

**HIGH THROUGHPUT SCREENING OF  
NANOPARTICLE FLOTATION COLLECTORS**

**HIGH THROUGHPUT SCREENING OF  
NANOPARTICLE FLOTATION COLLECTORS**

By

CARLA ABARCA, B. Chemistry

A Thesis

Submitted to the School of Graduate Studies

in Partial Fulfillment of the Requirements

for the Degree

Doctor of Philosophy

McMaster University

© Copyright by Carla Abarca, November 2016

DOCTOR OF PHILOSOPHY (2016)

McMaster University

(Chemical Engineering)

Hamilton, Ontario

TITLE: High Throughput Screening of Nanoparticle  
Flotation Collectors

AUTHOR: Carla Abarca  
B. Chemistry (Pontifical Catholic University of  
Chile)

SUPERVISOR: Professor Robert H. Pelton

NUMBER OF PAGES: x, 138

## Abstract

The selective separation of valuable minerals by froth flotation is a critical unit operation in mineral processing. Froth flotation is based on the ability of chemical reagents, called collectors, to selectively lower the surface energy of valuable mineral particles, facilitating attachment of the modified mineral particles to air bubbles in the flotation cell. The mineral laden bubbles rise to the surface forming a froth phase that can be isolated.

Novel cationic polystyrene nanoparticle collectors have been developed recently to be used as effective flotation collectors, aiming to recover challenging nickel sulfide ores that respond poorly to conventional molecular flotation collectors. However, optimizing nanoparticle flotation collectors is a challenge. An effective nanoparticle collector candidate should meet three requirements: (1) it should be colloidally stable in the flotation media; (2) it should be hydrophobic enough to change the mineral surface and induce an air bubble-mineral particle attachment; and (3) specifically and strongly bind to metal-rich minerals. Producing nanoparticles that are simultaneously colloidally stable and sufficiently hydrophobic presents a problematic task. Thus, a delicate balance of nanoparticle properties is required for commercially viable nanoparticle collectors.

This thesis presents a promising approach for discovering and characterizing novel nanoparticle collectors by using high throughput screening techniques. Developed was a workflow for fast fabrication and testing of nanoparticle candidates, including: (1) parallel production of large nanoparticle libraries covering a range of surface chemistries, (2) a high throughput colloidal stability assay to determine whether a nanoparticle type is stable in flotation conditions; (3) an automated contact angle assay to reject nanoparticles that are not hydrophobic enough to induce efficient bubble-particle attachment, and; (4) a laboratory flotation test in sodium carbonate (pH~10) with the best nanoparticle candidates.

The automated colloidal stability assay was based on the optical characterization of diluted nanoparticle dispersions in multiwell plates, yielding critical coagulation concentrations (CCCs) of sodium carbonate. To pass this screening test, the CCC of candidate nanoparticles must be greater than the effective carbonate concentration in commercial flotation cells. Since the nanoparticle size affects the intrinsic light scattering properties of the nanoparticles, two routes were developed. The colloid stability assay was suitable for nanoparticles ranging between 50 nm and 500 nm, since nanoparticle size.

The automated contact angle assay used a miniature 16-well plate format where flat glass slides were exposed to 200  $\mu$ L nanoparticle dispersions. The cationic nanoparticles



formed a saturated adsorbed monolayer on the glass, and after rinsing and drying, the water contact angle was automatically measured. Effective nanoparticle candidates had contact angles greater than 50 degrees, a criterion developed with model experiments.

During the development of the automated workflow platform, a series of nanoparticles with methyl-ended PEG-methacrylate monomers were prepared. Although the PEG chains greatly enhanced colloidal stability, the particles were too hydrophilic to be effective collectors. Interestingly, nanoparticles with long PEG chains acted as froth modifiers, giving wetter and more robust foams as well as increased entrainment of materials that did not adhere to bubbles.

Conventional laboratory scale latex synthesis methodologies are far too inefficient to generate large library of candidate nanoparticles. Instead, we started with a few parent nanoparticle types and then used Click chemistry to generate a large range of surface chemistries. Specifically copper-mediated azide alkyne cycloaddition reaction was used to functionalize the surface of azide nanoparticles with different chemical groups, ranging from hydrophilic amine-terminated PEG chains, to hydrophobic hexane-terminated materials.

The Click library exhibited an extensive range of critical coagulation concentrations and contact angle values. For example, for a given parent azide nanoparticle, the contact angles ranged from 62 to 101 degrees, depending upon the density and type of click reagent. A novel paper chromatographic method was developed for the quantitative determination surface azide. This assay was critical for determining the surface density of functional groups from the click reactions.

Overall, high throughput screening techniques were designed and applied to the development of nanoparticle collectors for froth flotation. Automated screening assays of critical coagulation concentration and contact angle proved to be effective in obtaining flotation domain maps, and finding the most promising nanoparticle collectors for froth flotation. I believe the work in this thesis is one of the first reported uses of high throughput methodologies for the development of mineral flotation reagents.

## Acknowledgments

First of all, I would like to show the most sincere gratitude to my supervisor Dr. Robert Pelton, for his wise guidance, continuous support, patience and immense knowledge. He has been supportive since the day I arrived to Canada and began working on my Ph.D. research. Dr. Pelton has not only provided me with academic advice, but also the most valuable professional and emotional support I required to finish this thesis. Thank you for being generous and caring, thank you for letting me learn from you and explore novel - and sometimes wild- ideas, and especially thank you for always being positive and believing in me.

I would also like to deeply thank my thesis committee: Dr. Carlos Filipe, from the Chemical Engineering department and Dr. Kenneth Coley, from the department of Materials Science and Engineering, for their invaluable advice and clever interpretations, generous encouragement and always positive attitude. Their insightful recommendations, out-of-the-box questions and unique thinking made me a better researcher and allowed me to expand my research from different views.

My sincere thanks also goes to Mr. Doug Keller, our lab manager, for his guidance and great assistance in all the matters related to my laboratory work, and Ms. Sally Watson, Ms. Kristina Trollip and Ms. Michelle Whalen, for helping me handle all the administrative work. Thanks to Mr. Paul Gatt, Mechanical Technician, for his immediate and important assistance in fabricating different gaskets for my project.

Also, I would like to sincerely thank some researchers that were fundamental in conducting my research project: Dr. Danielle Covelli and Dr. Mehdi Keramane, from the Biointerfaces Institute, Dr. Bob Berno and Dr. Steve Kornic, from the Department of Chemistry, and Ms. Marcia Reid, from the Faculty of Health Science. Thank you for giving me the proper training and for all the interesting science discussions we had all these years.

Furthermore, I am immensely grateful of Dr. Monsur Ali, for all his generous support, guidance and stimulating discussions about science and life. I am also very grateful of the summer students that worked with me: Mr. Devon Bowie, Mr. Michael Kiriakou, Mr. Patrick Morkus and Mr. Gerard Bruin. Your contributions and hard work were very important to accomplish this thesis.

I would like to thank the financial support of Vale Base Metals, the National Sciences and Engineering Research Council of Canada (NSERC) and CONICYT - Becas Chile Scholarship Program.

I would also like to thank my research group, in particular to Dr. Songtao Yang, Ms. Nazanin Moshtagh, Ms. Zela Li, Dr. Sophia Dong and Mr. Dong Yang; my friends at the EGS and my friends at OLAS. Thank you so much for all our entertaining discussions and support all these years.

Last but not the least; I would like to thank from the bottom of my heart all my friends at McMaster, which have given me the strength to complete this hard but beautiful journey. In particular, I profoundly thank Angie Perez, Cristina Gonzalez, Paula Guerra, Oscar Tirado and Marco Franco for always being there, for good and for bad.

Agradezco a mi familia, especialmente a mi madre, Patricia Segura, por amarme y darme las herramientas para conquistar el mundo. A mi abuelita, María Elena Inostroza, por rezar por mí y esperarme pacientemente todos estos años. A mi abuelito, Juan Segura, por cuidarme desde arriba. A mi hermano Francisco y a mi tío Juan José, por amar, acompañar y cuidar a mi mamá y a nuestra familia. A mi suegro, Pedro Krisch y a su maravillosa familia venezolana-canadiense que me ha aceptado como su nueva hija; a mis hermanos y sus hermosas familias, a mi padre, Carlos Abarca, a mis tíos y mis primos; a mis amigos PUC, a mis amigos y colegas de Redicec y a mi amiga de la niñez, Lilian Alvear. A todos ellos y ellas, muchas gracias por alentarme todo el tiempo a la distancia con su amor y consejos.

Finally, I heartily express thanks to my husband, Andres Krisch Bordy. El hombre que me protege en sus brazos a cada instante, el hombre que me enseña la luz en los días oscuros, el hombre que entibia mi corazón y me hace cada día más feliz. Thank you for walking by my side and supporting me emotionally throughout this thesis and my life. You are one of the best things that has happened to me in Canada and for that I will be always grateful of this wonderful country and this Ph.D. life.

“Our thoughts are like bubbles, waiting to be popped”

## Table of Contents

<b>Abstract .....</b>	<b>iii</b>
<b>Acknowledgments .....</b>	<b>v</b>
<b>Table of Contents .....</b>	<b>vii</b>
<b>List of Abbreviations .....</b>	<b>ix</b>
<b>Chapter 1: Introduction .....</b>	<b>1</b>
1.1. Nickel Mineral Processing Overview .....	1
1.2. Froth Flotation Overview .....	3
1.2.1. Steps of Froth Flotation .....	3
1.2.1.1. Surface modification of minerals .....	4
1.2.1.2. Collision between Minerals and Bubbles .....	4
1.2.1.3. Attachment between minerals and bubbles .....	5
1.2.1.4. Transport of the particle-bubble aggregate to the surface .....	5
1.2.2. Entrainment .....	7
1.3. Froth Flotation Additives .....	7
1.3.1. Collectors .....	7
1.3.2. Frothers .....	9
1.3.3. Other Flotation Reagents .....	9
1.4. Nanoparticle Collectors for Froth Flotation .....	9
1.4.1. Polymerization of Nanoparticle Collectors .....	10
1.4.2. Requirements of Nanoparticle Collectors .....	11
1.4.2.1. Nanoparticle Hydrophobicity .....	12
1.4.2.2. Nanoparticle Colloidal Stability .....	14
1.4.2.3. Nanoparticle Selectivity .....	16
1.4.2.4. Nanoparticle Size and Softness .....	17
1.4.3. Challenges of Nanoparticle Collectors .....	18
1.5. High Throughput Screening .....	18
1.5.1. HTS Polymerization Techniques .....	20
1.5.2. Click Chemistry .....	20

---

1.6. Objectives .....	22
1.7. Thesis Outline .....	24
1.8. References .....	25
<b>Chapter 2: Towards High Throughput Screening of Nanoparticle Flotation Collectors</b> .....	<b>37</b>
Appendix: Supporting Information for Chapter 2 .....	46
<b>Chapter 3: A Colloidal Stability Assay Suitable for High-Throughput Screening .....</b>	<b>57</b>
Appendix: Supporting Information for Chapter 3 .....	66
<b>Chapter 4: A Simple Assay for Azide Surface Groups on Clickable Polymeric Nanoparticles.....</b>	<b>72</b>
Appendix: Supporting Information for Chapter 4 .....	78
<b>Chapter 5: High Throughput Screening of Click Nanoparticle Collectors: a Platform for Modular Functionalization .....</b>	<b>91</b>
5.1. Abstract .....	92
5.2. Introduction .....	93
5.3. Experimental .....	94
5.4. Results and Discussion .....	99
5.5. Conclusions .....	112
5.6. References .....	114
Appendix: Supporting Information for Chapter 5 .....	117
<b>Chapter 6: Concluding Remarks .....</b>	<b>135</b>
6.1. Key Findings and Contributions .....	135
6.2. Future Work Outlook .....	137

## List of Abbreviations

AmPEG4	Amino-PEG <sub>4</sub> -alkyne
ATR	Attenuated Total Reflection (in FT-IR technique)
Az	Azide
BMA	Butyl methacrylate
BocPrAm	N-boc-propargylamine
BrBu	4-bromo-1-butyne
BuTos	3-butynyl tosylate
CCC	Critical coagulation concentration
cen	Centrifugation
CMC	Carboxymethyl cellulose
Cp	Chalcopyrite, CuFeS <sub>2</sub>
CTAB	Cetyl trimethyl ammonium bromide
CuACC	Copper-catalyzed azide-alkyne cycloaddition
D	Diameter
DADMAC	Diallyldimethyl ammonium chloride
DCC	N,N'-dicyclohexyl carbodiimide
DDA	Dodecyl amine
DETA	Diethylene triamine
DLS	Dynamic Light Scattering
DLVO	Derjaguin-Landau-Verwey-Overbeek
DMAP	4-dimethyl amino pyridine
DMSO	Dimethyl sulfoxide
FT-IR	Fourier Transform Infrared
HEMA	2-hydroxyethyl methacrylate
Hex	1-hexyne
HTS	High Throughput Screening
I <sub>azide</sub>	Proton peak intensity for azide (in NMR)
ICP-AES	Inductively coupled plasma atomic emission spectroscopy
m	Mass concentration
M	Molar concentration
MAPTAC	3-(methacryloylamino) propyl trimethyl ammonium chloride
MIBC	Methyl isobutyl carbinol
MP	Microwell plate
MW	Molecular weight
NaAsc	(+)-sodium L-ascorbate
NdMPrAm	N,N-dimethyl propargyl amine
NMR	Nuclear Magnetic Resonance
ODP	Octadecyl dihydrogen phosphate
Parg	Pargyline or N-methyl-N-propargylbenzylamine
PAX	Potassium amyl xanthate

---

PDI	Polydispersity Index
PEG4IM	Alkyne-PEG <sub>4</sub> -maleimide
PEGMA or PEG-methacrylate	Poly(ethylene glycol) methyl ether methacrylate
Pen	1-pentyne
PMDETA	N,N,N',N'',N'''-pentamethyldiethylenetriamine
Pn	Pentlandite, (Ni,Fe) <sub>9</sub> S <sub>8</sub>
PrAm	Propargyl amine
PrBr	Propargyl bromide
PrOH	Propargyl alcohol
PS	Polystyrene
Py	Pyrrhotite, Fe <sub>7</sub> S <sub>8</sub>
Rho-Alk	Rhodamine alkyne
SA	Azide Nanoparticle
SDS	Sodium dodecyl sulfate
sed	Sedimentation
SEM	Scanning Electron Microscopy
Sp	Serpentine, (Mg,Fe) <sub>3</sub> Si <sub>2</sub> O <sub>5</sub> (OH) <sub>4</sub> , Mg/Si slime coating
St	Styrene
TA	Triazole nanoparticle
TPC	Three phase contact
$\tau_p$	Relative turbidity
V	Volume
V44	2,2'-azobis[2-(2-imidazolin-2-yl)propane] dihydrochloride
V50	2,2'-azobis(2-methylpropionamidine) dihydrochloride
VBAz	Vinyl benzyl azide
VBCl	4-vinylbenzylchloride
VBTMAC	4-vinylbenzyltrimethyl ammonium chloride
VI	Vinyl imidazole
$\gamma$	Interfacial tension
$\theta, CA$	Contact angle
$\lambda_{SAz}$	Surface azide concentration ( $\mu\text{mol/g}$ )
$\lambda_{TAz}$	Total azide concentration ( $\mu\text{mol/g}$ )
$\sigma_{NP}$	Specific surface area of the nanoparticle
$\Gamma_{SAz}$	Surface azide units per area

## Chapter 1: Introduction

Froth flotation is an essential practice in mineral processing and is the most effective purification technique for sulfide ores processing<sup>[1]</sup>. Chemical industries have used flotation in various applications, ranging from wastewater treatment<sup>[2]</sup> to flotation deinking in paper recycling<sup>[3,4]</sup>. Froth Flotation is used to separate valuable solids from heterogeneous mixtures, by promoting the affinity of wanted material to air bubbles. The selected material are then transported by the bubbles to the surface of the flotation cell, where the froth layer is separated mechanically<sup>[5]</sup>.

Chemical additives called collectors are used to enhance the selective attachment of minerals to bubbles. These reagents increase the hydrophobicity at the surface of the valuable mineral, incrementing its adhesion to the air bubble<sup>[6]</sup>.

This thesis summarizes a project focused on the development of nanoparticle collectors for froth flotation. A promising approach to discover and accelerate this development is the use of combinatorial surface modification and high throughput techniques. These methods have been implemented in the fields of polymer science, pharmaceuticals, and material science with great success, giving researchers an opportunity to develop new materials faster and more effectively<sup>[7,8]</sup>.

The overall goal of this thesis is to develop high throughput screening techniques for the surface modification and characterization of nanoparticles collectors for froth flotation in mineral processing.

### 1.1. Nickel Mineral Processing Overview

The mining industry is an integration of several chemical processes<sup>[9]</sup>, including extraction, separation and purification of mineral ores. The industry has developed advanced operations to recover valuable metals, such as nickel, copper, gold, silver, etc. A number of factors are considered when extracting and purifying mineral ores. The type of mineral, final product specifications, unitary operations efficiency, and environmental requirements are all weighed-in when evaluating mining projects.

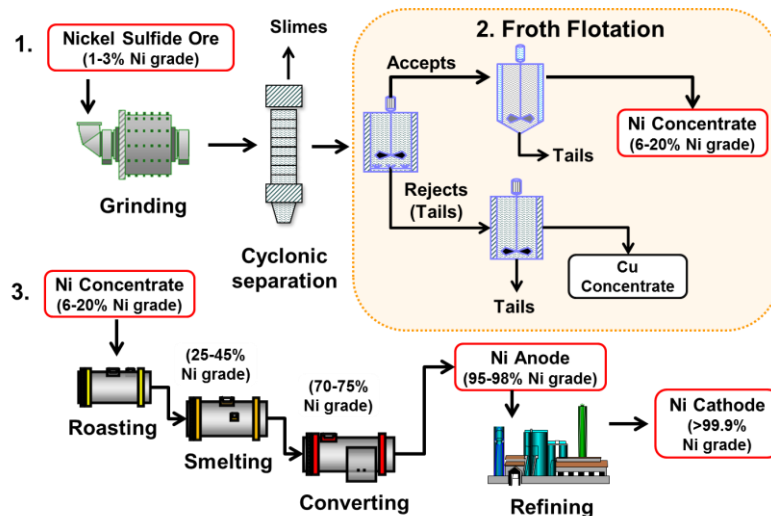
Nickel can be extracted from different mineral ores including sulfide oxide, arsenide, antimonide, and silicate ores; however, the main resources of nickel are presented in lateritic ores and sulfide ores. Nickel sulfide ores consist mainly of pentlandite (Pn,  $(\text{Ni,Fe})_9\text{S}_8$ ), pyrrhotite (Py,  $\text{Fe}_7\text{S}_8$ ), chalcopyrite (Cp,  $\text{CuFeS}_2$ ), mixed with other gangue minerals such as quartz, feldspar, amphibole, biotite and chlorite. Pentlandite surfaces are



normally anionic in mineral ores <sup>[10]</sup>. Nickel sulfide ores contain a nickel percent concentration, also referred as grade, between 0.4% and 2.0% <sup>[11]</sup>. Pentlandite rich-ores comprise around 40% of the world's nickel production <sup>[12, 13]</sup>, to a total of 2.5 million tons in 2015 <sup>[14]</sup>.

Figure 1-1 illustrates a typical process workflow for nickel ore processing. The first step involves the extraction of mineral ores that contains a nickel grade higher than 1%. These ores are ground, mixed with water and separated from some of their impurities by cyclonic separation. The second step is froth flotation in series, in which the addition of collectors, depressants and pH controllers allows the separation of valuable minerals from the gangue, or commercially worthless material. During froth flotation the mineral is concentrated up to 20% of nickel concentration, or grade <sup>[15]</sup>. A higher nickel grade in the flotation step will allow reduced energy consumption in the smelting step: roasting, smelting and converting <sup>[13]</sup>. After this processing, a nickel-copper molten material is molded as an anode and usually brought to electro-refining. At this step the purity of nickel metal cathodes reach 99.9% or higher. Other valuable materials, such as cobalt and copper can be recovered in the anode residues.

**Figure 1-1:** A typical nickel ore process workflow (Adapted from Kirk-Othmer Encyclopedia of Chemical Technology <sup>[13]</sup> and Ullmann's Encyclopedia of Industrial Chemistry <sup>[12]</sup>).



One of the main sources of pentlandite in Canada is ultramafic ores. Canada is the second largest producers of nickel and its sub-products in the world <sup>[14]</sup>. Vale, the main mining company in Canada for nickel sulfide ore processing <sup>[13]</sup>, has operations in four mine sites in Canada. Thompson Complex, a northern city in the boreal forest of Manitoba, has

extensive deposits of nickel ultramafic ores that have not been exploited due to their expensive mineral processing. The focus of this project is to find novel flotation collectors that would allow an effective processing of ultramafic ores.

In the geological classification, ultramafic ores are rocks that present a low content of silica (usually lower than 44%)<sup>[16]</sup>. These ores are well known for having a challenging recovery by flotation process due to the deposition of a great amount of Serpentine,  $(\text{Mg,Fe})_3\text{Si}_2\text{O}_5(\text{OH})_4$ <sup>[17]</sup>, fibrous materials on the surface, commonly referred as “Mg/Si slime coating”<sup>[18]</sup>. These hydrophilic slimes, generally cationic and rich in magnesium<sup>[19]</sup>, reduce the interaction between collectors and the mineral, lowering the air bubble attachment efficiency and thus decreasing the recovery of the valuable minerals<sup>[20]</sup>.

## 1.2. Froth Flotation Overview

In froth flotation, air bubbles are introduced into an aqueous pulverized ore slurry, where adherence to hydrophobic minerals happens, producing solid-air aggregates that are subsequently carried out to the surface by a pressure gradient, forming a froth layer that can be separated from undesirable materials by mechanical methods<sup>[11]</sup>, as shown in Figure 1-2.

Flotation performance is characterized by two parameters: recovery and grade. Recovery is a measure of flotation efficiency, referring to the percentage of valuable material that has been effectively removed from the mixture in a flotation experiment<sup>[16]</sup>. The recovered mineral is generally called concentrate or accepts, while the rejected material is known as tails or tailings<sup>[16]</sup>. The grade is the percent concentration of a valuable metal or compound in the recovered material. For instance, nickel grade, MgO grade, iron grade or sulfur grade are typically obtained from an analytical assay (e. g. ICP-AES, Inductively coupled plasma atomic emission spectroscopy) in samples of concentrate and tailings. The grade is reported in flotation as a measure of selectivity efficiency<sup>[16]</sup>.

### 1.2.1. Steps of Froth Flotation

Ralston *et al.*<sup>[21]</sup> proposed that the collection efficiency is determined by: the collision efficiency, attachment efficiency and stability of the bubble-particle aggregate efficiency. This process is also called orthokinetic hetero-coagulation in flotation science<sup>[22]</sup>.

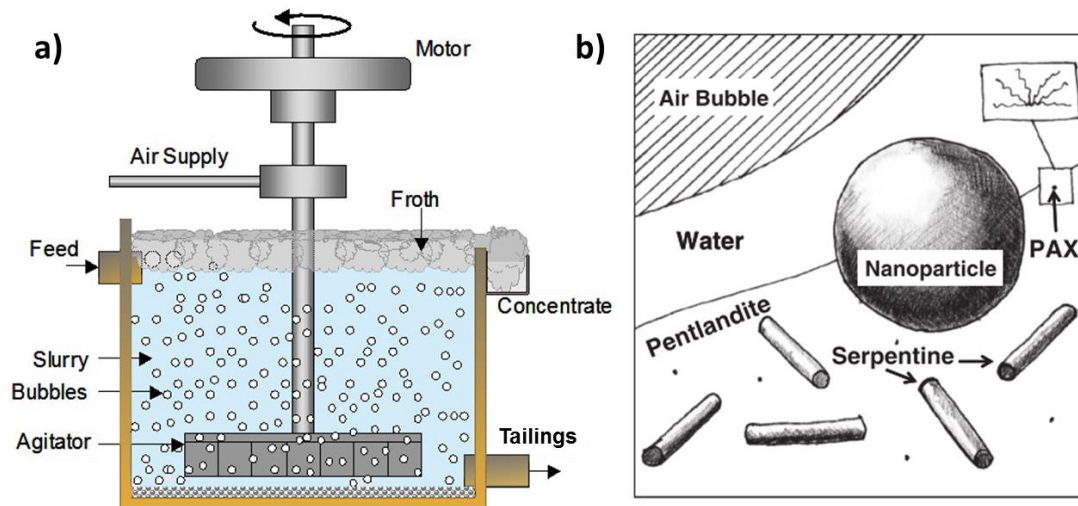
From that perspective, the science of froth flotation can be defined as a sequence of events: 1) Surface modification of minerals by collectors; 2) Collision between the bubbles and the hydrophobic valuable minerals; 3) Adherence of the required mineral to

the bubble and; 4) Transport to the surface of the bubble-particle aggregates to join the froth layer<sup>[23]</sup>.

### 1.2.1.1. Surface modification of minerals

Most of the minerals in froth flotation do not show natural floatability<sup>[24]</sup>, since their surfaces tend to be wetted by water or absorb water, thus they are normally hydrophilic<sup>[24]</sup>. Bubbles will attach to mineral particles as long as the surfaces of minerals are sufficiently hydrophobic to induce a selective bubble-mineral attachment. A mineral surface with a contact angle between 30 to 50° is generally enough to promote attachment to the bubbles<sup>[25]</sup>. In the presence of collectors, this attachment can happen since the minerals have been hydrophobized by the chemical collectors<sup>[26, 27]</sup> (two examples of collectors, molecular and nanoparticle, are shown in Figure 1-2. b).

**Figure 1-2:** a) Froth Flotation Cell Scheme (Adapted from Haldar<sup>[28]</sup>); b) Illustration of molecular collectors and nanoparticle collectors onto a pentlandite ore surface (Reprinted from Yang *et al.*<sup>[29]</sup>).



### 1.2.1.2. Collision between Minerals and Bubbles

In froth flotation, the probability of collision between minerals and bubbles is dictated by hydrodynamic forces, including: shear force in the flotation cell, viscous forces on the flotation mixture, and gravity. Ralston's research group<sup>[30]</sup> has published a complete review of collision probability in flotation. Further investigations<sup>[31, 32]</sup> have also included the impact of particle size, aqueous film thickness and contaminations to correct numerical models that explain collision. Laskowski<sup>[33]</sup> mentioned the importance of bubbles at the collision stage, since they are the primary vehicle of flotation agents to

reach the zone of collision. Other variables that increase the collision probability, such as air flowrate, gas dispersion and slurry flowrate, are always optimized and controlled in the system<sup>[34]</sup>, and can greatly affect the performance of the flotation process.

### **1.2.1.3. Attachment between minerals and bubbles**

When a mineral particle collides against a bubble, two phenomena can happen: the particle attach to the bubble, or the particle rebound, coming back into the liquor. The probability of attachment of the particle to the bubble is mainly determined by the hydrophobicity of the mineral and the stability of the wetting film at the bubble surface. Studies have shown that the more hydrophobic a mineral, the more efficient the flotation<sup>[6, 35]</sup>.

The mechanism of attachment has been extensively studied theoretically<sup>[21, 36]</sup> and experimentally<sup>[37, 38]</sup>; however it is still not fully understood. Ralston *et al.* also established that the attachment of minerals to bubbles is a process that involves three steps<sup>[39]</sup>: 1) the thinning of the liquid film between both surfaces, 2) the liquid film rupture to form the three-phase contact (TPC) nucleus, and 3) the expansion of this TPC line to lead to a stable wetting perimeter.

Figure 1-3a shows the deformation effect produced by a particle attached to a bubble. Scheludko *et al.*<sup>[40]</sup> determined the equation to obtain the force necessary to pull apart a particle from a bubble in case of complete de-wetting (when the wetting film has been broken by the particle-bubble attachment) (Figure 1-3. a). Yang and Pelton have also obtained a pull-off force relationship for a partial de-wetting<sup>[41]</sup>. From these equations the correlation between the contact angle ( $\theta$ ) at the TPC line and the pull-off force can be established. A higher contact angle will lead to a higher pull-off force, therefore a more hydrophobic surface will attach more strongly to the bubbles.

### **1.2.1.4. Transport of the particle-bubble aggregate to the surface**

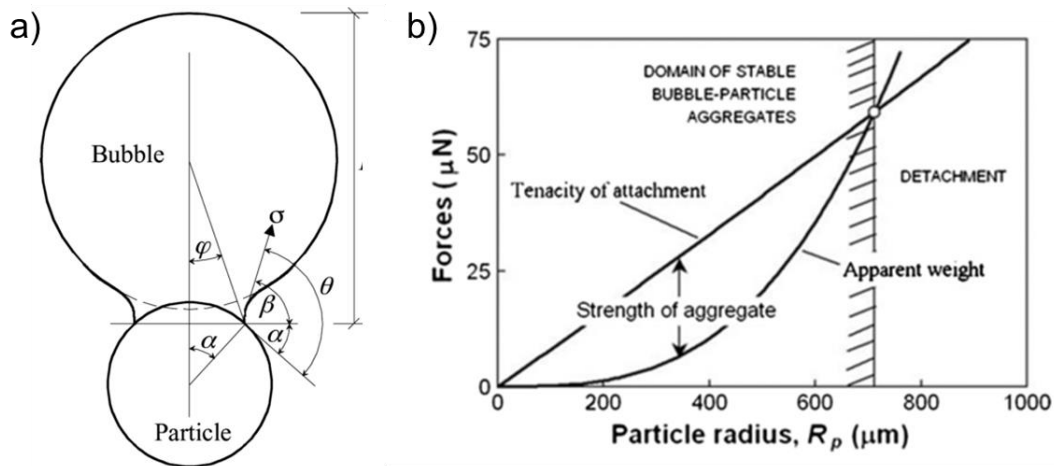
The particle-bubble aggregate recently formed must overcome the detachment forces in order to be recovered in the froth layer (Figure 1-3. b). Thus, the stability of the bubble-particle aggregate and the stability of the froth layer become crucial for achieving high recoveries and grade of minerals<sup>[25, 42, 43]</sup>.

In a flotation cell where turbulence is absent, the particle-bubble aggregate stability is determined by thermodynamics<sup>[22]</sup>. However, in a real case, dynamic conditions (e. g. turbulence) are always going to exist. Since flotation is a kinetic process, the particle-bubble aggregate has a probability to detach, lowering the recovery of flotation.

Wang *et al.* [43] published a recent review on detachment models, based on forces, energy and particle size. Shear force and turbulence play an important role on the detachment. If the shear force overcomes the capillary force, the particle will detach from the bubble [44]. Also, if the mineral particle size is negligible compared to the bubble size, the aggregate will act as a bubble; hence the turbulence of the system does not influence the stability of the aggregate in a great extent. By contrast, if the particle size becomes dominant over the bubble size, the aggregate will start rotate with the turbulent flow, diverging and promoting detachment [45]. Therefore, coarse minerals will also increase the detachment probability, decreasing the collection efficiency [22].

In case of the froth layer, the transport of the particle-bubble aggregates to the froth-pulp interface is determined by bubble size, rate of aeration, wash water, froth depth, among others [46]. Bubble coalescence within the froth layer also promotes detachment [47]. Consequently, a stable and structured layer is important to increase collection efficiency [47]. However, a stable froth, with small bubbles, can also recover unwanted material by entrainment [29, 48], which affects the grade of the mineral recovered.

**Figure 1-3:** a) Geometry of a particle attached to a bubble (Reprinted from Nguyen [49]) note: drawing is not at scale; b) Firmness of the particle-bubble attachment, and apparent weight of the particle in water versus the particle radius (Reprinted from Wang *et al.* [43]).



In summary, the essential challenge is to ensure that the adhesive force acting on the bubble-particle aggregate is enough to overcome the detachment forces in a dynamic system [22], to promote a high collection efficiency.

### 1.2.2. Entrainment

The size of the bubbles also plays an important role on the recovery. If the bubbles at the froth layer are small, the surface area at which the minerals and collectors can interact will be larger, enhancing true flotation. However, smaller bubbles can also increase the thickness of the aqueous lamella that surrounds the surface of the bubbles<sup>[50, 51]</sup>, incrementing the amount of liquid that will be recovered from flotation. If more liquid is recovered, the more probable it is that the liquid carries mineral particles along with it without a bubble-particle attachment. This situation is called entrainment<sup>[29, 48]</sup>.

Entrainment is a major detrimental effect for the selectivity of minerals, since the particles brought to the froth layer via this mechanism may have not been necessarily recovered due to the particle-bubble collision and attachment, leading to more gangue materials recovered. Furthermore, this mechanism becomes dominant when the bubble size decreases<sup>[26, 27, 52]</sup>.

## 1.3. Froth Flotation Additives

Chemical additives are fundamental to promote flotation of valuable minerals and decrease the recovery of unwanted materials. Collectors, depressants, frothers and pH-modifiers are among the most typical types of additives used in flotation.

### 1.3.1. Collectors

Since hydrophobicity is the most important factor affecting attachment of the valuable mineral to the bubble and stability of the particle-bubble aggregate, collectors are needed to increase the hydrophobicity at the surface of the valuable mineral and allow a selective separation.

The collectors most widely used in froth flotation include alkyl dithiocarbonates (xanthates), xanthogen formates, dixanthogens, alkyl dithiocarbamates, thionocarbamates, and dithiophosphates<sup>[53]</sup>.

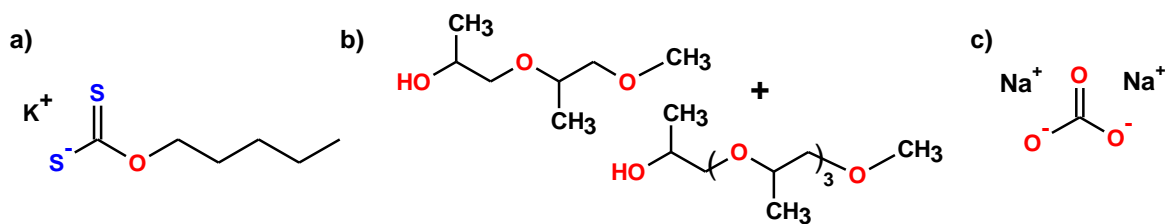
Pearse<sup>[54]</sup> has published a complete overview on froth flotation reagents in 2005, including frothers, collectors, depressants and modifiers. In the review it is acknowledged that divalent sulfur collectors, also known as xanthates, are the most used in nickel sulfide flotation since sulfide surfaces already have some inherited hydrophobicity in their natural state. Xanthates technology is based in electrochemical reactions onto the surface of the mineral, therefore it is dependent on the electronegativity of sulfur group and metal species<sup>[55]</sup>. The reactions involve cathodic reductions to produce hydroxyl groups, anodic

oxidation to generate sulfur and/or sulfates, chemisorption and physical adsorption, among other reactions <sup>[55]</sup>.

Potassium amyl xanthate (PAX) is the most used collector in nickel sulfide ore froth flotation, and contains an alkali metal salt of amyl xanthic acid with a hydrophilic dithiocarbonyl-head and hydrophobic short tail of 5 members, as shown in Figure 1-4. Most of the xanthate salts are yellow pale solids with a disagreeable odor (due to their decomposition in water), which are relatively stable in aqueous and mild conditions depending on the length of their carbonyl tail, pH, and ionic strength, among others. Their decomposition mostly releases carbon disulfide (CS<sub>2</sub>), hydrosulfide (HS<sup>-</sup>), hydrogen sulfide (H<sub>2</sub>S), carbonyl sulfide (COS), pseudo-xanthates, alcohols, hydroxides, among others <sup>[56, 57]</sup>. Some of these decomposition products are flammable, toxic and poisonous for the human health and environment. This decomposition may occur during the process of froth flotation, smelting, tailings treatment, or as a discard of residues. Therefore, these materials have presented several environmental concerns, specifically for mine workers, and neighboring areas around mines <sup>[58, 59, 60]</sup>.

Amine-based collectors have also shown some selectivity and good recoveries; and even though their performance has been tested more widely in silicate minerals <sup>[54]</sup>, it is a technology that could also be used in sulfide minerals. Consequently, the development of new types of collectors is one of the key aspects in mining research & development. For example, more than 200 patents have been published since the first xanthates collector technology was patented, back in 1924 <sup>[61]</sup>. However, these patents are mostly related to the applications of mixing collectors systems rather than developing technologies to minimize the environmental impact caused by these collectors and their unwanted side reactions.

**Figure 1-4:** Three important additives for froth flotation: a) collector: PAX (potassium amyl xanthate); b) frother: Unifroth 250C (di-propylene glycol monomethyl ether and poly-propylene glycol monomethyl ether (250 Da) mixture); c) pH controller: Sodium carbonate, Na<sub>2</sub>CO<sub>3</sub>.



### 1.3.2. Frothers

Frothers are non-ionic chemical additives, which are added to the flotation cell to form and enhance the froth phase by reducing the interfacial tension at the water-air interface, allowing the bubbles to agglomerate and become stable in the flotation buffer<sup>[53]</sup>.

The characteristic chemical moiety in a frother is the hydroxyl, generally as alcohol or glycol form<sup>[54]</sup>. Poly-propylene glycol derivatives<sup>[62]</sup>, such as Unifroth series (Figure 1-4) and methyl isobutyl carbinol (MIBC) are the most common frothers used in sulfide mineral processing. These molecules can play a fundamental role in the kinetics and feasibility of the flotation process when interacting with the bubbles and other chemicals, since they co-adsorb on the surface of the bubbles, sometimes allowing the solubilization of collectors, stronger attachment with the selected minerals or controlling the bubble size<sup>[54, 63]</sup>.

### 1.3.3. Other Flotation Reagents

Modifiers, depressants, flocculants, dispersants, thickeners, among others, are additives that can be added to the flotation liquor for different purposes. They can either be inorganic or organic compounds, and their function is to improve the separation or recovery of the valuable minerals. pH controllers regulate pH and ionic strength at the mineral slurry, resulting in depressing other minerals to float, helping minerals to disperse or flocculate. The most common flotation buffer in sulfide mineral processing is sodium carbonate (Figure 1-4) ( $pK_a = 10.33$ ) that allows the flotation slurry to maintain at  $pH \sim 9-10$ , at which the slime coating can present a negative surface charge and therefore, is less likely to adsorb onto the mineral surface<sup>[18]</sup>. Depressants allow separating the gangue from wanted minerals by depositing onto the most hydrophilic material. Most of the depressants are based on hydroxyl group structure<sup>[54]</sup>, very hydrophilic in nature. Typically used depressants are polysaccharides such as sodium carboxymethyl cellulose (CMC) or starch<sup>[64]</sup>.

## 1.4. Nanoparticle Collectors for Froth Flotation

The Interfacial Technologies Group at McMaster University, led by Robert Pelton, has been working in this field for the past few years, aiming to develop new classes of froth flotation collectors, nanoparticle collectors, and understanding their mechanism of action applied to nickel sulfide compounds.



Important providers of collector technologies, such as Dow Chemical<sup>[65]</sup>, Lubrizol<sup>[66]</sup> and Cytec<sup>[67]</sup>, have been mostly focused on patenting applications of their own brands of molecular collectors in conjunction with other water soluble chemical compounds containing heteroatoms as sulfur, nitrogen and oxygen, which can enhance the mechanism of action in the flotation systems. However, there were no patented applications on the development of cationic hydrophobic polymeric nanoparticle collectors. Hence, Pelton and colleagues filled an patent application in 2011 to protect and investigate this new technology further<sup>[68]</sup>.

As molecular collectors can have low efficiency in the recovery of valuable minerals in challenging ultramafic ores, the hypothesis is that larger hydrophobic nanoparticles may be less susceptible to Mg/Si slime coating than molecular collectors; offering advantages over molecular collectors. These nanoparticles must meet three requirements in order to act as good collectors: 1) must be hydrophobic enough to promote the particle-bubble attachment, 2) must be colloidally stable in flotation conditions, and 3) must have selectivity for Pentlandite and no other materials in ultramafic ores.

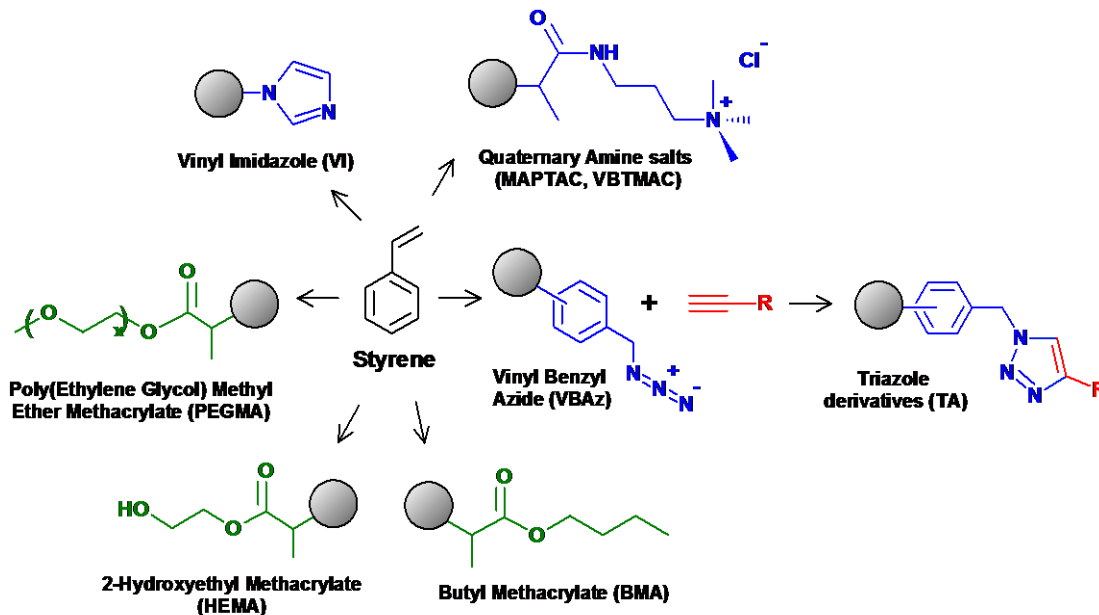
#### **1.4.1. Polymerization of Nanoparticle Collectors**

Polystyrene (PS) lattices have been extensively studied and used in various applications, such as coatings<sup>[69, 70]</sup>, biological applications<sup>[71]</sup>, water treatment<sup>[72]</sup>, etc. They are easily produced by emulsion polymerization, a type of radical polymerization, in which the monomers and the final product are insoluble in the continuous phase, typically water<sup>[73]</sup>. The monomer used, styrene, presents the ability to co-polymerize with other functional monomers, whether they have hydrophilic or hydrophobic properties, or whether they are organic or inorganic by nature; thus allowing the fabrication of numerous copolymers and morphologies<sup>[74, 75, 76]</sup>.

The starting point to produce nanoparticle collectors involves emulsion polymerization with monomer controlled addition. Based on recipes published by Pelton and Goodwin<sup>[77, 78]</sup>, with modifications; an extensive nanoparticle collectors library has been produced, as shown in Figure 1-5.

Several monomers were used individually or in conjunction at increasing ratios to gain insights on the mechanism of flotation of nanoparticle collectors, along with practical experiments in glass beads (as a mineral model) and real pentlandite ores, at laboratory scale, from 100 mL to 5 L flotation vessels.

**Figure 1-5:** Nanoparticle Collectors Library developed by the Interfacial Technologies group at McMaster.



#### 1.4.2. Requirements of Nanoparticle Collectors

Our research group has published several investigations on the fundamentals of this technology. The most important requirements that a nanoparticle must have to work effectively as a collector are: 1) a high hydrophobicity, 2) a high colloidal stability and, 3) a selectivity to nickel sulfide minerals.

In the first publication related to the nanoparticle collectors technology<sup>[41]</sup>, Yang and Pelton showed that polystyrene nanoparticles can function as collectors of silica glass beads, a negatively charged mineral model, in similarity to pentlandite ores<sup>[10]</sup>. Furthermore, they presented a micromechanics experiment to investigate the adhesion force between nanoparticles, glass beads and bubbles. From this work it was concluded that, to be effective collectors, nanoparticles must be: sufficiently hydrophobic to attach to the bubbles and sufficiently small to efficiently cover the glass beads and produce a wet patch at the glass beads-nanoparticle-bubble interface.

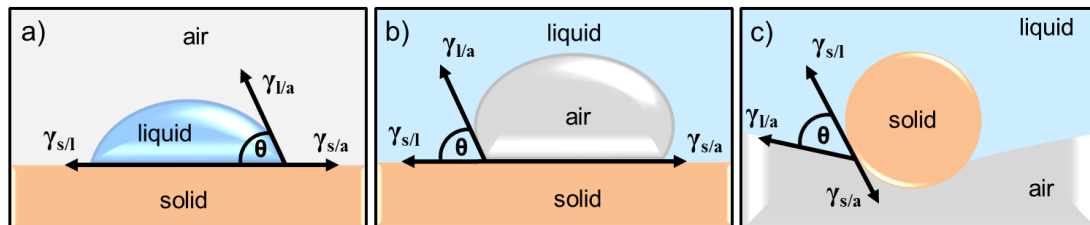
Some further questions arose from this work, such as, why did the nanoparticles aggregate on the glass beads? Why did smaller and more hydrophobic nanoparticles give better recoveries? What surface groups will selectively float nickel sulfide minerals? Those questions led to more investigations, and the requirements herein are the main focus of this thesis.

### 1.4.2.1. Nanoparticle Hydrophobicity

One of the keys aspects of flotation collectors is their ability to provide hydrophobicity to the mineral to promote bubble-particle attachment. Most of the mineral surfaces are in nature hydrophilic, having water contact angles from  $0^\circ$  up to  $30^\circ$  (practically total spreading) <sup>[79]</sup>. To increase the contact angle of these mineral surfaces, nanoparticles must be more hydrophobic than the mineral surfaces. The water contact angle measured at the surface of a nanoparticle coating allows to measure hydrophobicity. The contact angle at the TPC line is related to the interfacial tensions (Figure 1-6) by the Young-Dupré equation. However, roughness and nature of the sample also affects the contact angle, as described by theories of Wenzel <sup>[80]</sup> and Cassie-Baxter <sup>[81]</sup>, as extensions of Young's theory <sup>[82]</sup>. Spori *et al.* <sup>[83]</sup> explained that while the Wenzel's equation to calculate interfacial tensions and contact angle is based in a chemically homogeneous but rough surface, the Cassie-Baxter's theory established its calculations on a chemically heterogeneous underlying and rough surface.

In mineral processing, most of the studies involve experiments of contact angle directly on minerals surfaces, either bare or coated with collectors <sup>[35, 79, 84]</sup>. Prestidge and Ralston <sup>[35]</sup>, published the influence that surface treatment and size of galena minerals have on the contact angle results of different samples with and without PAX as a collector, showing its variability and difficulty to correlate results to flotation. Kelebek and Yoruk <sup>[79]</sup> showed the bubble captive contact angle dependency with the pH solution and sample preparation in clean chalcopyrite, galena and chalcocite. In this study they concluded that low pH and short bubble-mineral contact periods increased contact angles and promoted self-induced flotation.

**Figure 1-6:** Water contact angles ( $\theta$ ) and interfacial tensions ( $\gamma$ ) in a: a) droplet sitting on a mineral surface; b) bubble sitting on a mineral surface in liquid media (adapted from Chau *et al.* <sup>[82, 85]</sup>), and; c) a mineral particle attached to an air bubble (adapted from Scheludko *et al.* <sup>[40]</sup>).



Also, mineral models as quartz have been used; for instance, Schwarz and colleagues<sup>[47]</sup> used methylated quartz with different contact angles as mineral models to run flotation experiments. They analyzed the effect of hydrophobicity and particle size in the flotation recovery and froth phase. Their findings revealed that while more hydrophobic quartz particles gave higher recoveries, increasing hydrophobicity also affected the froth phase, promoting coalescence, and therefore decreasing recovery.

Another approach was shown by Yang and Pelton<sup>[86]</sup> when studying effects of hydrophobicity of nanoparticle collectors on flotation. They correlated flotation recoveries with the contact angle for some coatings of nanoparticle collectors, showing that nanoparticles with more hydrophobic surface chemistry gave higher recoveries. In this study, contact angles were measured on glass surfaces (as a mineral model) covered by nanoparticle collectors instead of mineral surfaces to eliminate the variability of contact angle on the mineral surfaces. However, contact angles obtained by this method were still subject to some variability, especially receding contact angles of droplets, since deposition of nanoparticles onto the glass surfaces was heterogeneous, provoking a pinning effect.

In other fields, a few other studies have shown the use of nanoparticles to change the surface of hydrophilic materials<sup>[87, 88]</sup>. Generally, this modification is done to produce super-hydrophobic surfaces with advanced chemical and physical techniques relying heavily in changing the roughness of the materials<sup>[89, 90, 91]</sup>. Bala and colleagues<sup>[92]</sup> published the synthesis of barium sulfate nanoparticles and its surface modification with ODP (Octadecyl dihydrogen phosphate) to obtain contact angles between  $17^\circ$  and  $111^\circ$ , for applications such as fillers in coatings, as shown in Figure 1-7.

**Figure 1-7:** Water contact angles of various BaSO<sub>4</sub> nanoparticles modified with increasing concentration of ODP (Octadecyl dihydrogen phosphate) (Reprinted from Bala *et al.*<sup>[92]</sup>).

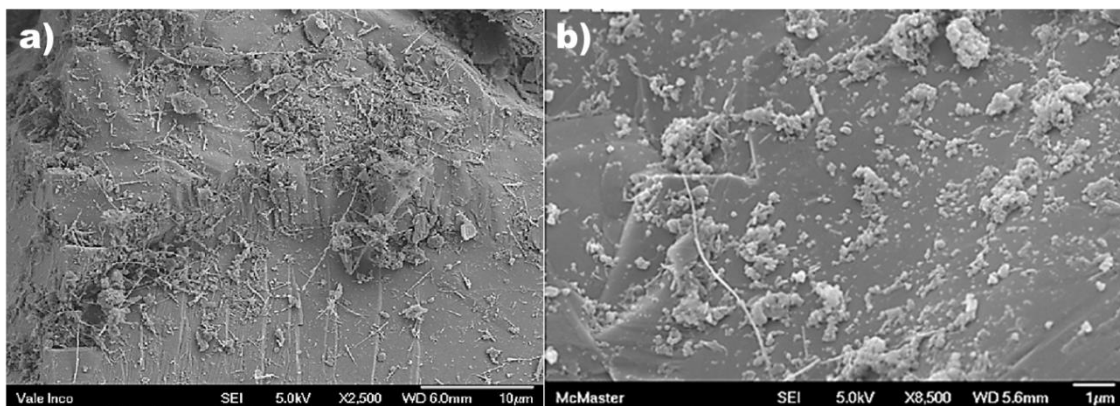


#### 1.4.2.2. Nanoparticle Colloidal Stability

As extreme conditions of pH and ionic strength characterize froth flotation in nickel sulfide minerals, similar conditions should be established as a starting point for the application of delicate nanoparticle collectors. The flotation conditions to be met by nanoparticles to remain stable and avoid aggregation are: pH higher than 10, conductivity over 3000  $\mu\text{S}/\text{cm}$ , and variable concentration of ions, such as  $\text{Na}^{2+}$ ,  $\text{Mg}^{2+}$ ,  $\text{Ca}^{2+}$ ,  $\text{CO}_3^{-2}$ ,  $\text{Cl}^-$ ,  $\text{SO}_4^{-2}$ . Thus, the froth flotation pulp is a mixture of species that can interact with each other to produce secondary structures, to form aggregate with other species, or to enhance/reduce the recovery of valuable species <sup>[54, 93, 94]</sup>.

One of the challenges of nanoparticle collectors technology is the aggregation of the nanoparticles at the mineral surface <sup>[29, 95]</sup> (as shown in Figure 1-8). Aggregated nanoparticles will have less contact surface area to cover the mineral surface, leading to a decrease in their efficiency and consequently, the recovery of minerals. Therefore, the colloidal stability of collectors in froth flotation conditions is a key aspect in the process.

**Figure 1-8:** Pentlandite micrographs: a) bare pentlandite with MgO slimes (fibers) on the surface (Reprinted from Yang *et al.* <sup>[29]</sup>); b) Recovered pentlandite with aggregates of nanoparticle collectors at the surface (Reprinted from Yang <sup>[95]</sup>).



To aggregate, colloidal particles must overcome the barrier of inter-particle repulsive energy <sup>[96]</sup>. This process has been explained by different approaches to the Deryagin & Landau, Verwey & Overbeek (DLVO) theory <sup>[97]</sup>, which combines electrostatic, hydrophobic and hydration forces to describe mechanisms of destabilization or compression of the electrical double layer <sup>[98]</sup>. Also, the extended DLVO theory presented by Hoek *et al.* <sup>[99]</sup>, used interactions between spherical particles and rough surfaces to show that additionally to the traditional theory, nanoscale roughness and particle size also

influence coagulation. From this study, they proposed that rougher surfaces are more prone to form aggregates because the electrostatic and acid-base interactions of repulsion cannot overcome the van der Waals force of attraction at long distance<sup>[99]</sup>. Therefore, smooth nanoparticles should work better.

In a series of publications by van de Ven and colleagues, “The micro-rheology of colloidal dispersions”, they examined the micro-rheology of colloidal dispersions<sup>[100]</sup>, discussing perikinetic and orthokinetic coagulation in various systems conformed by latex spheres of 1 to 2  $\mu\text{m}$ . Perikinetic coagulation is the aggregation of destabilized colloidal particles driven by Brownian motion (random molecules bombardment)<sup>[101, 102]</sup>. Orthokinetic coagulation, is the aggregation of colloidal particles by inducing velocity gradients, in which fast particles can collide against slow particles to produce aggregation<sup>[103, 104]</sup>, for instance flotation systems. Hence, a suitable nanoparticle should be able to remain stable in orthokinetic coagulation conditions.

Polyelectrolyte effect in coagulation of latex particles has also been studied theoretically and experimentally<sup>[105, 106, 107]</sup>. Interestingly, in one of the last publications of the series<sup>[107]</sup>, they experimented with mixtures of latex particles, glycerol and KCl as polyelectrolyte. They found that high concentrations of glycerol would impede coagulation, and they attributed it to the surface roughness or hydration forces. It is now known that glycerol and polymers also promote steric stabilization, hydrogen bonding, and other non-DLVO interactions<sup>[108]</sup>.

Grasso *et al.*<sup>[108]</sup> published a systematic review in where all forces that influence coagulation are explained. In froth flotation and the thesis presented herein, coagulation of nanoparticles is mostly produced by a polyelectrolytes effect (e. g. flotation buffer) and an external shear (e. g. turbulence). The former compresses the electrical double layer, while the latter introduces velocity gradients into the system. Both phenomena make the nanoparticles collide, aggregate and lose their efficiency to recover minerals by flotation.

#### ***1.4.2.2.1. Mechanisms of Colloidal Stabilization***

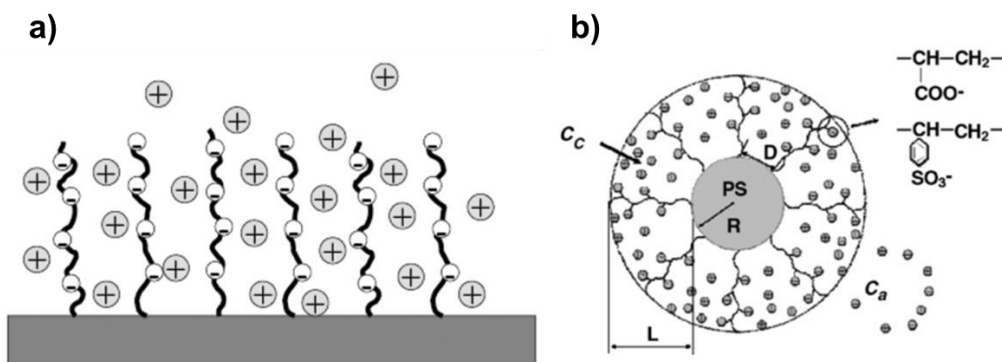
Electrostatic, acid-base, steric and electrosteric interactions are the main forces that promote stability in colloidal systems. Studies of the effect of anionic electrolytes and adsorption of anionic polymers on positively charged latex particles and vice versa, have been published by Gillies *et al.*<sup>[109]</sup> and Bouyer *et al.*<sup>[110]</sup>, to investigate how adsorption of polymers on the surface of latex particles is capable of increasing electrostatic stabilization by changing the surface charge on the particles.

Steric stabilization<sup>[111, 112, 113]</sup> is the most used method to stabilize colloidal particles. The term refers to the stabilization of any colloidal systems by non-ionic macromolecules<sup>[111]</sup>.

Steric stabilizers confer an extended interparticle separation, offsetting attraction forces. Therefore, the thickness and density of the steric layer becomes the most important parameter to control when producing steric stabilized particles<sup>[114]</sup>. Steric stabilization is an efficient tool that can be used to stabilize particles in polar and non-polar systems<sup>[115]</sup> and it can provide the particle with resistance to high concentrations of salts<sup>[116]</sup>. Polymerization techniques (e. g. macromonomers<sup>[113, 117]</sup>), chemical grafting<sup>[118]</sup> or physical adsorption<sup>[119]</sup> are the techniques used by polymer scientists to produce these particles, normally leading to good yields. These mechanism and particles are exploited in several industries to produce functional and long-term stable compounds.

Electrosteric stabilization<sup>[120]</sup> is the combination of both stabilization methods. The compounds fabricated with this type of mechanisms contain charged macromolecules that can form the required steric layer and also give a specific charge to the particles, by keeping counterions contained by the brush layer<sup>[121]</sup>, as shown in Figure 1-9.

**Figure 1-9:** Polyelectrolyte brushes (electrosteric stabilization: a) planar view, b) spherical view (Reprinted from Ballauf *et al.*<sup>[122]</sup>).



#### 1.4.2.3. Nanoparticle Selectivity

To achieve higher recoveries and grades the collector must selectively adsorb onto wanted mineral surfaces<sup>[123]</sup>. Several problems at the surface of the minerals can reduce the ore beneficiation<sup>[17]</sup>, such as the slime coating, grinding process, particle size, aeration, pH and water, etc. Senior *et al.*<sup>[124]</sup> published a procedure to reject talc and pyrrhotite from pentlandite ores by optimizing pH, collectors and depressant conditions. As long as the collector presents a selective interaction for a mineral and that interaction promotes the hydrophobicity at the surface, the collector can be effective.

Depressants can also help to increase the grade of the recovered material when reacting with gangue minerals. Xanthates seem to be the premier collectors for sulfide ores due to their electrochemical reactions on the surface of the minerals<sup>[57]</sup>. Xanthate thermo-responsive polymers have been recently tested by Franks *et al.*<sup>[125, 126]</sup>, in efforts to find more applications to xanthate derivatives. Some amine compounds have shown action as depressants and collectors. For instance, diethylenetriamine (DETA), showed to be beneficial as pyrrhotite depressants in nickel sulfide operations<sup>[64, 127]</sup>, while other nitrogen derivatives, such as dodecylamine (DDA), can act as collectors<sup>[128, 129]</sup> by adsorbing on the surface.

Investigations have shown imidazole-compounds as chelating collectors as well<sup>[130, 131, 132]</sup>. Imidazole moieties can coordinate nickel sulfide surfaces by the coordination of the electron-rich nitrogen of the imidazole to the electron-acceptor nickel atom in the sulfide mineral. Our previous publications in nanoparticle collectors showed that sulfide minerals containing metals such nickel and copper can interact with imidazole moieties by chelation<sup>[29]</sup>, as well as help the flotation of small-sized mineral pentlandite particles (also called fine particles)<sup>[133]</sup>. Nanoparticle collectors would promote selectivity as long as they have species that can interact with the nickel metal on their surface, by means of coordination, electrostatic attraction, chemisorption or physical adsorption.

#### **1.4.2.4. Nanoparticle Size and Softness**

The importance of the mineral particle size<sup>[134, 135]</sup> and bubble size<sup>[27, 136]</sup> has been widely studied by froth flotation scientists. Genc *et al.*<sup>[137]</sup> stated that the recovery of fine mineral particles depends on many factors, such as particle size, shape, particle-particle interaction, solids concentration and rheological aspects in the pulp. Fine particles are more prone to be recovered by entrainment. Also, smaller bubbles are prone to cause more entrainment. Although the size of molecular collectors is not a problem as it usually does not affect the recovery, when working with nanoparticle collectors, the size of these compounds can also affect froth flotation.

Yang *et al.*<sup>[138]</sup> investigated the role of nanoparticle diameter in froth flotation of glass beads as a mineral model, concluding that smaller nanoparticles collectors are more effective because: 1) they deposited more quickly than larger nanoparticles as they diffuse more easily in the water/mineral interface, 2) with a larger surface area and a larger number of nanoparticles, smaller nanoparticles would increase the hydrophobicity of the mineral, and 3) as the TPC line is expanded with smaller nanoparticles, attachment of minerals to bubbles is assisted. Recent investigations in our research group also propose that a glass beads collision would desorb larger nanoparticles from the surface of the glass



beads more easily than small ones, a phenomenon that Pelton and colleagues defined as the nano-scale ball milling effect<sup>[139]</sup>.

The softness of nanoparticle collectors was also studied in our research group<sup>[140]</sup>. It was proposed that softer nanoparticles, for instance, nanoparticles made of styrene/n-butylacrylate copolymers, would attach more firmly to the glass beads due to a greater contact area leading to a stronger adhesion.

### **1.4.3. Challenges of Nanoparticle Collectors**

One of the main challenges of the nanoparticle collectors' technology is to balance the nanoparticle properties described to produce good candidates for froth flotation. Hydrophobicity and colloidal stability in aqueous media are known to be opposite parameters. Generally, a more stable nanoparticle is more hydrophilic. In consequence, a delicate balance on the surface chemistry of the nanoparticles is necessary to achieve both requirements. If for instance, selectivity to the minerals, size and softness of the nanoparticles are to be included in the balance, the problem becomes the ability to test countless possible combinations of monomers that can produce good nanoparticle candidates for froth flotation.

The design, fabrication and testing of nanoparticles collectors is a time consuming process; hence, high throughput techniques applied to their fabrication and characterization is a promising method for faster discovery of new nanoparticle candidates.

## **1.5. High Throughput Screening**

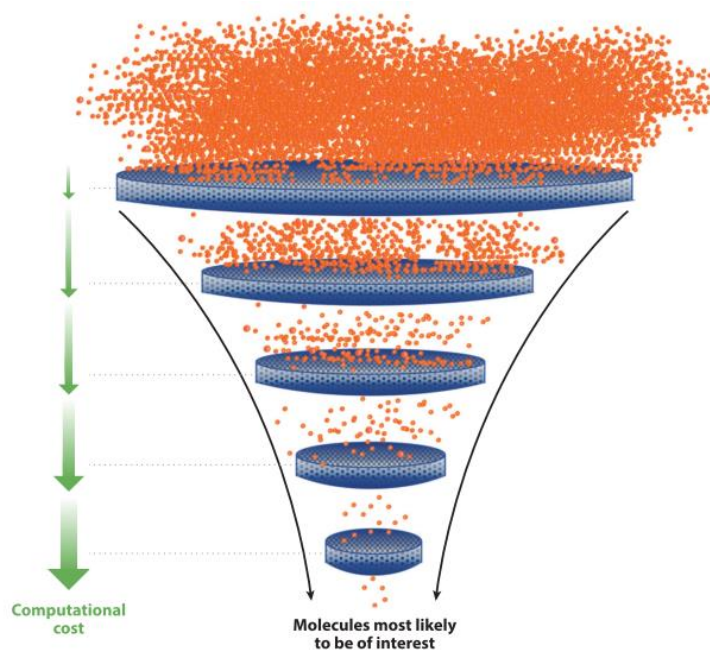
Nowadays, there is very little time for trial/error experimentation. In several industries such as coatings<sup>[141, 142]</sup>, combinatorial chemistry<sup>[8, 143]</sup> and pharmaceuticals<sup>[144, 145]</sup>, they have been taking advantage of new automated technologies, robotic and computational systems to create innovative ways for discovering and analyzing new combinations of materials. This new approach of experimentation is usually called “high throughput screening” (HTS)<sup>[145, 146]</sup>, in which the term high throughput refers to fast and automated analyses of a variety of substances.

The use of these techniques offers many benefits, as they represent a fast and simple test to discard non-interesting samples and it can expand the knowledge and development of

“unknown” components, avoiding human error, and achieving even more than 7,000 tests in a single day<sup>[147, 148]</sup>.

The development of new materials during the last two decades has been greatly influenced by HTS methodologies<sup>[149]</sup>. HTS is equivalent to a “materials funnel” (Figure 1-10), which brings the parallel production of several materials, in conjunction with different measurements (generally high throughput as well) to characterize intrinsic or performance properties in the target materials<sup>[8]</sup>, and collect the promising candidates. These techniques respond to the need of covering the wide possibilities of combinations that components can have, referring as components as every single variable, as materials compositions, operation conditions and process factors that is possible to change in a determined development.

**Figure 1-10:** High throughput screening funnel. Filtering by intrinsic or performance properties of materials will lead to “target candidates” for a specific application (Reprinted from Pyzer-Knapp *et al.*<sup>[146]</sup>).



In order to achieve a high throughput development, the automation of experiments, miniaturization, data collection and data management are key aspects<sup>[150]</sup>. Also, it is important to note that polymer discovery has many challenges as mentioned by Meredith<sup>[151]</sup>, for instance: most of the variables are continuous (just a few yes/no tests available),

there is usually no universal screen for properties, and sometimes the properties are “size-dependant”. Therefore, the need of useful assays and a large sample library is fundamental.

In the nanoparticle collectors research project it is a challenge to find surface chemistries that will act as good collectors. Polymerization and cleaning steps of a single batch of nanoparticles can take weeks; nonetheless a very thorough fabrication does not ensure its success as a minerals collector. Consequently, a high throughput polymerization looked promising to accelerate the discovery of promising nanoparticle collectors.

### 1.5.1. HTS Polymerization Techniques

There are several polymerization techniques that can be transformed into a high throughput polymerization. Hoogenboom *et al.* <sup>[152]</sup> reviewed combinatorial methods for polymerization. They reported types of polymerizations such as: polycondensation, free-radical and controlled-radical polymerization, ring-opening polymerization, supramolecular polymerization. Furthermore, these reactions can be carried in different conditions such as: suspension, emulsion, photo/thermal initiated and imprinted polymerizations. Also, most of the high throughput polymerizations are carried out with very low volumes, usually less than 1 mL, even though some automated parallel systems can prepare samples even up to volumes of 100 mL <sup>[153, 154]</sup>.

The challenges of high throughput polymerization of nanoparticle collectors are: 1) to implement parallel equipment and dosage to automate emulsion polymerizations of polystyrene; 2) to find a surface modification easily adjustable to be used in high throughput polymerization; 3) to determine which types of surface chemistry could be suitable as nanoparticle collectors, and; 4) to find or develop automated and rapid methods to characterize the relevant properties on the nanoparticles collectors (e. g. hydrophobicity, colloidal stability, surface chemistry). In the present work, click chemistry was identified as a possible route to produce several nanoparticle surface chemistries and automate the modification.

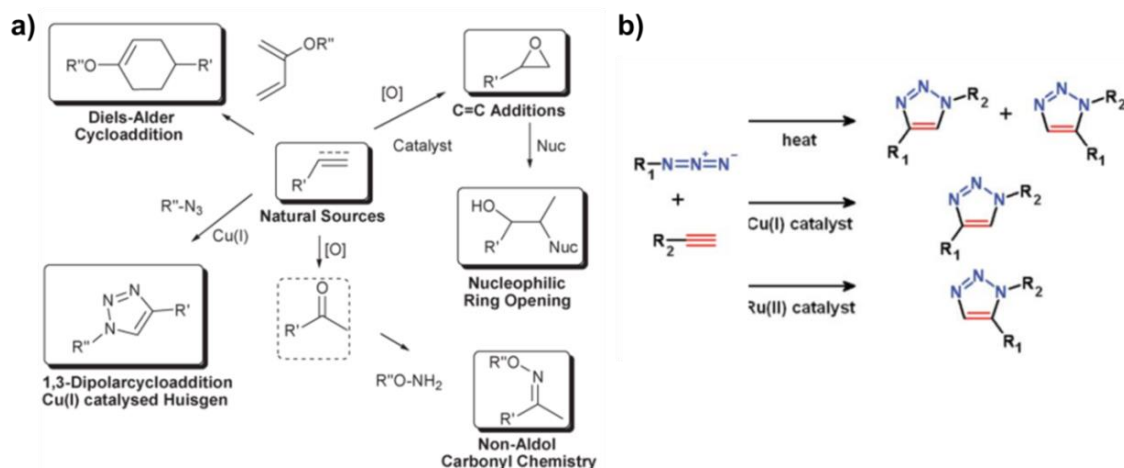
### 1.5.2. Click Chemistry

Synthetic chemistry and polymer science researchers have recognized how useful high throughput techniques can be to accelerate the materials discovery process <sup>[143, 147, 155]</sup>. Click chemistry is another powerful tool that organic chemists have used to synthesize a wide range of materials for different applications <sup>[156, 157, 158]</sup>. Combining these tools can be the perfect solution for screening large libraries of materials.

The term *click chemistry* was just recently introduced by Sharpless *et al.* <sup>[159]</sup>, in 2001. It was defined as a set of carbon-heteroatom reactions with bond forming that satisfied some requirements such as: being modular, lead to high yields, being stereospecific, generate innocuous by-products that can be removed by non-chromatographic techniques and with a wide scope of applications <sup>[160]</sup>. Click reactions also include: mild conditions of reaction, readily available reagents, and simple product separation. These reactions are known by their high thermodynamic driving force that allows them to be selective and achieve high yields. Figure 1-11a, illustrates a selection click reactions that comply with the criteria.

One of the most attractive examples of click reactions is the copper-catalyzed Huisgen 1,3-dipolar cycloaddition of azides to terminal alkynes to produced triazole compounds <sup>[161]</sup> (also known as *CuACC*, copper-catalyzed Azide-Alkyne Cycloaddition), as illustrated in Figure 1-11b, Meldal and colleagues published a detailed review on these copper-catalyzed click reactions in 2008 <sup>[162]</sup>. Advantages of the CuAAC reaction are: versatility of reagents, solvents, reaction conditions and platforms.

**Figure 1-11:** a) Selection of click reactions (Reprinted from Moses *et al.* <sup>[163]</sup>); b) 1,3-dipolar cycloaddition of azides to terminal alkynes, activated by three different catalytic systems (Reprinted from Fournier *et al.* <sup>[164]</sup>).



Investigations on quantum mechanics show that the azide group is a weak electrophile, but it can have an electrophilic activation from methyl or phenyl groups <sup>[165]</sup>, allowing the nucleophilic alkyne to react with it to form triazole groups <sup>[166]</sup>. When adding the catalytic system, copper (I), the reaction reaches shorter times and gives stereoselective compounds. Although the mechanism is still in discussion <sup>[162, 166]</sup>, an intermediate

formed between the alkyne, activated by two chemically equivalent copper atoms, and the terminal nitrogen on the azide, seems to be the more accepted mechanism<sup>[166]</sup>. These reactions have been reported as stable and irreversible, assuring that once the triazole group is formed, the reaction would not revert<sup>[167]</sup>.

Click reactions have been also exploited in nanotechnology, such as bio-nanotechnology<sup>[168]</sup>, cellulose materials<sup>[169]</sup>, and polymer science<sup>[170]</sup>. Manfield *et al.*<sup>[170]</sup> published a complete review on how click reagents are used by polymer scientists to produce macromolecular structures. Either azide or alkyne monomers can be attached to nanoparticles to generate macromolecules with different surface architectures.

When selectivity to mineral is needed, triazole groups in nanoparticles could interact with minerals by chemical coordination<sup>[171]</sup> in a similar manner to other heterocyclic molecules containing nitrogen, sulfur or other electron pair donor<sup>[172, 173]</sup>.

As a result, click chemistry is an interesting way to quickly produce a large library of polystyrene nanoparticle collectors with different surface chemistries that can influence the balance between stable, hydrophobic and selective nanoparticles.

## 1.6. Objectives

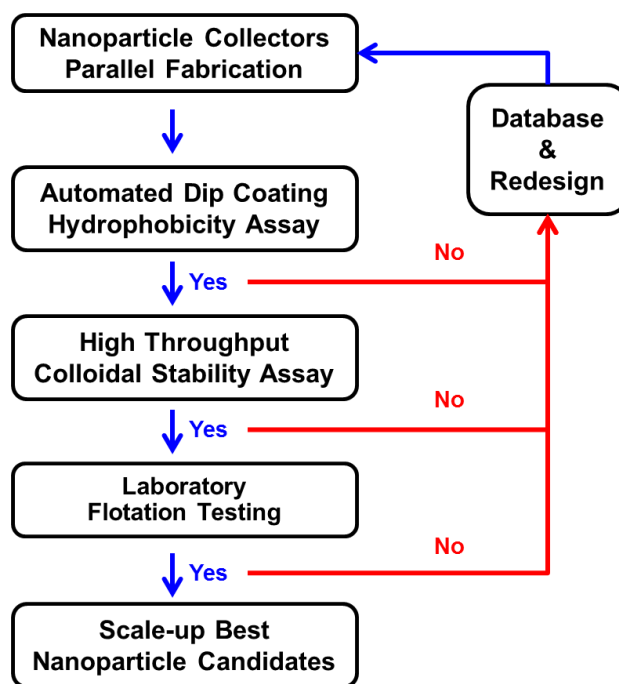
The development of nanoparticle collectors has been our research focus for 8 years and, although we have achieved several milestones on understanding the fundamentals of this technology, the need for accelerating the development of nanoparticle candidates has led us to introduce high throughput screening techniques into the process.

The overall objective of this project is the development of novel nanoparticle collectors by using high throughput screening techniques in order to accelerate the design, fabrication and testing of nanoparticle candidates. The specific objectives of this work include:

1. To generate nanoparticle collectors libraries, to further investigate different properties of nanoparticles that affects the flotation performance, such as nanoparticle colloidal stability and hydrophobicity.
2. To fabricate hydrophilic nanoparticles and study their action as collectors – frothers in flotation, investigating how hydrophilic chains in nanoparticles affect the recovery of glass beads and minerals.
3. To develop a parallel production platform of clicked nanoparticles through CuACC reactions, in order to fabricate nanoparticle collectors with different surface

- chemistries. Additionally, to design and optimize a quick and reproducible assay to quantify azide moieties on the surface of nanoparticles and estimate the coupling yield with different alkynes via sequential reactions.
4. To develop a high throughput colloidal stability assay that can be effectively used with any nanoparticle collectors library and that can be extrapolated to other colloidal systems. This assay also aims to assist investigations on the effect of the colloidal stability of nanoparticle collectors under high pH and ionic strength used in the flotation process.
  5. To develop an automated, rapid and reproducible contact angle measurement that can be applied to the nanoparticles collectors' library to find correlations between colloidal stability and hydrophobicity of nanoparticles.
  6. To establish a sequential workflow (Figure 1-12) for the development of nanoparticles, in which the surface chemistry design, the fabrication and the testing of colloidal stability and hydrophobicity can lead us to find the most promising nanoparticle collectors for froth flotation in a harsh flotation environment.

**Figure 1-12:** Sequential workflow for nanoparticle collectors' development involving design, fabrication, testing and scale-up of best nanoparticle candidates.



## 1.7. Thesis Outline

*Chapter 1: Introduction.* This chapter summarizes a literature review and the fundamental principles related to this project, including an overview of mining processes, froth flotation principles and reagents, implications for the development of nanoparticle collectors, high throughput technology and click chemistry fundamentals. This chapter also includes the research objectives and the thesis outline.

*Chapter 2: “Towards High Throughput Screening of Nanoparticle Flotation Collectors”.* This chapter presents our investigations on hydrophilic modification of nanoparticle collectors, aiming to relate colloidal stability and contact angle with their flotation performance and generate a library of PEG-methacrylate nanoparticles. It was demonstrated that the correlations between critical coagulation concentration and advancing water contact angle can be used to screen promising nanoparticle candidates, and that entrainment is a major challenge for hydrophilic modification of nanoparticle collectors. This work has been published in the *Journal of Colloid and Interface Science* [174].

*Chapter 3: “A Colloidal Stability Assay Suitable for High-Throughput Screening”.* This chapter investigates the development of a high throughput assay to study colloidal stability in colloidal systems, specifically in nanoparticle collectors of sizes ranging between 50 nm and 400 nm. 32 nanoparticle collectors candidates library was tested in order to optimize the assay for a wide range of nanoparticle diameters. The assay was developed in 96-microwell plates, giving a robust approach for larger nanoparticles. This work allows us to continue our high throughput development of nanoparticle collectors. This manuscript has been published in *ACS Analytical Chemistry* [175].

*Chapter 4: “A Simple Assay for Azide Surface Groups on Clickable Polymeric Nanoparticles”.* To create a practical nanoparticle collectors library that could be tested by high throughput methods, we fabricated azide-modified nanoparticles that could be reacted with different alkynes. A rapid and reproducible chromatographic assay was developed to determine the amount of azide moieties on the surface of nanoparticles. This assay allowed us to estimate the coupling yield of any alkyne by proceeding with a second step click reaction with a fluorescent alkyne. This work has been published in the *Journal Colloids and Surfaces A: Physicochemical and Engineering Aspects* [176].

*Chapter 5: “Fabrication and High Throughput Screening of Click Nanoparticle Collectors: A Platform for Modular Functionalization”.* This chapter describes the high throughput polymerization and characterization of novel clicked nanoparticle collectors,

and investigates automated colloidal stability vs. hydrophobicity maps to correlate and predict their performance as collectors. Additionally, it summarizes the progress on an automated sample preparation and contact angle measurement that could allow us to rapidly analyze over 100 nanoparticle samples. This manuscript is in preparation for publication.

*Chapter 6: Concluding Remarks.* The final chapter explores main conclusions, major contributions and future work for this research project.

## 1.8. References

- [1] Wills, B.A. and T. Napier-Munn, *Froth Flotation*, in *Wills' mineral processing technology: an introduction to the practical aspects of ore treatment and mineral recovery*. 2015, Butterworth-Heinemann. p. 265-368.
- [2] Rubio, J., M. Souza, and R. Smith, *Overview of flotation as a wastewater treatment technique*. *Minerals engineering*, 2002. **15**(3): p. 139-155.
- [3] Ajersch, M., *Mechanisms of pulp loss in flotation deinking*. 1997, McMaster University.
- [4] Hubbe, M.A., A. Sundberg, P. Mocchiutti, Y. Ni, and R.H. Pelton, *Dissolved and colloidal substances (DCS) and the charge demand of papermaking process waters and suspensions: A review*. *BioResources*, 2012. **7**(4): p. 6109-6193.
- [5] Fuerstenau, M.C., G.J. Jameson, and R.-H. Yoon, *Froth flotation: a century of innovation*. 2007, Littleton, Colorado: Society for Mining, Metallurgy, and Exploration.
- [6] Rao, S.R., *Surface Chemistry of Froth Flotation: Volume 1: Fundamentals*. 2013: Springer Science & Business Media.
- [7] Meier, M.A.R. and U.S. Schubert, *Combinatorial polymer research and high-throughput experimentation: powerful tools for the discovery and evaluation of new materials*. *Journal of Materials Chemistry*, 2004. **14**(22): p. 3289.
- [8] Potyrailo, R., K. Rajan, K. Stoewe, I. Takeuchi, B. Chisholm, and H. Lam, *Combinatorial and high-throughput screening of materials libraries: review of state of the art*. *ACS Comb Sci*, 2011. **13**(6): p. 579-633.
- [9] Krüger, J., J. Reisener, M. Reuter, and K. Richter, *Metallurgy*, in *Ullmann's Encyclopedia of Industrial Chemistry*. 2002, Wiley-VCH Verlag GmbH & Co. KGaA: Weinheim.
- [10] Bremmell, K.E., D. Fornasiero, and J. Ralston, *Pentlandite–lizardite interactions and implications for their separation by flotation*. *Colloids and Surfaces A: Physicochemical and Engineering Aspects*, 2005. **252**(2-3): p. 207-212.
- [11] Yarar, B., *Flotation*, in *Ullmann's Encyclopedia of Industrial Chemistry*. 2000, Wiley-VCH Verlag GmbH & Co. KGaA.
- [12] Kerfoot, D.G.E., *Nickel*, in *Ullmann's Encyclopedia of Industrial Chemistry*. 2000, Wiley-VCH Verlag GmbH & Co. KGaA.



- 
- [13] Tundermann, J.H., J.K. Tien, T.E. Howson, and S. Updated by, *Nickel and Nickel Alloys*, in *Kirk-Othmer Encyclopedia of Chemical Technology*. 2000, John Wiley & Sons, Inc.
- [14] Kuck, P.H., *Nickel*, in *Mineral commodity summaries 2016: U.S. Geological Survey*. 2016, U.S. Geological Survey: Virginia. p. 114-115.
- [15] Duby, P.F., *Metallurgy, Extractive*, in *Kirk-Othmer Encyclopedia of Chemical Technology*. 2000, John Wiley & Sons, Inc.
- [16] Neuendorf, K.K., *Glossary of geology - American Geosciences Institute*. 2005: Springer Science & Business Media.
- [17] Kirjavainen, V. and K. Heiskanen, *Some factors that affect beneficiation of sulphide nickel–copper ores*. *Minerals Engineering*, 2007. **20**(7): p. 629-633.
- [18] Edwards, C.R., W.B. Kipkie, and G.E. Agar, *The effect of slime coatings of the serpentine minerals, chrysotile and lizardite, on pentlandite flotation*. *International Journal of Mineral Processing*, 1980. **7**(1): p. 33-42.
- [19] Feng, B., Y.-p. Lu, Q.-m. Feng, P. Ding, and N. Luo, *Mechanisms of surface charge development of serpentine mineral*. *Transactions of Nonferrous Metals Society of China*, 2013. **23**(4): p. 1123-1128.
- [20] Trahar, W., *A rational interpretation of the role of particle size in flotation*. *International Journal of Mineral Processing*, 1981. **8**(4): p. 289-327.
- [21] Ralston, J., D. Fornasiero, and R. Hayes, *Bubble–particle attachment and detachment in flotation*. *International Journal of Mineral Processing*, 1999. **56**(1): p. 133-164.
- [22] Ralston, J., S. Dukhin, and N. Mishchuk, *Wetting film stability and flotation kinetics*. *Advances in colloid and interface science*, 2002. **95**(2): p. 145-236.
- [23] Subrahmanyam, T. and E. Forssberg, *Froth stability, particle entrainment and drainage in flotation—a review*. *International Journal of Mineral Processing*, 1988. **23**(1-2): p. 33-53.
- [24] Aghazadeh, S., S.K. Mousavinezhad, and M. Gharabaghi, *Chemical and colloidal aspects of collectorless flotation behavior of sulfide and non-sulfide minerals*. *Advances in Colloid and Interface Science*, 2015. **225**: p. 203-217.
- [25] Ata, S., *Phenomena in the froth phase of flotation — A review*. *International Journal of Mineral Processing*, 2012. **102-103**: p. 1-12.
- [26] Trahar, W. and L. Warren, *The flotability of very fine particles—a review*. *International Journal of Mineral Processing*, 1976. **3**(2): p. 103-131.
- [27] Ahmed, N. and G.J. Jameson, *The effect of bubble size on the rate of flotation of fine particles*. *International Journal of Mineral Processing*, 1985. **14**(3): p. 195-215.
- [28] Haldar, S.K., *Mineral Exploration: Principles and Applications*. 2012, Newnes: Elsevier. 372.
- [29] Yang, S., R.H. Pelton, C. Abarca, Z. Dai, M. Montgomery, M. Xu, and J.-A. Bos, *Towards nanoparticle flotation collectors for pentlandite separation*. *International Journal of Mineral Processing*, 2013. **123**: p. 137-144.
- [30] Dai, Z., D. Fornasiero, and J. Ralston, *Particle–bubble collision models—a review*. *Advances in Colloid and Interface Science*, 2000. **85**(2): p. 231-256.

- [31] Firouzi, M., A.V. Nguyen, and S.H. Hashemabadi, *The effect of microhydrodynamics on bubble–particle collision interaction*. Minerals Engineering, 2011. **24**(9): p. 973-986.
- [32] Huang, Z., D. Legendre, and P. Guiraud, *Effect of interface contamination on particle–bubble collision*. Chemical Engineering Science, 2012. **68**(1): p. 1-18.
- [33] Laskowski, J.S., *Flotation Thermodynamics: Can We Learn anything from It?* Canadian Metallurgical Quarterly, 2007. **46**(3): p. 251-258.
- [34] Shean, B.J. and J.J. Cilliers, *A review of froth flotation control*. International Journal of Mineral Processing, 2011. **100**(3–4): p. 57-71.
- [35] Prestidge, C.A. and J. Ralston, *Contact angle studies of particulate sulphide minerals*. Minerals Engineering, 1996. **9**(1): p. 85-102.
- [36] Krasowska, M., J. Zawala, and K. Malysa, *Air at hydrophobic surfaces and kinetics of three phase contact formation*. Advances in Colloid and Interface Science, 2009. **147–148**: p. 155-169.
- [37] Beaussart, A., L. Parkinson, A. Mierczynska-Vasilev, J. Ralston, and D.A. Beattie, *Effect of Adsorbed Polymers on Bubble–Particle Attachment*. Langmuir, 2009. **25**(23): p. 13290-13294.
- [38] Nguyen, A.V., J. Nalaskowski, and J.D. Miller, *A study of bubble–particle interaction using atomic force microscopy*. Minerals Engineering, 2003. **16**(11): p. 1173-1181.
- [39] Nguyen, A., H. Schulze, and J. Ralston, *Elementary steps in particle–bubble attachment*. International journal of mineral processing, 1997. **51**(1): p. 183-195.
- [40] Scheludko, A., B. Toshev, and D. Bojadjev, *Attachment of particles to a liquid surface (capillary theory of flotation)*. Journal of the Chemical Society, Faraday Transactions 1: Physical Chemistry in Condensed Phases, 1976. **72**: p. 2815-2828.
- [41] Yang, S., R.H. Pelton, A. Raegen, M. Montgomery, and K. Dalnoki-Veress, *Nanoparticle flotation collectors: mechanisms behind a new technology*. Langmuir, 2011. **27**(17): p. 10438-46.
- [42] Farrokhpay, S., *The significance of froth stability in mineral flotation — A review*. Advances in Colloid and Interface Science, 2011. **166**(1–2): p. 1-7.
- [43] Wang, G., A.V. Nguyen, S. Mitra, J.B. Joshi, G.J. Jameson, and G.M. Evans, *A review of the mechanisms and models of bubble-particle detachment in froth flotation*. Separation and Purification Technology, 2016. **170**: p. 155-172.
- [44] Nguyen, A. and H. Schulze, *Colloidal Science of Flotation*. 2004, New York: Marcel Dekker. 840.
- [45] Wang, G., S. Zhou, J. Joshi, G.J. Jameson, and G.M. Evans, *An energy model on particle detachment in the turbulent field*. Minerals Engineering, 2014. **69**: p. 165-169.
- [46] Van Deventer, J., D. Feng, and A. Burger, *Transport phenomena at the pulp–froth interface in a flotation column: II. Detachment*. International Journal of Mineral Processing, 2004. **74**(1): p. 217-231.
- [47] Schwarz, S. and S. Grano, *Effect of particle hydrophobicity on particle and water transport across a flotation froth*. Colloids and Surfaces A: Physicochemical and Engineering Aspects, 2005. **256**(2-3): p. 157-164.

- [48] Bushell, G.C., Y.D. Yan, D. Woodfield, J. Raper, and R. Amal, *On techniques for the measurement of the mass fractal dimension of aggregates*. *Advances in Colloid and Interface Science*, 2002. **95**(1): p. 1-50.
- [49] Nguyen, A.V., *New method and equations for determining attachment tenacity and particle size limit in flotation*. *International Journal of Mineral Processing*, 2003. **68**(1-4): p. 167-182.
- [50] Hemmings, C., *On the significance of flotation froth liquid lamella thickness*. *Institution of Mining and Metallurgy Transactions*, 1981. **90**.
- [51] Pelton, R., *A review of antifoam mechanisms in fermentation*. *J Ind Microbiol Biotechnol*, 2002. **29**(4): p. 149-54.
- [52] Tao, D., *Role of Bubble Size in Flotation of Coarse and Fine Particles—A Review*. *Separation Science and Technology*, 2005. **39**(4): p. 741-760.
- [53] Rao, S.R., *Surface Chemistry of Froth Flotation: Volume 2: Reagents*. 2013: Springer Science & Business Media.
- [54] Pearse, M.J., *An overview of the use of chemical reagents in mineral processing*. *Minerals Engineering*, 2005. **18**(2): p. 139-149.
- [55] Hu, Y., W. Sun, and D. Wang, *Electrochemistry of Flotation of Sulphide Minerals*. 2009: Springer.
- [56] Sun, Z. and W. Forsling, *The degradation kinetics of ethyl-xanthate as a function of pH in aqueous solution*. *Minerals Engineering*, 1997. **10**(4): p. 389-400.
- [57] Harris, G.H., *Xanthates*, in *Kirk-Othmer Encyclopedia of Chemical Technology*. 2000, John Wiley & Sons, Inc.
- [58] Shaohua, C., G. Wenqi, and M. Guangjun. *Study on Biodegradation of Alkyl Xanthate Collectors*. in *Bioinformatics and Biomedical Engineering (iCBBE), 2010 4th International Conference on*. 2010.
- [59] Webb, M., H. Ruber, and G. Leduc, *The toxicity of various mining flotation reagents to rainbow trout (Salmo gairdneri)*. *Water Research*, 1976. **10**(4): p. 303-306.
- [60] Agar, G.E., *Flotation of chalcopyrite, pentlandite, pyrrhotite ores*. *International journal of mineral processing*, 1991. **33**(1): p. 1-19.
- [61] Sayre, R.E., *Concentration of Ores by Flotation*, U.S. Patent 1924.
- [62] Laskowski, J. and E.T. Woodburn, *Frothing in Flotation II: Recent Advances in Coal Processing*. Vol. 2. 1998: CRC Press. 336.
- [63] Melo, F. and J.S. Laskowski, *Fundamental properties of flotation frothers and their effect on flotation*. *Minerals Engineering*, 2006. **19**(6-8): p. 766-773.
- [64] Mu, Y., Y. Peng, and R.A. Lauten, *The depression of pyrite in selective flotation by different reagent systems – A Literature review*. *Minerals Engineering*, 2016. **96-97**: p. 143-156.
- [65] Klimpel, R.R. and R.D. Hansen, *Collector compositions for the froth flotation of mineral values*, The Dow Chemical Company. WIPO. WO 87/03222. 1987, Worldwide.
- [66] Bush, J.H., *Flotation process using a mixture of collectors*, The Lubrizol Corporation. WIPO. WO1991019570A1. 1992, Worldwide.

- [67] Nagaraj, D.R., *Dithiocarbamate collectors and their use in the beneficiation of mineral ore bodies*, Cytec Technology Corp. WIPO. WO2008097707A1. 2008, Worldwide.
- [68] Pelton, R. and S. Yang, *Nanoparticle flotation collectors*, McMaster University. WIPO. WO2008097707A1. 2011, Worldwide.
- [69] Fuchs, A.D. and J.C. Tiller, *Contact-Active Antimicrobial Coatings Derived from Aqueous Suspensions*. *Angewandte Chemie International Edition*, 2006. **45**(40): p. 6759-6762.
- [70] Thickett, S.C., C. Neto, and A.T. Harris, *Biomimetic surface coatings for atmospheric water capture prepared by dewetting of polymer films*. *Adv Mater*, 2011. **23**(32): p. 3718-22.
- [71] Pichot, C., T. Taniguchi, T. Delair, and A. Elaissari, *Functionalized thermosensitive latex particles: Useful tools for diagnostics*. *Journal of dispersion science and technology*, 2003. **24**(3-4): p. 423-437.
- [72] Pelton, R., D. Zhang, K.L. Thompson, and S.P. Armes, *Borate binding to polyol-stabilized latex*. *Langmuir*, 2011. **27**(6): p. 2118-23.
- [73] Antonietti, M. and K. Tauer, *90 Years of Polymer Latexes and Heterophase Polymerization: More vital than ever*. *Macromolecular Chemistry and Physics*, 2003. **204**(2): p. 207-219.
- [74] Wang, X., J.E. Hall, S. Warren, J. Krom, J.M. Magistrelli, M. Rackaitis, and G.G.A. Bohm, *Synthesis, Characterization, and Application of Novel Polymeric Nanoparticles*. *Macromolecules*, 2007. **40**(3): p. 499-508.
- [75] Tissot, I., J.P. Reymond, F. Lefebvre, and E. Bourgeat-Lami, *SiOH-Functionalized Polystyrene Latexes. A Step toward the Synthesis of Hollow Silica Nanoparticles*. *Chemistry of Materials*, 2002. **14**(3): p. 1325-1331.
- [76] Haruma, K., *Functional polymer microspheres*. *Progress in Polymer Science*, 2000. **25**(8): p. 1171-1210.
- [77] Goodwin, J.W., R.H. Ottewill, and R. Pelton, *Studies on the preparation and characterization of monodisperse polystyrene latices V.: The preparation of cationic latices*. *Colloid and Polymer Science*, 1979. **257**(1): p. 61-69.
- [78] Goodwin, J.W., R.H. Ottewill, R. Pelton, G. Vianello, and D.E. Yates, *Control of particle size in the formation of polymer latices*. *British Polymer Journal*, 1978. **10**(3): p. 173-180.
- [79] Kelebek, S. and S. Yoruk, *Bubble contact angle variation of sulphide minerals in relation to their self-induced flotation*. *Colloids and Surfaces A: Physicochemical and Engineering Aspects*, 2002. **196**(2-3): p. 111-119.
- [80] Wenzel, R.N., *Resistance of solid surfaces to wetting by water*. *Industrial & Engineering Chemistry*, 1936. **28**(8): p. 988-994.
- [81] Cassie, A.B.D. and S. Baxter, *Wettability of porous surfaces*. *Transactions of the Faraday Society*, 1944. **40**: p. 546.
- [82] Chau, T.T., W.J. Bruckard, P.T.L. Koh, and A.V. Nguyen, *A review of factors that affect contact angle and implications for flotation practice*. *Advances in Colloid and Interface Science*, 2009. **150**(2): p. 106-115.

- [83] Spori, D.M., T. Drobek, S. Zürcher, M. Ochsner, C. Sprecher, A. Mühlebach, and N.D. Spencer, *Beyond the lotus effect: roughness influences on wetting over a wide surface-energy range*. Langmuir, 2008. **24**(10): p. 5411-5417.
- [84] Drelich, J., *Contact angles measured at mineral surfaces covered with adsorbed collector layers*. Minerals and Metallurgical Processing, 2001. **18**(1): p. 31-37.
- [85] Chau, T.T., *A review of techniques for measurement of contact angles and their applicability on mineral surfaces*. Minerals Engineering, 2009. **22**(3): p. 213-219.
- [86] Yang, S. and R. Pelton, *Nanoparticle flotation collectors II: the role of nanoparticle hydrophobicity*. Langmuir, 2011. **27**(18): p. 11409-15.
- [87] Takeshita, N., L.A. Paradis, D. Öner, T.J. McCarthy, and W. Chen, *Simultaneous tailoring of surface topography and chemical structure for controlled wettability*. Langmuir, 2004. **20**(19): p. 8131-8136.
- [88] Hsieh, C.-T., J.-M. Chen, R.-R. Kuo, T.-S. Lin, and C.-F. Wu, *Influence of surface roughness on water-and oil-repellent surfaces coated with nanoparticles*. Applied Surface Science, 2005. **240**(1): p. 318-326.
- [89] Zhang, X., F. Shi, J. Niu, Y. Jiang, and Z. Wang, *Superhydrophobic surfaces: from structural control to functional application*. Journal of Materials Chemistry, 2008. **18**(6): p. 621-633.
- [90] Westcott, S.L., S.J. Oldenburg, T.R. Lee, and N.J. Halas, *Formation and adsorption of clusters of gold nanoparticles onto functionalized silica nanoparticle surfaces*. Langmuir, 1998. **14**(19): p. 5396-5401.
- [91] Tolnai, G., F. Csempezs, M. Kabai-Faix, E. Kálmán, Z. Keresztes, A.L. Kovács, J.J. Ramsden, and Z. Hörvölgyi, *Preparation and Characterization of Surface-Modified Silica-Nanoparticles*. Langmuir, 2001. **17**(9): p. 2683-2687.
- [92] Bala, H., W. Fu, Y. Guo, J. Zhao, Y. Jiang, X. Ding, K. Yu, M. Li, and Z. Wang, *In situ preparation and surface modification of barium sulfate nanoparticles*. Colloids and Surfaces A: Physicochemical and Engineering Aspects, 2006. **274**(1-3): p. 71-76.
- [93] Leppinen, J.O., *FTIR and flotation investigation of the adsorption of ethyl xanthate on activated and non-activated sulfide minerals*. International Journal of Mineral Processing, 1990. **30**(3-4): p. 245-263.
- [94] Song, S., A. Lopez-Valdivieso, J.L. Reyes-Bahena, and C. Lara-Valenzuela, *Floc flotation of galena and sphalerite fines*. Minerals Engineering, 2001. **14**(1): p. 87-98.
- [95] Yang, S., *Nanoparticle Flotation Collectors*, in *Ph.D. Thesis*. 2012, McMaster University: Hamilton, Canada.
- [96] Chan, K., R. Pelton, and J. Zhang, *On the formation of colloidally dispersed phase-separated poly (N-isopropylacrylamide)*. Langmuir, 1999. **15**(11): p. 4018-4020.
- [97] Ninham, B.W., *On progress in forces since the DLVO theory*. Advances in Colloid and Interface Science, 1999. **83**(1-3): p. 1-17.
- [98] Hunter, R.J., *Foundations of colloid science*. 2001: Oxford University Press. 806.
- [99] Hoek, E.M. and G.K. Agarwal, *Extended DLVO interactions between spherical particles and rough surfaces*. J Colloid Interface Sci, 2006. **298**(1): p. 50-8.

- [100] van de Ven, T.G.M., *Colloidal Hydrodynamics*. 1989, London: Academic Press.
- [101] van de Ven, T.G.M. and S.G. Mason, *The microrheology of colloidal dispersions: VIII. Effect of shear on perikinetic doublet formation*. Colloid and Polymer Science, 1977. **255**(8): p. 794-804.
- [102] Vadas, E.B., R.G. Cox, H.L. Goldsmith, and S.G. Mason, *The microrheology of colloidal dispersions II. Brownian diffusion of doublets of spheres*. Journal of Colloid and Interface Science, 1976. **57**(2): p. 308-326.
- [103] van de Ven, T. and S. Mason, *The microrheology of colloidal dispersions VII. Orthokinetic doublet formation of spheres*. Colloid and Polymer Science, 1977. **255**(5): p. 468-479.
- [104] van de Ven, T.G.M. and S.G. Mason, *The microrheology of colloidal dispersions VI. Chains of spheres in shear flow*. Journal of Colloid and Interface Science, 1976. **57**(3): p. 535-546.
- [105] Le Berre, F., G. Chauveteau, and E. Pefferkorn, *Perikinetic and orthokinetic aggregation of hydrated colloids*. Journal of colloid and interface science, 1998. **199**(1): p. 1-12.
- [106] Takamura, K., H.L. Goldsmith, and S.G. Mason, *The microrheology of colloidal dispersions. IX. Effects of simple and polyelectrolytes on rotation of doublets of spheres*. Journal of Colloid and Interface Science, 1979. **72**(3): p. 385-400.
- [107] Takamura, K., H.L. Goldsmith, and S.G. Mason, *The microrheology of colloidal dispersions XII. Trajectories of Orthokinetic Pair-Collisions of Latex Spheres in a Simple Electrolyte*. Journal of Colloid and Interface Science, 1981. **82**(1): p. 175-189.
- [108] Grasso, D., K. Subramaniam, M. Butkus, K. Strevett, and J. Bergendahl, *A review of non-DLVO interactions in environmental colloidal systems*. Reviews in Environmental Science and Biotechnology, 2002. **1**(1): p. 17-38.
- [109] Gillies, G., W. Lin, and M. Borkovec, *Charging and Aggregation of Positively Charged Latex Particles in the Presence of Anionic Polyelectrolytes*. The Journal of Physical Chemistry B, 2007. **111**(29): p. 8626-8633.
- [110] Bouyer, F., A. Robben, W.L. Yu, and M. Borkovec, *Aggregation of Colloidal Particles in the Presence of Oppositely Charged Polyelectrolytes: Effect of Surface Charge Heterogeneities*. Langmuir, 2001. **17**(17): p. 5225-5231.
- [111] Napper, D.H., *Steric stabilization*. Journal of Colloid and Interface Science, 1977. **58**(2): p. 390-407.
- [112] Thompson, K.L., S.P. Armes, D.W. York, and J.A. Burdis, *Synthesis of Sterically-Stabilized Latexes Using Well-Defined Poly(glycerol monomethacrylate) Macromonomers*. Macromolecules, 2010. **43**(5): p. 2169-2177.
- [113] Amalvy, J., G.-F. Unali, Y. Li, S. Granger-Bevan, S. Armes, B. Binks, J. Rodrigues, and C. Whitby, *Synthesis of sterically stabilized polystyrene latex particles using cationic block copolymers and macromonomers and their application as stimulus-responsive particulate emulsifiers for oil-in-water emulsions*. Langmuir, 2004. **20**(11): p. 4345-4354.
- [114] Akpınar, B., L.A. Fielding, V.J. Cunningham, Y. Ning, O.O. Mykhaylyk, P.W. Fowler, and S.P. Armes, *Determining the Effective Density and Stabilizer Layer*

- Thickness of Sterically Stabilized Nanoparticles*. *Macromolecules*, 2016. **49**(14): p. 5160-5171.
- [115] Smith, G.N., S.D. Finlayson, D.A.J. Gillespie, J. Peach, J.C. Pegg, S.E. Rogers, O. Shebanova, A.E. Terry, S.P. Armes, P. Bartlett, and J. Eastoe, *The internal structure of poly(methyl methacrylate) latexes in nonpolar solvents*. *Journal of Colloid and Interface Science*, 2016. **479**: p. 234-243.
- [116] Beal, L. and Y. Chevalier, *Mechanisms involved in the stabilization of latex particles by adsorbed block copolymers in emulsion polymerization process*. *Colloids and Surfaces A: Physicochemical and Engineering Aspects*, 2005. **270–271**: p. 26-32.
- [117] Thompson, K.L., I. Bannister, S.P. Armes, and A.L. Lewis, *Preparation of biocompatible sterically stabilized latexes using well-defined poly(2-(methacryloyloxy)ethyl phosphorylcholine) macromonomers*. *Langmuir*, 2010. **26**(7): p. 4693-702.
- [118] Rixman, M.A., D. Dean, and C. Ortiz, *Nanoscale Intermolecular Interactions between Human Serum Albumin and Low Grafting Density Surfaces of Poly(ethylene oxide)*. *Langmuir*, 2003. **19**(22): p. 9357-9372.
- [119] Chong, J.Y.T., X. Mulet, L.J. Waddington, B.J. Boyd, and C.J. Drummond, *High-Throughput Discovery of Novel Steric Stabilizers for Cubic Lyotropic Liquid Crystal Nanoparticle Dispersions*. *Langmuir*, 2012. **28**(25): p. 9223-9232.
- [120] Fritz, G., V. Schädler, N. Willenbacher, and N.J. Wagner, *Electrosteric stabilization of colloidal dispersions*. *Langmuir*, 2002. **18**(16): p. 6381-6390.
- [121] Ballauff, M., *Spherical polyelectrolyte brushes*. *Progress in Polymer Science*, 2007. **32**(10): p. 1135-1151.
- [122] Ballauff, M. and O. Borisov, *Polyelectrolyte brushes*. *Current Opinion in Colloid & Interface Science*, 2006. **11**(6): p. 316-323.
- [123] Urbina, R.H., *Recent developments and advances in formulations and applications of chemical reagents used in froth flotation*. *Mineral Processing and Extractive Metallurgy Review*, 2003. **24**(2): p. 139-182.
- [124] Senior, G.D., W.J. Trahar, and P.J. Guy, *The selective flotation of pentlandite from a nickel ore*. *International Journal of Mineral Processing*, 1995. **43**(3): p. 209-234.
- [125] Ng, W.S., E. Forbes, G.V. Franks, and L.A. Connal, *Xanthate-Functional Temperature-Responsive Polymers: Effect on Lower Critical Solution Temperature Behavior and Affinity toward Sulfide Surfaces*. *Langmuir*, 2016. **32**(30): p. 7443-7451.
- [126] Ng, W.S., L.A. Connal, E. Forbes, and G.V. Franks, *Xanthate-functional temperature-responsive polymers as selective flocculants and collectors for fines recovery*. *Minerals Engineering*, 2016.
- [127] Marticorena, M.A., G. Hill, A.N. Kerr, D. Liechti, and D.A. Pelland, *INCO develops new pyrrhotite depressant*. *Innovations in Mineral Processing*, 1994. **3**: p. 15-33.

- [128] Ma, X., Y. Hu, H. Zhong, S. Wang, G. Liu, and G. Zhao, *A novel surfactant S-benzoyl-N,N-diethyldithiocarbamate synthesis and its flotation performance to galena*. Applied Surface Science, 2016. **365**: p. 342-351.
- [129] Liu, Z. and F.M. Doyle, *Ion flotation of Co<sup>2+</sup>, Ni<sup>2+</sup>, and Cu<sup>2+</sup> using dodecyldiethylenetriamine (Ddien)*. Langmuir, 2009. **25**(16): p. 8927-34.
- [130] Ackerman, P., G. Harris, R. Klimpel, and F. Aplan, *Use of chelating agents as collectors in the flotation of copper sulfides and pyrite*. Minerals & metallurgical processing, 1999. **16**(1): p. 27-35.
- [131] Khalek, M.A., *Separation of dolomite from phosphate minerals by flotation with a new amphoteric surfactant as collector*. Mineral Processing and Extractive Metallurgy, 2001. **110**(2): p. 89-93.
- [132] Saitoh, T., F. Satoh, and M. Hiraide, *Concentration of heavy metal ions in water using thermoresponsive chelating polymer*. Talanta, 2003. **61**(6): p. 811-817.
- [133] Yang, S., C. Abarca, Z. Dai, M. Xu, and R.H. Pelton. *Nanoparticle Flotation Aids For Pentlandite Fines*. in *Proceedings of the 47th Annual Canadian Mineral Processors Conference*. 2015. Ottawa.
- [134] Kusuma, A.M., *Impact of the Fine Minerals Particles on Pentlandite Flotation*. 2014, University of Alberta.
- [135] Shahbazi, B., B. Rezai, and S.M. Javad Koleini, *Bubble-particle collision and attachment probability on fine particles flotation*. Chemical Engineering and Processing: Process Intensification, 2010. **49**(6): p. 622-627.
- [136] Nguyen, A.V., C.M. Phan, and G.M. Evans, *Effect of the bubble size on the dynamic adsorption of frothers and collectors in flotation*. International Journal of Mineral Processing, 2006. **79**(1): p. 18-26.
- [137] Merve Genc, A., I. Kilickaplan, and J.S. Laskowski, *Effect of pulp rheology on flotation of nickel sulphide ore with fibrous gangue particles*. Canadian Metallurgical Quarterly, 2012. **51**(4): p. 368-375.
- [138] Yang, S., R.H. Pelton, M. Montgomery, and Y. Cui, *Nanoparticle flotation collectors III: the role of nanoparticle diameter*. ACS Appl Mater Interfaces, 2012. **4**(9): p. 4882-90.
- [139] Dong, X., H.S. Marway, E.D. Cranston, and R.H. Pelton, *Relating Nanoparticle Shape and Adhesiveness to Performance as Flotation Collectors*. Industrial & Engineering Chemistry Research, 2016. **55**(36): p. 9633-9638.
- [140] Yang, S., R.H. Pelton, B.B. Razavizadeh, and G. Bruin, *Nanoparticle flotation collectors - the influence of particle softness*. ACS Appl Mater Interfaces, 2013. **5**(11): p. 4836-42.
- [141] Chisholm, B.J., S.J. Stafslie, D.A. Christianson, C. Gallagher-Lein, J.W. Daniels, C. Rafferty, L.V. Wal, and D.C. Webster, *Combinatorial materials research applied to the development of new surface coatings*. Applied Surface Science, 2007. **254**(3): p. 692-698.
- [142] Banerjee, I., R.C. Pangule, and R.S. Kane, *Antifouling coatings: recent developments in the design of surfaces that prevent fouling by proteins, bacteria, and marine organisms*. Adv Mater, 2011. **23**(6): p. 690-718.



- [143] Collins, K.D., T. Gensch, and F. Glorius, *Contemporary screening approaches to reaction discovery and development*. Nat Chem, 2014. **6**(10): p. 859-71.
- [144] Macarron, R., M.N. Banks, D. Bojanic, D.J. Burns, D.A. Cirovic, T. Garyantes, D.V.S. Green, R.P. Hertzberg, W.P. Janzen, J.W. Paslay, U. Schopfer, and G.S. Sittampalam, *Impact of high-throughput screening in biomedical research*. Nat Rev Drug Discov, 2011. **10**(3): p. 188-195.
- [145] Bleicher, K.H., H.-J. Bohm, K. Muller, and A.I. Alanine, *Hit and lead generation: beyond high-throughput screening*. Nat Rev Drug Discov, 2003. **2**(5): p. 369-378.
- [146] Pyzer-Knapp, E.O., C. Suh, R. Gómez-Bombarelli, J. Aguilera-Iparraguirre, and A. Aspuru-Guzik, *What Is High-Throughput Virtual Screening? A Perspective from Organic Materials Discovery*. Annual Review of Materials Research, 2015. **45**(1): p. 195-216.
- [147] Maier, W.F., K. Stowe, and S. Sieg, *Combinatorial and high-throughput materials science*. Angew Chem Int Ed Engl, 2007. **46**(32): p. 6016-67.
- [148] Capelle, M.A., R. Gurny, and T. Arvinte, *High throughput screening of protein formulation stability: practical considerations*. Eur J Pharm Biopharm, 2007. **65**(2): p. 131-48.
- [149] Meier, M.A.R., R. Hoogenboom, and U.S. Schubert, *Combinatorial Methods, Automated Synthesis and High-Throughput Screening in Polymer Research: The Evolution Continues*. Macromolecular Rapid Communications, 2004. **25**(1): p. 21-33.
- [150] Chisholm, B.J. and D.C. Webster, *The development of coatings using combinatorial/high throughput methods: a review of the current status*. Journal of Coatings Technology and Research, 2007. **4**(1): p. 1-12.
- [151] Meredith, J., *A current perspective on high-throughput polymer science*. Journal of materials science, 2003. **38**(22): p. 4427-4437.
- [152] Hoogenboom, R., M.A. Meier, and U.S. Schubert, *Combinatorial Methods, Automated Synthesis and High-Throughput Screening in Polymer Research: Past and Present*. Macromolecular rapid communications, 2003. **24**(1): p. 15-32.
- [153] Martín-Esteban, A., *Molecularly-imprinted polymers as a versatile, highly selective tool in sample preparation*. TrAC Trends in Analytical Chemistry, 2013. **45**: p. 169-181.
- [154] Hook, A.L., C.Y. Chang, J. Yang, D.J. Scurr, R. Langer, D.G. Anderson, S. Atkinson, P. Williams, M.C. Davies, and M.R. Alexander, *Polymer microarrays for high throughput discovery of biomaterials*. J Vis Exp, 2012(59): p. e3636.
- [155] Briehn, C.A., M.-S. Schiedel, E.M. Bonsen, W. Schuhmann, and P. Bäuerle, *Single-Compound Libraries of Organic Materials: From the Combinatorial Synthesis of Conjugated Oligomers to Structure–Property Relationships*. Angewandte Chemie International Edition, 2001. **40**(24): p. 4680-4683.
- [156] Nandivada, H., X. Jiang, and J. Lahann, *Click Chemistry: Versatility and Control in the Hands of Materials Scientists*. Advanced Materials, 2007. **19**(17): p. 2197-2208.

- [157] Berg, R. and B.F. Straub, *Advancements in the mechanistic understanding of the copper-catalyzed azide-alkyne cycloaddition*. Beilstein J Org Chem, 2013. **9**: p. 2715-50.
- [158] Kantheti, S., R. Narayan, and K.V.S.N. Raju, *The impact of 1,2,3-triazoles in the design of functional coatings*. RSC Adv., 2015. **5**(5): p. 3687-3708.
- [159] Kolb, H.C., M. Finn, and K.B. Sharpless, *Click chemistry: diverse chemical function from a few good reactions*. Angewandte Chemie International Edition, 2001. **40**(11): p. 2004-2021.
- [160] Thirumurugan, P., D. Matosiuk, and K. Jozwiak, *Click chemistry for drug development and diverse chemical–biology applications*. Chemical reviews, 2013. **113**(7): p. 4905-4979.
- [161] Tornøe, C.W., C. Christensen, and M. Meldal, *Peptidotriazoles on solid phase:[1, 2, 3]-triazoles by regioselective copper (I)-catalyzed 1, 3-dipolar cycloadditions of terminal alkynes to azides*. The Journal of organic chemistry, 2002. **67**(9): p. 3057-3064.
- [162] Meldal, M. and C.W. Tornøe, *Cu-Catalyzed Azide–Alkyne Cycloaddition*. Chemical Reviews, 2008. **108**(8): p. 2952-3015.
- [163] Moses, J.E. and A.D. Moorhouse, *The growing applications of click chemistry*. Chem Soc Rev, 2007. **36**(8): p. 1249-62.
- [164] Fournier, D., R. Hoogenboom, and U.S. Schubert, *Clicking polymers: a straightforward approach to novel macromolecular architectures*. Chem Soc Rev, 2007. **36**(8): p. 1369-80.
- [165] Pérez, P., L.R. Domingo, M. José Aurell, and R. Contreras, *Quantitative characterization of the global electrophilicity pattern of some reagents involved in 1,3-dipolar cycloaddition reactions*. Tetrahedron, 2003. **59**(17): p. 3117-3125.
- [166] Worrell, B., J. Malik, and V. Fokin, *Direct evidence of a dinuclear copper intermediate in Cu (I)-catalyzed azide-alkyne cycloadditions*. Science, 2013. **340**(6131): p. 457-460.
- [167] Halford, B., *Doubts About Unclick Reaction*, in *Chemical and Engineering News*. 2014, American Chemical Society: Washington.
- [168] Sapsford, K.E., W.R. Algar, L. Berti, K.B. Gemmill, B.J. Casey, E. Oh, M.H. Stewart, and I.L. Medintz, *Functionalizing nanoparticles with biological molecules: developing chemistries that facilitate nanotechnology*. Chem Rev, 2013. **113**(3): p. 1904-2074.
- [169] Yang, H. and T.G.M. van de Ven, *A Bottom-up Route to a Chemically End-to-End Assembly of Nanocellulose Fibers*. Biomacromolecules, 2016. **17**(6): p. 2240-2247.
- [170] Mansfeld, U., C. Pietsch, R. Hoogenboom, C.R. Becer, and U.S. Schubert, *Clickable initiators, monomers and polymers in controlled radical polymerizations – a prospective combination in polymer science*. Polymer Chemistry, 2010. **1**(10): p. 1560.
- [171] Schweinfurth, D., C.Y. Su, S.C. Wei, P. Braunstein, and B. Sarkar, *Nickel complexes with "click"-derived pyridyl-triazole ligands: weak intermolecular*

- interactions and catalytic ethylene oligomerisation*. Dalton Trans, 2012. **41**(41): p. 12984-90.
- [172] Douthwaite, R.E., D. Häüssinger, M.L. Green, P.J. Silcock, P.T. Gomes, A.M. Martins, and A.A. Danopoulos, *Cationic nickel (II) complexes of chelating N-heterocyclic carbenes*. Organometallics, 1999. **18**(22): p. 4584-4590.
- [173] Török, I., P. Surdy, A. Rockenbauer, L. Korecz Jr, G.J. Anthony A. Koolhaas, and T. Gajda, *Nickel(II)-, copper(II)- and zinc(II)-complexes of some substituted imidazole ligands*. Journal of Inorganic Biochemistry, 1998. **71**(1–2): p. 7-14.
- [174] Abarca, C., S. Yang, and R.H. Pelton, *Towards high throughput screening of nanoparticle flotation collectors*. Journal of colloid and interface science, 2015. **460**: p. 97-104.
- [175] Abarca, C., M.M. Ali, S. Yang, X. Dong, and R.H. Pelton, *A Colloidal Stability Assay Suitable for High-Throughput Screening*. Analytical Chemistry, 2016. **88**(5): p. 2929-2936.
- [176] Abarca, C., M.M. Ali, D. Bowie, and R.H. Pelton, *A simple assay for azide surface groups on clickable polymeric nanoparticles*. Colloids and Surfaces A: Physicochemical and Engineering Aspects, 2016. **508**: p. 192-196.

## **Chapter 2: Towards High Throughput Screening of Nanoparticle Flotation Collectors**

---

In Chapter 2, most of the project design, experiments and data analysis were performed by me. Dr. Songtao Yang provided assistance with scanning electron microscopy, flotations and useful discussions about the project. Patrick Morkus and Gerard Bruin (undergraduate students) aided with some polymerizations and contact angle measurements. Dr. Robert Pelton provided much useful discussion about project design, experiments and data analysis.

The manuscript was initially drafted by myself, proofread by Dr. Yang and Andres Krisch, and edited to the final version by Dr. Robert Pelton. This chapter has been published in the *Journal of Colloid and Interface Science*, 460 (2015) pp. 97–104. DOI: [10.1016/j.jcis.2015.08.052](https://doi.org/10.1016/j.jcis.2015.08.052) Permission from © Elsevier Inc. All rights reserved.



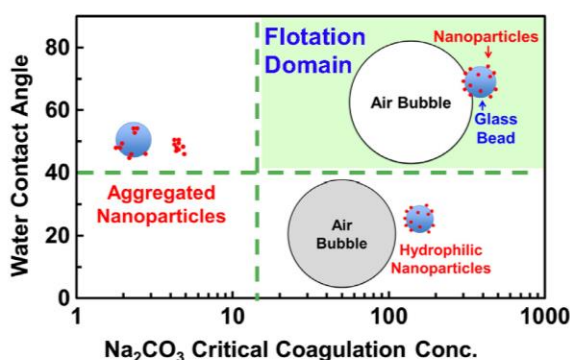
## Towards high throughput screening of nanoparticle flotation collectors



Carla Abarca, Songtao Yang, Robert H. Pelton\*

Department of Chemical Engineering, McMaster University, Hamilton, Ontario L8S 4L8, Canada

## GRAPHICAL ABSTRACT



## ARTICLE INFO

*Article history:*  
Received 2 July 2015  
Revised 16 August 2015  
Accepted 22 August 2015  
Available online 24 August 2015

*Keywords:*  
Froth flotation  
Flotation collectors  
Flotation  
Colloidal stability  
Nanoparticle hydrophobicity  
Latex synthesis

## ABSTRACT

To function as flotation collectors for mineral processing, polymeric nanoparticles require a delicate balance of surface properties to give mineral-specific deposition and colloidal stability in high ionic strength alkaline media, while remaining sufficiently hydrophobic to promote flotation. Combinatorial nanoparticle surface modification, in conjunction with high throughput screening, is a promising approach for nanoparticle development. However, efficient automated screening assays are required to reject ineffective particles without having to undergo time consuming flotation testing. Herein we demonstrate that determining critical coagulation concentrations of sodium carbonate in combination with measuring the advancing water contact angle of nanoparticle-saturated glass surfaces can be used to screen ineffective nanoparticles. Finally, none of our first nanoparticle library based on poly(ethylene glycol) methyl ether methacrylate (PEG-methacrylate) were effective flotation collectors because the nanoparticles were too hydrophilic.

© 2015 Elsevier Inc. All rights reserved.

## 1. Introduction

Froth flotation is one of the cornerstones of most mineral processing operations because flotation can efficiently isolate valuable mineral particles diluted in large quantities of unwanted gangue materials [1]. A critical step in flotation is the selective adsorption

of hydrophobic collectors onto the surfaces of mineral particles to facilitate particle attachment to air bubbles. Although most conventional collector chemicals are very low molecular weight surfactants, over the last few years we have shown that it is possible, and sometime advantageous, to replace conventional collectors with hydrophobic nanoparticles [2–6]. Our work follows the established use of calcium soap colloidal particles generated *in situ* in flotation deinking [7] and sulfide flotation. There are three fundamental requirements for nanoparticle flotation collectors: (1)

\* Corresponding author.

E-mail address: [peltonrh@mcmaster.ca](mailto:peltonrh@mcmaster.ca) (R.H. Pelton).

the nanoparticles must be colloidally stable in the flotation medium; (2) the nanoparticles must be sufficiently hydrophobic to promote the attachment of mineral particles to air bubbles; and, (3) the nanoparticles must bear surface functionalities that promote selective deposition only onto the desired minerals surfaces. These requirements are contradictory – functional groups that increase colloidal stability will invariably decrease hydrophobicity. Similarly, chelating groups and other mineral specific surface groups will reduce nanoparticle hydrophobicity. Summarized herein are results of a study with two goals. First, we wanted to develop simple assays that could be used for high throughput screening of potential nanoparticle flotation collectors. Second, we wanted to evaluate macromonomers based poly(ethylene glycol) methyl ether methacrylate as a route to increase nanoparticle colloidal stability.

Although our ultimate goal is the development of flotation collectors for pentlandite (nickel sulfide mineral) ores, much of our initial information was obtained from the flotation of glass beads with cationic polystyrene latex particles. Key findings included: surfactant-free cationic polystyrene latex will promote glass bead flotation [2], however, such particles are too colloidally unstable function in the ionic strengths typical of commercial flotation; [8] nanoparticle coverages on the mineral particle surfaces as low as 5–10% can perform well; [2] generally smaller ~50 nm diameter particles are superior to larger >100 nm particles; [4] and, softer copolymers perform better than hard polystyrene [3]. In subsequent work with ore flotation, we demonstrated that the copolymerization of imidazole surface functional groups can promote selective nanoparticle deposition onto nickel sulfide rich surfaces [8].

In spite of much success, we have struggled to optimize nanoparticle surface chemistry because of the broad design space for polymeric nanoparticles. If there exists a domain in the property space where hydrophobicity, colloidal stability and deposition specificity are all appropriate, we are unlikely to discover it by tedious large-scale polymerization, latex characterization and flotation evaluation protocols. Instead we are designing combinatorial synthesis approaches to generate a large nanoparticle library which we plan to interrogate for potentially useful nanoparticles by screening based on two properties: (1) the nanoparticle critical coagulation concentration in sodium carbonate solution; and, (2) the water contact angle on a hydrophilic glass surface saturated with adsorbed nanoparticles. In previous work, we have shown that the advancing water contact angle should be greater than 40° for good flotation performance [6]. In future reports, we will describe the nanoparticle library development and subsequent

screening. In this paper we present the validation of our screening assay based on contact angle and colloidal stability measurements. In addition, we assess the utility of poly(ethylene glycol) methyl ether methacrylate surface functional groups as agents to increase colloidal stability.

## 2. Experimental

### 2.1. Materials

Unless stated otherwise, all chemicals and supplies were purchased from Sigma Aldrich. Styrene (99%) with <15 ppm of 4-tert-butylcatechol as inhibitor, was purified using inhibitor-removing preppacked columns. 1-vinylimidazole (99%), three macromonomer derivatives, poly(ethylene glycol) methyl ether methacrylate (PEG-methacrylate) average molecular weight, Mn: 300 Da (<100%), 950 Da (<100%) and 2000 Da (50 wt.% in H<sub>2</sub>O), and 2,2'-azobis(2-methylpropionamide) dihydrochloride (V50) were used as supplied. A mixture of dipropylene glycol monomethyl ether and monomethyl polypropylene glycol (250 Da), commercially called UNIFROTH 250C (99%) was provided by VALE Canada (Mississauga, ON) and was used as a frother in the experiments. Glass beads with a nominal diameter of 30–50 μm were purchased from Polysciences Inc. The particle size distribution of the beads was measured, and is given in the [Supporting Materials file](#). The corresponding surface area mean diameter is  $d_{32} = 43 \mu\text{m}$ , and the specific surface area  $\sigma = 0.056 \text{ m}^2/\text{g}$ .

### 2.2. Emulsion polymerization

Experiments were conducted in a 250 mL three-neck round-bottom flask connected to a condenser, under a nitrogen stream. The temperature (70 °C) and stirring (750 RPM) were controlled using a hot plate/magnetic stirrer (RCT IKAMAG, IKA-Werke GmbH & Co. KG) equipped with an IKA ETS-D5 temperature controller. For P2000-4, 95 mL of water was added to the reactor and purged with a nitrogen stream for 30 min at 70 °C followed with 0.5 mL of styrene, and 2 mL of 50 wt.% 2000 Da PEG-methacrylate macromonomer. After 10 min 0.1 g of V50 initiator dissolved in 5 mL of water was added to start polymerization. The rest of the styrene (4.5 mL) and 0.25 mL 1-vinylimidazole were added in a monomer-starved semi-batch configuration with a monomer addition rate of 1 mL/h, using a 10 mL syringe fitted to a syringe pump (NE-1600, New Era Pump System Inc.). The chemical compositions of the latexes are shown in [Table 1](#). After polymerization, the latexes were dialyzed for at least 7 days in semi-permeable mem-

**Table 1**  
Nanoparticle recipes and PEG contents, measured by NMR. The surface density of PEG chains was estimated assuming all PEG chains were at the polymer/water interface.

Nanoparticle designation	Batch			Semi-batch		Solids content, mg/mL	PEG/styrene, wt/wt	PEG surface density, $\sigma$ , mg/m <sup>2</sup>	Reduced grafting density index, $\Sigma$
	St (g)	V50 (g)	PEGMA (g)	St (g)	VI (g)				
P300-1	0.5	0.1	0.1	4.5	0.13	39.7	0.01	0.21	0.25
P300-2	0.5	0.1	0.25	4.5	0.13	46.0	0.03	0.98	1.17
P300-3	0.5	0.1	0.5	4.5	0.13	50.5	0.07	1.96	2.35
P300-4	0.5	0.1	1	4.5	0.13	41.1	0.15	4.23	5.06
P950-1	0.5	0.1	0.1	4.5	0.13	38.5	0.01	0.37	0.74
P950-2	0.5	0.1	0.25	4.5	0.13	40.4	0.02	0.75	1.52
P950-3	0.5	0.1	0.5	4.5	0.13	39.3	0.05	0.96	1.94
P950-4	0.5	0.1	1	4.5	0.13	38.4	0.17	2.01	4.07
P2000-1	0.5	0.1	0.1	4.5	0.13	34.2	0.02	0.95	2.33
P2000-2	0.5	0.1	0.25	4.5	0.13	34.8	0.04	1.40	3.42
P2000-3	0.5	0.1	0.5	4.5	0.13	32.7	0.07	2.14	5.24
P2000-4	0.5	0.1	1	4.5	0.13	24.9	0.26	6.12	14.9
PS-62 <sup>a</sup>	0.5	0.1	0	4.5	0	43.3	/	/	/
PSVI-52 <sup>a</sup>	0.5	0.1	0	4.5	0.13	30.0	/	/	/
PSVI-75 <sup>a</sup>	0.5	0.1	0	4.5	0.38	32.1	/	/	/

<sup>a</sup> Preparations used 0.1 g CTAB as a surfactant to achieve small nanoparticles.

brane tubing (MWCO 14000 Da) to remove any unreacted material. Latex concentrations were determined gravimetrically. 1 mL of cleaned latex was placed in a 5 mL glass vial and heated to 110 °C to remove water, until no mass change was recorded.

### 2.3. Nuclear magnetic resonance

<sup>1</sup>H NMR, <sup>13</sup>C NMR, 2D-HSQC and 2D-HMBC were obtained in all the samples to calculate the final concentration of polyethylene glycol residues in the final nanoparticles. In a typical experiment, a measured amount between 10 and 15 mg of dry sample was dissolved in 1 mL of deuterated chloroform, CDCl<sub>3</sub>, and measured in a 600 MHz NMR spectrophotometer at 25 °C. Example spectra are shown in the Supporting Materials file.

### 2.4. Scanning electron microscopy

Photographs of the nanoparticles deposited on glass beads with a nominal diameter of 30–50 μm, were acquired by a JEOL JSM-7000F SEM equipped with a Schottky Field Emission Gun (FEG) filament with an accelerating voltage of 2.8 keV. Before starting the experiment, the edges of the samples were coated with silver coating and dried at 50 °C for 45 min. The samples were then sputter coated under vacuum with a thin layer of 5 nm of platinum. The SEM photographs were digitized using JEOL image processing software.

### 2.5. Hydrodynamic diameter

Dynamic Light Scattering measurements were conducted with a Zetasizer Nano ZS (Malvern Instruments) equipped with a He–Ne laser (633 nm), a non-invasive backscattering detector positioned at a scattering angle of 173°, and a temperature controlled jacket. Nanoparticle dispersions, 0.01 mg/mL in 5 mM NaCl at neutral pH with conductivities ~0.4 mS/cm, were measured in triplicate using polystyrene cuvettes at 20 °C. Diameters were calculated with the method of cumulants and the results are summarized in Table 2.

### 2.6. Electrophoretic mobility

Dispersions of nanoparticles in 5 mM NaCl (0.01 mg/mL) were measured in a Zetasizer Nano ZS (Malvern Instruments) equipped with a He–Ne laser (633 nm) and an electrode-dip cell, using a

multi frequency phase analysis light scattering technique (M3-PALS) at 20 °C, pH ~7 and conductivity ~0.4 mS/cm. Measurements were repeated 3 times, in which the electrophoretic mobilities of the nanoparticles were measured. The obtained values and standard error are displayed in Table 2.

### 2.7. Critical coagulation concentration (CCC)

The colloidal stability of nanoparticle dispersions was determined by measuring their relative turbidity in 3 mL cuvettes. In a typical experiment, each cuvette was filled with combinations of sodium carbonate stock solutions (50 mM, 250 mM, or 1000 mM) and water to give final Na<sub>2</sub>CO<sub>3</sub> concentrations between 0 and 1000 mM. After agitation in a mini vortex mixer (VWR VM3000) at 500 RPM for 30 s, sufficient 5 g/L nanoparticle dispersion required to give an initial maximum absorbance of 0.3 UA (or 50% transmittance) at 550 nm measured by a UV–vis spectrophotometer (Beckman Coulter, DU800) giving a total volume of 2 mL. The final dispersion was vortexed at 500 RPM for 60 s. Absorbance values at 550 nm were recorded after 5 min and 24 h. A nanoparticle suspension in electrolyte was considered to be coagulated if the ratio was either  $A_s/A_c > 1.3$  or  $A_s/A_c < 0.75$  where  $A_s$  is the suspension absorbance, and  $A_c$  is the suspension absorbance without salt.

### 2.8. Advancing water contact angle

Contact angle measurements were performed with a OCA 35 DataPhysics Instruments GmbH contact angle apparatus, equipped with a motorized stage. In a typical experiment, glass microscope slides (75 mm × 25 mm, VWR) were cut into 10 mm<sup>2</sup> squares, cleaned with Hellmanex III (Hellma GmbH & Co. KG) and immersed in nanoparticle suspensions with a concentration of 0.5 mg/mL in 5 mM NaCl up to 30 min. The treated glass slides were rinsed in 1000 mL of water to remove unbound nanoparticles. Sessile drop water/air contact angle measurements were performed on dry, latex-treated glass slides. The contact angle results were calculated with ellipse fitting settings in the drop shape analysis software (SCA202 4.3.19, DataPhysics Instruments GmbH).

### 2.9. Quartz crystal microbalance with dissipation measurements (QCM-D)

The measurement of the deposition of selected nanoparticles onto silica coated sensors was performed using a QCM-D

**Table 2**  
Nanoparticle properties and activities as glass bead flotation collectors.

Nanoparticle designation	Diameter, <sup>a</sup> nm (PDI)	Electrophoretic mobility, $\times 10^{-8} \text{ m}^2 \text{ s}^{-1} \text{ V}^{-1}$ (std error)		CCC in sodium carbonate, mM	Water contact angle, $\theta$ (std error)	Glass beads flotation recovery, % (std error)	Liquid recovery, % (std error)
		NaCl <sup>a</sup>	Na <sub>2</sub> CO <sub>3</sub> <sup>a</sup>				
P300-1	202 (0.07)	2.96	-0.15 (±0.07)	2.5	43.5 (±1.3)	22.3 (±1.9)	41.5 (±0.5)
P300-2	173 (0.02)	2.84	0.30 (±0.21)	5	36.0 (±0.8)	19.1 (±1.4)	40.2 (±0.1)
P300-3	160 (0.12)	1.43	0.17 (±0.08)	7.5	35.0 (±1.0)	17.6 (±1.6)	39.0 (±0.9)
P300-4	158 (0.16)	1.15	0.03 (±0.06)	140	33.0 (±1.1)	24.3 (±1.6)	37.3 (±0.6)
P950-1	227 (0.10)	3.04	-0.39 (±0.11)	5	41.2 (±1.3)	27.2 (±1.1)	40.5 (±0.3)
P950-2	187 (0.01)	2.32	-0.16 (±0.04)	12.5	34.5 (±0.9)	25.4 (±1.1)	37.0 (±0.9)
P950-3	105 (0.05)	1.73	0.32 (±0.10)	310	33.1 (±1.2)	22.1 (±1.9)	35.0 (±0.2)
P950-4	69 (0.05)	0.68	-0.33 (±0.19)	470	30.0 (±1.4)	36.1 (±1.6)	34.1 (±0.3)
P2000-1	245 (0.03)	2.35	0.03 (±0.12)	15	29.7 (±1.2)	24.5 (±1.1)	40.5 (±0.3)
P2000-2	223 (0.01)	1.29	-0.02 (±0.02)	200	24.0 (±1.4)	18.9 (±2.1)	38.8 (±0.7)
P2000-3	175 (0.01)	1.13	0.02 (±0.11)	320	21.2 (±1.1)	16.7 (±1.1)	35.9 (±0.5)
P2000-4	137 (0.04)	0.93	-0.05 (±0.09)	450	19.7 (±1.0)	53.4 (±2.9)	47.1 (±1.3)
PS-62	62 (0.01)	3.33	1.91 (±0.08)	8	71.2 (±1.1)	81.1 (±1.5)	31.1 (±0.7)
PSVI-52	56 (0.04)	2.93	-0.05 (±0.08)	4	61.0 (±1.4)	65.9 (±2.3)	33.4 (±1.2)
PSVI-75	76 (0.02)	3.10	1.80 (±0.04)	12.5	62.0 (±0.8)	54.8 (±1.0)	32.6 (±2.1)

<sup>a</sup> Measured in 5 mM NaCl or 5 mM Na<sub>2</sub>CO<sub>3</sub>.



(E4 model from Q-Sense, Sweden). In a typical experiment, a new SiO<sub>2</sub> sensor was cleaned by UV–ozone treatment for 10 min, and the QCM-D baseline was stabilized in 5 mM Na<sub>2</sub>CO<sub>3</sub> for about 30 min. A nanoparticle dispersion of concentration 100 mg/L in 5 mM Na<sub>2</sub>CO<sub>3</sub> was injected into the QCM-D module with a flow speed of 100 µL/min at 25 °C. After 3–4 h, the experiment was stopped and air was injected into the QCM-D module to dry the sensor. The resulting sensor surfaces were imaged by SEM to show the nature of the surfaces after nanoparticle deposition.

#### 2.10. Flotation of glass beads in sodium carbonate

Laboratory scale flotation of glass beads was performed in the presence of 5 mM of sodium carbonate at pH ~9–10. In a typical experiment, 100 ppm of a nanoparticle suspension was mixed with 2 g of glass beads in 120 mL solution of 5 mM sodium carbonate in a 150 mL plastic beaker, placed on a 90 mm diameter plastic petri dish, on top of a magnetic stirring plate (Cimarec, Thermo Scientific). The bead and latex mixture was stirred for 5 min using a 25 × 25 mm cross-shape stirring bar at approximately 600 rpm, to allow deposition of nanoparticles onto the glass beads. Next, 10 ppm of frother (0.12 mL of 1% Unifroth 250C) was added and stirred for 30 s. Flotation was started by passing nitrogen controlled by a flow controller (1355-EDA-7BLC1A, Brooks Instruments) at a rate of 2.0 L/min through a Corning Pyrex gas dispersion tube with a 30 mm coarse fritted disc at a 90° elbow (11-137E, Fisher Scientific). During the flotation experiment, the stirring rate was increased to 900 rpm to avoid sedimentation of the glass beads. The froth layer formed in the surface was collected in the plastic petri dish positioned beneath the plastic beaker. After 30 s, the contents of the petri dish were weighed, and filtered with a vacuum Büchner ceramic funnel supporting Whatman #1 filter paper. The quantity of dry collected beads was determined gravimetrically.

#### 2.11. Pentlandite ore flotation

Industrial laboratory flotation tests using pentlandite ore were performed at the Vale laboratory in Mississauga, Ontario. In a typical experiment 1.0 kg of ultramafic nickel ore, crushed at 6-mesh, was mixed with a simulated process water (fabricated with sodium carbonate at pH 10.1 in tap water) and ground in a laboratory rod mill where the grind size was 80% passing 106 µm. The ground slurry was then exposed to a desliming process employing a Mozley 1-in. hydrocyclone. The flotation feed coming from the hydrocyclone was placed into a 4.2 L Denver flotation cell and topped up with simulated process water. Incremental flotation procedure was performed according to Vale's standard, obtaining eight incremental concentrates collected at 2 min flotation per concentrate. In the conditioning step, the pH was adjusted with sodium carbonate to 9.8–10.1 (desired range for pentlandite flotation). Subsequently, the nanoparticle collector was added and stirred for 5 min before each incremental flotation, and 10 ppm of frother (Unifroth 250C) was added 30 s before starting each incremental flotation. The nickel and magnesium oxide content for each collected sample was measured with a Varian Vista inductively coupled plasma–optical emission spectrophotometer (ICP–OES). For each sample, approximately 0.25 g of sample was placed into a zirconium crucible containing 3.4 g of sodium peroxide and 2–3 pellets of sodium hydroxide. The sample was mixed and the crucible was then inserted in a muffle furnace at 710 °C for 35 min. The resulting cake was leached with a hydrochloric acid–water solution. The solution was then diluted to a 250 mL volume and measured directly on the ICP–OES.

### 3. Results

#### 3.1. The nanoparticles

A series of cationic polystyrene latexes was prepared by semi-batch emulsion polymerization – the recipes are shown in Table 1. The molecular weight and concentrations of PEG macromonomers were the main variables in this series. The particle surface groups included amidine from the initiator, PEG groups from the macromonomer, and imidazole groups from the second stage polymerization. Proton NMR was used to measure the total PEG content – see examples in the supporting information (SI). The corresponding surface density values ( $\sigma$  mg/m<sup>2</sup>) in Table 1 were estimated by assuming that all of the PEG chains were present on the particle surface. The final column in Table 1 shows the corresponding values of Brittain's reduced grafting density parameter,  $\Sigma$ , defined as the number of grafted chains divided by the projected coil area for the equivalent untethered polymer in solution. Values above 5 correspond to surface brushes, whereas values below 1 describe grafted chains in the mushroom configuration.

Table 2 summarizes some properties of the nanoparticles and their efficacy as glass bead flotation collectors. We now link these properties to the ability of the nanoparticles to function as flotation collectors.

#### 3.2. Nanoparticle adsorption onto silica and glass

To function as flotation collectors, the nanoparticles must spontaneously adsorb onto the target mineral particles. For our mechanistic studies, the targets were glass beads. The nanoparticles were positively charged, whereas glass is negative, suggesting an electrostatic driving force. However, the flotation experiments were performed in 5 mM sodium carbonate at pH ~10. The electrophoresis results, summarized in Table 2, reveal that under these conditions the mobilities had very low positive or negative values. Only PS-62, the polystyrene latex with no PEG surface groups and PSVI-75, nanoparticle with high amount of imidazole surface groups, had mobilities greater than 1 in the carbonate solution. The low electrophoretic mobilities are due to both the high ionic strength and low degree of ionization of amidine [9] (from the initiator) and imidazole groups at pH 10. With the attenuation of the electrostatic driving force for deposition in 5 mM sodium carbonate, we were concerned that the nanoparticles might not adsorb onto the glass beads. Most of our previous work with glass bead flotation was performed in low ionic strength NaCl.

In spite of our concerns, SEM examination of glass beads collected in flotation experiments showed the presence of adsorbed nanoparticles. For example, Fig. 1 shows SEMs of collected glass beads floated with P2000-4, the most hydrophilic nanoparticles, and with P300-1, the most hydrophobic PEG-containing nanoparticles. In both cases there were sufficient deposited nanoparticles to promote flotation. The micrographs reveal some other details. P300-1 was present as aggregates, indicating limited colloidal stability whereas the P2000-4 micrographs showed no aggregates. Most of the P2000-4 particles were present as zones of ordered particles. These patterns typically occur when surface tension forces drag the particles together during drying. These structures are indicative of uniform particle size and low particle/glass adhesion forces.

Nanoparticle adsorption onto silica surfaces was followed by quartz crystal microbalance (QCM-D) measurements in flow. The results are summarized in Fig. 2, and SEM images of the sensor surfaces, after nanoparticle adsorption are shown in Supporting Materials Fig. S8. The simple cationic polystyrene latex, PS-62, rapidly adsorbed to give a high coverage with little aggregation. The PEG



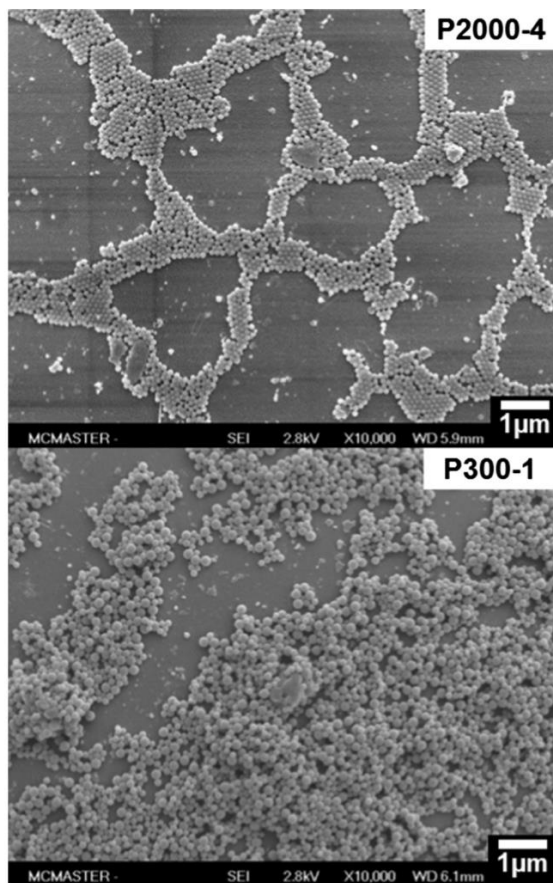


**Fig. 1.** SEM micrographs of glass bead surfaces collected from the froth flotation experiments in 5 mM of  $\text{Na}_2\text{CO}_3$  with P2000-4 and with P300-1 nanoparticles. The P300-1 sample appears to be partially aggregated.

coated P2000-4 particles gave a much lower coverage with no aggregation. The P2000-4 SEMs for the QCM-D sensor look very similar to the glass micrographs in Fig. 1. Finally the P300-3 gave a very small QCM-D response, and the SEM showed the deposited particles to be highly aggregated. Note the initial particle number concentrations in these experiments were not constant. In spite of the PEG coatings, the high pH and the high ionic strength, the main conclusion is that the nanoparticles adsorb onto glass surfaces.

### 3.3. Glass bead flotation

Glass bead flotation recovery measurements were performed in 150 mL scale flotation experiments, and the results are summarized in Table 2. These glass recovery values are the mass fraction of beads collected in the froth during the first 30 s of flotation. In these experiments glass beads were suspended in 5 mM sodium carbonate containing 100 mg/L nanoparticles. This dosage was sufficient to cover between 51% and 181% of the glass bead surface, with the smallest diameter nanoparticle giving the highest potential coverage on the glass beads. This dosage represents a large excess of nanoparticles. Earlier work has shown that 10% coverage is sufficient to give good recoveries with an effective nanoparticle [2].

Table 2 reveals that none of the nanoparticles bearing PEG surface groups were good flotation collectors; P2000-4 gave the

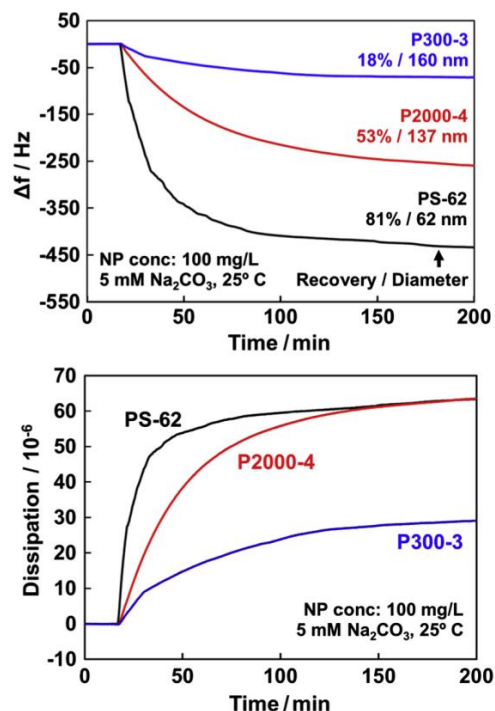


**Fig. 2.** Deposition of latex particles onto silica QCM-D sensor surfaces. Measurements were performed in 5 mM sodium carbonate at pH 10. 18%/160 nm refers to glass bead flotation recovery values and particle diameters from Table 2.

higher recovery of only 53%. By contrast, the smaller simple cationic polystyrene PS-62 recovered 81% of the glass beads. Note that PS-62 is not a useful collector for pentlandite flotation because it is too colloidal unstable and because it has no nickel chelating surface groups required for selectivity in mixtures of pentlandite and unwanted gangue.

PEG macromonomers were employed to increase the colloidal stability of the polystyrene nanoparticles. Critical coagulation concentrations (CCC) in sodium carbonate were used as a measure of colloidal stability. In our target industrial application, flotation is conducted in ~7 to 13 mM sodium carbonate, suggesting a useful nanoparticle must have a CCC above 12 mM.

In addition to colloidal stability, the nanoparticles must be sufficiently hydrophobic to promote adhesion to air bubbles. In previous work we observed a direct correlation between the advancing water contact angle ( $\theta$ ) and flotation efficiency [6]. For these contact angle measurements, nanoparticles were allowed to form a saturated adsorbed layer on clean glass slides. After gently rinsing and drying the slide, advancing water contact angles were measured. Based on our earlier results, we assumed herein that a promising nanoparticle for glass bead flotation must have an advancing water contact angle greater than  $40^\circ$ .

Fig. 3 shows the nanoparticle properties mapped onto the  $\theta$  vs CCC plane. The green area of the plane, labeled “Predicted Flotation Domain” denotes the predicted combinations of contact angle and CCC values that will support flotation. We see that many of the nanoparticles have CCC values  $>12$  mM suggesting sufficient colloidal stability. However, all but two of the PEG-based nanoparticles have an advancing water contact angle less than  $40^\circ$ . Our hypothesis was that only the nanoparticles within the green “Predicted Flocculation Domain” would be effective. The numbers beside the data points in Fig. 3 give the measured glass bead recovery values. PSVI-75, a polystyrene latex with surface imidazole

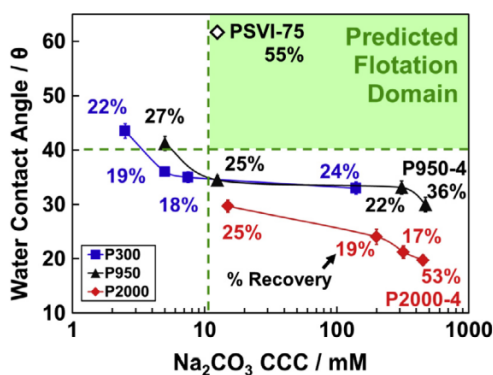


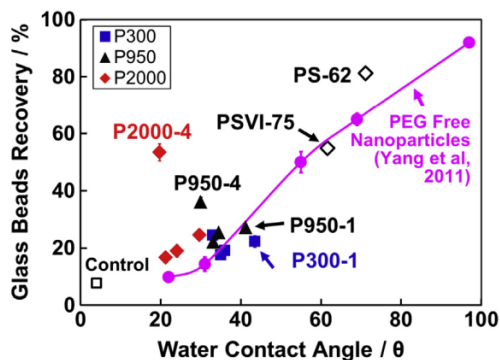
**Fig. 3.** Mapping of nanoparticles properties in Table 2 onto the  $\theta$  vs. CCC surface. The assignment of the flotation domain is based on our earlier work [6]. Each data point corresponds to one nanoparticle type in Table 2. The colored nanoparticle groupings indicate the PEG macromonomer molecular weight (300, 950 or 2000 Da). (For interpretation of the references to color in this figure legend, the reader is referred to the web version of this article.)

groups, was the only nanoparticle within the “Flotation Domain” and it showed some flotation efficacy. With the exception of PSVI-75 and two outliers (P2000-4 and P950-4), all the glass bead recoveries were less than 40%, which is low. Based on these criteria, none of the PEG-based nanoparticles showed any promise.

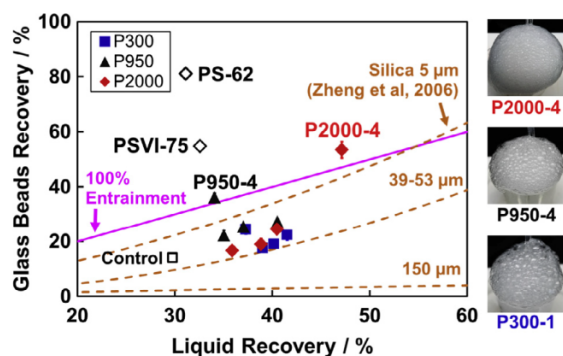
The deviant behavior of the two outliers is further illustrated in Fig. 4 that shows flotation recoveries as a function of contact angle. Included in the plot are Yang’s data [6] for glass bead flotation with PEG-free polystyrene. We propose that the contact angles reflect the relative hydrophobicity of the nanoparticles. For the three PEG macromonomer types, the contact angle decreases with increasing PEG contents giving lower recoveries, except for the two outliers that give somewhat higher recoveries.

### 3.4. Explaining the outliers

When performing the flotation experiments, we observed that the froth (foam) bubble size seemed much smaller and foam more durable in the case of the outliers (P2000-4 and P950-4) – see photographs in Fig. 5. One of the flotation recovery mechanisms is entrainment, whereby soluble and dispersed particles are carried over with the liquid phase in the foam [10,11]. Materials recovered by entrainment are not attached to the air bubbles.



**Fig. 4.** Glass bead flotation recoveries as functions of the advancing water contact angles on glass beads saturated with adsorbed nanoparticle. P2000-4 and P950-4 are outliers that gave relatively high recoveries.



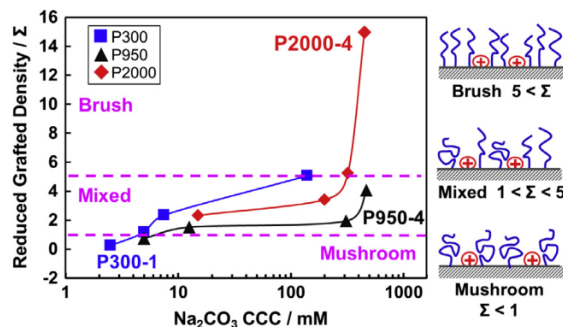
**Fig. 5.** Glass bead recovery as a function of the quantity of liquid collected with the froth. Also shown are results from Zheng et al. showing silica entrainment; smaller size fractions of silica are more efficiently entrained.

Fig. 5 shows our flotation data plotted as a function of the percentage of added liquid that was recovered with the froth. Most of the PEG-based nanoparticles gave liquid recoveries in the range 35–42%, whereas the outlier P2000-4 entrained much more water in finer foam. Also shown are the curves representing the data of Zheng et al. for the entrainment of silica as a function of particle size [11]. The larger the dispersed particles, the less entrainment of particles with the water. In summary, we propose that the somewhat enhanced recoveries of outliers P2000-4 were due to more entrained aqueous phase and suspended particles carried over in finer, more stable foams.

### 3.5. Influence of PEG surface chains on colloidal stability

The PEG-based nanoparticle covered a wide range of PEG densities. We estimated the reduced grafted density indices [12],  $\Sigma$ , for our nanoparticles assuming all of the measured PEG functionality was on the particle surface (see Supporting Materials for details).  $\Sigma$  is defined as the number of grafted chains that occupy the projected coil area on the bead surface of a free PEG coil in solution. Fig. 6 show the experimental CCC values mapped on the  $\Sigma$ –CCC surface. The PEG surface chains on most of the nanoparticles were in the mixed “mushroom/brush” configuration, whereas the P2000-4, again an outlier, supported a dense surface PEG brush. This dense PEG layer is the origin of the high colloidal stability (i. e. highest CCC) and low contact angle for the P2000-4 and P950-4 nanoparticles.

We evaluated the P2000-4 nanoparticle as a potential flotation collector for pentlandite ore. Fig. 7 compares the 4 L scale batch flotation results in nickel ore with two non-PEG nanoparticles.



**Fig. 6.** Reduced grafted density indices,  $\Sigma$ , as a function of the critical coagulation concentration in sodium carbonate.



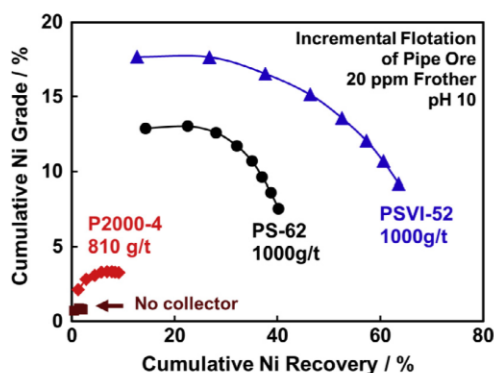


Fig. 7. Comparison of P2000-4 PEG-containing nanoparticles with PEG-free PS-62 (polystyrene) and PSVI-52 (polystyrene-co-vinyl imidazole) as collectors for a nickel sulfide ore. The PEG-free cationic polystyrene nanoparticles were more effective.

The results are shown as plots of nickel grade (wt.% Ni in recovered material) versus nickel recovery (percentage of total nickel in ore recovered). The points along each line represent a sequence of batch flotation runs – the more flotation steps, the higher the total recovery, at the expense of product purity. A perfect separation giving pure pentlandite in the froth would give a horizontal line with a nickel grade of 34% going across to 100% recovery.

The best nickel separation in Fig. 7 was obtained with PSVI-52, which has similar to nanoparticle PSVI-75. This is a pristine polystyrene latex with a few surface imidazole groups, which have an affinity to nickel ions. PS-62, a similarly sized polystyrene, but without imidazole surface groups, was next best. Finally the P2000-4 was ineffective with only slightly better separation than the control with not collector. However, PS-62 (CCC = 8 mM), PSVI-52 (CCC = 4 mM) and related particles are not colloidal stable in the high ionic strength flotation media. Therefore the very high nanoparticle dosages shown in Fig. 7 were required.

#### 4. Discussion

This work is one of our first steps towards the implementation of combinatorial synthesis and high throughput screening of potential nanoparticle flotation collectors. In this work we have focused on validating screening assays to accept/reject candidate particles. For example, if we consider the thirteen nanoparticle types plotted on the contact angle vs. CCC plane in Fig. 3, only PSVI-75 would be considered a candidate for time and material consuming flotation testing. To validate the assay, we performed flotation testing on entire set. However, for thirteen hundred or thirteen thousand nanoparticle particles types from combinatorial nanoparticle synthesis, flotation testing would not be practical. In summary, the results in Fig. 3 support our contention that mapping nanoparticles onto the contact angle/CCC surface, provides an initial screening to reject candidate nanoparticles before laboratory and pilot scale flotation testing.

Effective nanoparticle flotation collectors must be sufficiently hydrophobic. We used the water contact angle as a measure of hydrophobicity, and as a criterion for rejecting particles. Of course, it has been long known that mineral contact angles alone cannot predict flotation efficiencies [13]. Thus, the link between nanoparticle hydrophobicity and flotation is tenuous. In other words, we believe that nanoparticle hydrophobicity is a necessary but not sufficient condition for effective nanoparticle flotation collectors.

Our semi-automated contact angle assay consists of placing concentrated latex drops on a patterned glass surface with circular hydrophilic domains. The glass is rinsed and allowed to dry. The

advancing water contact angle is then measured. Previously, we compared this advancing water contact angle with two other types of contact angle measurement: (1) smooth film measurements where an adsorbed latex layer was partially dissolved in solvent and dried to give a smooth film; and (2) receding contact angles where air bubbles were attached to latex coated surfaces immersed in buffer [6]. The three types of contact angle measurements gave different values, however, all showed a positive correlation with flotation performance. However, defining a “cut-off” contact angle to differentiate promising from poor candidate nanoparticles is problematic. Fig. 4 shows that the slope of recovery vs. contact angle is not steep and data are somewhat spread, making the definition of a specific cut-off contact angle below which nanoparticles are ineffective, somewhat arbitrary. In our  $\theta$  vs. CCC mapping (Fig. 3), we chose  $40^\circ$  as the cut-off defining the flotation domain. However,  $70^\circ$  is arguably a more useful cut-off value.

In this work we used traditional, 100 mL scale polymerizations to prepare a small library of PEG-containing nanoparticles. However, traditional latex polymerization, cleaning, characterization and flotation testing is too slow to explore an extensive nanoparticle property space. Our future publications will describe high throughput colloidal stability measurements employing 96 multi-wall plates and robotic sample preparation. This stability assay, coupled with our medium throughput contact angle assay, described herein, will be used to screen a large library of nanoparticle flotation collector candidates, prepared with click chemistry.

#### 5. Conclusions

The conclusions from this work are:

1. Critical coagulation concentration values (CCC) and advancing water contact angle measurements ( $\theta$ ) can be used to screen potential nanoparticle flotation agents. Mapping nanoparticle properties onto the  $\theta \times$  CCC plane gives a useful screening assay for rejecting nanoparticles not suitable as flotation collectors.
2. PEG-methacrylate (MW 300–2000 Da) stabilized polystyrene nanoparticles are too hydrophilic to perform as pentlandite flotation collectors.
3. Polystyrene particles with a dense PEG surface layer stabilize smaller bubbles during flotation, giving anomalous higher apparent flotation recovery due to enhanced entrainment.
4. We hypothesize that latex stabilizing species smaller than PEG macromonomers are required for nanoparticle flotation collectors – particles stabilized by higher molecular weight PEG chains are too hydrophilic.

#### Acknowledgments

The authors acknowledge useful discussions and technical assistance of Dr. Berno from the McMaster Nuclear Magnetic Resonance (NMR) Facility. We are indebted to Drs. Zongfu Dai and Manqiu Xu from VALE for help, samples, and advice. We thank the National Sciences and Engineering Research Council of Canada (NSERC) and VALE Base Metals for funding this project. Some measurements were performed in the McMaster Biointerfaces Institute funded by the Canadian Foundation for Innovation. R.P. holds the Canada Research Chair in Interfacial Technologies.

#### Appendix A. Supplementary data

The supporting material file includes: NMR characterization, glass bead particle size distribution, details on the calculation of

coverage and reduced grafted density, and SEMs of QCM-D sensor surfaces after latex deposition experiments. Supplementary data associated with this article can be found, in the online version, at <http://dx.doi.org/10.1016/j.jcis.2015.08.052>.

## References

- [1] M. Fuerstenau, G. Jameson, R. Yoon, Froth flotation: a century of innovation, Society for Mining, Metallurgy, and Exploration, Littleton, Colorado, 2007.
- [2] S. Yang, R. Pelton, A. Raegen, M. Montgomery, K. Dalnoki-Veress, Nanoparticle flotation collectors – mechanisms behind a new technology, *Langmuir* 27 (2011) 10438–10446.
- [3] S. Yang, B.M. Razavizadeh, R. Pelton, G. Bruin, Soft nanoparticle flotation collectors, *ACS Appl. Mater. Interfaces* 5 (2013) 4836–4842.
- [4] S. Yang, R. Pelton, M. Montgomery, Y. Cui, Nanoparticle flotation collectors III – the role of nanoparticle diameter, *ACS Appl. Mater. Interfaces* 4 (2012) 4882–4890.
- [5] S. Yang, R. Pelton, M. Xu, Z. Dai, Nanoparticle flotation collectors for pentlandite, in: Proceedings of the 44th Annual Canadian Mineral Processors Conference, Canadian Institute of Mining Metallurgy and Petroleum, Ottawa, 2012, pp. 225–236.
- [6] S. Yang, R. Pelton, Nanoparticle flotation collectors II: the role of nanoparticle hydrophobicity, *Langmuir* 27 (2011) 11409–11415.
- [7] I.J. McLennan, R. Pelton, Some factors influencing the morphology of flexo ink calcium soap particles, *J. Pulp Paper Sci.* 23 (1997) J263–J269.
- [8] S. Yang, R. Pelton, C. Abarca, Z. Dai, M. Montgomery, M. Xu, J.-A. Bos, Towards nanoparticle flotation collectors for pentlandite separation, *Int. J. Miner. Process.* 123 (2013) 137–144.
- [9] J.W. Goodwin, R.H. Ottewill, R. Pelton, Studies on the preparation and characterization of monodisperse polystyrene lattices. 5. Preparation of cationic lattices, *Colloid Polym. Sci.* 257 (1979) 61–69.
- [10] T.V. Subrahmanyam, E. Forsberg, Froth stability, particle entrainment and drainage in flotation—a review, *Int. J. Miner. Process.* 23 (1988) 33–53.
- [11] X. Zheng, N.W. Johnson, J.P. Franzidis, Modelling of entrainment in industrial flotation cells: water recovery and degree of entrainment, *Miner. Eng.* 19 (2006) 1191–1203.
- [12] W.J. Brittain, S. Minko, A structural definition of polymer brushes, *J. Polym. Sci., Part A: Polym. Chem.* 45 (2007) 3505–3512.
- [13] R. Crawford, J. Ralston, The influence of particle size and contact angle in mineral flotation, *Int. J. Miner. Process.* 23 (1988) 1–24.

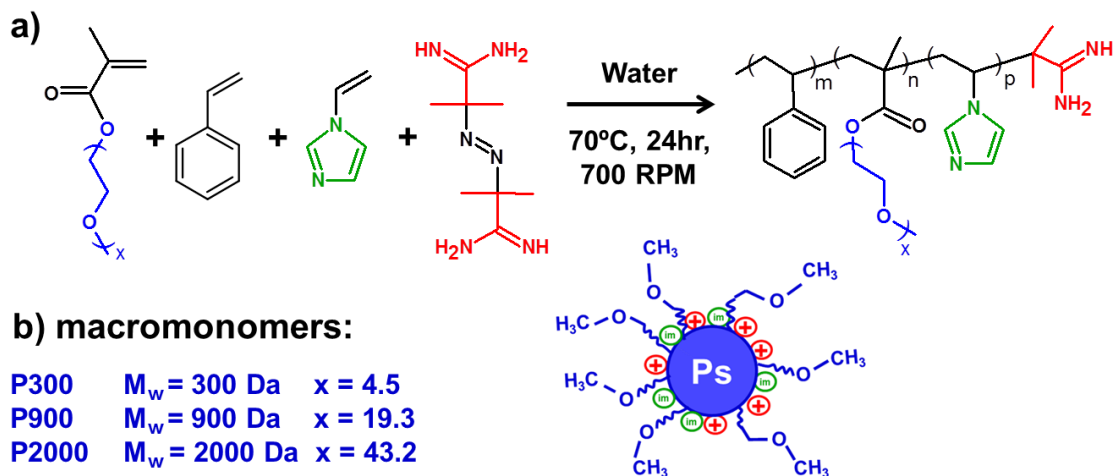
**Appendix: Supporting Information for Chapter 2****Towards High Throughput Screening of Nanoparticle  
Flotation Collectors**

Carla Abarca, Songtao Yang and Robert H. Pelton\*

Appendix: Supporting Information for Chapter 2.....	46
Nanoparticle synthesis.....	47
Nanoparticle <sup>1</sup> H-NMR characterization .....	48
Glass bead particle size distribution .....	50
Calculation of nanoparticle coverages on glass beads.....	50
Calculation of reduced grafted density indices, $\Sigma^{[2]}$ .....	51
Results of surface coverage calculations of PEG-methacrylate nanoparticles.....	52
Colloidal Stability Maps .....	53
SEM Micrographs of QCM-D sensors for selected nanoparticles .....	54
Flotation of Pentlandite .....	55
Surface tension measurements in selected nanoparticles .....	55
References Appendix Chapter 2 .....	56

## Nanoparticle synthesis

**Figure A 2-1:** a) Schematic synthesis of sterically stabilized nanoparticles by using styrene, 1-vinylimidazole and poly(ethylene glycol) methyl ether methacrylate macromonomers and V50 as initiator; b) Properties of three types of poly(ethylene glycol) methyl ether methacrylate macromonomers used in the polymerizations.



### Nanoparticle $^1\text{H-NMR}$ characterization

**Figure A 2-2:**  $^1\text{H-NMR}$  spectrum for P2000-4 in  $\text{CDCl}_3$  used for ethylene glycol final content calculations. The integral at 3.36 ppm corresponds to 3 protons from the methyl ether group at the end of the macromonomer. Spectra for each nanoparticle were used for calculations of the macromonomer content in the nanoparticles.

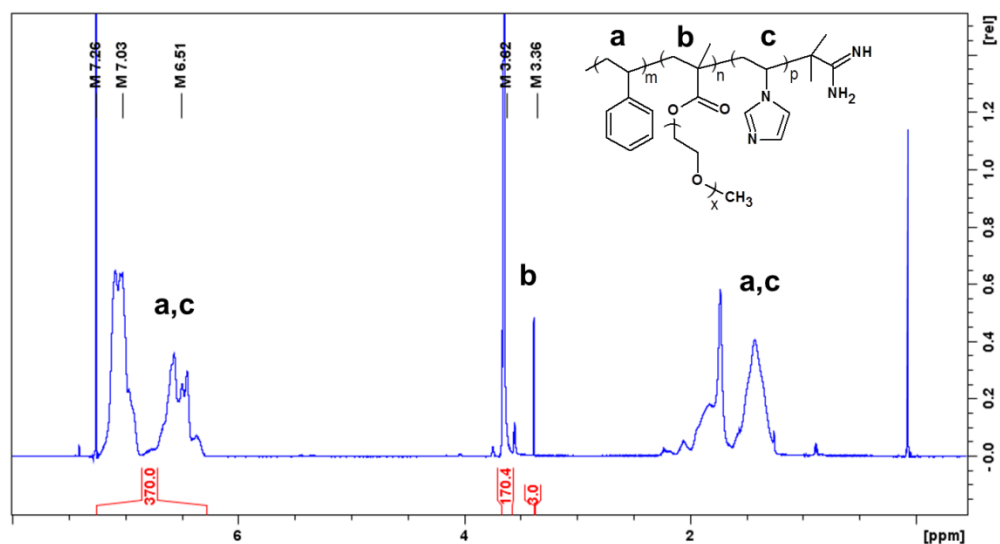


**Figure A 2-3:** Heteronuclear Single Quantum Coherence (HSQC) spectrum for P2000-4 zoomed in PEG region to show correlations of first bond hydrogens and carbons couplings in PEG-methacrylate macromonomer.

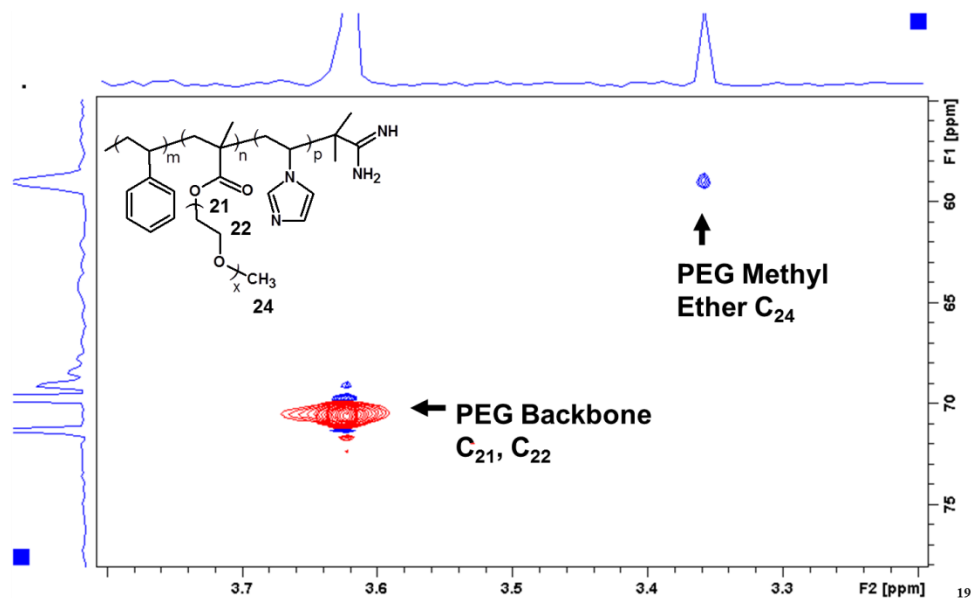
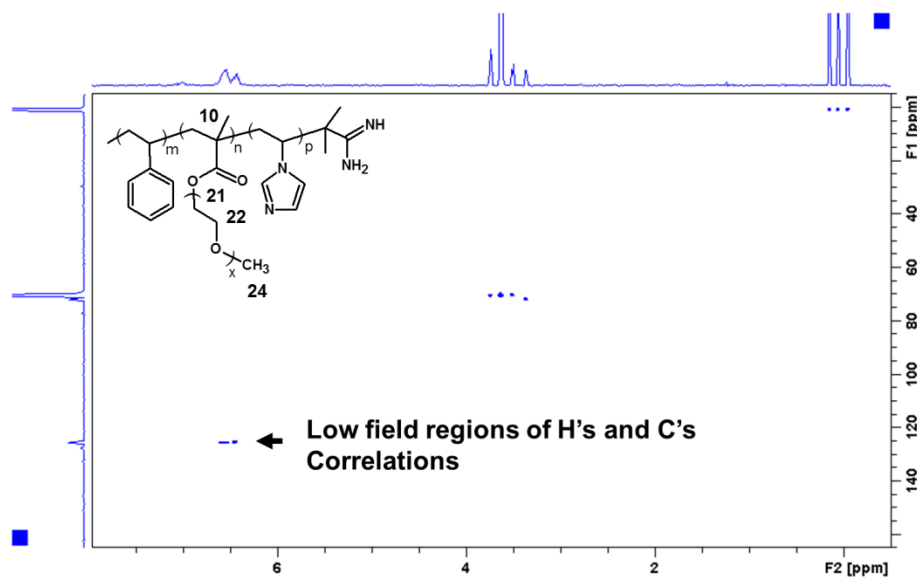


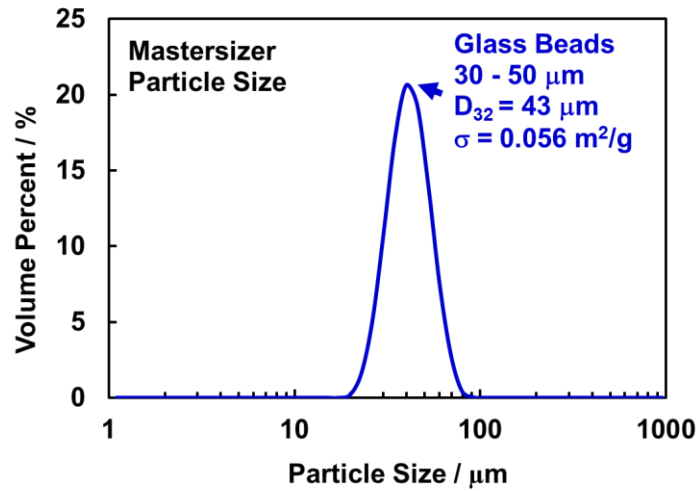
**Figure A 2-4:** Heteronuclear multiple-bond correlation spectroscopy (HMBC) spectrum for P2000-4. Low field regions of hydrogen and carbon 2D-spectra show that PEG-methacrylate is connected to the main chain of the polymer, due to low field aromatic hydrogens in styrene displays correlation with low field quaternary carbons ( $C_{10}$ ) of the PEG-methacrylate macromonomer.





### Glass bead particle size distribution

**Figure A 2-5:** The particle size distribution of glass beads used as a model mineral suspension was measured with a Mastersizer laser diffraction Malvern 2000 instrument. The surface area mean diameter ( $D_{32}$ ) is equivalent to the diameter of a sphere with the same volume/surface area ratio as the glass beads suspension in 5 mM NaCl, and  $\sigma$  is its specific surface area.



### Calculation of nanoparticle coverages on glass beads

Considering the nanoparticles as round spheres cover the surface area of each glass beads, the coverage calculation is:

$$\lambda_{np\_gb} = \frac{A_{NP} C_{NP}}{\sigma_{GB} C_{GB} V_{NP} \rho_{NP}} FC_{rand} [\%] \quad \text{Equation A 2-1}$$

Where  $A_{NP}$  is the projected area of the nanoparticle,  $C_{NP}$  is the mass concentration of the nanoparticle in flotations experiments,  $V_{NP}$  is the volume of the nanoparticle,  $\rho_{NP}$  is the density of polystyrene,  $\sigma_{GB}$  is the specific surface area of the glass beads and  $C_{GB}$  is the concentration of the glass beads in flotation experiments and  $FC_{rand}$  is the maximum random fractional coverage, 0.82<sup>[1]</sup>.

### Calculation of reduced grafted density indices, $\Sigma$ <sup>[2]</sup>

For the analysis of the PEG concentration on the nanoparticle and its grafted density on the surface, a hexagonal packing model was used following some applicable assumptions. The first assumption considers that all the PEG chains coexist on the surface of nanoparticles to calculate the mass of PEG-methacrylate chains per surface area of nanoparticle. Following that, the grafted density ( $\sigma_{\text{peg}}$ ), or the coverage by the number of PEG-methacrylate chains per area of nanoparticle, with sphere-based equations, is calculated as shown in Equation A 2-2.

$$\sigma_{\text{peg}} = \zeta_{\text{peg}} \frac{V_{\text{NP}} \rho_{\text{NP}}}{SA_{\text{NP}}} \frac{N_A}{MW_{\text{pegma}}} F_{\text{out}} \left[ \text{chains/nm}^2 \right] \quad \text{Equation A 2-2}$$

Where  $SA_{\text{NP}}$  and  $V_{\text{NP}}$  were the surface area and volume of a nanoparticle with the corresponding hydrodynamic diameter of the nanoparticle ( $d_{\text{NP}}$ ),  $\zeta_{\text{peg}}$  is the PEG to Styrene experimental mass ratio in the nanoparticle (obtained from <sup>1</sup>H-NMR data calculations),  $N_A$  is Avogadro's number,  $MW_{\text{pegma}}$  is the molecular weight of the correspondent PEG-methacrylate macromonomer and  $F_{\text{out}}$  is the fraction of PEG-methacrylate on the outmost surface of the nanoparticle (assumed to be 1 for all calculations). Other approximations to calculate the grafted density include that the PEG chains maintain a spherical shape (in the same manner as a free PEG chain in solution) with a size determined by its radius of gyration, and remains flat on the surface of the nanoparticle <sup>[3]</sup>. This radius of gyration,  $R_g$ , was obtained using an empirical formula based on static light-scattering, published by Kawaguchi et al., <sup>[4]</sup> is shown in Equation A 2-3.

$$R_g = 0.181 N_{\text{units}}^{0.58} \quad \text{Equation A 2-3}$$

In which  $N_{\text{units}}$  is the number of repeat units of ethylene glycol in the macromonomer. By combining these values it is possible to calculate the reduced grafted density <sup>3</sup>,  $\Sigma$ , which corresponds to the number of chains of macromonomer that would fill the same area as a free polymer chain that is not overlapping at the same experimental conditions <sup>3</sup>, as shown in. Equation A 2-4

$$\Sigma = \pi \sigma_{\text{peg}} R_g^2 \quad \text{Equation A 2-4}$$

The reduced grafted density can be used as a comparison index to judge either the mushroom-like or the brush-like character of a sample.

### Results of surface coverage calculations of PEG-methacrylate nanoparticles

Table A 2-1 summarizes experimental and theoretical results for calculations related to PEG nanoparticles. In experimental results,  $\zeta_{\text{peg}}$  was obtained from  $^1\text{H-NMR}$  data calculations, while in theoretical results,  $\zeta_{\text{peg}}$  corresponded to a theoretical mass ratio of PEG to styrene with a monomer conversion of 100% for both monomers. As the rest of the parameters in the calculations were kept the same, the discrepancies in the results are due to the conversion of each monomer on its corresponding polymerization.

**Table A 2-1:** PEG methacrylate surface coverage calculations. Radius of gyration of each macromonomer, experimental and theoretical values of PEG-methacrylate surface density, PEG-methacrylate grafting density,  $\sigma_{\text{peg}}$ , and reduced grafted density index,  $\Sigma$ , for each nanoparticle dispersion.

Nanoparticle designation	Radius of Gyration PEG, Rg, nm	PEG Grafting Density, $\sigma_{\text{peg}}$ , (chains/nm <sup>2</sup> )		Reduced Grafting Density Index, $\Sigma$	
		Exp	Theo	Exp	Theo
P300-1	0.44	0.42	1.42	0.25	0.85
P300-2	0.44	1.97	3.03	1.17	1.81
P300-3	0.44	3.94	5.63	2.35	3.36
P300-4	0.44	8.49	11.1	5.06	6.60
P950-1	1.01	0.23	0.50	0.74	1.61
P950-2	1.01	0.48	1.04	1.52	3.31
P950-3	1.01	0.61	1.17	1.94	3.73
P950-4	1.01	1.27	1.54	4.07	4.90
P2000-1	1.61	0.29	0.26	2.33	2.10
P2000-2	1.61	0.42	0.59	3.42	4.77
P2000-3	1.61	0.65	0.92	5.24	7.49
P2000-4	1.61	1.84	1.44	14.9	11.7

\* Calculations based on experimental macromonomer mass ratio from  $^1\text{H-NMR}$  measurements.

\*\* Calculations based on initial macromonomer added to the reactor and a 100% conversion and experimental hydrodynamic diameter.

### Colloidal Stability Maps

In order to understand correlations between the colloidal stability of the nanoparticles with other properties, the following graphs are presented:

**Figure A 2-6:** Hydrodynamic diameter as a function of the critical coagulation concentration in sodium carbonate for three series of nanoparticles, in which the optimum flotation domain is shown (green area). Blue squares: P300; black triangle: P950; red diamond: P2000.

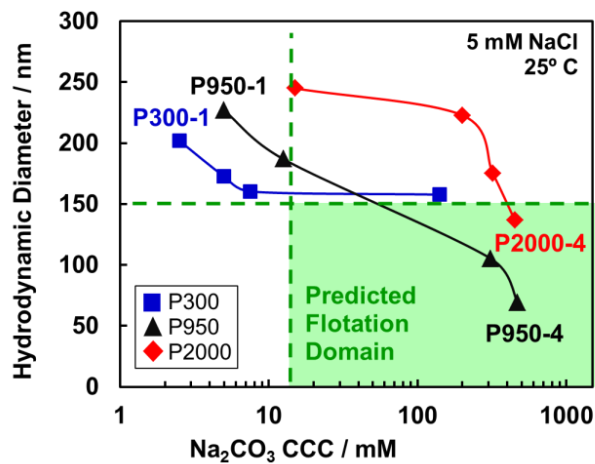
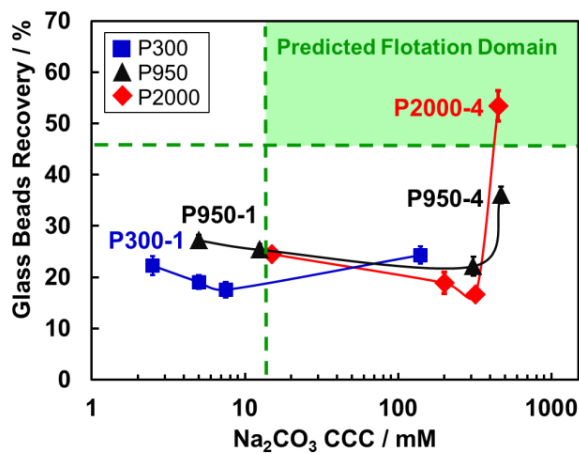


**Figure A 2-7:** Glass beads recovery in the first dish flotation as a function of the critical coagulation concentration in sodium carbonate for three series of nanoparticles, in which the optimum flotation domain is shown (green area). Blue squares: P300; black triangle: P950; red diamond: P2000.



### SEM Micrographs of QCM-D sensors for selected nanoparticles

**Figure A 2-8:** SEM micrographs of QCM-D sensors for representative nanoparticles, showing adsorption and aggregation correlation in an adsorption experiment at 5 mM Na<sub>2</sub>CO<sub>3</sub> buffer that simulates flotation environment of high pH and high ionic strength at which sterically stabilized nanoparticles show low electrophoretic mobilities (Table 2 of manuscript).

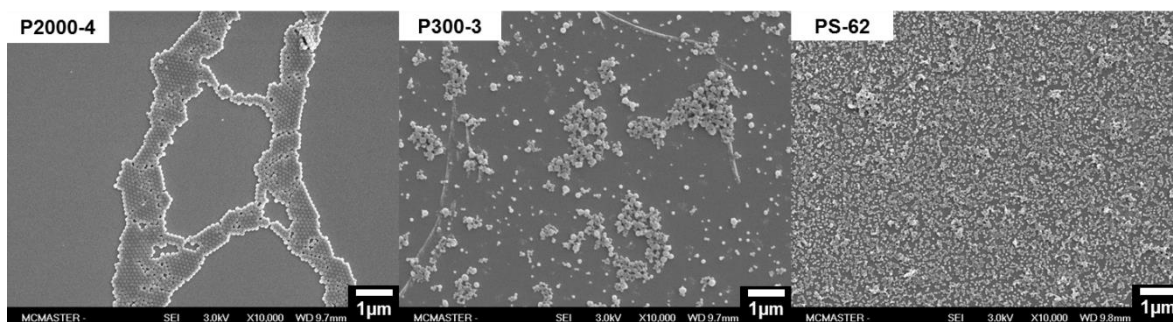
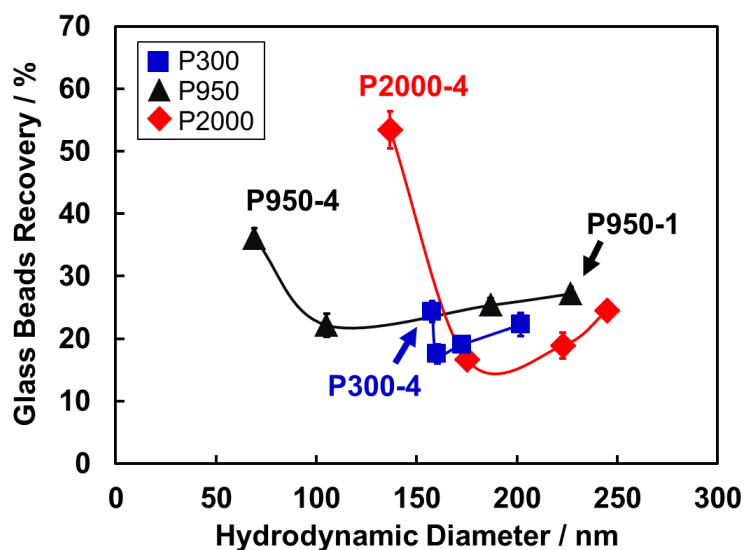
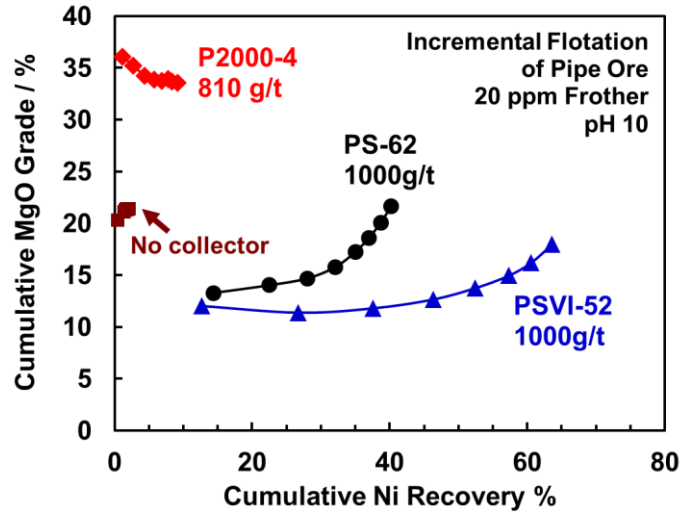


**Figure A 2-9:** The influence of nanoparticle diameter on glass bead recovery. (Helpful for QCM)



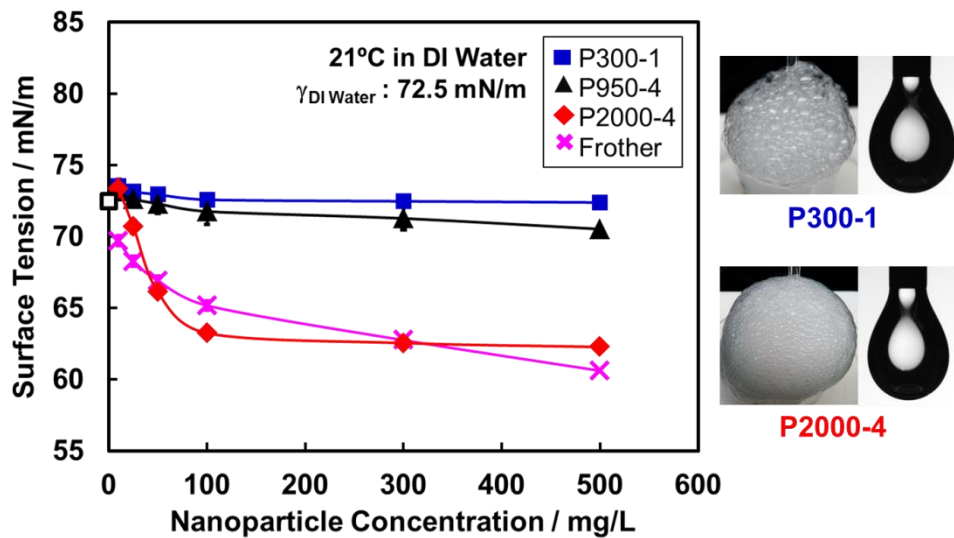
**Flotation of Pentlandite**

**Figure A 2-10:** Cumulative MgO grade as function of Cumulative nickel recovery. These graphs may suggest the use of this nanoparticle as a depressant of slimes. Results obtained by ICP technique.



**Surface tension measurements in selected nanoparticles**

**Figure A 2-11:** Water-air surface tension as a function of the nanoparticle concentration for selected nanoparticles and frother used in laboratory flotation tests.



**References Appendix Chapter 2**

- [1] Kausch, H., D. Fesko, and N. Tschoegl, *The random packing of circles in a plane*. Journal of Colloid and Interface Science, 1971. **37**(3): p. 603-611.
- [2] Brittain, W.J. and S. Minko, *A structural definition of polymer brushes*. Journal of Polymer Science Part A: Polymer Chemistry, 2007. **45**(16): p. 3505-3512.
- [3] Pasche, S., S.M. De Paul, J. Vörös, N.D. Spencer, and M. Textor, *Poly (l-lysine)-g raft-poly (ethylene glycol) Assembled Monolayers on Niobium Oxide Surfaces: A Quantitative Study of the Influence of Polymer Interfacial Architecture on Resistance to Protein Adsorption by ToF-SIMS and in Situ OWLS*. Langmuir, 2003. **19**(22): p. 9216-9225.
- [4] Kawaguchi, S., G. Imai, J. Suzuki, A. Miyahara, T. Kitano, and K. Ito, *Aqueous solution properties of oligo-and poly (ethylene oxide) by static light scattering and intrinsic viscosity*. Polymer, 1997. **38**(12): p. 2885-2891.

### **Chapter 3: A Colloidal Stability Assay Suitable for High-Throughput Screening**

---

In Chapter 3, the methodology design, experiments and data analysis were done almost entirely by me. Dr. M. Monsur Ali provided much assistance with Chemidoc instrumentation and analysis along with helpful discussion and help towards the project completion. Michael Kiriakou (undergraduate student) aided with some microplate experiments. Dr. Songtao Yang and Sophia Dong provided me with a few nanoparticle samples to complete the database tested. Dr. Robert Pelton contributed with very important guidance and discussion during the project design, experiments and data analysis.

This work was originally drafted by me, proofread by Andres Krisch, and revised to the final version by Dr. Robert Pelton. This manuscript has been published in ACS Analytical Chemistry, 2016. **88**(5): p. 2929-2936 DOI: [10.1021/acs.analchem.5b04915](https://doi.org/10.1021/acs.analchem.5b04915) Permission from © 2016 American Chemical Society.



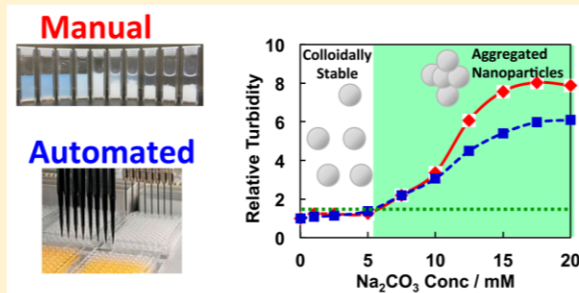
# A Colloidal Stability Assay Suitable for High-Throughput Screening

Carla Abarca, M. Monsur Ali, Songtao Yang, Xiaofei Dong, and Robert H. Pelton\*

Department of Chemical Engineering, McMaster University, Hamilton, Ontario Canada L8S4L8

## Supporting Information

**ABSTRACT:** A library of 32 polystyrene copolymer latexes, with diameters ranging between 53 and 387 nm, was used to develop and demonstrate a high-throughput assay using a 96-well microplate platform to measure critical coagulation concentrations, a measure of colloidal stability. The most robust assay involved an automated centrifugation–decantation step to remove latex aggregates before absorbance measurements, eliminating aggregate interference with optical measurements made through the base of the multiwell plates. For smaller nanoparticles (diameter <150 nm), the centrifugation–decantation step was not required as the interference was less than with larger particles. Parallel measurements with a ChemiDoc MP plate scanner gave indications of aggregation; however, the results were less sensitive than the absorbance measurements.



In most applications involving colloidal and nanoparticle suspensions, it is critical to control particle aggregation. In applications like papermaking and water treatment, the usual emphasis is on inducing colloidal aggregation. By contrast, many consumer products, such as paints, cosmetics and foods, are formulated to prevent colloidal aggregation. Herein we describe an automated colloid stability assay to distinguish colloidally stable from unstable samples in a high-throughput screening (HTS) workflow. High-throughput screening methodologies have been widely used in the pharmaceutical industry to identify possible target drugs in large candidate libraries.<sup>1,2</sup> The two essential requirements for HTS are large sample libraries and useful assays to reject poor candidates for a target application. Herein we focus on the assay development. Although we developed the stability assay specifically for the optimization of latex surface chemistry for a mineral processing application, described below, we propose that HTS methods are attractive as methods to optimize nanoparticle suspensions.

The tendency for colloids to aggregate, driven by van der Waals attraction,<sup>3</sup> can be overcome by introducing particle–particle repulsive interactions based upon electrostatic and steric interactions.<sup>4</sup> Starting with the famous DLVO theory developed in the mid 1900s,<sup>5</sup> the theoretical framework describing colloid stability is well-developed. Colloidal aggregation is a kinetic process influenced by interparticle forces including hydrodynamic interactions. Experimentally, aggregation kinetics have been measured by light scattering,<sup>6–9</sup> rheology,<sup>10,11</sup> and particle counting.<sup>12</sup> Indeed, any method giving particle-size distributions as functions of time yield aggregation kinetic details. However, from a more practical perspective, we often only want to know whether or not a colloidal suspension is aggregating in a time scale of interest. For this, simply monitoring turbidity or the visual appearance

of a colloidal dispersion often resolves the stable versus unstable question.

The critical coagulation concentration (CCC) is a related parameter for assessing the sensitivity of a colloidal dispersion to the presence of a coagulant. Typically, a series of colloidal samples is prepared with increasing concentrations of the coagulant, which is usually a salt. The CCC is defined as the concentration of coagulant corresponding to the onset of aggregation. CCC values are convenient single parameters for comparing the colloidal stability of multiple samples.

For the past few years, our laboratory has been developing polymeric latexes that function as flotation collectors in mineral processing operations.<sup>13–15</sup> This application has stringent requirements for our nanoparticles, including the following: the particles must be sufficiently hydrophobic to induce bubble attachment; the particles must specifically deposit onto the surfaces of only the mineral particles of interest; and the nanoparticles must be colloidally stable in the high ionic strengths typical of most mineral flotation operations. These are conflicting requirements, and the optimization of nanoparticle surface chemistries required the development of high-throughput strategies for identification of the best candidate particles. Our initial work employed classical manual methods to show that CCC values were correlated to flotation performance in sodium carbonate solutions.<sup>13</sup> As a step toward HTS of a large nanoparticle library, we required a colloidal stability assay that could be automated. We have found only one other publication focused on automated colloidal stability measurements. Chong et al. described a clever method that was

Received: December 29, 2015

Accepted: February 9, 2016

Published: February 9, 2016

Table 1. Nanoparticle Library of Polystyrene Copolymer Latexes<sup>a</sup>

nanoparticle designation	additional polymerization reagents	content of solids (g/L)	diameter, nm (PDI)	EM, $\times 10^{-8} \text{ m}^2 \text{ s}^{-1} \text{ V}^{-1}$ (std error)		CCC in $\text{Na}_2\text{CO}_3$ , mM	
				NaCl	$\text{Na}_2\text{CO}_3$	cuvette	microplate
PS-62	V50, CTAB	43	62 (0.01)	3.3	1.9 ( $\pm 0.08$ )	5	5
PS-62-44	V44, CTAB	45	62 (0.04)	3.0	1.5 ( $\pm 0.06$ )	7.5	7
PS-370-50	V50	30	374 (0.03)	4.4	1.3 ( $\pm 0.02$ )	5	2.5*
PS-385-50	V50	32	387 (0.10)	2.0	0.8 ( $\pm 0.26$ )	1	1*
PSM-120	V50, CTAB, MAPTAC	25	120 (0.06)	2.7	1.4 ( $\pm 0.13$ )	15	12.5*
PSVI-52	V50, CTAB, imidazole	30	56 (0.04)	2.9	-0.1 ( $\pm 0.08$ )	3	2.5
PSVI-75	V50, CTAB imidazole	32	76 (0.02)	3.1	1.8 ( $\pm 0.04$ )	12.5	12.5
SA-507	V50, CTAB, VBAAzide: 2.5% - 20 wt %/wt initial addition	39	55 (0.05)	3.2	1.5 ( $\pm 0.05$ )	5.0	4.0
SA-508		40	62 (0.06)	2.6	1.4 ( $\pm 0.1$ )	5.0	5.0
SA-510		40	53 (0.06)	2.7	1.6 ( $\pm 0.01$ )	5.0	4.0
SA-511		38	53 (0.05)	2.4	1.6 ( $\pm 0.07$ )	2.5	3.0
SA-512		39	59 (0.07)	2.3	1.6 ( $\pm 0.03$ )	2.5	3.0
SA-513		48	59 (0.05)	3.2	1.5 ( $\pm 0.02$ )	2.5	3.0
SA-514		49	57 (0.07)	2.7	1.6 ( $\pm 0.06$ )	2.5	2.5
SA-401	V44, CTAB, VBAAzide: 2.5% - 20 wt %/wt initial addition	41	58 (0.05)	2.8	1.5 ( $\pm 0.03$ )	2.5	2.5
SA-402		46	53 (0.06)	2.1	1.6 ( $\pm 0.04$ )	7.5	5.0
SA-403		43	61 (0.03)	2.5	1.8 ( $\pm 0.06$ )	7.5	5.0
SA-404		44	54 (0.09)	2.4	1.7 ( $\pm 0.04$ )	2.5	3.0
SA-406		49	64 (0.03)	3.4	1.8 ( $\pm 0.03$ )	5.0	5.0
SA-410		46	58 (0.02)	3.2	1.7 ( $\pm 0.06$ )	2.5	1.0
P300-1	V50, PEG300, imidazole	40	202 (0.07)	3.0	-0.2 ( $\pm 0.07$ )	2.5	1.0*
P300-2		46	173 (0.02)	2.8	0.3 ( $\pm 0.21$ )	5	2.5*
P300-3		50	160 (0.12)	1.4	0.2 ( $\pm 0.08$ )	7.5	7.5*
P300-4		41	158 (0.16)	1.1	0.0 ( $\pm 0.06$ )	140	160*
P950-1	V50, PEG950, imidazole	39	227 (0.10)	3.0	-0.4 ( $\pm 0.11$ )	5	5.0*
P950-2		40	187 (0.01)	2.3	-0.2 ( $\pm 0.04$ )	12.5	7.5*
P950-3		39	105 (0.05)	1.7	0.3 ( $\pm 0.10$ )	310	330
P950-4		38	69 (0.05)	0.7	-0.3 ( $\pm 0.19$ )	470	450
P2000-1	V50, PEG2000, Imidazole	34	245 (0.03)	2.4	0.0 ( $\pm 0.12$ )	15	20*
P2000-2		35	223 (0.01)	1.3	-0.0 ( $\pm 0.02$ )	200	180*
P2000-3		33	175 (0.01)	1.1	0.0 ( $\pm 0.11$ )	320	320*
P2000-4		25	137 (0.04)	0.9	-0.1 ( $\pm 0.09$ )	410	410*

<sup>a</sup>Average diameters were measured by dynamic light scattering, and electrophoretic mobilities (EM) were measured in 5 mM NaCl and in 5 mM  $\text{Na}_2\text{CO}_3$ . The microplate CCC measurements were based on either the direct *MP-sed-0.25* or the *MP-cen-24\** methods. Abbreviations: V50 (2,2'-azobis(2-methylpropionamide) dihydrochloride); V44 (2,2'-azobis[2-(2-imidazolin-2-yl)propane]dihydrochloride); CTAB (cetyl trimethylammonium bromide); MAPTAC (methacrylamidopropyl trimethylammonium chloride); imidazole (1-vinylimidazole); VBAAzide (4-vinylbenzylazide); and PEG300, PEG950, and PEG2000 (poly(ethylene glycol) methyl ether methacrylate, Mw: 300, 950, and 2000 Da).

based on the difference in fluorescent intensity from a water-soluble fluorophore before versus after centrifuging the dispersion.<sup>16</sup> However, we are concerned about the interaction of aromatic fluorophores with our relatively hydrophobic latex particles. Instead, we developed an assay exploiting the intrinsic light-scattering properties of our particles. There are a few publications describing turbidity-based assays for assessing protein stability<sup>17</sup> and drug solubility.<sup>18,19</sup> Considerable efforts were required to develop an automated robust colloidal stability assay. The results of that work are summarized herein.

## EXPERIMENTAL SECTION

**Materials.** Sodium carbonate and sodium chloride salt high purity, sodium bicarbonate (Sigma-Aldrich, 99.5%), and water type 1 (as per ASTM D1193-6,<sup>20</sup> resistivity 18 M $\Omega$ -cm, from either EMD Millipore Milli-Q Advantage A10 System or Barnstead Nanopure Diamond system) were used in all the experiments.

**Nanoparticle Library.** Thirty-two polystyrene copolymer latexes were prepared, and their properties are summarized in

Table 1. The synthesis, purification, and characterization details for the polyethylene glycol (PEG) modified particles were published previously.<sup>13</sup> The azide bearing particles were prepared by copolymerization of styrene and 4-vinylbenzylazide. For the stability assay development, this small library of particle types spans a large range of particle sizes and intrinsic colloidal stability.

**Assay Overview.** Visible light absorbance measurements were used to monitor nanoparticle stability. Table 2 summarizes five colloid stability assays—one traditional, manual cuvette-based and four automated multiwell plate methods. The following paragraphs give detailed descriptions, and Figure 1 shows a schematic illustration of the four automated work flows.

**Absorbance Measurements in Cuvettes (Cuv-sed-t).** This is a variation of the classical manual method. The initial nanoparticle concentration, in the absence of coagulant, was adjusted to give absorbance readings of approximately 0.3 at 500 nm (Beckman Coulter, DU800). In a typical coagulation experiment, 3 mL cuvettes were filled with combinations of

**Table 2. Five Assays to Access Colloidal Stability—One Manual and Four Automated**

designation	details
Cuv-sed-t	absorbance (550 nm) using 3 mL cuvettes with a Beckman Coulter, DU800 spectrophotometer; light path passes horizontally across the cell; measurements recorded $t$ hours after last mixing step.
MP-sed-t	absorbance (550 nm) using 96-well microplates with TECAN Infinite M1000; light path from top and down through the base of the microplate; measurements recorded $t$ hours after last mixing step.
MP-cen-t	sample is centrifuged and absorbance measurements made on the centrifuged multiwell plate; nanoparticles were allowed $t$ hours to aggregate before centrifugation.
MPS-sed-t	sample is allowed to sediment for $t$ hours and absorbance measurements made on isolated supernatant in a multiwell plate.
MPS-cen-t	sample sat for $t$ hours and centrifuged for 15 min at 2500 rpm (1360g); absorbance measurements made on its supernatant in a clean multiwell plate.

sodium carbonate stock solutions (50, 250, or 1000 mM) and water to give final  $\text{Na}_2\text{CO}_3$  concentrations between 0 and 1000 mM. After agitation in a mini vortex mixer (VWR VM3000) at 500 rpm for 1 min, typically 0.04 to 0.4 mL of 5 g/L nanoparticle dispersion was added to give a final total volume in each cuvette of 2 mL. After a second vortexing at 500 rpm for 60 s, absorbance values at 550 nm were recorded typically after  $t = 24$  h sedimentation (“sed”) time.

**Direct Absorbance Measurements in Multiwell Plates (MP-sed-t).** In some cases, absorbance measurements could be made directly in the wells where nanoparticles were mixed with electrolyte. To optimize the initial nanoparticle concentration, several wells of a 96-well microplate (Falcon 96-well flat-bottom microplate, black with clear bottom, no. 353219) were filled with a 5 g/L nanoparticle dispersion at volumes between 10 and 100  $\mu\text{L}$ . This was diluted in water to a total volume of 200  $\mu\text{L}$  to determine the final nanoparticle dispersion concentration needed to give an initial absorbance of approximately 0.3 at 550 nm. UV–vis measurements were then made with an Infinite M1000 spectrophotometer (Tecan Group Ltd.), equipped with a high energy Xenon arc discharge lamp, a silicon photodiode, and a multiwavelength excitation monochromator.

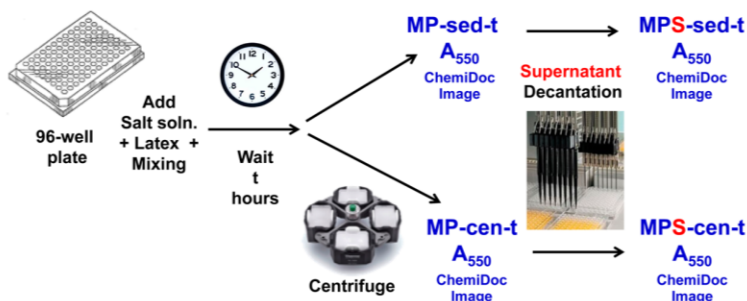
Using a Tecan Freedom Evo 200 liquid handling robot, combinations of sodium carbonate stock solutions (50, 500, or 1000 mM) and water were added to 9 wells and mixed to give final sodium carbonate concentration between 0 to 500 mM. The corresponding volumes of sodium carbonate stock solutions ranged between 0 and 80  $\mu\text{L}$ . To the sodium carbonate solutions were added 40  $\mu\text{L}$  of either 0.5 g/L or 5 g/L nanoparticle dispersions to give nanoparticle concentrations in the range of 0.1 g/L and 1 g/L. The total volume in each

well was 200  $\mu\text{L}$ . Microplates were agitated at 500 rpm in an orbital shaker (VWR Microplate Shaker 1706, no. 12620-926, orbital shaking amplitude of 3 mm) for 5 min after which the microplate with lid was wrapped with Parafilm and placed in a 4 °C refrigerator to avoid evaporation. UV–vis absorbance measurements at a wavelength of 550 nm were acquired for each well after sedimentation time intervals between 5 min and 24 h. For a given well, the final absorbance was based on 16 readings taken across the well. The error bars in our plots were the standard errors based on 16 absorbance readings. The experiment scripts were developed in the Freedom EVOware Standard 2.3 software that comes with the liquid handling robot (photographs of the robot and instruments are presented in the Supporting Information file).

**Automated Absorbance Measurements of Decanted Supernatant (MPS-cen-t or MPS-sed-t).** In some cases, nanoparticle aggregates sitting on the well bottoms interfered with direct absorbance measurements. In these cases, the larger aggregates were deposited on the well bottom, and 100  $\mu\text{L}$  of supernatant solution was withdrawn and placed in a clean 96-well microplate for absorbance measurements. The assays based on isolated supernatants are designated MPS (microplate supernatant). We employed two variations of MPS assays. With MPS-cen-t aggregate sedimentation was promoted by centrifugation for 15 min at 2500 rpm (1360g) in a Sorvall Legend XT/XF (Thermo Scientific) swigging rotor TX 750 multiwell plate centrifuge minutes after mixing. In the MPS-sed-t method, the microplate sat at 4 °C for  $t$  hours to give the aggregates enough time to settle before supernatant decantation.

**Imaging Scanning of Microplates by ChemiDoc MP Scanner.** Images of sediments on the well bottoms were captured with a ChemiDoc MP imaging system (Biorad, no. 170-8280) equipped with a supercooled CCD detector. The microplate was placed on top of the white screen and scanned by using the software ImageLab with the protocol “stain gel free”, in a white light mode, with a UV Trans illumination light source, a standard emission filter, and automatic exposure time. To aid visual sensitivity, inverted images are presented, with a gray absorbance signal on a white background.

**Hydrodynamic Diameter.** Dynamic Light Scattering measurements to analyze the importance of the nanoparticle size in these experiments were conducted with a Zetasizer Nano ZS, ZEN3600 (Malvern Instruments) equipped with a noninvasive backscattering detector positioned at a scattering angle of 173° at a 633 nm wavelength (He–Ne laser), and a temperature controlled jacket. Nanoparticle dispersions with a concentration of 0.01 mg/mL in 5 mM NaCl at neutral pH with conductivities  $\sim 0.4$  mS/cm, were measured in triplicate

**Figure 1.** Illustrating four variations of colloid stability assay for high-throughput screening.



using polystyrene cuvettes at 20 °C. Hydrodynamic diameters were calculated with the method of cumulants using Zetasizer software version 7.01, and the results are summarized in Table 1.

**Electrophoretic Mobility (EM).** Dispersions of nanoparticles in 5 mM NaCl (0.01 mg/mL) were measured in a Zetasizer Nano ZS, ZEN3600 (Malvern Instruments) equipped with a He–Ne laser (633 nm) and an electrode-dip cell, using a multi frequency phase analysis light scattering technique (M3-PALS) at 20 °C, pH ~ 7 and conductivity ~0.4 mS/cm. Measurements were repeated three times, and the resulting values and standard error are displayed in Table 1.

## RESULTS

The goal of this work was to develop a high-throughput colloid stability assay capable of characterizing thousands of samples in a short time. For assay development, we employed a library of 32 polystyrene copolymer latexes, ranging from weakly electrostatically stabilized suspensions to very stable particles bearing grafted polyethylene glycol (PEG) chains. The latex properties are summarized in Table 1.

Visible light absorbance measurements were used to probe the onset of aggregation with increasing concentrations of sodium carbonate. Compared are results from measurements using conventional cuvettes in a spectrophotometer with measurements in microplates. Unlike the case with cuvettes, with microplates, the light path is through the bottom of the wells where precipitates can collect. Table 2 describes four different procedures used to measure absorbance in microplates. In all cases, a small volume of concentrated latex was added to the electrolyte solution, followed by mixing. The two MP methods (MP-sed-t and MP-cen-t) were the simplest “one-well” procedures. After mixing, the wells were allowed to sit, MP-sed-t, or were centrifuged, MP-cen-t, before the absorbance measurements. However, as shown below, the simple “one-well” methods often gave poor results. In these cases, the more complex MPS methods were used with aggregate-free supernatant samples, isolated by either sedimentation MPS-sed-t or by centrifugation, MPS-cen-t.

**Absorbance Values for Stable Nanoparticle Suspensions.** Absorbance values for a subset of our nanoparticles in water were measured and the results are shown in Figure 2 as functions of particle size. The range of particle diameters spans the Rayleigh and Mie scattering domains. As expected, the absorbance increased with particle size for a constant mass concentration. Cuvette-based measurements in a conventional spectrophotometer showed the same features as the microplate results. However, the light path length in the cuvette was 10 mm, whereas in the microplates, the path length was only 5.5 mm, explaining the detailed differences in the absorbance versus diameter curves.

Ideally, the absorbance of the stable, control nanoparticles (i.e., with no coagulant),  $A_0$ , should be about 0.3. The corresponding nanoparticle concentration must be determined experimentally. However, for our nanoparticle library, a nanoparticle concentration of 1 g/L was suitable for particles less than 150 nm, whereas the larger particles should be diluted to 0.1 g/L. The remaining absorbance results herein are presented as relative turbidity values, which we define as  $\tau_R = A/A_0$ , where  $A$  is the absorbance in the presence of the sodium carbonate, the electrolyte used as a coagulant. In the following sections, we compare methods for measuring nanoparticle stability as functions of sodium carbonate concentration.

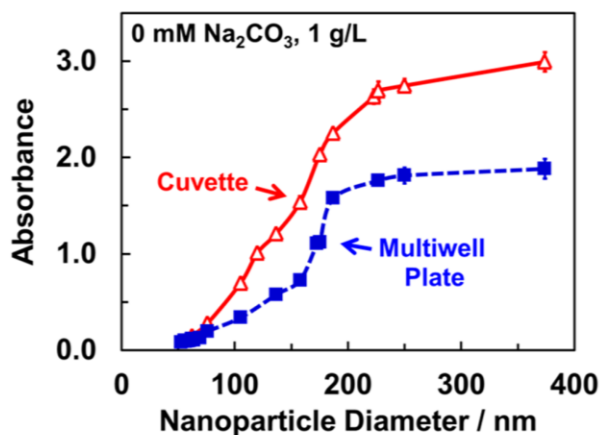


**Figure 2.** Influence of nanoparticle diameter and concentration on optical absorbance at 550 nm. Compared are results obtained with 1 cm cuvettes in a Beckman DU 800 with those obtained in 96-well microplates measured with an Infinite M1000 plate reader. The error bars for the multiwell results are the standard errors of 16 measurements. In most cases, the error bars are smaller than the symbol.

**Direct Measurements of Aggregation in Microplates (MP-sed-t) and Cuvettes (Cuv-sed-t).** The simplest procedures summarized in Table 2 for assessing nanoparticle stability are the direct methods in which nanoparticles are mixed with sodium carbonate in wells or cuvettes and the absorbance values directly measured. An example of this approach is given in Figure 3, which compares results for the automated MP-sed-0.25 assay with the manual Cuv-sed-0.25.

We used plots of  $\tau_R$  versus sodium carbonate concentration to determine the critical coagulation concentration (CCC) for our nanoparticles. We arbitrarily defined CCC as the lowest sodium carbonate concentration where the relative turbidity ( $\tau_R$ ) was either  $\tau_R > 1.4$  or  $\tau_R < 0.80$ . With small nanoparticles, the onset of aggregation results in higher absorbance, whereas with larger particles the opposite occurs. In the case of Figure 3, the nanoparticles are small and aggregation gives a substantial increase in light scattering. According to our definition, the CCC corresponds to the intersection of the green dashed line with the experimental curves, giving a CCC of 5 mM. The cuvette and the microplate assays gave the same sodium carbonate concentration for the onset of coagulation.

The photograph of the cuvettes clearly illustrates the onset of aggregation. At high electrolyte concentrations, the aggregates settle on the bottom of cuvettes. The ChemiDoc images of the microplates show more subtle indications of aggregation (Figure 3B).

Although the direct method has the least complex workflow, it is not robust. Figure 4 shows results for two particle sizes at two concentrations. With the smaller particles, SA-S08 (62 nm), shows the onset of aggregation with increasing sodium carbonate concentration; however, the assignment of a CCC value is sensitive to nanoparticle concentrations Figure 4A. Of more concern are the results from the larger 385 nm particles (Figure 4B). Although there was obvious visible coagulation with electrolyte addition, the relative turbidity curves were flat. With the larger particles, sedimented aggregates are interfering with the microplate absorbance measurements.

To further illustrate the problems with direct microplate turbidity measurements, we have plotted the cuvette turbidity

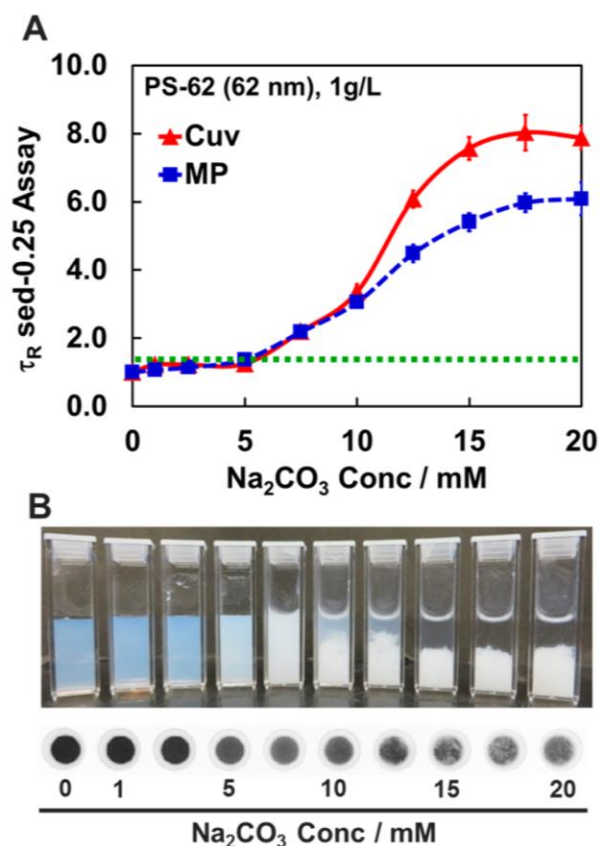


**Figure 3.** Comparison between the cuvette assay (Cuv-sed-0.25) and the microplate assay (MP-sed-0.25) of PS-62 polystyrene nanoparticles. Measurements were made 0.25 h after mixing. The intersection of the green line with the experimental curves gives the CCC = 5 mM. The images below the cuvettes are the inverted ChemiDoc scans.

measurements against the corresponding microplate measurements, and the results are shown in Figure 5. These data involve the results of a number of nanoparticles in a range of sodium carbonate concentrations giving varying degrees of aggregation. The nanoparticles with initial diameters less than 150 nm (the red data squared symbols) gave a reasonable correlation between the two methods. By contrast, with the larger particles, the microplate turbidity values were nearly independent of cuvette turbidity values because of interference by deposits on the microwell base.

**Supernatant Decantation.** To circumvent problems from the presence of aggregates, aggregate free supernatants were obtained by centrifugation or sedimentation. The advantage of using centrifuged supernatant for absorbance measurements is illustrated in Figure 6, which compares the manual cuvette method (Cuv-sed-24), the “one-well” microplate method (MP-sed-24), and the microplate supernatant method (MPS-cen-24) centrifugal method. The latex was 187 nm nanoparticles stabilized with grafted PEG groups and was fairly tolerant to sodium carbonate. The cuvette and supernatant method gave similar results, whereas the direct, “one-well” method results were more attenuated and did not agree.

In our initial work, centrifugations were performed after 24 h. Are these long reaction/sedimentation times necessary? Figure 7 compares three variations of supernatant measurement

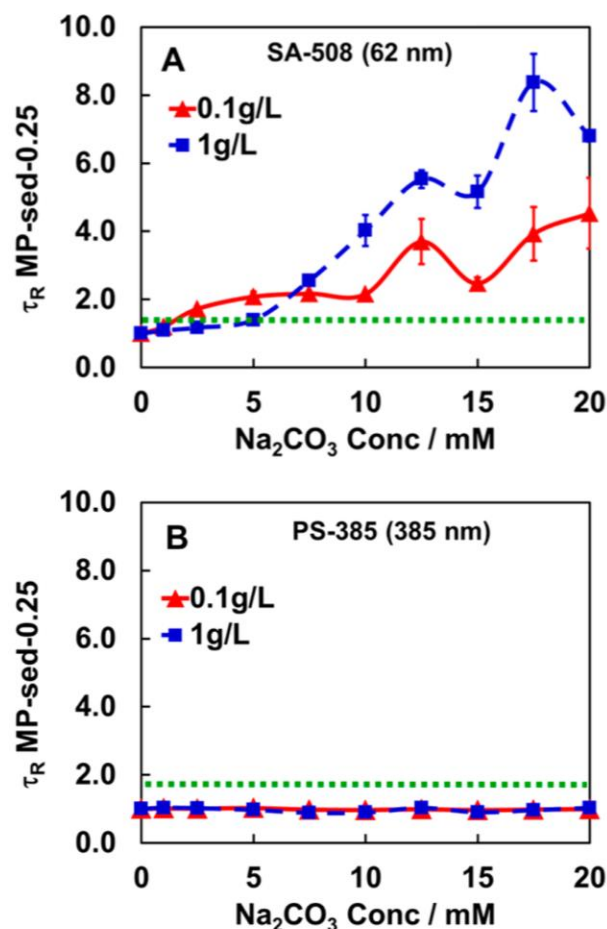


**Figure 4.** Two problem examples of the “one-well” direct (MP-sed-0.25) assay. (A) SA-508 (62 nm azide-coated nanoparticle), CCC is dependent on concentration; and (B) PS-385, relative turbidity was independent of the extent of aggregation.

methods for a 227 nm nanoparticle (P950-1). The samples centrifuged after mixing, MPS-cen-0.25, gave essentially the same results obtained after 24 h, MPS-cen-24. In this case, sedimentation (MPS-sed-24) was not effective; the relative turbidity changes due to aggregation were small. Presumably some of the aggregates were too small to settle within 24 h.

Table 1 includes CCC values for the entire nanoparticle library obtained by the classical, manual cuvette method and either the direct or the supernatant automated microplate assay. Figure 8 correlates the cuvette methods to the various types of microplate assays. Assay MPS-cen-0.25 gave the best correlation with the cuvette method. The other two methods gave reasonable correlation for the more stable nanoparticles giving high CCC values, whereas the correlations were poor for the less stable particles—see Figure 8A.

We have taken ChemiDoc images of most microplates used in this work with a view to having a very simple method to judge stability. Many of the figures herein have been reproduced in the Supporting Information file, together with the corresponding ChemiDoc images. Generally, the trends in the turbidity curves are reflected in the ChemiDoc images. Such images may be useful for rapid but less accurate assessments. The Supporting Information file also includes CCC values for



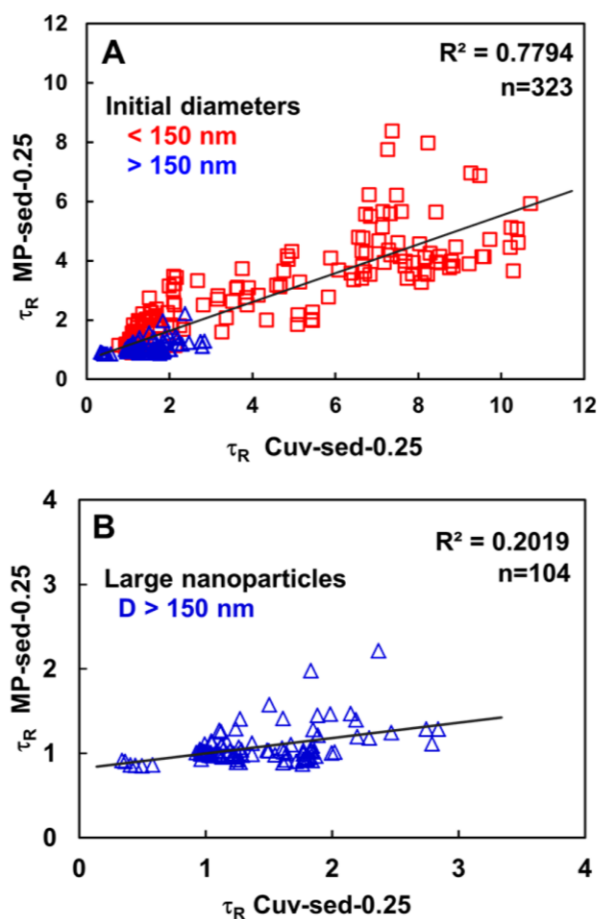


**Figure 5.** Correlation of relative turbidity results from microplates with those from cuvettes. Nanoparticle diameters (before aggregation) ranged from 50 to 350 nm. Data were extracted from plots of relative turbidity versus sodium carbonate concentration. Many of the points represent aggregated particles.

all 33 nanoparticles as measured by each of the five assay types described in Table 2.

## DISCUSSION

We have compared four microplate assays with the manual cuvette method for assessing colloidal stability. Of all the microplate assays described in Table 1, the most robust is the MPS-cen-t, where a centrifugation step is used to isolate the supernatant from aggregates that complicate the optical measurements. Important issues when setting up this assay are the following: (1) the nanoparticle concentrations in the stable, control samples must give absorbance values within the working range of the spectrophotometer; and (2) the centrifugation conditions must be such that the absorbance of the control dispersion does not change with centrifugation. The polymeric nanoparticles used in this work have specific gravities only slightly larger than one and thus were tolerant to the mild microplate centrifugation. With denser inorganic particles, the choice of centrifugation conditions will be more important.

The reaction/sedimentation time (see  $t$  in Figure 1) was varied between 15 min and 24 h. Shorter times are better for high-throughput assays. How short is too short? In the absence of particle–particle repulsive forces, coagulation is fast. The

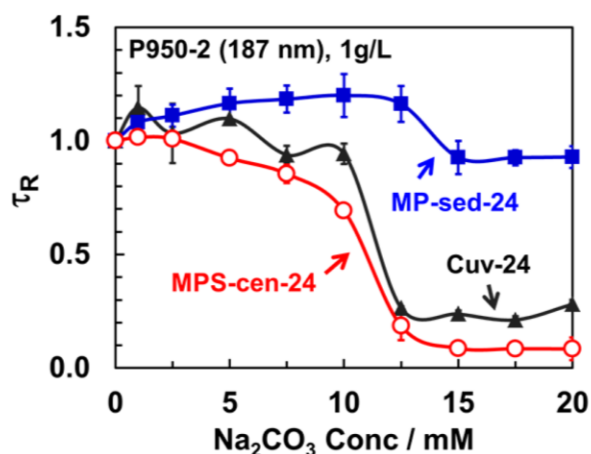


**Figure 6.** Comparing classic cuvette-based, manual turbidity results (Cuv-24) with automated microwell measurements after 24 h sedimentation (MP-sed-24) and with measurements made with isolated supernatant in microwell plates (MPS-cen-24). The isolated supernatant (MPS) results were close to the manual method, whereas results from the simpler MP-sed-24 did not agree with the manual Cuv-24 results.

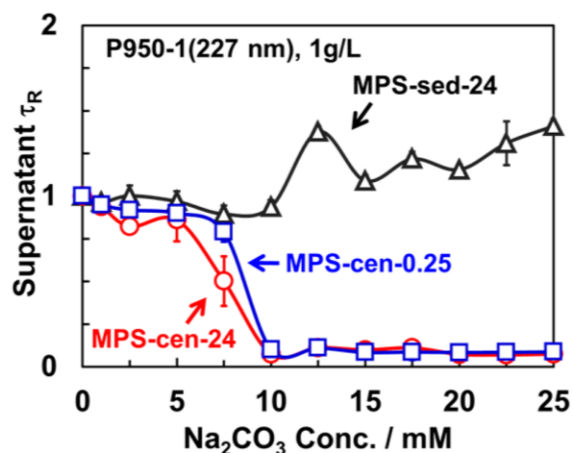


**Figure 7.** Demonstrating that there is no advantage in long waiting times before centrifugation (MPS-cen-0.25 versus MPS-cen-24) and that, in some cases, sedimentation does not remove aggregates from the supernatant (MPS-sed-24).

Smoluchowski equation, combined with the Stokes–Einstein equation for the diffusion coefficient, gives the following expressions for the half-life of an unstable suspension:<sup>21</sup>

$$t_{1/2} = \frac{3\eta}{4kTP_0} \quad (1)$$

where  $\eta$  is viscosity,  $k$  is Boltzmann's constant,  $T$  is temperature, and  $P_0$  is the initial number concentration ( $\text{m}^{-3}$ ) of particles. For a 1 g/L dispersion of 50 nm particles, the corresponding Smoluchowski half-life is 0.01 s. At the other extreme, a 0.1 g/L unstable dispersion of 400 nm particles has a theoretical half-life of 57 s. The large difference arises because for a given mass concentration, the nanoparticle number concentration is inversely related to the cube of the particle radius. In summary, for polymer particles, the particle concentrations required to give reasonable absorbance are

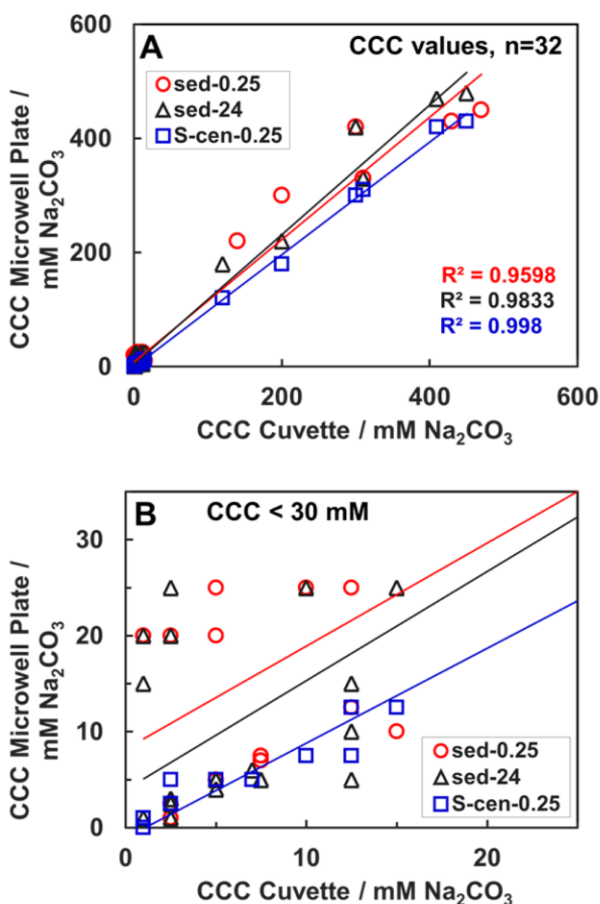


**Figure 8.** Correlating the critical coagulation concentrations of sodium carbonate from the new, automated microplate assays (y-axis) with the classical cuvette method (x-axis). (A) Shows all values for the library. (B) Expands the scale to show more clearly CCC values less than 30 mM  $\text{Na}_2\text{CO}_3$ . The assay in microwell MPS-cen-0.25 shows the closest correlation with the cuvette assay.

sufficiently high to not require aggregation times beyond a few minutes.

In contrast to aggregation kinetics, sedimentation is a much slower process, particularly with small polystyrene particles having a specific gravity of 1.05. With the recommended MPS-cen-t assay, centrifugation drives floc sedimentation, and so it is not necessary to have any extra reaction/sedimentation time. In addition, with small nanoparticles, the onset of aggregation is apparent by an increase in turbidity (e.g., see photograph in Figure 3)—again no sedimentation time is required in this situation. Long sedimentation times are only required with larger particles and when a multiwell plate centrifuge is not available.

Hydrodynamic forces from mixing can induce aggregation of larger particles and can break apart large aggregates.<sup>22</sup> In our work, microplate mixing at 200 and 500 rpm gave similar absorbance readings over 1 and 15 min. Hydrodynamic effects tend to be more important in the micrometer particle size range. Mixing conditions should be evaluated in these cases.<sup>22</sup>

The simplest role of a colloidal stability assay in HTS workflow is to determine whether or not suspensions are colloidally stable in a specific solution. The multiwell

absorbance assays described herein can perform this function. In our application, we determined CCC values to give a more quantitative ranking for our library of particles. We require nanoparticles that are colloidally stable in 11 mM sodium carbonate. For our application, a nanoparticle with CCC of 50 mM sodium carbonate is more promising than one with a CCC = 15 mM sodium carbonate even though both types of nanoparticles would pass the 11 mM yes/no assay. Nevertheless, we recognize that CCC values are not absolute quantities. Instead, CCC values depend upon the details of the aggregation test (i.e., times, nanoparticle concentrations, etc.) and on the criteria used to extract the CCC from the experimental data.

In applications requiring colloidal suspensions with very long shelf lives, very slowly aggregating systems may not give turbidity changes that are rapid enough to detect with our assay. In these cases, dynamic light scattering might be a better way to detect the initial stages of aggregation.

Finally, our work focused on polystyrene latexes. Our assay would have to be tuned for other types of colloids. For example, with colloidal  $\text{TiO}_2$  the particle concentration ranges would be lower because of the higher refractive index, giving a higher scattering intensity. On the other hand, centrifugation conditions would have to be less severe with these dense particles to differentiate aggregates from individual particles.

## CONCLUSIONS

1. The most robust approach to automating CCC determination for high-throughput screening of colloids, involves the following steps in multiwell plates: (1) addition of coagulant; (2) addition of nanoparticles with mixing; (3) centrifugation; (4) supernatant transfer to a clean well; and (5) supernatant turbidity measurement. With fluid handling robots, optical plate readers, and multiwell plate centrifuges, the elapsed time for the five steps is 30 min. If a microplate centrifuge is not available, 24 h of sedimentation generally gives good results.
2. For nanoparticle latex with diameters less than 150 nm, good results were obtained with simpler procedure (MP-sed-0.25) consisting of the following: (1) addition of coagulant; (2) addition of nanoparticles with mixing; and (3) turbidity measurement.
3. The ChemiDoc MP plate scanner, which images the microplate wells, gives an indication of flocculation. However, the absorbance measurements are more sensitive and more robust.
4. Because our plate readers measured through the bottom of the multiwell plates, floc sediments interfered with the optical measurements with large particles or with concentrated suspensions when the supernatants were not isolated.

## ASSOCIATED CONTENT

### Supporting Information

The Supporting Information is available free of charge on the ACS Publications website at DOI: 10.1021/acs.analchem.5b04915.

Additional CCC data; ChemiDoc images and the corresponding turbidity graphs; comparison of centrifugation in microplates to microtubes centrifugation; and photographs of our liquid handling robot (PDF)

## AUTHOR INFORMATION

### Corresponding Author

\*E-mail: peltonrh@mcmaster.ca.

### Notes

The authors declare no competing financial interest.

## ACKNOWLEDGMENTS

The authors acknowledge useful discussions and technical assistance of Dr. Kornic from the McMaster Combustion Analysis and Optical Spectroscopy (CAOS) facility. We are indebted to Drs. Zongfu Dai and Manqiu Xu from VALE for help, samples, and advice. We thank the National Sciences and Engineering Research Council of Canada (NSERC CRD 451944-13) and VALE Base Metals for funding this project. C.A. acknowledges the support of Becas-Chile program from the National Commission for Scientific and Technological Research of Chile (CONICYT). Some measurements were performed in the McMaster Biointerfaces Institute funded by the Canadian Foundation for Innovation. R.P. holds the Canada Research Chair in Interfacial Technologies.

## REFERENCES

- (1) Bleicher, K. H.; Bohm, H.-J.; Muller, K.; Alanine, A. I. *Nat. Rev. Drug Discovery* **2003**, *2*, 369–378.
- (2) Alsenz, J.; Kansy, M. *Adv. Drug Delivery Rev.* **2007**, *59*, 546–567.
- (3) Israelachvili, J. N. *Intermolecular and Surface Forces*, 3rd ed.; Academic Press: San Diego, CA, 2011.
- (4) Napper, D. H. J. *Colloid Interface Sci.* **1977**, *58*, 390–407.
- (5) Ninham, B. W. *Adv. Colloid Interface Sci.* **1999**, *83*, 1–17.
- (6) Berka, M.; Rice, J. A. *Langmuir* **2004**, *20*, 6152–6157.
- (7) Yang, Z.; Yang, H.; Jiang, Z.; Huang, X.; Li, H.; Li, A.; Cheng, R. *Colloids Surf., A* **2013**, *423*, 11–19.
- (8) Holthoff, H.; Egelhaaf, S. U.; Borkovec, M.; Schurtenberger, P.; Sticher, H. *Langmuir* **1996**, *12*, 5541–5549.
- (9) Yu, W. L.; Matijević, E.; Borkovec, M. *Langmuir* **2002**, *18*, 7853–7860.
- (10) Bolto, B.; Gregory, J. *Water Res.* **2007**, *41*, 2301–2324.
- (11) Kusters, K. A.; Wijers, J. G.; Thoenes, D. *Chem. Eng. Sci.* **1997**, *52*, 107–121.
- (12) Bushell, G. C.; Yan, Y. D.; Woodfield, D.; Raper, J.; Amal, R. *Adv. Colloid Interface Sci.* **2002**, *95*, 1–50.
- (13) Abarca, C.; Yang, S.; Pelton, R. H. J. *Colloid Interface Sci.* **2015**, *460*, 97–104.
- (14) Yang, S.; Pelton, R.; Raegen, A.; Montgomery, M.; Dalnoki-Veress, K. *Langmuir* **2011**, *27*, 10438–10446.
- (15) Yang, S.; Pelton, R.; Abarca, C.; Dai, Z.; Montgomery, M.; Xu, M.; Bos, J.-A. *Int. J. Miner. Process.* **2013**, *123*, 137–144.
- (16) Chong, J. Y. T.; Mulet, X.; Boyd, B. J.; Drummond, C. J. *ACS Comb. Sci.* **2014**, *16*, 205–210.
- (17) Capelle, M. A.; Gurny, R.; Arvinte, T. *Eur. J. Pharm. Biopharm.* **2007**, *65*, 131–148.
- (18) Morrison, J. S.; Nophsker, M. J.; Haskell, R. J. *J. Pharm. Sci.* **2014**, *103*, 3022–3032.
- (19) Bard, B.; Martel, S.; Carrupt, P. A. *Eur. J. Pharm. Sci.* **2008**, *33*, 230–240.
- (20) ASTM. *D1193 - 06 Standard Specification for Reagent Water*; ASTM International: West Conshohocken, PA, 2006 (2011), p 6.
- (21) Stokes, R. J.; Evans, D. F. *Fundamentals of interfacial engineering*; John Wiley & Sons: Hoboken, NJ, 1997.
- (22) Van de Ven, T. *Colloidal Hydrodynamics*; Academic Press: London, 1989; p 582.



## **Appendix: Supporting Information for Chapter 3**

# **A Colloidal Stability Assay Suitable for High Throughput Screening**

Carla Abarca, M. Monsur Ali, Songtao Yang, Xiaofei Dong and Robert H. Pelton\*

Appendix: Supporting Information for Chapter 3.....	66
Critical coagulation concentration values for all nanoparticle series. ....	67
Selected ChemiDoc™ images with their corresponding turbidity graphs. ....	68
Centrifugation on Microplates versus Centrifuge Microtubes. ....	70
Liquid Handling Robot TECAN Freedom Evo® 200. ....	71

### Critical coagulation concentration values for all nanoparticle series.

**Table A 3-1:** Critical coagulation concentration values at different methods for all nanoparticle series.

Nanoparticle designation	Diameter*, nm (PDI)	Cuvette CCC, mM Na <sub>2</sub> CO <sub>3</sub>		Microwell Plate CCC, mM Na <sub>2</sub> CO <sub>3</sub>		Supernatant CCC mM Na <sub>2</sub> CO <sub>3</sub>	
		sed-0.25	sed-24	sed-0.25	sed-24	S-cen-0.25	S-cen-24
PS-62	62 (0.01)	5.0	5.0	5.0	5.0	5.0	5.0
PS-62-44	62 (0.04)	7.5	7.0	7.0	6.0	5.0	N/D
PS-370-50	374 (0.03)	5.0	1.0	20.0	15.0	1.0	0.0
PS-385-50	387 (0.10)	1.0	1.0	20.0	20.0	1.0	0.0
PSM-120	120 (0.06)	15.0	12.5	10.0	10.0	12.5	10.0
PSVI-52	56 (0.04)	2.5	2.5	1.0	1.0	2.5	2.5
PSVI-75	76 (0.02)	12.5	12.5	12.5	15.0	10.0	10.0
SA-507	55 (0.05)	5.0	5.0	5.0	4.0	N/D	N/D
SA-508	62 (0.06)	5.0	5.0	5.0	5.0	N/D	N/D
SA-510	53 (0.06)	5.0	5.0	5.0	4.0	N/D	N/D
SA-511	53 (0.05)	2.5	2.5	2.5	3.0	N/D	N/D
SA-512	59 (0.07)	2.5	2.5	2.5	3.0	N/D	N/D
SA-513	59 (0.05)	2.5	2.5	2.5	3.0	N/D	N/D
SA-514	57 (0.07)	2.5	2.5	2.5	2.5	N/D	N/D
SA-401	58 (0.05)	2.5	2.5	2.5	2.5	N/D	N/D
SA-402	53 (0.06)	7.5	7.5	7.0	5.0	N/D	N/D
SA-403	61 (0.03)	7.5	7.5	7.5	5.0	N/D	N/D
SA-404	54 (0.09)	2.5	2.5	2.5	3.0	N/D	N/D
SA-406	64 (0.03)	5.0	5.0	5.0	5.0	N/D	N/D
SA-410	58 (0.02)	2.5	2.5	1.0	1.0	N/D	N/D
P300-1	202 (0.07)	1.0	1.0	20.0	1.0	0.0	1.0
P300-2	173 (0.02)	2.5	2.5	20.0	20.0	2.5	2.5
P300-3	160 (0.12)	7.5	12.5	7.5	5.0	7.5	7.5
P300-4	158 (0.16)	140.0	120.0	220.0	180.0	120.0	160.0
P950-1	227 (0.10)	5.0	2.5	25.0	25.0	5.0	5.0
P950-2	187 (0.01)	10.0	10.0	25.0	25.0	7.5	7.5
P950-3	105 (0.05)	310.0	310.0	330.0	330.0	310.0	330.0
P950-4	69 (0.05)	470.0	450.0	450.0	480.0	430.0	450.0
P2000-1	245 (0.03)	12.5	15.0	25.0	25.0	12.5	20.0
P2000-2	223 (0.01)	200.0	200.0	300.0	220.0	180.0	180.0
P2000-3	175 (0.01)	300.0	300.0	420.0	420.0	300.0	320.0
P2000-4	137 (0.04)	430.0	410.0	430.0	470.0	420.0	410.0

### Selected ChemiDoc™ images with their corresponding turbidity graphs.

**Figure A 3-1:** A, B) The influence of nanoparticle diameter and concentration on optical absorbance at 550 nm for cuvettes and microwell plates. C, D) Selected ChemiDoc™ pictures of microwells for turbidity plots in A and B (corresponding to Figure 2 in manuscript).

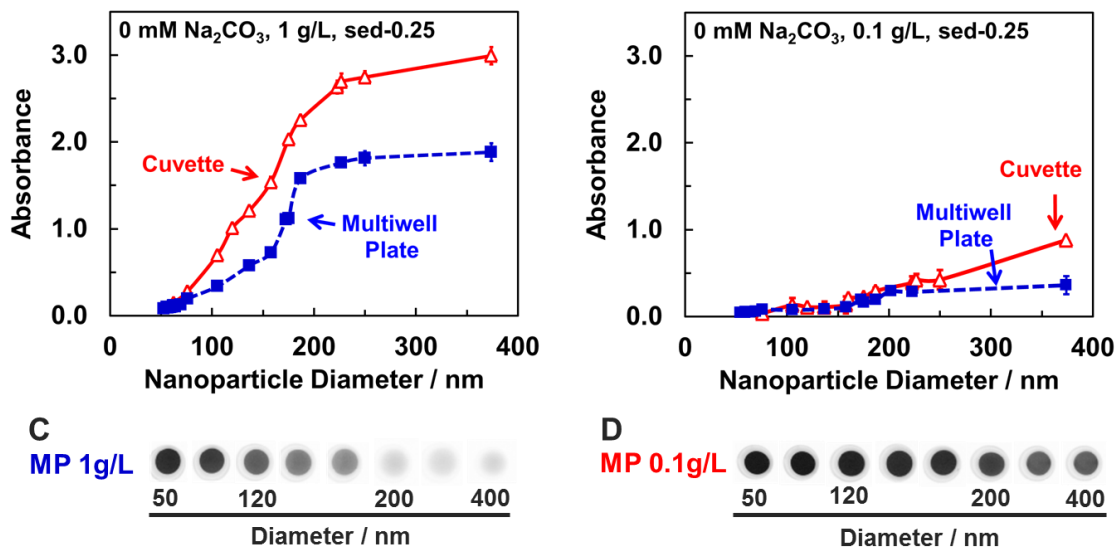


**Figure A 3-2:** C, D) ChemiDoc™ images for turbidity trends on A and B respectively (presented in Figure 4 of manuscript).

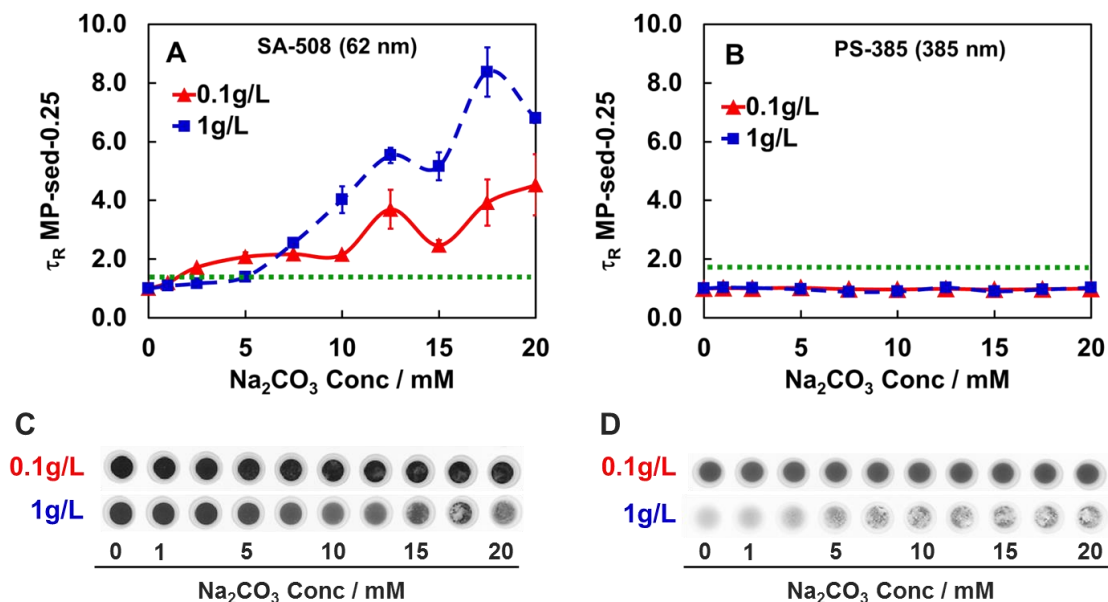


**Figure A 3-3:** B) ChemiDoc™ pictures for 187 nm (P950-2) nanoparticle for turbidity trends on A, corresponding to the figure 6 in manuscript.

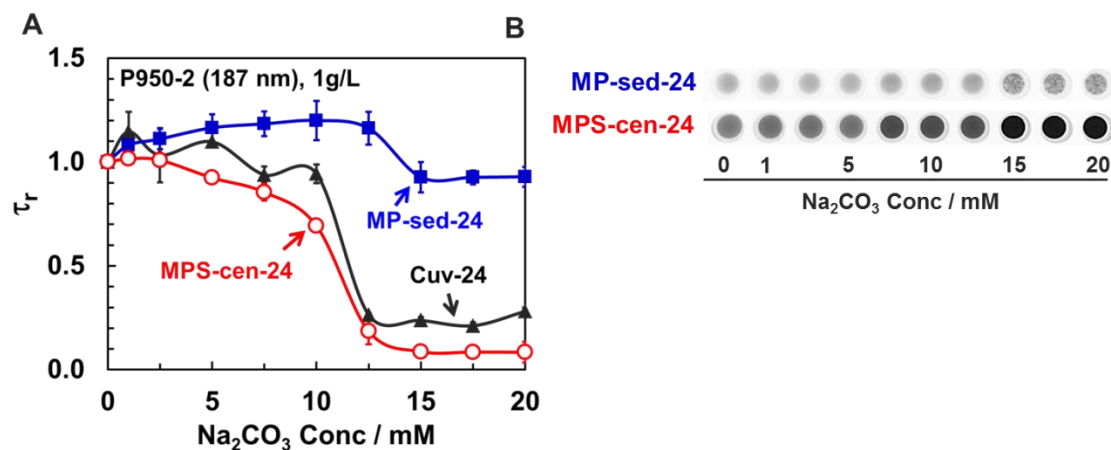
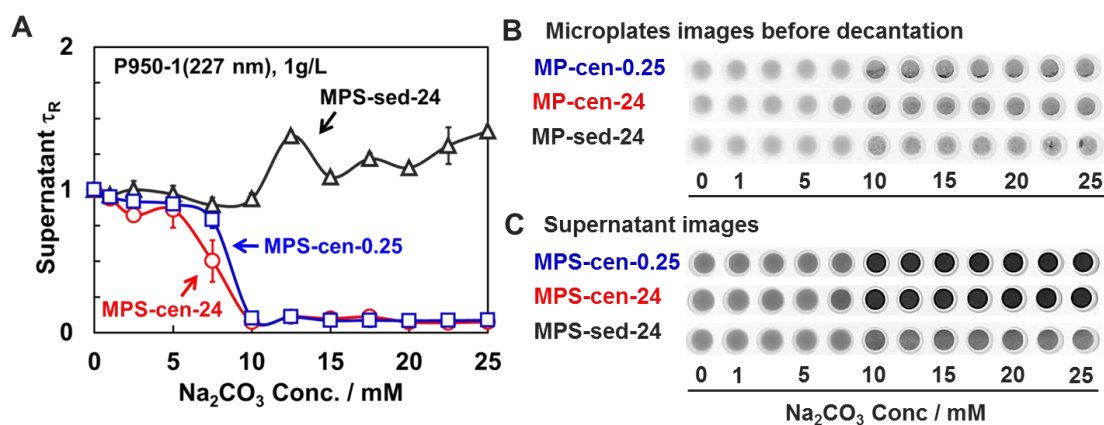


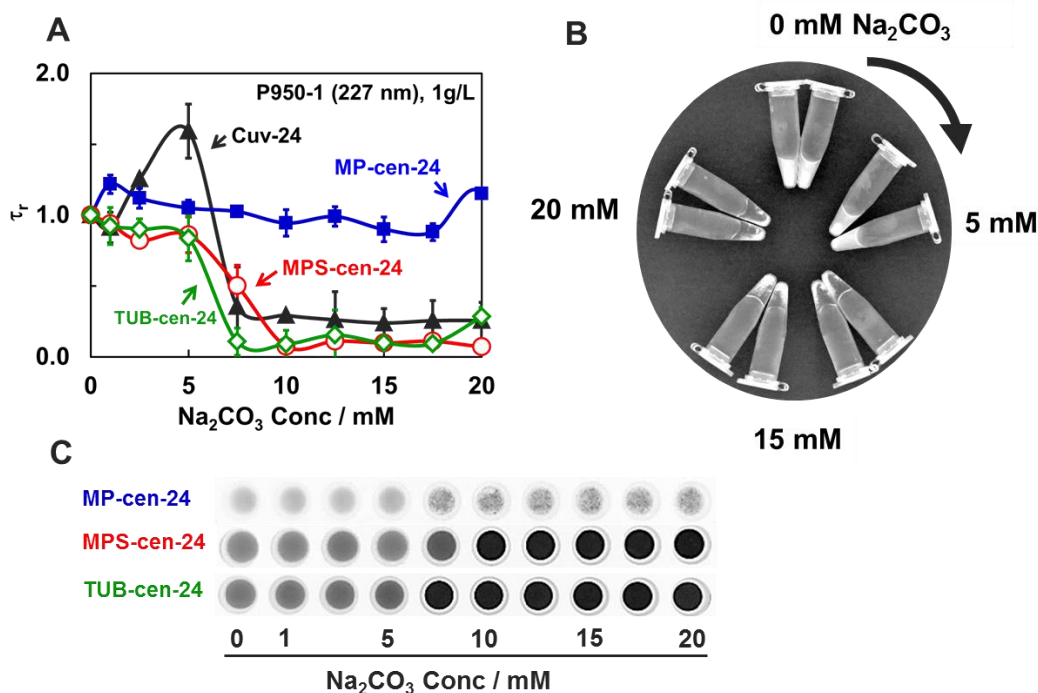
**Figure A 3-4:** ChemiDoc™ images before and after decantation for a 227 nm nanoparticle, to compare three supernatant microplate assays (corresponding to figure 7 in manuscript).



### Centrifugation on Microplates versus Centrifuge Microtubes.

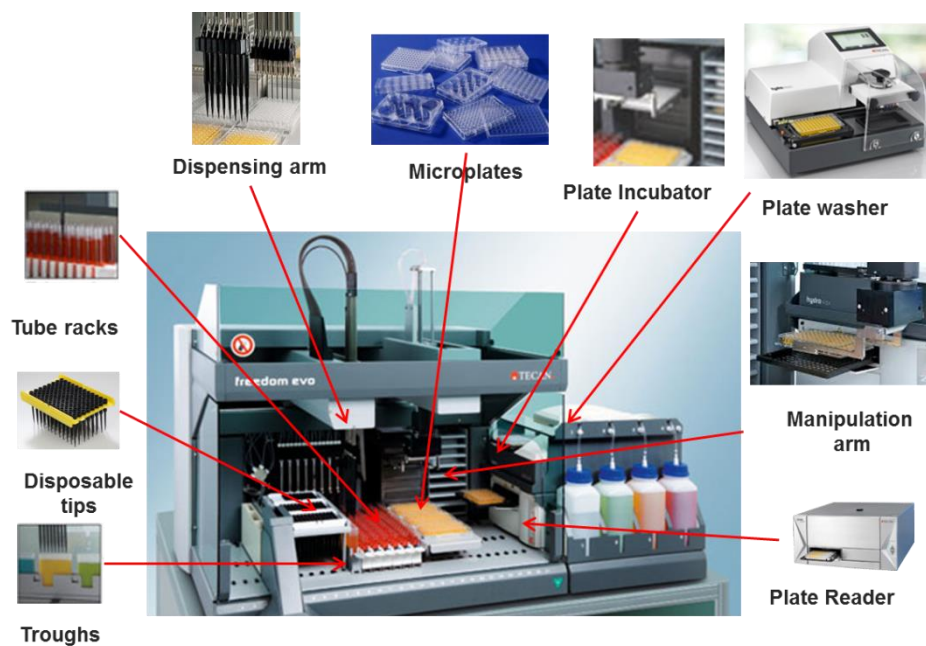
The method involving centrifugation and supernatant decantation was also tested using 1-mL centrifuge microtubes (CELLTREAT® CLS-4310-105, Chemglass). The centrifugation of nanoparticle dispersions in microplates was compared to centrifugation of the same sample and amount in 1-mL centrifuge microtubes to compare centrifugal effectivity. For most of the nanoparticles analyzed in microplates and microtubes, both of the supernatants  $\tau_r$  trends are in concordance with the traditional cuvettes assay at 24 hrs. However, the microtubes experiments are more prone to human error due to the liquid handling robot is not programmed to work with microtubes and the manual multi-channel micropipettes cannot reach all the microtubes at the same time. This is another advantage of using microplates to microtubes and cuvettes, even though centrifugation in microplates can be used in the same manner as in typical microtubes centrifugation experiments.

**Figure A 3-5:** Comparison of supernatant extraction assays using three different carriers: A) relative turbidity trends B) ChemiDoc™ image of tubes before supernatant decantation; C) ChemiDoc™ images of microplates and tubes supernatant.



### Liquid Handling Robot TECAN Freedom Evo® 200.

**Figure A 3-6:** Scheme with parts of liquid handling robot Tecan Freedom Evo® 200.



## **Chapter 4: A Simple Assay for Azide Surface Groups on Clickable Polymeric Nanoparticles**

---

In Chapter 4, the development of the chromatography technique, experiments and data analysis were performed by me with the useful and committed assistance of Devon Bowie (undergraduate student). Michael Kiriakou (undergraduate student) aided with some chromatography experiments as well. Dr. M. Monsur Ali gave essential advice and discussion in all the steps of the project, assuring its success. Dr. Robert Pelton and Dr. Carlos Filipe provided insightful discussion about the fluorescence and paper-based techniques, to enrich the project design, experiments and data analysis.

The first draft was written by myself, with proofreading by Dr. M. Monsur Ali and Andres Krisch, and finished to its final version by Dr. Robert Pelton. This manuscript has been published in the Journal Colloids and Surfaces A: Physicochemical and Engineering Aspects, 2016.508: p. 192-196. DOI: [10.1016/j.colsurfa.2016.08.015](https://doi.org/10.1016/j.colsurfa.2016.08.015) Permission from © 2016 Elsevier B. V. All rights reserved.



## A simple assay for azide surface groups on clickable polymeric nanoparticles



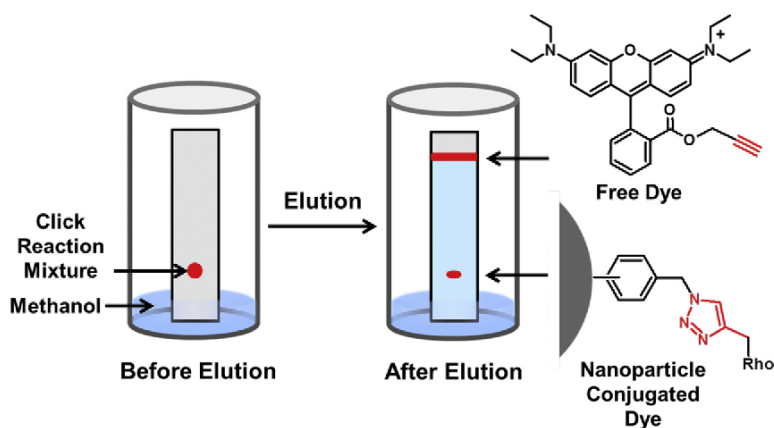
Carla Abarca, M. Monsur Ali, Devon Bowie, Robert H. Pelton\*

Department of Chemical Engineering, McMaster University, Hamilton, Ontario, L8S4L8, Canada

### HIGHLIGHTS

- Robust fluorescence quantification of azides on clickable nanoparticles.
- Conjugation of clickable Rhodamine.
- Paper chromatographic separation of free dye.

### GRAPHICAL ABSTRACT



### ARTICLE INFO

*Article history:*  
 Received 27 May 2016  
 Received in revised form 24 July 2016  
 Accepted 13 August 2016  
 Available online 23 August 2016

*Keywords:*  
 Clickable nanoparticles  
 Click reaction yield  
 Paper chromatography  
 Rhodamine alkyne

### ABSTRACT

The surface azide content of polymeric nanoparticles (latex) was measured in three steps: 1) conjugating an alkyne derivative of Rhodamine (Rho-Alk); 2) using paper chromatography to separate the immobile latex particles from unreacted fluorophore; and, 3) on-paper fluorescence quantification of the latex-bound Rho-Alk. Paper chromatography with methanol elution was effective because the nanoparticles did not migrate during elution, whereas the unreacted dye did. This assay can be used to estimate the coupling yield of any alkyne simply by conducting a second stage click reaction with Rho-Alk to determine the content of azides not consumed in the first click reaction.

© 2016 Elsevier B.V. All rights reserved.

### 1. Introduction

Clickable polymeric nanoparticles show promise for many applications including medical imaging [1] and as biosensor com-

ponents [2]. With a history going back to the 1950s, polymeric nanoparticles (latex, polymer colloids) are relatively easy to prepare. However, quantitative surface characterization remains a challenge. Particle surface chemistry always differs from the bulk polymer concentration, an analytical challenge that becomes more difficult with increasing particle diameter. For example, in lyophobic colloids, ionisable groups, representing a trivial mass fraction of hydrophobic polymers, accumulate on nanoparticle surfaces,

\* Corresponding author.  
 E-mail address: [peltonrh@mcmaster.ca](mailto:peltonrh@mcmaster.ca) (R.H. Pelton).



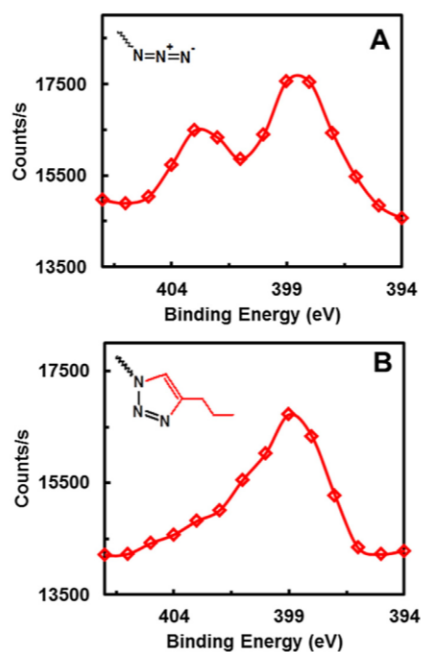


Fig. 1. XPS spectra narrowed for N1s region on SA-513: (A) functionalized azide nanoparticle before click reaction with pentyne, (B) functionalized triazole nanoparticle after click reaction with pentyne.

contributing to colloidal stability. We have been employing click chemistry [3–5] to prepare a large library of polystyrene copolymer nanoparticles for possible applications in mineral flotation [6]. For this work, we needed not only a library with large range of nanoparticle surface compositions, but also needed accurate values for the density of accessible surface azides, before and after click derivatization reactions. Several publications described the use of clickable fluorescent probes for azide characterization [7–9]. However, the published methods described extensive sample cleaning procedures before analysis. Herein, we describe the use of clickable probes, together with a simple paper chromatographic separation that gives rapid results suitable for a high throughput workflow.

## 2. Experimental

The preparation and characterization of several 4-vinylbenzylazide, poly(styrene-co-4-vinylbenzylazide) latexes, and Rhodamine-alkyne (Rho-Alk) [9] is described in the Supplementary materials file.

### 2.1. Click reaction between azide nanoparticles and rhodamine alkyne

In a typical experiment, a 2-mL glass vial was filled with water, 10  $\mu\text{L}$  of 1 mM copper sulfate, 10  $\mu\text{L}$  of 1 mM  $N,N,N',N',N''$ -pentamethyldiethylenetriamine (PMDETA) and 10  $\mu\text{L}$  of 10 mM sodium ascorbate, reagents that act as catalysts in the click reaction. The vial was mixed in a vortex mixer at 500 RPM for 10 s, and 100  $\mu\text{L}$  of 0.5 mM Rhodamine Alkyne solution was added to the vial. The mixture was shaken again in the vortex, and 50  $\mu\text{L}$  of 10 g/L nanoparticle dispersion was added to the vial, completing a total volume of 1000  $\mu\text{L}$ . After shaking the mixture for 10 s at 500 RPM in a vortex, the vial was placed in a 3D rocking shaker at 24 RPM with a tilt  $\pm 20^\circ$  (Benchmark Scientific Inc., Biomixer B3D1020) at room temperature. The reaction was monitored by paper chromatography over time intervals up to 7 days.

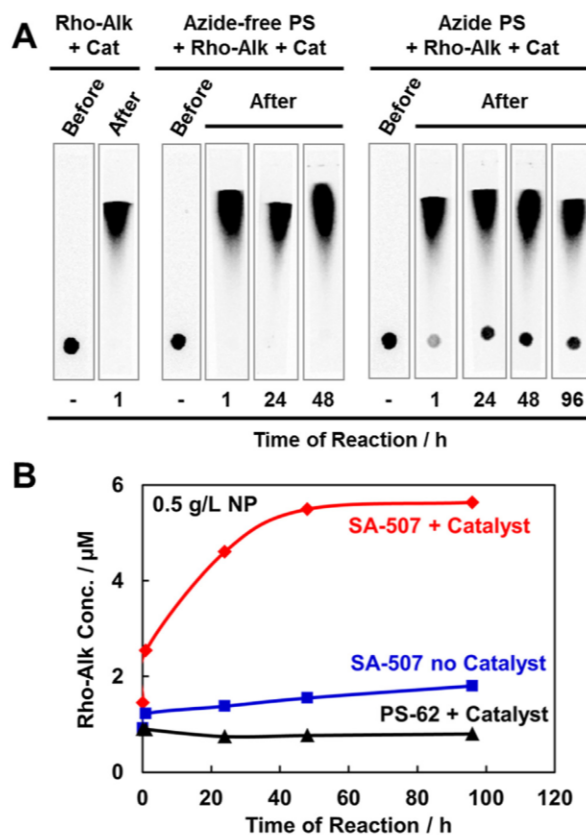


Fig. 2. (A) Fluorescent images from ChemiDoc™ for controls, azide-free polystyrene nanoparticles, and test azide coated nanoparticle samples at different time reaction intervals. (B) Influence of reaction time of fluorescence signal. Reactions were conducted in 0.01 mM copper sulfate, 0.01 mM PMDETA and 0.1 mM sodium ascorbate as the catalysis system.

### 2.2. Paper chromatography assay

In a typical experiment, Whatman #1 filter paper was cut in strips 7.6 cm long by 1.3 cm wide. 3  $\mu\text{L}$  of reaction sample was withdrawn from the click reaction vial using a 10  $\mu\text{L}$  micropipette and spotted 1.3 cm above the bottom of the filter paper strip. The strip was left to dry for 30 min. Then the strip was suspended in a 400 mL beaker filled with 25 mL of methanol 99.8% and covered with PARAFILM®. The elution was carried out for 15 min, then the strip was removed from the beaker and dried in a dark room for 30 min and imaged using a ChemiDoc fluorescent scanner. Details of the ChemiDoc scanning and the assay calibration are given in the Supplementary materials file.

### 2.3. X-ray photoelectron spectroscopy (XPS) experiments

Elemental surface characterization was conducted in samples before and after reaction with alkynes. Nanoparticles were deposited onto clean silicon wafers. Sample preparation details are given in the Supplementary information. X-ray photoelectron spectroscopy (XPS) was performed using a Physical Electronics (PHI) Quantera II spectrometer equipped with an Al anode source for X-ray generation, and a quartz crystal monochromator for focusing the generated X-rays. A monochromatic Al K- $\alpha$  X-ray (1486.7 eV) source was operated at 50W 15 kV. The system base pressure was no higher than  $1.0 \times 10^{-9}$  Torr, with an operating pressure that did not exceed  $2.0 \times 10^{-8}$  Torr. A pass energy of 280 eV and a dual beam

**Table 1**

Properties of poly(styrene-*co*-4-vinylbenzylazide) latexes. The 500 series was initiated with V50 whereas the 400 series was made with V44—Supplementary file for more details. The overall compositions were measured by  $^1\text{H}$  NMR, whereas surface azide content was from our new assay. Particle diameters and electrophoretic mobilities (EM) were measured in 5 mM NaCl. diameters.

Sample Designation	Azide Monomer, mg	Azide/Styrene Mole%	Solids Content, g/L	Diameter, nm (PDI)	EM, $\times 10^{-8} \text{ m}^2 \text{ s}^{-1} \text{ V}^{-1}$	Total Azide, $\lambda_{\text{Taz}}$ ( $\mu\text{mol/g}$ )	Surface Azide, $\lambda_{\text{SAz}}$ ( $\mu\text{mol/g}$ )
PS-62	/	/	43	62 (0.01)	3.3	/	/
SA-507	125	59.8	39	55 (0.05)	3.2	94.2	11.3
SA-508	125	60.4	40	62 (0.06)	2.6	94.2	10.8
SA-510	250	40.1	40	53 (0.06)	2.7	125.6	8.6
SA-511	375	50.2	38	53 (0.05)	2.4	245.0	12.6
SA-512	500	67.3	39	59 (0.07)	2.3	452.3	13.1
SA-513	750	46.8	48	59 (0.05)	3.2	471.1	13.2
SA-514	1000	37.8	49	57 (0.07)	2.7	521.4	14.6
PS-62-4	/	/	45	62 (0.04)	3.0	/	/
SA-402	125	62.5	46	53 (0.06)	2.1	100.5	12.2
SA-403	250	44.4	43	61 (0.03)	2.5	144.5	10.8
SA-404	375	49.0	44	54 (0.09)	2.4	238.7	15.4
SA-406	750	42.0	46	58 (0.02)	3.2	427.2	15.5
SA-410	1000	31.3	49	64 (0.03)	3.4	414.6	13.6

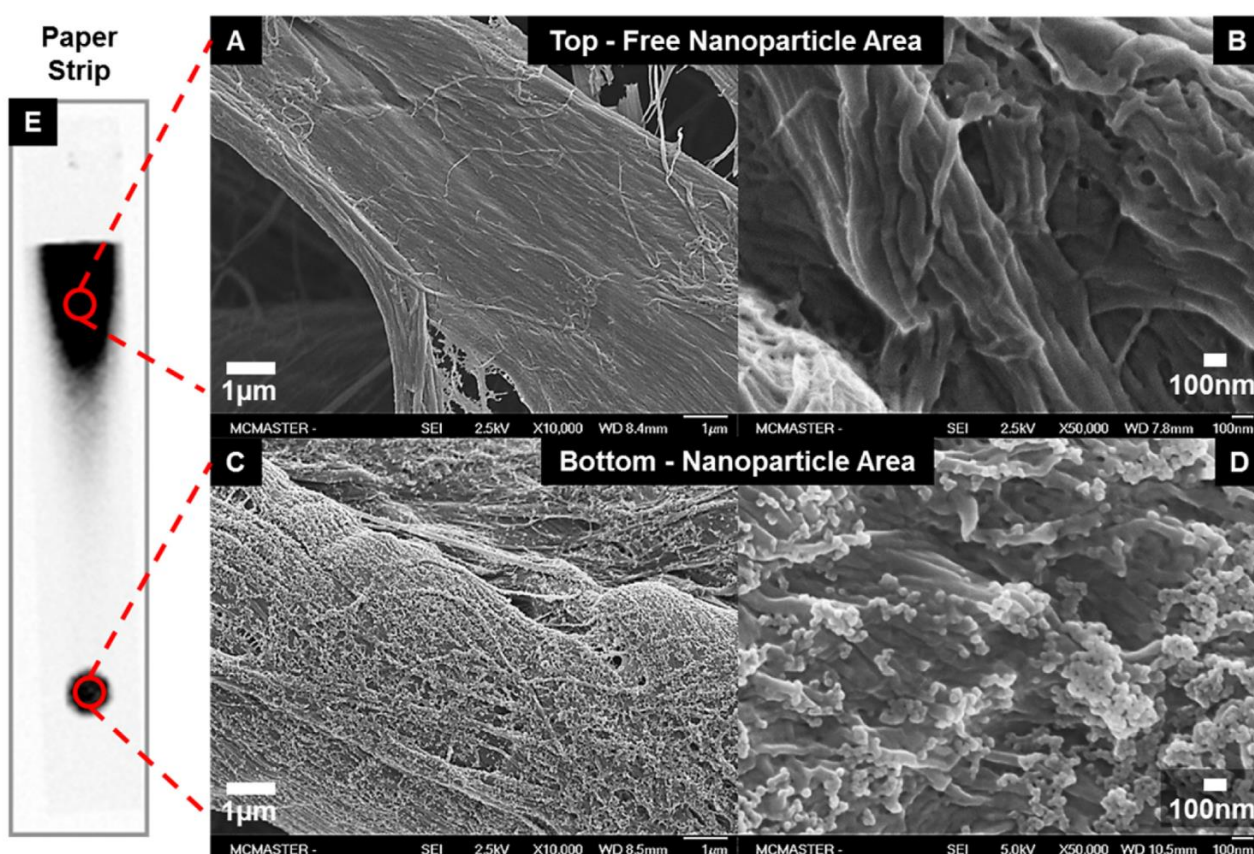


**Fig. 3.** Scanning Electron microscope micrographs of the top and bottom of paper strips. (A,B) Top dark area of strips, free of nanoparticles; (C, D) bottom spot of strip, decorated with fluorescent nanoparticles, (E) example of paper strips at 24 h of reaction of SA-507 + Rho-Alk + Catalyst.

charge compensation system for neutralization of all samples were used to obtain all survey spectra. Experiments were obtained at  $45^\circ$  and  $10^\circ$  take off angles to achieve a more surface sensitive detection. On average,  $45^\circ$  angle gave a detection depth of about 10 nm.

### 3. Results and discussion

We prepared two series of poly(styrene-*co*-4-vinylbenzylazide) latexes by emulsion copolymerization using starved azide

monomer addition. Synthesis of the azide monomer was based on Ouadahi's method [10]. Polymerization procedures are given in the Supplementary materials file, and the latex properties are summarized in Table 1. The total azide content, inside and on the surface of the nanoparticles, was measured by proton NMR and FT-IR.

High-resolution XPS measurements were performed before and after reaction with pentyne, and the results for the N1s region are shown in Fig. 1. The click reactions caused the high-energy peak at 403 eV, characteristic of the central nitrogen in the azide groups, to decrease, together with the enhancement of the peak at



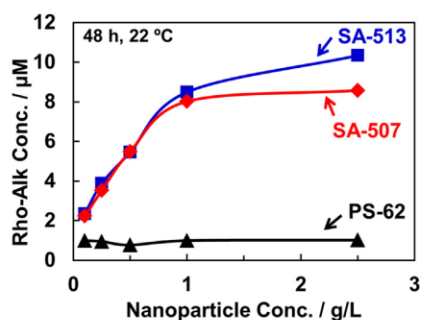


**Fig. 4.** The measured Rho-Alk content versus the concentration of added nanoparticle. Reactions were conducted for 48 h in 0.01 mM copper sulfate, 0.01 mM PMDETA, 0.1 mM sodium ascorbate, and 0.05 mM Rho-Alk.

399 eV, characteristic of the substituted triazole. These results mirror published XPS studies of click reactions [11] and they show that click reactions have occurred. From the low-resolution spectra, the atomic ratio of nitrogen to carbon decreased from 5.61% to 2.93% after the coupling of pentyne to the nanoparticle surface. XPS spectra for reactions of azide nanoparticle with Rhodamine Alkyne, and also the control, PS-62, with the fluorescent dye and pentyne, have been included in the Supplementary information. XPS gave qualitative evidence for the click reactions, but is not quantitative because, with a penetration depth of 10 nm, XPS probes only 35% of the volume of a layer of 61 nm particles. Measurement of the density of accessible surface azide groups requires another method.

Instead, we have developed an assay consisting of three steps: 1) conjugating an alkyne derivative of Rhodamine (Rho-Alk) to the surface azide moieties; 2) using ascending paper chromatography to separate the immobile latex particles from unreacted fluorophore; and, 3) on-paper fluorescence quantification of latex particles – see the abstract graphic.

To maximize the yield of accessible azide conversion to triazoles, the reaction conditions were systematically investigated. We chose a known active catalyst consisting of copper/sodium ascorbate and a ligand, PMDETA [12]. Excess of rhodamine alkyne was employed. The kinetics of the Rho-Alk click reaction with azide latex SA-507 were investigated. Fig. 2A illustrates fluorescent images of paper strips from the azide assay. The bottom dark spot in each paper strip indicates the fluorescent signal of the Rhodamine dye conju-

gated to the particles, while the top dark region denotes the free dye. The fluorescent signals from the dye-conjugated particles on the paper strips were quantified and plotted as a function of click reaction time, and shown in Fig. 2B. The aqueous click reaction at room temperature required 48 h to achieve maximum conversion, with no further reaction for up to 7 days.

Results from two negative controls are also shown, azide-free PS-62 that has no azide groups and a mixture of fluorescent dye and copper catalyst without nanoparticles. Neither control showed significant changes with time (Fig. 2B), demonstrating that physical adsorption or other artefacts were negligible.

Fig. 3 compares electron micrographs taken on the bottom spot with those taken in the upper fluorescence region on the paper chromatography strips. Clearly, the latex particles are concentrated on the bottom and did not travel with the unbound Rho-Alk. This is partially because the cationic latex naturally adheres to negatively charged paper, and partially because our nanoparticles would not disperse in methanol during chromatographic elution.

Table 1 includes the total azide contents of the particles, as well as the surface azide, determined by our assay. The surface azide densities ranged over 11–21 nm<sup>2</sup> per azide. Most of the added azide monomer was buried in the polymer particles and it was not accessible for reaction. Example calculations are available in the Supplementary materials file.

In developing the assay, it was necessary to optimize the nanoparticle and Rho-Alk concentrations. The total Rho-Alk dosages were chosen to be in the linear range of the calibration curve (Supplementary materials file). Fig. 4 indicates that a nanoparticle concentration of 0.5 g/L was within the linear range of the assay.

Our assay was used to compare the yields of four click reactions, and the results are summarized in Fig. 5. Yields were calculated from the differences between the initial surface azide concentrations and the corresponding azide concentration after the click reaction. The yields ranged from 33 to 47%, with the most hydrophobic reagent, pentyne giving the highest yield.

#### 4. Conclusions

In conclusion, our assay is simple, rapid and gave reproducible results with our azide-coated latexes. The main assumption in the assay, also made by others [7–9], is that the density of azides accessible for Rho-Alk is the same for other alkynes. The results in Fig. 5

#### A

Yield	SA-507	N-BocPrAm	PrAm	N-dMPrAm	Pentyne
Small Alkyne Reaction	0%	33%	40%	42%	47%
Rho-Alk Reaction	100%	67%	60%	58%	53%

#### B

Paper spot after 48 h Rho-Alk reaction

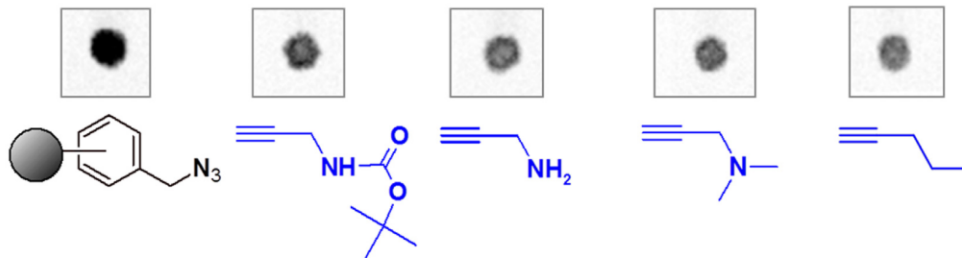


**Fig. 5.** (A) Sequential reactions results for the reaction of four small alkynes with SA-507, followed by the reaction between Rho-Alk and the partially reacted nanoparticle. (B) Paper spots after chromatography and chemical structure of alkynes.

support this assumption. If, for example, only a small percentage of surface azide groups were conjugated to Rho-Alk, we would expect at least one of the other alkynes in Fig. 5 to be more reactive than Rho-Alk, leaving no sites for subsequent Rho-Alk coupling – this was not the case.

A key advantage of our method is that it can be applied to any alkyne click reagent without optimizing an assay for each new reagent. Instead we optimized only the Rho-Alk coupling. In addition, the simple and rapid paper chromatographic sample preparation makes this assay particularly attractive when working with large nanoparticle libraries in high throughput workflows.

### Disclosure

The authors report no conflicts of interest in this work.

### Acknowledgments

The authors acknowledge useful discussions and technical assistance of Dr. Songtao Yang from AuTec Innovative Extractive Solutions Ltd., Dr. Berno from the McMaster Nuclear Magnetic Resonance (NMR) Facility, Danielle Covelli from the McMaster Biointerfaces Institute and Mr. Michael Kiriakou, undergraduate research assistant. We thank the National Sciences and Engineering Research Council of Canada (NSERC) and VALE Base Metals for funding this project. Some measurements were performed in the McMaster Biointerfaces Institute funded by the Canadian Foundation for Innovation. R.P. holds the Canada Research Chair in Interfacial Technologies. C. Abarca thanks the National Commission for Scientific and Technological Research of Chile, CONICYT – Becas Chile Scholarship program.

### Appendix A. Supplementary data

Supplementary data associated with this article can be found, in the online version, at <http://dx.doi.org/10.1016/j.colsurfa.2016.08.015>.

### References

- [1] E.Y. Sun, L. Josephson, R. Weissleder, Clickable nanoparticles for targeted imaging, *Mol. Imaging* 5 (2006) 122.
- [2] K. Welsler, M.D.A. Perera, J.W. Aylott, W.C. Chan, A facile method to clickable sensing polymeric nanoparticles, *Chem. Commun.* (2009) 6601–6603.
- [3] H. Nandivada, X. Jiang, J. Lahann, Click chemistry: versatility and control in the hands of materials scientists, *Adv. Mater.* 19 (2007) 2197–2208.
- [4] R. Berg, B.F. Straub, Advancements in the mechanistic understanding of the copper-catalyzed azide-alkyne cycloaddition, *Beilstein J. Org. Chem.* 9 (2013) 2715–2750.
- [5] S. Kantheti, R. Narayan, K.V.S.N. Raju, The impact of 1,2,3-triazoles in the design of functional coatings, *RSC Adv.* 5 (2015) 3687–3708.
- [6] C. Abarca, S. Yang, R.H. Pelton, Towards high throughput screening of nanoparticle flotation collectors, *J. Colloid Interface Sci.* 460 (2015) 97–104.
- [7] K. Zhu, Y. Zhang, S. He, W. Chen, J. Shen, Z. Wang, X. Jiang, Quantification of proteins by functionalized gold nanoparticles using click chemistry, *Anal. Chem.* 84 (2012) 4267–4270.
- [8] G. Yue, H. Ye, X. Huang, W. Ye, S. Qiu, B. Qiu, Z. Lin, G. Chen, Quantification of DNA through a fluorescence biosensor based on click chemistry, *Analyst* 139 (2014) 5669–5673.
- [9] R.H. Staff, J. Willersinn, A. Musyanovych, K. Landfester, D. Crespy, Janus nanoparticles with both faces selectively functionalized for click chemistry, *Polym. Chem.* 5 (2014) 4097–4104.
- [10] K. Ouadahi, E. Allard, B. Oberleitner, C. Larpent, Synthesis of azide-functionalized nanoparticles by microemulsion polymerization and surface modification by click chemistry in aqueous medium, *J. Polym. Sci. A: Polym. Chem.* 50 (2012) 314–328.
- [11] A.C. Gouget-Laemmel, J. Yang, M.A. Lodhi, A. Siriwardena, D. Aureau, R. Boukherroub, J.N. Chazalviel, F. Ozanam, S. Szunerits, Functionalization of azide-terminated silicon surfaces with glycans using click chemistry: XPS and FTIR study, *J. Phys. Chem. C* 117 (2013) 368–375.
- [12] M. Meldal, C.W. Tornøe, Cu-catalyzed azide-alkyne cycloaddition, *Chem. Rev.* 108 (2008) 2952–3015.

**Appendix: Supporting Information for Chapter 4****A Simple Assay for Azide Surface Groups on Clickable Polymeric Nanoparticles**

Carla Abarca, M. Monsur Ali, Devon Bowie and Robert H. Pelton\*

Appendix: Supporting Information for Chapter 4.....	78
Experimental Section.....	79
Materials .....	79
Synthesis of monomer 4-vinylbenzylazide (VBAz) .....	79
Emulsion polymerization of azide-coated nanoparticles .....	80
Synthesis of Rhodamine Alkyne (Rho-Alk) .....	80
Click reaction between azide nanoparticles and rhodamine alkyne .....	81
Imaging scanning of paper strips by ChemiDoc™ MP scanner.....	81
Calibration curve preparation .....	82
Sequential reactions of nanoparticles with small alkynes and rhodamine alkyne..	83
Scanning Electron Microscopy (SEM) in paper strips .....	84
Nuclear Magnetic Resonance (NMR) .....	85
X-ray photoelectron spectroscopy (XPS).....	86
Miscellaneous Calculations .....	87
Calculations of total azide content by <sup>1</sup> H-NMR .....	87
Calculations of surface azide content by paper chromatography .....	88
Calculations of theoretical surface azide density ( $\lambda$ S).....	88
References Appendix Chapter 4.....	90

## Experimental Section

### *Materials*

All the reagents were purchased in Sigma Aldrich unless otherwise noted. In the fabrication of nanoparticles and synthesis of monomers, Styrene (99%) and 4-vinylbenzylchloride (90%) were purified using distillation. Sodium azide (99%) and sodium iodide (99%) were used without previous purification. 2,2'-Azobis(2-methylpropionamide) dihydrochloride (V50) (97%) and 2,2'-Azobis[2-(2-imidazolin-2-yl)propane]dihydrochloride (V44) (Wako Pure Chemical Industries, Ltd., 98%) were used as cationic initiators, and cetyl trimethylammonium bromide (CTAB) (99%) as surfactant. In the synthesis of a fluorescent alkyne, Rhodamine B (95%), 4-dimethylaminopyridine (DMAP) (99%), propargyl alcohol (99%), N,N'-Dicyclohexylcarbodiimide (DCC) (99%), were used without previous purification. In click reactions, copper sulfate (99%), N,N,N',N'',N''-pentamethyldiethylenetriamine (PMDETA) (98%) and (+)-Sodium L-ascorbate (98%) were used as catalyst system. Other solvents and reagents such as sodium bicarbonate (99.5%), anhydrous magnesium sulfate (97%), dimethyl sulfoxide (DMSO) (Caledon, 99.9%) and anhydrous diethyl ether (Caledon, 99%), dichloromethane (Caledon, 99.5%) and water type 1 (as per ASTM D1193-6<sup>[1]</sup>, resistivity 18 M $\Omega$ -cm) were used in all experiments.

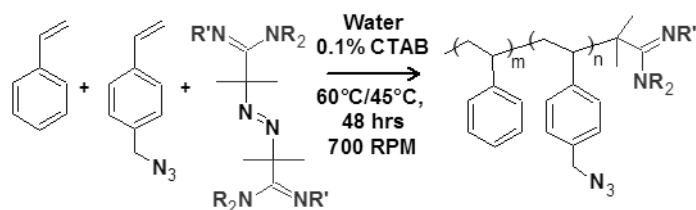
### *Synthesis of monomer 4-vinylbenzylazide (VBAz)*

The monomer was prepared by following Ouadahi et al<sup>[2]</sup> procedure with modifications. In a 50 mL 1-neck round bottom flask 10.2 g of sodium azide and 0.58 g of sodium iodide were slowly added to mixture of 5.95 g of 4-vinylbenzylchloride and 25 mL of DMSO. The reaction was stirred at room temperature for 24 hours. The reaction products were extracted in a separatory funnel with 100 mL of water and 100 mL of ether. The organic phase was washed two more times with 100 mL of water. The organic phase was dried with anhydrous magnesium sulfate and filtered by vacuum filtration. Organic solvents were evaporated under vacuum in a rotavapor at room temperature resulting in yellow oil (5.64 g, 94%). This product was analyzed by FT-IR and proton NMR. Relevant signals: at FT-IR (diamond crystal): 2092 (azide peak), 1288, 1250, 822 cm<sup>-1</sup>. <sup>1</sup>H-NMR (600 MHz, CDCl<sub>3</sub>):  $\delta$  7.43 (d, 2H, Ar-H),  $\delta$  7.28 (d, 2H, Ar-H),  $\delta$  6.73 (dd, 1H, CH=C),  $\delta$  5.77 (dd, 1H, C=CH<sub>2</sub>),  $\delta$  5.28 (dd, 1H, C=CH<sub>2</sub>),  $\delta$  4.32 (s, 2H, CH<sub>2</sub>N<sub>3</sub>).

### *Emulsion polymerization of azide-coated nanoparticles*

Two series of azide nanoparticles were synthesized by changing the initiator and the reaction temperature. V50 was used in polymerizations at 60 °C (500 series), while V44 was used for polymerizations conducted at 45 °C (400 series). In all cases, nanoparticles were fabricated in a 250 mL three-neck round-bottom flask connected to a condenser, under a nitrogen stream. A hot plate/magnetic stirrer (RCT IKAMAG, IKA-Werke GmbH & Co. KG) equipped with an IKA ETS-D5 temperature controller was used to regulate temperature and stirring (750 RPM). In a typical experiment, 100 mL of water was added to the reactor containing 0.1 g of CTAB surfactant and 0.1 g of initiator, and purged with a nitrogen stream for 30 minutes. Subsequently, 0.5 mL of styrene was added to start polymerization. After 15 minutes, the rest of the styrene (4.5 mL) was added in a monomer-starved semi-batch configuration with a monomer addition rate of 1 mL/h, using a 5 mL syringe fitted to a syringe pump (NE-1600, New Era Pump System Inc. ). At approximately 4 hours of reaction, a determined amount of VBAz and 0.01 g of initiator dissolved in 0.4 mL of water were added using two -a 3 and 1 mL- syringes fitted to the syringe pump. The reaction was stopped after 48 hrs. Table 1 in the paper summarizes the latex properties.

**Figure A 4-1:** Polymerization of Azide-coated nanoparticles



### *Synthesis of Rhodamine Alkyne (Rho-Alk)*

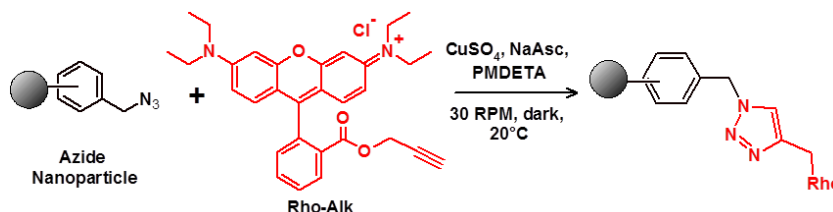
Alkyne functional groups were introduced onto Rhodamine B following a reported protocol by Staff and colleagues<sup>[3]</sup> with some modifications. 9.5 g of Rhodamine B, 0.024 g of 4-dimethylaminopyridine (DMAP) were added to a dried 3-neck round bottom flask with a stir bar. The mixture was purged in nitrogen for 30 minutes, and 1.27 mL of propargyl alcohol and 90 mL of dichloromethane were added. The flask was cooled to 0° C with an ice bath before adding 8.3 g of N,N'-dicyclohexyl carbodiimide (DCC) dissolved in 10 mL of dichloromethane. The mixture was stirred at 300 RPM for 30 minutes and then allowed to stir for 24 h at room temperature. The resulting mixture was filtered through a gravity funnel and washed in dichloromethane until approximately 200

mL of solution was obtained. The solution was added to a 500 mL separatory funnel and washed 2 more times with 200 mL of saturated sodium bicarbonate. A final wash step was conducted with water. The organic phase was collected and was dried overnight with magnesium sulfate. Vacuum filtration with a fritted glass funnel was used to remove the magnesium sulfate. The remaining dichloromethane was evaporated in a vacuum rotavap. The residue was re-dissolved in acetonitrile and re-precipitated in diethyl ether 3 times and filtrated by vacuum filtration in a ceramic funnel provided with a Whatman #1 filter paper. The residue was washed 3 times in diethyl ether and dried in a vacuum oven overnight. 5.1 g of a golden powder were produced (45%, relevant bands: atr FT-IR: 3322.9  $\text{cm}^{-1}$  alkyne band).

### Click reaction between azide nanoparticles and rhodamine alkyne

The reaction was monitored by paper chromatography, as explained in the article related to this supporting information.

**Figure A 4-2:** Reaction between an azide nanoparticle and Rhodamine Alkyne to produce a fluorescent triazole nanoparticle.



### Imaging scanning of paper strips by ChemiDoc™ MP scanner

A fluorescent imaging scanning system was used for determining the fluorescence intensity of the eluted paper strips. In a typical experiment, the paper strips are placed on top of a sample tray in the darkroom of a ChemiDoc™ MP imaging system (Biorad, nr. 170-8280) equipped with a supercooled CCD detector, several light sources and illuminators. The strips are scanned by using the Image Lab™ 4.1 software with the protocol *Rhodamine*, with a Green Epi illumination 520±50 nm excitation source, a 605±50 nm emission filter and automatic exposure time. To aid visual sensitivity, inverted images are presented, with a gray fluorescence signal on a white background. The fluorescence intensity of the gray spots at the bottom (conjugated rhodamine-nanoparticle) was obtained from a ChemiDoc™ image. To obtain quantitative



information for the amount of azide groups that reacted with Rhod-Alk, a calibration graph was made as described below.

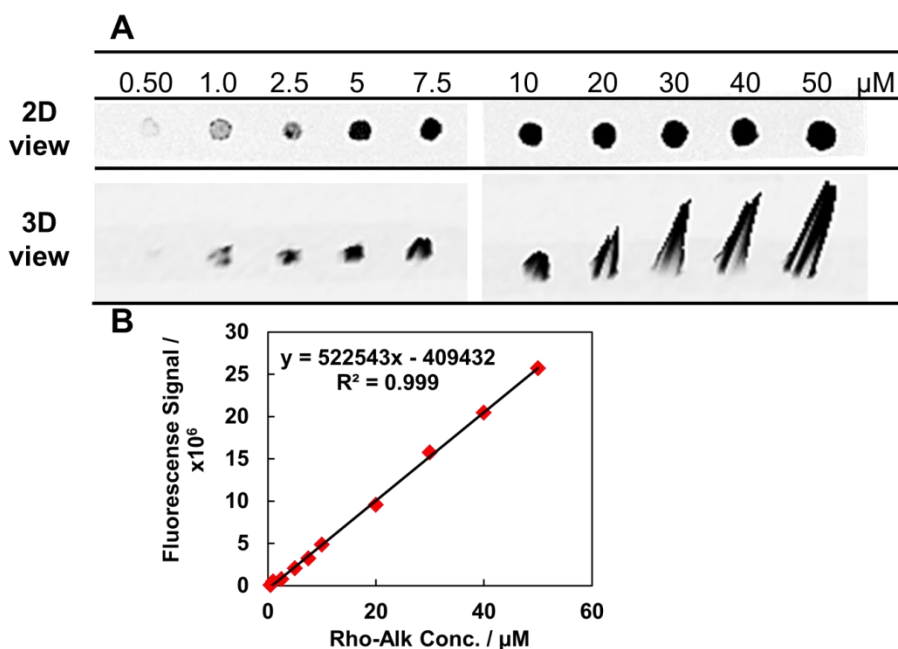
### **Calibration curve preparation**

10 stock solutions of Rhodamine-Alk at concentrations of 0.5, 1.0, 2.5, 5.0, 7.5, 10.0, 20.0, 30.0, 40.0, 50.0  $\mu\text{M}$  were prepared in water and 3  $\mu\text{L}$  of each solution was spotted in a paper strip starting from lower to higher concentrations (Figure A 4-3). The strip was left in the dark for 30 minutes to dry. The strip was scanned for fluorescence by the ChemiDoc™ scanner as described in the previous section. The calibration paper strip was scanned along with test strips every time a new image was taken.

The fluorescence intensity on each spot (test strips and calibration curve paper strip) was quantified by using Image Lab™ 4.1 software, in which the pictures were presented in a 2D view (fluorescent stain in a flat paper) and 3D view (fluorescent peak in a flat paper) (Figure A 4-3A). The 3D view option in the software allows seeing more clearly the increasing fluorescent signal, even though it does not have any effect in the fluorescence intensity results.

For each image, the fluorescent intensity values on each spot or stain were obtained by Image Lab™ 4.1, and plotted against the concentration of Rhodamine, obtaining a graph (and a linear regression equation) by Microsoft® Excel Software. In the fitted curve,  $y$  represents the fluorescence signal from ChemiDoc™, while  $x$  is the rhodamine alkyne concentration (Figure A 4-3B). The fluorescent amount obtained from the conjugated Rhodamine on PS beads was fit into this calibration to determine the amount of Rho-Alk on the beads. Note: since fluorescence is relative (ChemiDoc™ uses an auto-gain setting for intensities), a calibration curve equation was calculated for each experiment to avoid any false quantitative value.

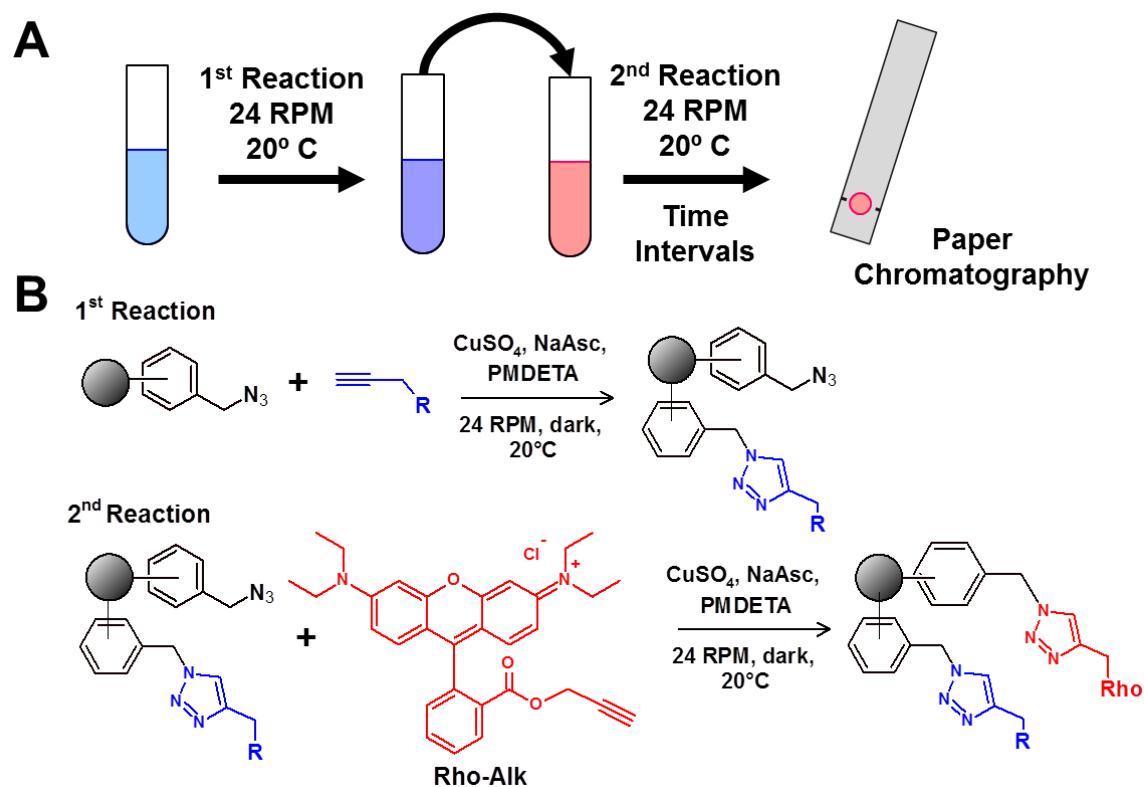
**Figure A 4-3:** A) 2D and 3D view of a ChemiDoc™ image for an internal calibration curve paper strips (produced by the software Image Lab™). B) Example of a calibration curve calculated in Microsoft® Excel, which has been obtained from the quantified fluorescence intensities by the software Image Lab™



### Sequential reactions of nanoparticles with small alkynes and rhodamine alkyne

Monitoring the reaction rates of non-fluorescence and small alkynes was needed as part of our nanoparticle collectors' library characterization. As explained in the article associated, we propose to monitor the reaction rates by using sequential reactions of nanoparticles with alkynes. As shown in Figure A 4-4, the first reaction will be conducted between a specific nanoparticle and non-fluorescent alkyne in click conditions. Volumes of this reaction will be withdrawn at different time intervals and dispensed in a new vial to continue with a second click reaction, between the partially reacted nanoparticles and Rho-Alk. Then, paper chromatography assays were conducted and the yield of the first reaction is simply calculated by subtracting the yield of the second reaction to a control nanoparticle reaction that has not being reacted with the small alkyne. Figure A 4-4A illustrates this idea in a scheme, while Figure A 4-4B shows the chemical reactions involved in this process.

**Figure A 4-4:** Sequential reactions pathway of nanoparticles with small alkynes in the first reaction and Rho-Alk in the second reaction. A) Pathway scheme; B) Chemical reactions involved on each step.



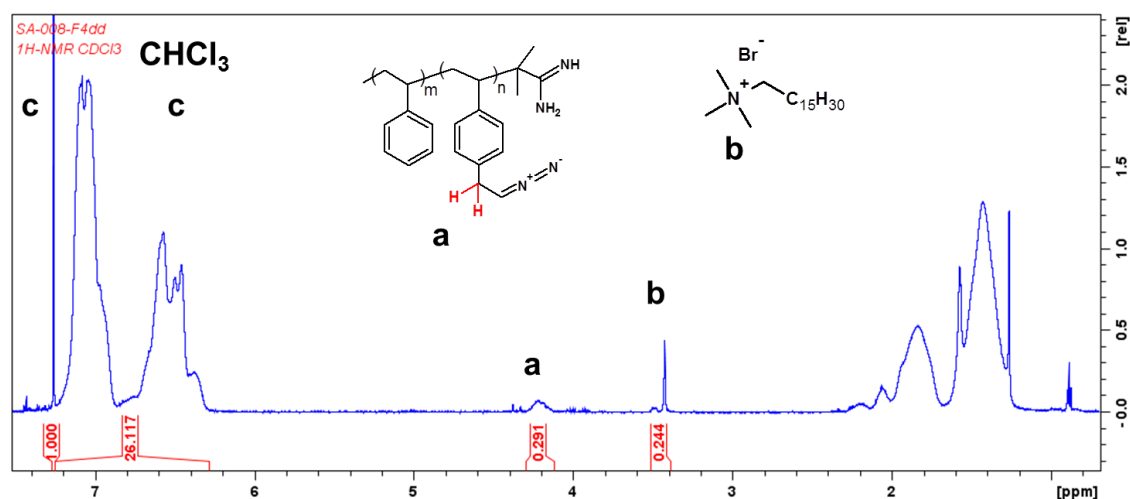
### Scanning Electron Microscopy (SEM) in paper strips

Selected paper strips were taken after chromatography and the regions of interest (fluorescent regions at bottom and top of strips) were carefully cut in small rectangular pieces of 4 x 4 mm and 4 x 1 mm (for cross-section view). The paper samples were pasted onto a stainless steel stubs with a conductive carbon tape, and some of the edges of the paper were coated with a thin layer of silver coating and dried at 50° C for 1 hour. The samples were then sputter coated under vacuum with a thin layer of 5 nm of platinum. Photographs of the paper samples were acquired by a JEOL JSM-7000F SEM equipped with a Schottky Field Emission Gun (FEG) filament with an accelerating voltage of 2.8 keV. Afterwards, SEM photographs were digitized using JEOL image processing software.

## Nuclear Magnetic Resonance (NMR)

$^1\text{H}$ -NMR spectra were obtained in all the nanoparticle samples to calculate the total azide content on each nanoparticle.  $^{13}\text{C}$ -NMR, 2D-HSQC and 2D-HMBC were acquired in selected nanoparticles to confirm the azide moieties and CTAB peak assignments on the samples. The azide peak was found between 4.2 – 4.0 ppm, while the CTAB peak was found between 3.45 – 3.30 ppm. The rest of the peaks correspond to polystyrene peaks, occluded water or chloroform peak from the solvent. In a typical experiment, a measured amount between 10-15 mg of dry sample was dissolved in 1 mL of deuterated chloroform,  $\text{CDCl}_3$ , and measured in a 600 MHz NMR spectrophotometer at 25 °C. The nanoparticles with a high concentration of azide needed longer time to dissolve in chloroform and in some cases mild sonication was required. Example spectrum is illustrated in Figure A 4-5.

**Figure A 4-5:** Example of  $^1\text{H}$ -NMR spectrum for an azide-coated nanoparticle, SA-008



### X-ray photoelectron spectroscopy (XPS).

Elemental surface characterization was conducted in samples before and after reaction with alkynes. Nanoparticles were deposited onto clean silicon wafers. Sample preparation: In a typical experiment, a silicon wafer of 1 cm<sup>2</sup> was cleaned in a UV-Ozone chamber for 5 minutes, followed by immersing in a solution of 2% sodium dodecyl sulfate (SDS) for 30 min. The wafer was rinsed and sonicated in MilliQ water for 10 min, dried with a nitrogen stream, and inserted again in a UV-Ozone chamber for 5 minutes. A 10 µL drop of a 0.5 g/L nanoparticle solution in water was dispensed in the recently cleaned wafer and dried in an argon stream. A typical XPS spectrum is presented in Figure A3- 1.

**Figure A 4-6:** Example of XPS spectrum for an azide coated nanoparticle, SA-513

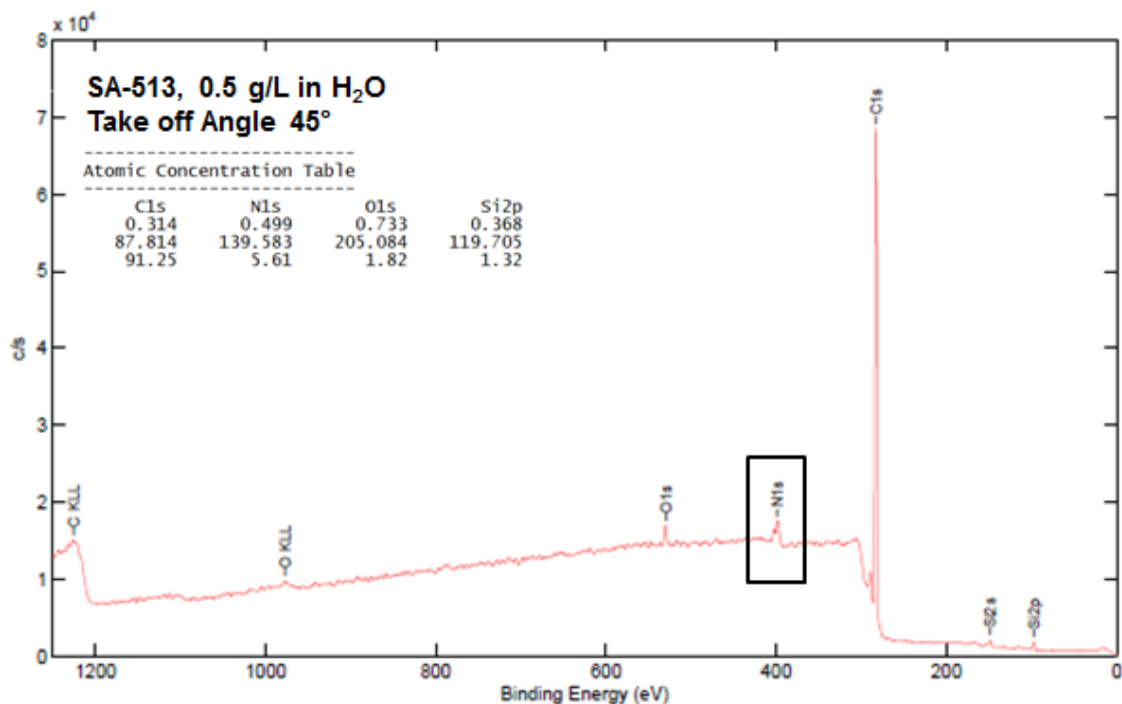


**Figure A 4-7:** XPS spectra narrowed for N1s region on SA-513: A) functionalized azide nanoparticle before click reaction with Rhodamine Alkyne, B) functionalized triazole nanoparticle after click reaction with Rhodamine Alkyne

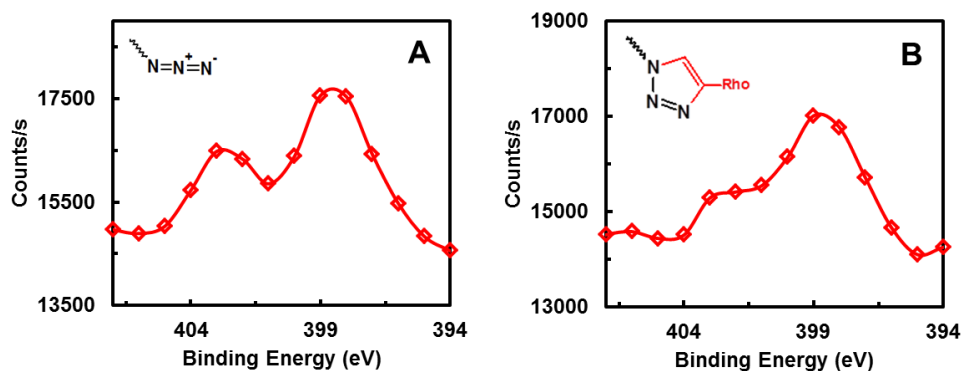
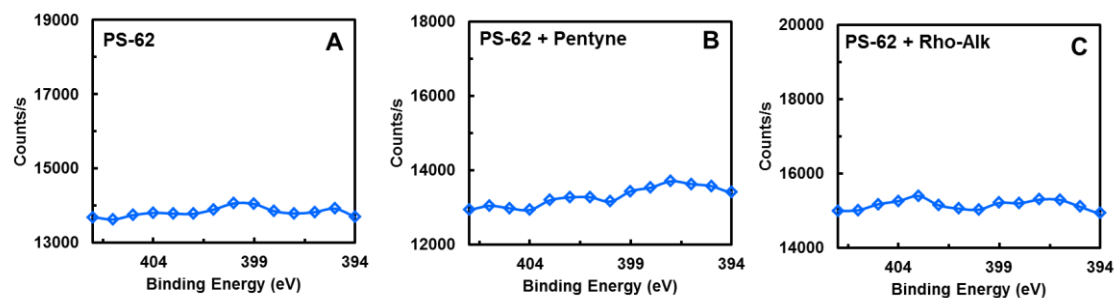


**Figure A 4-8:** XPS spectra narrowed for N1s region on azide-free PS-62: A) azide-free nanoparticle, B) free-azide nanoparticle after click reaction with pentyne, C) free-azide nanoparticle after click reaction with Rhodamine Alkyne



## Miscellaneous Calculations

### *Calculations of total azide content by $^1\text{H-NMR}$*

Azide proton peaks were obtained from nanoparticle spectra at  $\delta$  4.32 (s, 2H,  $\text{CH}_2\text{N}_3$ ). As a reference, we used a signal of 0.02% of  $\text{CHCl}_3$  solvent. The Azide/Styrene mass ratio was calculated since total mass and molecular weights of compounds are known by using Equation A 4-1.

$$\zeta_{Az} = \frac{I_{Azide} MW_{Azide} H_{St}}{I_{St} MW_{St} H_{Azide}} [\%] \quad \text{Equation A 4-1}$$

### *Calculations of surface azide content by paper chromatography*

From the molar concentration of conjugated Rhodamine Alkyne ( $M_{Rho}$ ) obtained from the ChemiDoc™ images and an internal calibration curve on each picture, the surface azide content is calculated as shown in Equation A 4-2, by assuming that the fluorescent dye has reacted 1:1 with the azide moieties available at the surface of the nanoparticle.

$$\lambda_{SAz} = \frac{M_{Rho} V_T}{m_{NP} V_{NP}} \left[ \frac{\mu mol}{g} \right] \quad \text{Equation A 4-2}$$

In where  $V_T$  is the total volume of solution,  $V_{NP}$  is the volume of nanoparticle in the reaction and  $m_{NP}$  is the initial mass concentration of nanoparticle. From the surface azide content obtained in Equation A 4-2 and the specific surface area of the nanoparticle ( $\sigma_{NP}$ ), the surface azide units per area ( $\Gamma_{SAz}$ ) can be calculated.

### *Calculations of theoretical surface azide density ( $\lambda_S$ )*

A theoretical value of the surface density of azide groups based on the total azide content of the nanoparticles was calculated by assuming that azide groups are uniformly distributed in the nanoparticles, and a defined surface zone of thickness,  $\delta$ , of 0.25 nm, is accessible to our surface measurement assay. Considering the nanoparticles as round spheres, the theoretical surface azide density is given by Equation A 4-3.

$$\lambda_S = \frac{\Gamma_S \sigma_{NP}}{N_A} \left[ \frac{\mu mol}{g} \right] \quad \text{Equation A 4-3}$$

In which, the theoretical surface azide units per area ( $\Gamma_S$ ) is defined by Equation A 4-4, the specific surface area of the nanoparticle ( $\sigma_{NP}$ ) is defined by Equation A 4-5, and  $N_A$  is the Avogadro's number.

$$\Gamma_S = \delta \cdot \rho \cdot \lambda_{TAz} \cdot N_A \left[ \frac{1}{m^2} \right] \quad \text{Equation A 4-4}$$

$$\sigma_{NP} = \frac{4\pi \left(\frac{d_{NP}}{2}\right)^2}{\frac{4}{3}\pi \left(\frac{d_{NP}}{2}\right)^3 \rho} \left[ \frac{m^2}{g} \right] \quad \text{Equation A 4-5}$$

In here,  $\rho$  is the density of latex nanoparticles,  $d_{NP}$  diameter of nanoparticles (obtained by dynamic light scattering), and  $\lambda_{TAz}$  is the total azide density, obtained from  $^1\text{H-NMR}$ .

**Table A 4-1:** Surface and total content of azide from paper chromatography results, unless otherwise noted. Experiments at 96 hrs, 0.5 g/L nanoparticle concentration, and 10  $\mu\text{L}$  of catalyst.

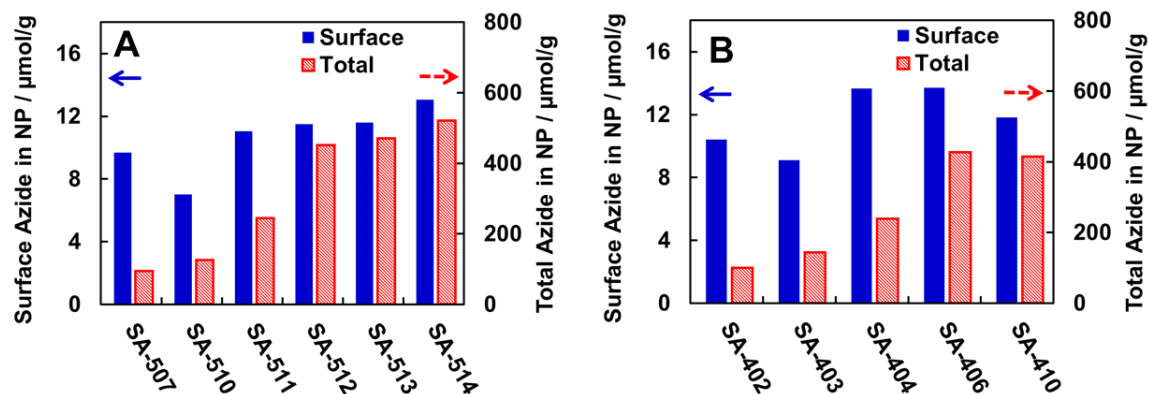
Nanoparticle	Azide/ Styrene (% wt/wt) <sup>a</sup>	Total Azide, $\lambda_{TAz}$ ( $\mu\text{mol/g}$ ) <sup>a</sup>	Theoretical Surface Azide, $\lambda_S$ ( $\mu\text{mol/g}$ )	Experimental Surface Azide, $\lambda_{SAz}$ ( $\mu\text{mol/g}$ ) <sup>b</sup>	Surface Azide Units/Area, $\Gamma_{SAz}$ (/nm <sup>2</sup> )	Area/ Surface Azide Units (nm <sup>2</sup> )
PS-62	/	/	/	/	/	/
SA-507	1.50	94.2	2.58	11.3	0.065	15.4
SA-508	1.51	94.2	2.26	10.8	0.071	14.1
SA-510	2.00	125.6	3.50	8.6	0.048	21.0
SA-511	3.76	245.0	6.90	12.6	0.070	14.3
SA-512	6.73	452.3	11.50	13.1	0.081	12.3
SA-513	7.02	471.1	11.90	13.2	0.082	12.1
SA-514	7.56	521.4	13.80	14.6	0.087	11.5
PS-62-4	/	/	2.85	/	/	/
SA-402	1.56	100.5	3.58	12.2	0.068	14.7
SA-403	2.22	144.5	6.61	10.8	0.069	14.5
SA-404	3.68	238.7	9.72	15.4	0.088	11.4
SA-406	6.30	427.2	10.97	15.5	0.095	10.5
SA-410	6.26	414.6	2.85	13.6	0.092	10.9

<sup>a</sup> Obtained by  $^1\text{H-NMR}$ .

<sup>b</sup> Obtained by Paper Chromatography Assay.



**Figure A 4-9:** Surface azide content vs. Total azide content for two series of nanoparticles. A) series of azide nanoparticles prepared with V50; B) series of azide nanoparticles prepared with V44 as initiator. Results from experiments conducted at 96 h and 0.5 g/L nanoparticle concentration.



#### References Appendix Chapter 4

- [1] ASTM, *D1193 - 06 Standard Specification for Reagent Water*. ASTM Standard Manual. 2006 (2011), West Conshohocken: ASTM International. 6.
- [2] Ouadahi, K., E. Allard, B. Oberleitner, and C. Larpent, *Synthesis of azide-functionalized nanoparticles by microemulsion polymerization and surface modification by click chemistry in aqueous medium*. *Journal of Polymer Science Part A: Polymer Chemistry*, 2012. **50**(2): p. 314-328.
- [3] Staff, R.H., J. Willersinn, A. Musyanovych, K. Landfester, and D. Crespy, *Janus nanoparticles with both faces selectively functionalized for click chemistry*. *Polymer Chemistry*, 2014. **5**(13): p. 4097.

## **Chapter 5: High Throughput Screening of Click Nanoparticle Collectors: a Platform for Modular Functionalization**

---

In Chapter 5, the project design, experiments and data analysis were conducted nearly completely by myself. Michael Kiriakou (undergraduate student) aided with some flotation of azide nanoparticle experiments. Dr. M. Monsur Ali assisted with important advice, discussion and support with some laboratory techniques. Dr. Pelton contributed with vital discussion advice throughout the whole project, especially in the design and development and analysis of the stability model for the high throughput techniques developed.

This chapter was written by myself, and proofread by Dr. M. Monsur Ali and Andres Krisch. Final revisions and proofreading were kindly provided Dr. Robert Pelton. The manuscript version of this chapter is being prepared for publication in 2017.

# High Throughput Screening of Click Nanoparticle Collectors: a Platform for Modular Functionalization

*Carla Abarca, M. Monsur Ali, and Robert H. Pelton\**

Department of Chemical Engineering, McMaster University, Hamilton, Ontario, Canada  
L8S4L8

CORRESPONDING AUTHOR: peltonrh@mcmaster.ca

**KEYWORDS** Nanoparticle Collectors, azide, triazole nanoparticles, Click chemistry, high throughput screening, colloidal stability maps, flotation, automated contact angle, automated dip coating

## 5.1. Abstract

High throughput techniques have been applied to fabricate azide nanoparticles with a wide variety of alkyne molecules with different chemical composition via click chemistry. These nanoparticles were analyzed and used as collectors for froth flotation of glass beads, a mineral model. Starting with a few parent azide nanoparticles, we achieved the parallel production of triazole compounds with diverse chemical moieties, ranging from hydrophobic hexane-terminated nanoparticles to hydrophilic amine-terminated PEG chains materials.

Two normally antagonizing requirements to function as collectors, hydrophobicity and colloidal stability, were screened by using a high throughput colloidal stability assay and an automated hydrophobicity assay. A colloidal stability map revealed the most promising nanoparticle candidates that were chosen for flotation experiments. The library of triazole compounds obtained from click chemistry presented a wide range of critical coagulation concentrations and contact angle values.

The automated contact angle assay was conducted in a multiwell plate format where glass slides were dip coated with nanoparticle dispersion. The automated dip coating multiwell format assay was also compared to the automated spot coating method. The dip coating multiwell plate assay was found to be more reproducible and give a more uniform coating. We were able to fabricate and reproducibly measure nanoparticles with contact angles ranging from 62 to 101 degrees from a single parent nanoparticle, by changing the density and click reagent chemical features.

Among the triazole nanoparticles, six fell into the flotation domain of the colloidal stability map. Their flotation performance was tested in alkaline media glass beads. Five of them showed improved glass beads recovery, demonstrating that colloidal stability maps can function as a screening framework to rapidly predict promising nanoparticle collectors for froth flotation.

## 5.2. Introduction

The development of high throughput screening techniques for rapidly measuring physicochemical properties in materials has gained interest in the last few years<sup>[1]</sup>. Such techniques have provided the most benefits in drug discovery for rapidly screening possible target molecules<sup>[2, 3]</sup>. These techniques have also been used as powerful tools for polymer science researchers, since they allow the quick screening of multiple compounds to find desired chemical and physical properties for an application<sup>[4, 5]</sup>.

Our application involves the screening of polystyrene nanoparticle candidates that can act as collectors for metal-enrichment of minerals through flotation<sup>[6]</sup>. Our previous studies have shown that an efficient nanoparticle collector must meet requirements, including being hydrophobic, being colloidally stable, being selective, being small and being adhesive<sup>[7, 8, 9]</sup>. In a preceding publication we introduced the idea of combining critical coagulation concentrations and contact angles of nanoparticles as criteria for identifying the best candidates for flotation<sup>[10]</sup>.

We analyzed a nanoparticle library of hydrophilic nanoparticles collectors and concluded that hydrophilic modifications of nanoparticles with long PEG chains generate too hydrophilic nanoparticles, even at low surface densities<sup>[10]</sup>. Hydrophilic nanoparticles are very stable in the flotation buffer but they do not promote flotation. We recently published a high throughput colloidal stability test for analyzing nanoparticles with a wide range of diameters<sup>[11]</sup>.

Another important requirement is the hydrophobicity of the nanoparticle, since collectors should promote the bubble-mineral attachment by changing the surface of the mineral. For screening, a quick and automated contact angle technique was needed. A few methods to measure contact angles in a high throughput manner have been published<sup>[12, 13]</sup>. However, most of the approaches did not implement automated techniques for the sample preparation. In our process, we have analyzed and implemented an automated dip coating technique for sample preparation, followed by automatic contact angle measurements to achieve this goal.

Post modification of nanoparticles with a variety of chemical surfaces seems to be a more effective route than directly synthesizing each surface-modified nanoparticle, optimizing materials consumption, time and instrumentation, in the search of nanoparticles with desired physicochemical properties<sup>[14]</sup>. High throughput screening and combinatorial chemistry are usually combined for achieving rapid and automated surface functionalization in nanoparticles<sup>[15]</sup>, and Click chemistry has shown to be a fundamental tool for researchers in this field<sup>[16]</sup>.

Sharpless *et al.*<sup>[17]</sup> defined Click chemistry as series of carbon-heteroatom chemical reactions that are characteristic because: they are highly modular or customizable, they are stereospecific, they give by-products that can be removed by non-chromatographic procedures and they can be done in mild reaction conditions. In our nanoparticle collectors development we used copper-catalyzed Huisgen 1,3-dipolar cycloaddition<sup>[18]</sup> of terminal alkynes to azide nanoparticles. Triazole nanoparticles could increase the colloidal stability without excessively compromising hydrophobicity, and they could also coordinate with nickel sulfide minerals as chelating agents, in similarity to imidazole collectors<sup>[19]</sup>.

In this manuscript we present investigations on a nanoparticle collectors' library produced via Click reactions and its parallel fabrication, along with the screening of the nanoparticles colloidal stability and hydrophobicity with high throughput and automated methods in order to find the most promising candidates for froth flotation.

### 5.3. Experimental

**Materials.** All the reagents were purchased from Sigma Aldrich unless otherwise noted. For the synthesis of parent azide nanoparticles, Styrene (99%) was purified using distillation. 2,2'-azobis(2-methylpropionamidine) dihydrochloride (V50) (97%) and 2,2'-azobis[2-(2-imidazolin-2-yl)propane]dihydrochloride (V44) (Wako Pure Chemical

Industries, Ltd. , 98%) were used as cationic initiators, and cetyl trimethylammonium bromide (CTAB) (99%) as surfactant. Copper sulfate (99%) (CuSO<sub>4</sub>), N,N,N',N'',N'''-pentamethyldiethylenetriamine (PMDETA) (98%) and (+)-sodium L-ascorbate (98%) (NaAsc) and sodium carbonate (99%), were used without previous purification. Water type 1 (as per ASTM D1193-6<sup>[20]</sup>) was used in all experiments.

The alkynes structures shown in Figure 5-3 are: propargylamine (PrAm), N,N-dimethyl propargylamine (N-dMPrAm), N-boc-propargylamine (BocPrAm), pargyline (or N-Methyl-N-propargylbenzylamine) (Parg), rhodamine alkyne (RhoAlk), amino-PEG4-alkyne (AmPEG4), alkyne-PEG4-maleimide (PEG4MI), 1-pentyne (Pen), 1-hexyne (Hex), propargyl bromide (PrBr) (80% in toluene), 4-bromo-1-butyne (BrBu), propargyl alcohol (PrOH), and 3-butynyl tosylate (or 3-butynyl p-toluenesulfonate) (BuTos), and they were used without previous purification.

The synthesis and characterization of 4-vinylbenzylazide<sup>[21]</sup> and rhodamine alkyne<sup>[22]</sup> are described in the supporting information file.

**Synthesis of parent azide-nanoparticles (SA series).** Two series of azide nanoparticles were synthesized via emulsion polymerization under two different conditions. V50 was used in polymerizations at 60 °C (SA-500 series), while V44 was used for polymerizations conducted at 45 °C (SA-400 series). In a typical experiment, the reaction was conducted in a 250 mL three-neck round-bottom flask connected to a condenser, under a nitrogen stream. A hot plate/magnetic stirrer (RCT IKAMAG, IKA-Werke GmbH & Co. KG) equipped with an IKA ETS-D5 temperature controller was used to regulate stirring (750 RPM) and temperature. A volume of 100 mL of water was added to the flask containing 0.1 g of CTAB surfactant and 0.1 g of initiator, and purged with a nitrogen stream for 30 minutes. Subsequently, 0.5 mL of styrene was added to start the polymerization. After 15 minutes, the rest of the styrene (4.5 mL) was added using a 5 mL syringe fitted to a syringe pump (NE-1600, New Era Pump System Inc.) with a monomer addition rate of 1 mL/h, in a monomer-starved configuration. At 4 hours of reaction, a determined amount of VBAz and 0.01 g of initiator were dissolved in water to complete up to 3 mL in separated syringes. The solutions were added using a syringe pump at 1 mL/h. The reaction was stopped after 48 hrs. The final product was cleaned by dialysis with a dialysis tubing cellulose membrane (molecular weight cut-off = 14,000). Table A 5-3 and Table A 5-4 in supporting information summarize the latex properties and Figure A 5-5 to Figure A 5-9 show FT-IR and <sup>1</sup>H-NMR spectra.

**Parallel synthesis of triazole nanoparticles via click reaction of azide nanoparticles (TR series).** Reactions were conducted in a parallel liquid-phase synthesizer, 24-vessel MiniBlock™ XT (Mettler Toledo) equipped with a shaking Bohdan MiniBlock™ station

(New Brunswick, model 18541). In a typical miniblock experiment, a volume of 10 mL on each vessel was completed by adding water, 200  $\mu$ L of 1 mM copper sulfate, 200  $\mu$ L of 1 mM PMDETA and 200  $\mu$ L of 10 mM sodium ascorbate, to act as catalysts in the click reaction. Reaction mixtures were shaken at 300 RPM for 2 minutes, and a determined volume of alkyne solution (e. g. 320  $\mu$ L of 1 mM Amine-PEG4-Alkyne) was added to the vessel. The miniblock was shaken again for 2 minutes, and 2 mL of 10 g/L nanoparticle dispersion was dispensed. The concentrations of alkynes added to each row in the miniblock were 32, 16 and 8  $\mu$ mol/L, corresponding to an alkyne surface density of 0.089, 0.045 and 0.022 molecules/nm<sup>2</sup>. Table A 5-3 summarizes recipes and properties for each reaction. As an example, Table A 5-2 (supplementary information shows experimental design for one of the miniblocks produced. The reactions were left in the dark, at room temperature and constant stirring at 300 RPM for up to 7 days. The progress of the reactions was monitored by paper chromatography following our recently published method<sup>[23]</sup>. After the reaction is completed, the nanoparticle dispersions were cleaned in a Dowex® MB mixed ion exchange resin when necessary.

**High throughput colloidal stability test.** Critical coagulation concentrations at ranges between 0 and 20 mM sodium carbonate were obtained for all the triazole nanoparticles and their parent nanoparticles by following the procedure previously published<sup>[11]</sup>.

**Parallel automated spot coating.** Squared borosilicate microscope coverglass slides (Fisherbrand™, 18 mm<sup>2</sup>) were cleaned in a UV-ozone chamber for 2 minutes. Three slides were placed in a slide adapter tray. A solution of 5 mM NaCl and triazole nanoparticle dispersion was prepared in 96-well microplates by using a liquid handling robot Tecan Freedom Evo® 200. The total volumes of the nanoparticle dispersions were 200  $\mu$ L, each with a final nanoparticle concentration of 0.5 g/L. 5  $\mu$ L of nanoparticle dispersions were dispensed onto the coverglass slides, spotting 2×2 arrays on each squared slide. Each experiment was run three times. The slides were left to dry in a humidity controlled chamber for 30 min at 60% humidity. Each slide was submerged in 1000 mL of water.

The slides were then placed in a custom tray that was positioned in the contact angle instrument and the experiments were completed by dispensing 1  $\mu$ L of water onto the treated slides and sessile drop water/air contact angle was measured on them. See supplementary material for scheme of the procedure (Figure A 5-14).

**Parallel automated dip coating.** In a typical experiment, 3 units of squared borosilicate microscope coverglass slides (18 mm<sup>2</sup>) were cleaned in a UV-ozone chamber for 2 minutes. The slides were aligned and fitted in a silicone gasket, and placed below a miniature 16-well chambered coverglass cell culture vessel (CultureWell™, Grace-Bio

Labs), forming a 2×2 well array on each squared slide. The 16-well vessel was positioned in a custom microplate adapter tray that can hold up to four 16-well vessels.

Each vessel was filled with a solution of 5 mM NaCl and triazole nanoparticle dispersion using a liquid handling robot Tecan Freedom Evo® 200, obtaining a total volume of 200 µL with a final nanoparticle concentration of 0.5 g/L. Each experiment was run in triplicates to assure reproducibility. The 16-well vessel was left with a lid at room temperature for 30 min to allow deposition of nanoparticles at the coverglass slides. The nanoparticle dispersions were removed from each well with the robot; the slides were detached from the silicone gasket and submerged in 1000 mL of water to remove unbound nanoparticles.

Contact angles were automatically obtained following the same procedure used for spot coated slides, previously described. Figure 5-1B shows a scheme of this procedure.

**Automated water contact angle.** Automated contact angle measurements were conducted using a high speed contact angle instrument (OCA 35, DataPhysics Instruments GmbH), equipped with a motorized station and software SCA202 V 4.3.19, which allowed creating and running a script for automatic positioning, water drop dispensing, baseline detection and sessile drop water/air contact angle measurements. The results were calculated from a drop shape analysis with an ellipse fitting setup using the same software, SCA202. In Figure 5-1B the sample preparation and automated contact angle procedure is shown.

**Imaging of coverglass slides by ChemiDoc™ MP fluorescent scanner.** A fluorescent imaging was used to compare coating densities between automated dip coating and automated spot coating on coverglass slides. The coverglass slides were placed on top of a white board and placed in a ChemiDoc™ MP imaging system (Biorad, nr. 170-8280). The slides were scanned and processed with the software ImageLab with the protocol *Rhodamine* with an automatic exposure time, a Green Epi illumination 520±50 nm excitation source, and a 605±50 nm emission filter. Since the images are presented in their original format, brighter areas represent a higher fluorescence signal.

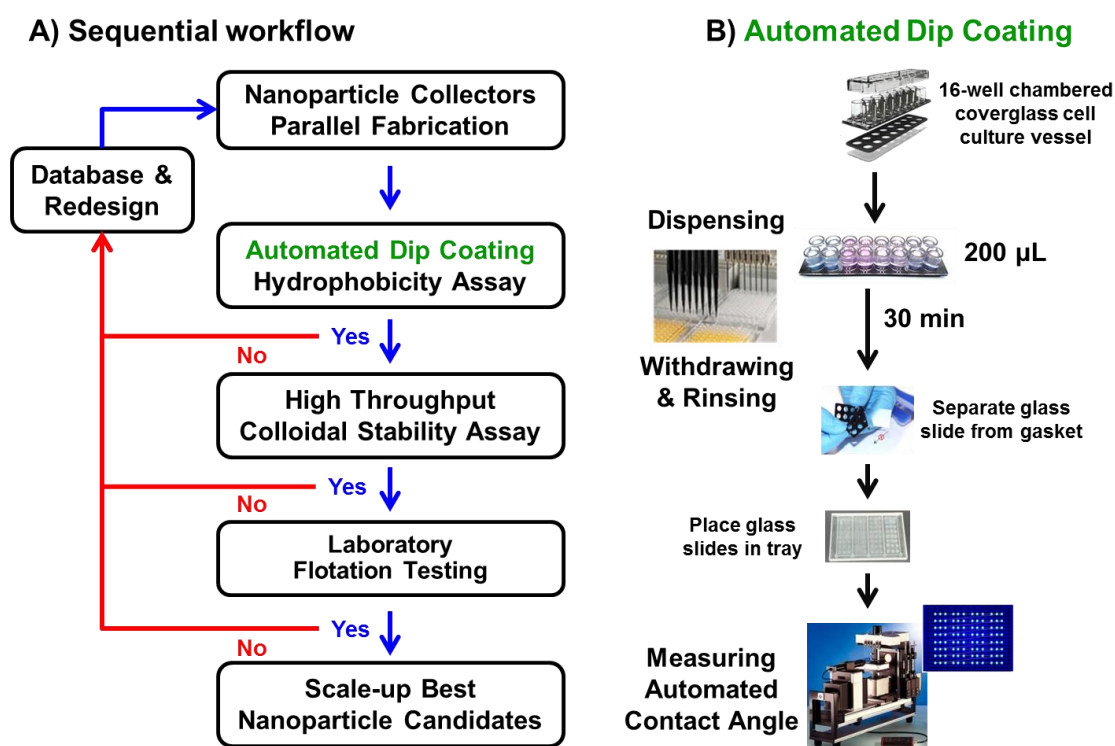
**Optical digital profilometry.** A surface optical digital profilometer (Veeco WYKO NT1100, DYMEK Company Ltd. ) was used to obtain images and analyze the topography of the glass slides prepared by dip and spot coating. The measurements were conducted and roughness was obtained in vertical scanning interferometry (VSI) mode at a magnification of 5.1 (5x objective) over an area of 240×368 µm<sup>2</sup>.

**Scanning Electron Microscopy (SEM).** Micrographs of the nanoparticles deposited on coverglass were obtained by a JEOL JSM-7000F SEM equipped with a Schottky Field



Emission Gun (FEG) filament with an accelerating voltage of 2.8 keV. Before starting the experiment, the edges and center of the slides were coated with silver coating and dried at 50° C for 60 min. The samples were then coated under vacuum with a thin layer of 5 nm of platinum. The SEM images were processed using JEOL image processing software.

**Figure 5-1:** A) Sequential workflow of discovery and testing of nanoparticle collectors; B) Automated dip coating hydrophobicity assay procedure.



**Flotation of glass beads coated with nanoparticles.** Flotation of glass beads was performed with the best nanoparticle candidates found by following the sequential workflow in Figure 5-1A. All the experiments were conducted in 5 mM of sodium carbonate at pH ~ 9-10. In a routine trial, 50 ppm of a nanoparticle suspension was mixed with 2 g of glass beads in 120 mL sodium carbonate solution. The beaker was placed on a 90 mm diameter plastic petri dish, on top of a magnetic stirring plate (Cimarec, Thermo Scientific). The mixture was stirred for 5 minutes at 700 rpm to allow deposition of nanoparticles onto the glass beads. 10 ppm of Unifroth 250C was added and the solution was stirred for 30 seconds. Flotation was initiated by passing nitrogen through a Corning

Pyrex gas dispersion tube with a coarse fritted disc (11-137E, Fisher Scientific) at a rate of 2.0 L/min, controlled by a flowmeter (1355-EDA-7BLC1A, Brooks Instruments). The froth layer formed in the surface was collected in a plastic petri dish placed beneath the beaker. After 30 seconds, the gas dispersion tube was removed from the solution, and the collected and remaining materials were filtered with a vacuum Büchner ceramic funnel using a filter paper (Whatman #1), dried and determined gravimetrically. Regardless the nanoparticles cleaning step after click reaction, separate control flotation experiments with the reagents (catalysts, alkynes) were conducted as well to ensure that reagents alone will not affect flotation.

## 5.4. Results and Discussion

We recently reported the usefulness of colloidal stability maps as a suitable prediction of the performance of nanoparticle candidates in nickel sulfides flotation<sup>[10]</sup>. In a later study, we also presented a high throughput assay of colloidal stability based on turbidity measurements<sup>[11]</sup>. To implement an efficient high throughput workflow, an automated design is necessary. We propose that by applying click chemistry it is possible to create several nanoparticle surfaces and rapidly test their effectiveness in flotation applications. In another recent manuscript<sup>[23]</sup>, we published a simple way to analyze surface content of azide nanoparticles. The goal of the present work was to produce a large library of nanoparticles with a variety of alkyne molecules by using click chemistry and evaluate them through colloidal stability maps.

### 5.4.1. Parent azide nanoparticles

More than 30 azide nanoparticles have been synthesized under different conditions to provide a wide range of azide contents in the nanoparticles. Table A 5-1, in supporting information, show the recipes and properties of the azide nanoparticles prepared. Figure 5-2 presents results for SA-400 series, while Figure A 5-10 (in supplementary information) shows SA-500 series. Surface to total azide concentration, relative turbidity plots and glass beads flotation at increasing nanoparticle dose were screened to find the most suitable parent nanoparticles for further modification.

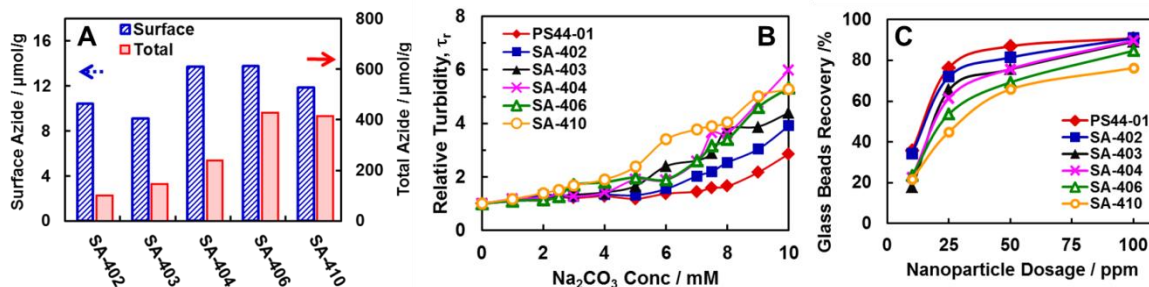
The azide surface concentration was measured by fluorescent paper chromatography in a recently published work<sup>[23]</sup>, while the total azide concentration was determined by proton NMR. In the paper chromatography experiment, a fluorescent dye reacted with the azide groups available at the surface of the nanoparticles. The excess of dye was removed by ascending paper chromatography<sup>[23]</sup>. Therefore the surface azide ( $\lambda_{SAz}$ ) presented in

Figure 5-2A was smaller than the total azide ( $\lambda_{TAz}$ ) in all cases. The azide nanoparticle SA-402 had the highest ratio of surface azide to total azide, corresponding to 12% of the total amount of azide in the nanoparticle.

Vinyl benzyl azide has polar mesomeric structures<sup>[24]</sup>, is prone to react with nucleophilic and electrophilic compounds<sup>[25]</sup>, by having attack on the terminal N by nucleophiles, or attacking electrophiles by the alkyl N. Thus, even though the azide monomer, vinyl benzyl azide, follows the stability rule described by Smith et al<sup>[26]</sup>, it was suspected to affect the nanoparticle colloidal stability, especially when adding salts to the system.

High throughput colloidal stability assay results (in Figure 5-2B), show that the colloidal stability is directly related to the ratio of surface azide to total azide. The higher the ratio, the more stable the particle is. SA-402 showed higher stability as it has the higher ratio of surface azide to total azide compared to the rest of the nanoparticle in the series.

**Figure 5-2:** Azide nanoparticle analysis for series SA-400: A) Surface azide ( $\lambda_{SAz}$ ), versus total azide ( $\lambda_{TAz}$ ); B) Relative turbidity map; and C) Glass beads flotation in 5 mM sodium carbonate at different nanoparticle dosage.



Additionally, flotation of azide nanoparticles was tested in 5 mM of sodium carbonate (Figure 5-2C). The results followed a similar path to their colloidal stability trend, suggesting that less stable nanoparticles will lead to poorer glass beads recoveries<sup>[9]</sup>. SA-402 gave high glass beads recoveries in a nanoparticles dose as low as 25 ppm. SA-508, from the SA-500 series with V50 as initiator, followed similar trends to their homologous SA-402 (see supplementary information, Figure A 5-10).

Therefore, among the nanoparticles produced, SA-402 and SA-508 were selected as the parent azide nanoparticles to react with alkyne molecules via click reactions. The criteria

used to choose these two nanoparticles include the ratio of surface azide to total azide in the nanoparticle, their colloidal stability and flotation results.

#### 5.4.2. Preparing libraries of triazole nanoparticles

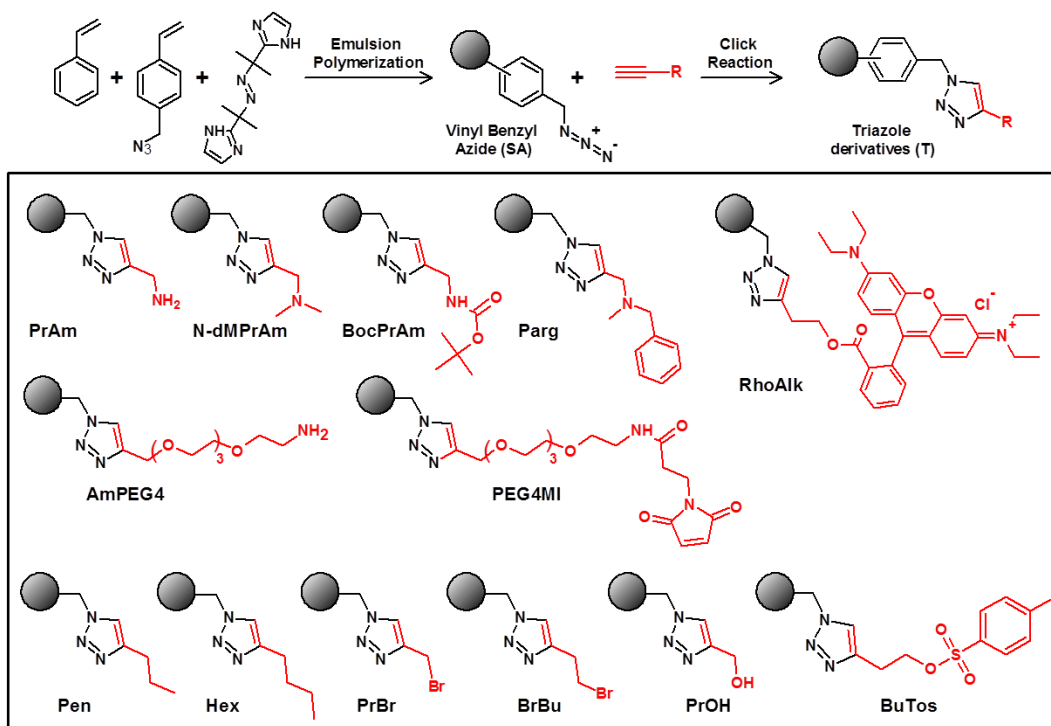
Several reagents, solvents and conditions were applied for click reactions between azides and alkynes<sup>[27]</sup>. In the preparation of the triazole nanoparticle library, we used water as solvent, thus, the nanoparticles produced after click reactions can be employed directly in flotation experiments without major modifications. We optimized the reaction conditions in terms of concentrations of nanoparticles, alkyne and catalyst. The progress of reaction was monitored by paper chromatography and X-ray photoelectron spectroscopy (XPS) as previously described in our publication<sup>[23]</sup>.

The optimized recipes for each derivative are shown in Table A 5-3 and Table A 5-4 in supplementary material. The catalyst system used, Cu (II), was reduced to Cu (I) by NaAsc (sodium ascorbate), with PMDETA as ligand to promote the 1,3-dipolar cycloaddition. Sodium ascorbate was added in excess to maintain the Cu in state +1, avoiding using an inert atmosphere.

Various catalyst concentrations were investigated in water as solvent to increase the yield of the reaction<sup>[27]</sup>. In our reaction, 20  $\mu\text{M}$  of Cu/PMDETA was found to be enough to efficiently couple alkynes to surface azides. The concentrations of alkynes used were 32, 16 and 8  $\mu\text{mol/L}$  and were calculated from ratios of surface azide to alkyne at 1:1, 1:0.5 and 1:0.25, to compare behavior of nanoparticles with different surface alkyne-saturations, resulting in alkyne surface densities of 0.089, 0.045 and 0.022 molecules/ $\text{nm}^2$ .

Figure 5-3 shows the alkyne structures that were reacted to SA-402. Research has shown that amine-based molecular collectors can be selective and can perform well in flotation<sup>[28]</sup>. Therefore, seven alkynes with amine derivatives were tested in click reactions ranging from hydrophilic quaternary ammonium, such as RhoAlk to more hydrophobic tertiary amines, such as pargyline, with the goal to test their ability to control the balance between hydrophobicity and colloidal stability. Also, hydrocarbon chains, bromide, alcohol and tosylate molecules were tested to investigate how they would affect flotation performance.

**Figure 5-3:** Polymerization and click reaction of triazole nanoparticles. 39 triazole nanoparticles were produced from a single parent azide nanoparticle. See materials section for complete alkynes names.



### 5.4.3. Automated dip coating and contact angle experiments

We developed a contact angle assay based on automated measurements. There are a few publications related to automatic contact angles measurements [12, 13]; however, all of them have used polymeric films or very smooth substrates made via spin coating. The application of automatic contact angles has been developed mostly for coatings, such as anti-fouling materials, therefore there is no need to test nanoparticles dispersed in water, which might bring complications on the sample preparation. In contact angle experiments, the homogeneity of the surface to measure is a key factor for reproducibility, especially when substrate preparation and contact angle measurements are intended to be automated.

First we attempted to measure the contact angles by preparing the coating with a parallel and automated spot coating method (as shown in Figure A 5-14, in supplementary information). Although, this method gave fairly good results, the standard deviation of the automatic measurements was still too high for contact angles (over  $\pm 5^\circ$  in several cases)

due to rapid evaporation and self-pinning. When humidity is not controlled, evaporation is fast and irregular in small drops<sup>[29]</sup>, and self-pinning of dispersed nanoparticles on the surface while evaporating is more likely to happen, producing a coffee ring effect or other irregularities, affecting the spreading dynamics and morphology of the substrates<sup>[30]</sup>.

A second attempt included dissolving the nanoparticle spots with chloroform after spotting and drying, to generate a semi-smooth film. Unfortunately, the nanoparticles dissolved and formed an uneven distorted polymer film, in where the polymer chains were dragged together by surface tension after the solvent evaporated, leaving holes in the film (Figure A 5-16).

Therefore, an automated dip coating method was adopted and optimized to obtain uniform coatings, minimizing surface irregularities that could lead to irreproducible results, as shown in Figure 5-1B. Hence, a parallel automated dip coating method can avoid these negative effects, as the deposition of nanoparticles is achieved by gravity in an aqueous environment. The nanoparticle coated surfaces were analyzed by fluorescence imaging and SEM to investigate discrepancies on contact angle results in the spot versus dip coating.

Figure 5-4 shows fluorescent images, SEM micrographs and profilometry analysis of triazole nanoparticles, in which the substrate was prepared via automated spot coating and dip coating. The fluorescent intensity of the surface by spot coating was much brighter than that by dip coating (

Figure 5-4A).

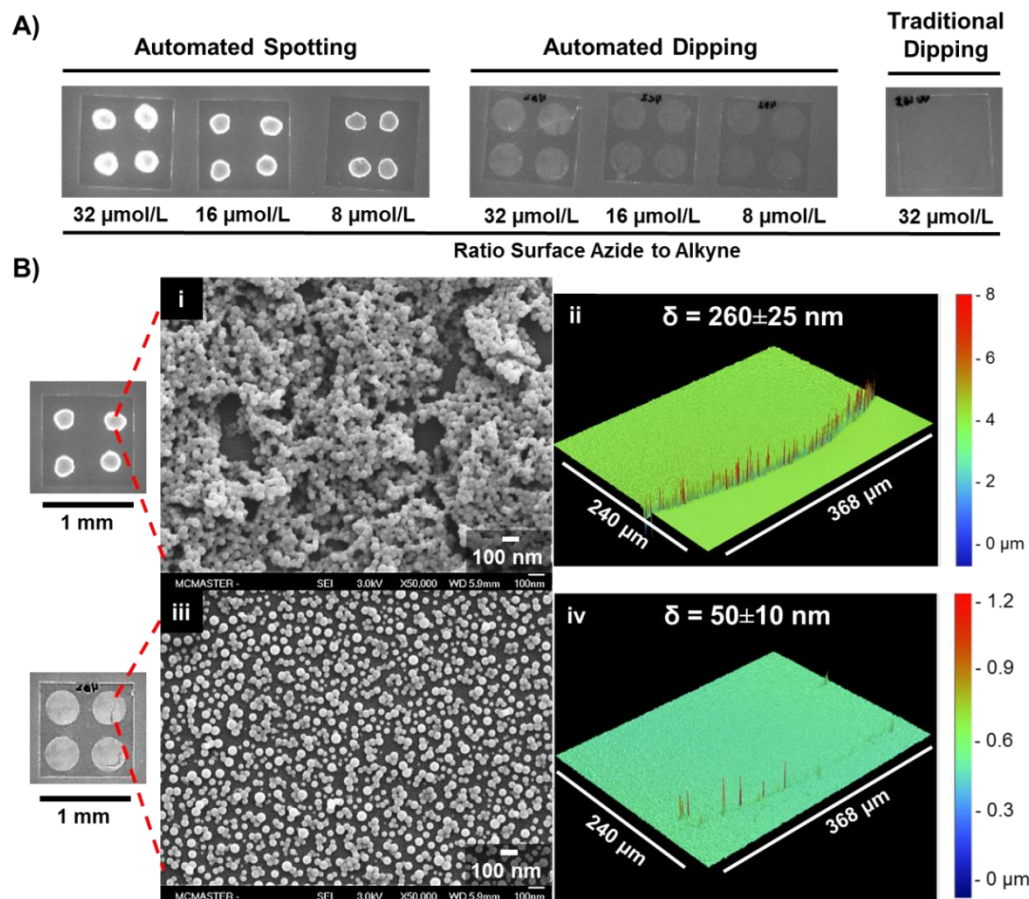
Additionally, SEM analysis indicated that the density of deposited nanoparticles was higher in spot coating than in dip coating, probably forming multilayers of nanoparticle in the spot due to surface tension and rapid evaporation (Figure 4B.i and iii). Analysis by profilometry also confirmed these results. The average thickness of the nanoparticle deposited layers was  $260 \pm 25$  nm for spot coating, and  $50 \pm 10$  nm for dip coating, suggesting that the second method gave a more uniform monolayer of nanoparticles (

Figure 5-4B.ii and iv).

Further investigations on the effect of salt and rinsing on the contact angle results showed that a contact angle can greatly vary if the rinsing step is avoided, especially in spot coating. For instance, a nanoparticle coating prepared via spot coating with rinsing presented a water contact angle of  $84^\circ \pm 2.7$ ; but, its contact angle decreased to  $74^\circ \pm 3.9$

when rinsing was absent. In SEM micrographs (Figure A 5-16 in supporting material) a cluster of salt inside the water contact angle footprint was found, suggesting that the water drop accumulates the remaining salt on the surface of the spot while evaporating. Cleaning the glass slide by immersion in water after the coating is, therefore, an important step to assure reproducibility of results as well.

**Figure 5-4:** A) Chemidoc™ Fluorescent images for slides coated through different methods; B) SEM micrographs and surface profiling images for: i, ii) automated spot coating of T-RhoAlk-32 triazole nanoparticle; iii, iv) automated dip coating of T-RhoAlk-32 triazole nanoparticle.

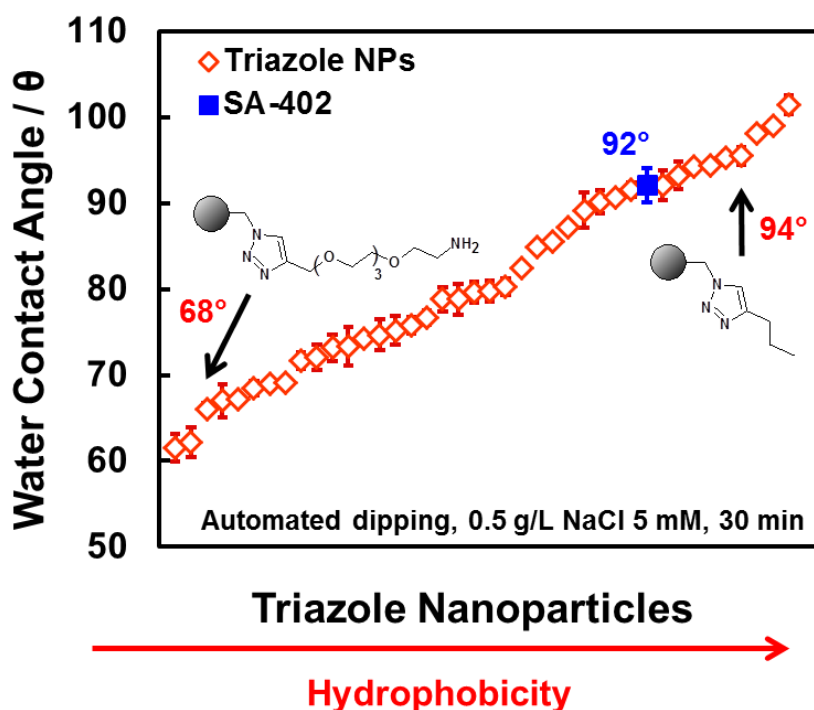


#### 5.4.4. Screening hydrophobicity of triazole nanoparticles

Contact angles of the triazole nanoparticles have been measured using parallel automated dip coating and automatic contact angle. This method was chosen since it gave the highest reproducibility and lowest standard deviation out of the preparation methods tested. Dip coating sample preparation reported contact angle results with a maximum standard deviation of  $\pm 2.0$  degrees, when running 3 repeats per each slide and experiment triplicates for each sample.

The results shown in Figure 5-5 indicated that the triazole nanoparticles contact angle ranged from  $62^\circ$  to  $101^\circ$ , while the parent nanoparticle, SA-402, had a contact angle of  $92^\circ$ . The contact angles mostly depend on the chemical nature of the alkyne such as: polarity, length of the alkyl chain, heteroatom groups present, etc. (Figure 5-3).

**Figure 5-5:** Surface wetting modification of a single parent azide nanoparticle only by changing surface groups and concentrations via click chemistry.



When analyzing results of contact angles by concentration for each alkyne, as seen in Figure A 5-11 (supporting information), it can be noticed that all the nanoparticles decreased their contact angle when the concentration of alkynes at the surface of the nanoparticle increased. Hydrophilic alkynes in greater concentrations were expected to lower the hydrophobicity of the nanoparticle and therefore, decrease their contact angle.



In contrast, more hydrophobic alkynes were expected to increase the nanoparticle contact angle when clicked to the surface.

Surprisingly, this only happened for T-pargyline, in which an increasing concentration increased its contact angle, reaching up to  $95^\circ \pm 1.0$ . The nanoparticles T-Pent and T-Hex did not show important variations on their contact angle when increasing their alkyne concentration. Consequently, we can conclude that our method is sensitive to the inherent hydrophobicity of the sample, which is a fundamental attribute for an optimized implementation of the method.

The lowest contact angle obtained was  $62^\circ \pm 1.6$ , corresponding to T-PrOH-32 nanoparticle. Propargyl alcohol was one of the most hydrophilic alkynes used. As a small molecule, it can easily react with azide groups at the surface and even inner moieties to produce hydrophilic triazoles.

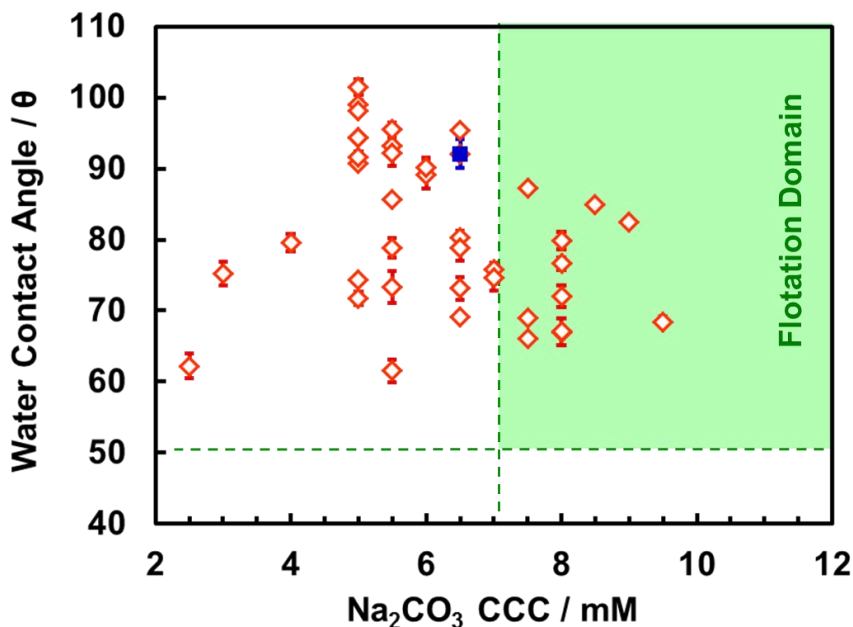
As seen in Figure A 5-11, in supplementary material, T-PrOH series presented the largest variation of contact angle, reaching up to  $85^\circ \pm 0.5$  for T-PrOH-8. Wetting properties depend upon the homogeneity of the surface and also the occlusion of water among the substrate. As hydroxyl presents a high water-affinity, the occlusion of water and also homogeneity of the layer formed at the surface could have had a great impact in the contact angle obtained. Similar wetting behavior was found in the amine-base nanoparticle T-PrAm, which presented contact angles between  $69^\circ \pm 0.4$  and  $87^\circ \pm 0.2$  with low standard deviations.

#### 5.4.5. Colloidal stability maps

Correlating the water contact angle of a nanoparticle with the critical coagulation concentration as a measurement of hydrophobicity versus colloidal stability can be useful for screening of nanoparticle candidates for flotation. In Figure 5-6, we established a flotation domain in which we expect nanoparticles to efficiently work as flotation collectors. We called this plot a colloidal stability map.

Considering industrial flotation conditions and previous studies in nanoparticle collectors, we have determined that a nanoparticle with a colloidal stability greater than 7 mM of sodium carbonate can be sufficiently stable to allow good flotation recoveries. Also, nanoparticles with a contact angle greater than 50 degrees should be sufficiently hydrophobic to show a good flotation performance. As a proof of concept we applied these criteria to all our nanoparticle candidates (40 samples for SA-402 parent nanoparticle) and plot the results in a colloidal stability map (Figure 5-6).

**Figure 5-6:** Colloidal stability map for triazole nanoparticles library. Nanoparticles that reach the flotation domain (green area at the right of the graph), should be able to act as good flotation collectors.



All our triazole nanoparticles presented a contact angle higher than 50 degrees; hence, all of them should be hydrophobic enough to conduct efficient flotation. Consequently, the limiting factor is their colloidal stability. The critical coagulation concentration of SA-402 was 6.5 mM of  $\text{Na}_2\text{CO}_3$ , thus any increment of colloidal stability can be beneficial for flotation performance.

The most effective way to colloidally stabilize a nanoparticle is to employ steric and electrostatic stabilizers and grafting them at the surface of the nanoparticle<sup>[31]</sup>. The problem is that grafting hydrophilic groups usually lower the contact angle of the nanoparticles dramatically, even in small amounts, as we showed when grafting PEG-methyl methacrylate groups onto nanoparticle collectors<sup>[10]</sup>. Orthokinetic coagulation is also a fundamental effect in flotation<sup>[32]</sup>, so keeping the nanoparticle stable without affecting flotation is a matter of balance of surface chemistries.

Two promising alkynes were tested as steric stabilizers. T-AmPEG4 and T-PEG4MI, included four PEG groups with an amine and a maleimide terminal groups. Both showed suitable contact angle results, even T-PEG4MI showed fairly high contact angles at 16 and 8  $\mu\text{mol/L}$  concentrations ( $75^\circ \pm 1.7$  and  $79^\circ \pm 1.2$ ); however, T-PEG4MI resulted to be the least colloidally stable nanoparticle of all the series, as shown Table A 5-3 in supporting material). Maleimide is a useful crosslinking group in molecular biology, but

at pH higher than 8.5, the compound hydrolyzes to a maleic acid<sup>[33]</sup>, opening its ring and losing stability.

T-AmPEG4 resulted to be a much better stabilizer for triazole nanoparticles. The highest concentration of this material increased the nanoparticle CCC to 9.5 mM Na<sub>2</sub>CO<sub>3</sub> (pH ~10), the highest of the series, without greatly affecting its contact angle ( $68^\circ \pm 0.8$ ). PEG chains conferred steric stabilization at the surface of nanoparticles to tolerate higher concentrations of sodium carbonate.

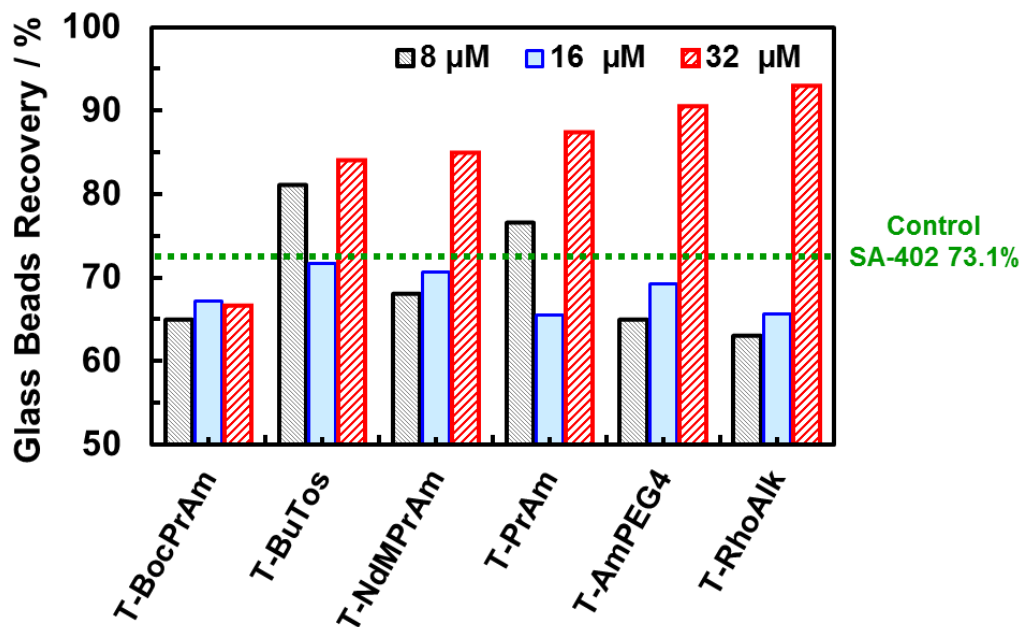
Other alkynes that resulted to greatly increase the colloidal stability were T-BocPrAm, T-PrAm, T-NdMPrAm and T-BuTos (see Figure A 5-12 in supporting info). The terminal Boc substituent is a common amine protector that hydrolyzes in acidic conditions but is stable at high pH, due to the tert-butyloxycarbonyl group coupled to the amine<sup>[34]</sup>. Therefore, it seemed to be a good candidate for flotation. T-PrAm and T-NdMPrAm are primary and tertiary amines with an alkyl substituent, increasing its pKa and tolerance to high pH.

T-Butos was another alkyne that showed unexpected increased stability. Tosylate terminal group are known for being good leaving groups in organic chemistry. However, in the colloidal stability assay this nanoparticle showed high tolerance to alkaline media. A reason could be the fact that tosylate has shown high stability up to pH ~ 12 when acting as a protecting group<sup>[34]</sup>, and similar to Boc groups, critical coagulation concentrations were higher than the non-conjugated nanoparticle.

Hydrophobic T-Pent and T-Hex showed a decreased colloidal stability in sodium carbonate, leaving them outside the green flotation domain. Pargyline did not pass the colloidal stability test either, although the lowest concentration of pargyline in the nanoparticle was a slightly more tolerant than the rest of its series.

In the colloidal stability map plotted (Figure 5-6), a high density of nanoparticles are found to be converging towards 70 degrees of contact angle. Out of the 40 triazole samples prepared from the parent nanoparticle SA-402, only 13 samples presented a CCC higher than 7 mM Na<sub>2</sub>CO<sub>3</sub>. Those reached the green flotation domain and corresponded to six alkynes: AmPEG4, BuTos, BocPrAm, RhoAlk, PrAm and N-dMPrAm, as shown in Table 1, flotation of glass beads in sodium carbonate was conducted on these alkynes series and the results are presented in Figure 5-7.

**Figure 5-7** Glass beads recovery of 6 most promising nanoparticle candidate series. Green line indicates parent nanoparticle, SA-402, value. Note: Results are grouped by alkyne molecule and by alkyne concentrations ( $\mu\text{M}$ ).



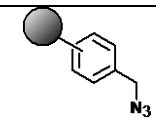
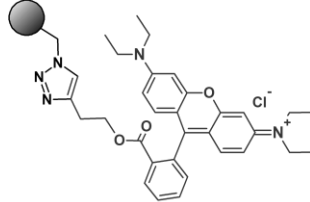
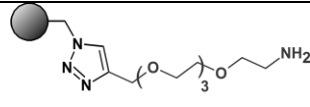
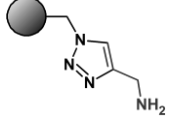
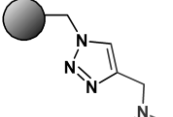
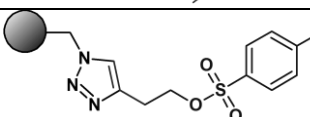
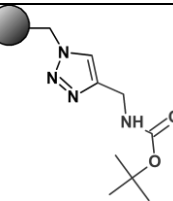
#### 5.4.6. Glass beads flotation with triazole nanoparticles

Flotation performance was tested for the best nanoparticle candidates as predicted from colloidal stability maps. Glass beads were used as a mineral model and all the experiments were conducted in 5 mM sodium carbonate (pH ~ 10).

Figure 5-7 reveals that 5 out of 6 nanoparticle candidates improved glass beads flotation in respect to SA-402 (73% recovery). Tests were run with 50 mg/L nanoparticle concentration in all cases, corresponding to a glass beads theoretical coverage of 117%, for a nanoparticle with 53 nm diameter. Interestingly, the highest concentration of RhoAlk at the surface of nanoparticles gave the best glass beads recovery with 93%, compared to lower amounts of RhoAlk (65% and 63%).

When comparing the colloidal stability results with the flotation results for the RhoAlk series, there is a correlation: higher the CCCs, the greater flotation recoveries (see Figure A 5-13 in supporting information). Other nanoparticles such as T-AmPEG4 and T-NdMPrAm also showed similar trends.

**Table 1** Best nanoparticle candidates according to colloidal stability map. Results of colloidal stability, hydrophobicity and activities as glass bead flotation collectors are shown. Results are ordered by glass beads flotation results.

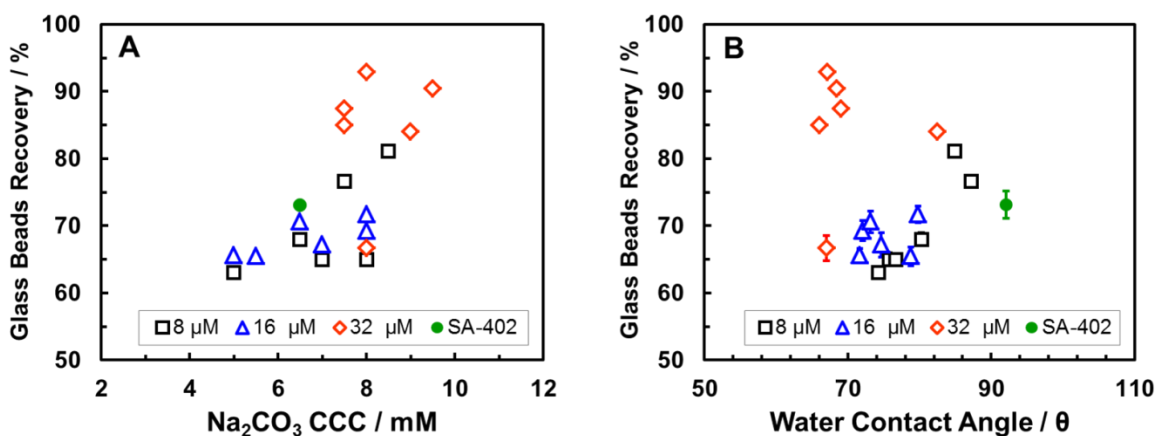
Sample Name	Alkyne Concentration, $\mu\text{mol/L}$	CCC in Sodium Carbonate, mM	Water Contact Angle, $\theta$ (std error)	Glass Beads Flotation Recovery, %	Nanoparticle Surface Coupled Structure
SA-402	0	6.5	92 ( $\pm 2.0$ )	73.1	
T-RhoAlk	8	5.0	74 ( $\pm 0.2$ )	63.0	
	16	5.0	72 ( $\pm 0.9$ )	65.6	
	32	8.0	67 ( $\pm 0.5$ )	92.9	
T-AmPEG4	8	7.0	76 ( $\pm 1.0$ )	65.0	
	16	8.0	72 ( $\pm 1.5$ )	69.3	
	32	9.5	68 ( $\pm 0.8$ )	90.4	
T-PrAm	8	7.5	87 ( $\pm 0.2$ )	76.6	
	16	5.5	79 ( $\pm 1.4$ )	65.5	
	32	7.5	69 ( $\pm 0.4$ )	87.4	
T-N-dMPrAm	8	6.5	80 ( $\pm 0.9$ )	68.0	
	16	6.5	73 ( $\pm 1.6$ )	70.6	
	32	7.5	66 ( $\pm 0.6$ )	85.0	
T-BuTos	8	8.5	85 ( $\pm 0.5$ )	81.1	
	16	8.0	80 ( $\pm 1.2$ )	71.7	
	32	9.0	82 ( $\pm 0.2$ )	84.0	
T-BocPrAm	8	8.0	77 ( $\pm 0.9$ )	65.0	
	16	7.0	75 ( $\pm 1.8$ )	67.2	
	32	8.0	67 ( $\pm 1.9$ )	66.7	

T-BuTos and T-PrAm had very good flotation results for alkyne concentrations of 32 and 16  $\mu\text{mol/L}$ , as seen in Table 1. Most of the triazole compounds that increased flotation recoveries showed a correlation with high colloidal stability, and in a lesser extent with high contact angles. We noted that more hydrophobic nanoparticles did not give high recoveries, regardless of their high hydrophobicity.

We also found that flotation recovery depends on the amount of alkyne molecules on the surface of nanoparticles. In most cases, most alkyne-saturated nanoparticles ( $32 \mu\text{mol/L}$ ,  $0.089 \text{ molecules/nm}^2$ ) exhibited the highest recoveries for glass beads (red diamond symbols in Figure 5-8), CCCs higher than 8 mM sodium carbonate, and contact angle results between  $65^\circ$  and  $75^\circ$ .

The blue triangle cluster corresponded to  $0.045 \text{ molecules/nm}^2$  alkyne surface densities, and showed the lowest glass beads flotation performance, even though three of them actually fell on the green flotation domain and were promising nanoparticles (T-RhoAlK-16, T-PrAm-16 and T-NdMPrAm-16 in Table A 5-3, in supplementary information). The black square cluster, with  $0.022 \text{ molecules/nm}^2$  alkyne surface densities, showed more spreading in the results, having four nanoparticles that fell in the green flotation domain but only two nanoparticles that increased the flotation recoveries when compared to the control, SA-402. These nanoparticles, T-BuTos-8 and T-PrAm-8, increased the flotation recovery by 8% and 4%, and both had quite high contact angle results,  $84.9^\circ$  and  $87.2^\circ$ , respectively.

**Figure 5-8:** Glass beads recovery of 6 most promising nanoparticle candidate series as a function of: A) critical coagulation concentrations; B) water contact angle. Green dot indicates value of control parent nanoparticle, SA-402. Note: Results are grouped by alkyne concentrations in  $\mu\text{M}$ .



## 5.5. Conclusions

Click chemistry was used to generate a large range of surface chemistries. Copper-mediated azide alkyne cycloaddition reaction was used to functionalize the surface of azide nanoparticles with different chemical groups, ranging from hydrophilic amine-terminated PEG chains, to hydrophobic hexane-terminated materials. The conclusions of this work are presented as follows:

- 1) At least 80 nanoparticles with different surface functionalization and densities were produced and analyzed to find the most promising nanoparticle candidates.
- 2) The parent azide nanoparticle, SA-402, was chosen as the most suitable for surface modification, since it presented the highest tolerance to sodium carbonate buffer along with a fairly high azide surface coverage and good glass beads recovery.
- 3) An automated contact angle assay was developed and used for screening nanoparticle candidates. A miniature 16-well plate format, where flat glass slides were exposed to 200  $\mu\text{L}$  nanoparticle dispersions, gave an efficient dip coating preparation and reproducible automated contact angle results, with a maximum standard deviation of  $\pm 2.0$  degrees, when running 3 repeats per each slide and experiment triplicates for each sample.
- 4) The click nanoparticles library exhibited an extensive range of critical coagulation concentrations and contact angle values. For example, for a given parent azide nanoparticle, the contact angles ranged from 62 to 101 degrees, depending upon the density and type of click reagent.
- 5) Successful nanoparticle candidates had contact angles greater than 50 degrees, a criterion developed with model experiments. However, a possible narrower criterion can be established for click triazole nanoparticles, since the best candidates had contact angles between 65 and 75 degrees.
- 6) The alkynes terminated in amine-PEG4, butyl-tosylate and rhodamine alkyne-saturated surfaces, 12  $\mu\text{mol/g}$  (1:1 ratio of alkyne to surface azide), showed the highest CCCs and the highest glass beads recovery. The colloidal stability demonstrated to be a more accurate predictor of glass beads recovery than water contact angle, when nanoparticles have a contact angle higher than 50 degrees, as a higher critical coagulation concentration value led to higher glass beads recovery in most of the nanoparticle samples that have previously fell in the green flotation domain.
- 7) From the studied library, five alkynes derivatives showed good flotation results in glass beads; therefore, a systematic study on analyzing more in detail their chemical structures and flotation of real ore minerals would be useful to

complement the design and application of the screening process proposed in this work.

- 8) We used stability map analysis for finding the best candidates for flotation. This method has the advantage of revealing how far specific nanoparticles are from target properties, when comparing to the typical pass/fail assays typically used in high throughput screening. Consequently, the design of new nanoparticle candidates via high throughput screening can consider models of target properties in narrower thresholds of colloidal stability and hydrophobicity.

Overall, the automation of the fabrication and colloidal stability along with hydrophobicity methods for screening nanoparticle candidates, are the framework for discovery and expansion of suitable surface chemistries for nanoparticle candidate for flotation.

#### **\*SUPPORTING MATERIAL**

The supporting material file includes detailed descriptions of the azide monomer and fluorescent dye synthesis; tables and plots of azide parents and triazole nanoparticles; experimental design, methodology schemes, SEM micrographs and plots of the best nanoparticles.

#### **ACKNOWLEDGMENTS**

The authors acknowledge useful discussions and technical assistance of Dr. Songtao Yang from AuTec Innovative Extractive Solutions Ltd. , Dr. Berno from the McMaster Nuclear Magnetic Resonance Facility and Dr. Keramane from the McMaster Biointerfaces Institute. We thank the National Sciences and Engineering Research Council of Canada (NSERC) and Vale Base Metals for funding this project. Most of the experiments were conducted at the McMaster Biointerfaces Institute, funded by the Canadian Foundation for Innovation. R. Pelton holds the Canada Research Chair in Interfacial Technologies. C. Abarca thanks the National Commission for Scientific and Technological Research of Chile, CONICYT - Becas Chile Scholarship Program.

#### **DISCLOSURE**

The authors report no conflicts of interest in this work.



## 5.6. References

- [1] Potyrailo, R., K. Rajan, K. Stoewe, I. Takeuchi, B. Chisholm, and H. Lam, *Combinatorial and high-throughput screening of materials libraries: review of state of the art*. ACS Comb Sci, 2011. **13**(6): p. 579-633.
- [2] Macarron, R., M.N. Banks, D. Bojanic, D.J. Burns, D.A. Cirovic, T. Garyantes, D.V.S. Green, R.P. Hertzberg, W.P. Janzen, J.W. Paslay, U. Schopfer, and G.S. Sittampalam, *Impact of high-throughput screening in biomedical research*. Nat Rev Drug Discov, 2011. **10**(3): p. 188-195.
- [3] Bleicher, K.H., H.-J. Bohm, K. Muller, and A.I. Alanine, *Hit and lead generation: beyond high-throughput screening*. Nat Rev Drug Discov, 2003. **2**(5): p. 369-378.
- [4] Meredith, J.C., *Advances in combinatorial and high-throughput screening of biofunctional polymers for gene delivery, tissue engineering and anti-fouling coatings*. Journal of Materials Chemistry, 2009. **19**(1): p. 34-45.
- [5] Collins, K.D., T. Gensch, and F. Glorius, *Contemporary screening approaches to reaction discovery and development*. Nat Chem, 2014. **6**(10): p. 859-71.
- [6] Yang, S., R.H. Pelton, A. Raegen, M. Montgomery, and K. Dalnoki-Veress, *Nanoparticle flotation collectors: mechanisms behind a new technology*. Langmuir, 2011. **27**(17): p. 10438-46.
- [7] Yang, S. and R. Pelton, *Nanoparticle flotation collectors II: the role of nanoparticle hydrophobicity*. Langmuir, 2011. **27**(18): p. 11409-15.
- [8] Yang, S., R.H. Pelton, M. Montgomery, and Y. Cui, *Nanoparticle flotation collectors III: the role of nanoparticle diameter*. ACS Appl Mater Interfaces, 2012. **4**(9): p. 4882-90.
- [9] Yang, S., R.H. Pelton, C. Abarca, Z. Dai, M. Montgomery, M. Xu, and J.-A. Bos, *Towards nanoparticle flotation collectors for pentlandite separation*. International Journal of Mineral Processing, 2013. **123**: p. 137-144.
- [10] Abarca, C., S. Yang, and R.H. Pelton, *Towards high throughput screening of nanoparticle flotation collectors*. Journal of colloid and interface science, 2015. **460**: p. 97-104.
- [11] Abarca, C., M.M. Ali, S. Yang, X. Dong, and R.H. Pelton, *A Colloidal Stability Assay Suitable for High-Throughput Screening*. Analytical Chemistry, 2016. **88**(5): p. 2929-2936.
- [12] Thaburet, J.-F., H. Mizomoto, and M. Bradley, *High-Throughput Evaluation of the Wettability of Polymer Libraries*. Macromolecular Rapid Communications, 2004. **25**(1): p. 366-370.
- [13] Wijnans, S., B.-J. de Gans, F. Wiesbrock, R. Hoogenboom, and U.S. Schubert, *Characterization of a Poly(2-oxazoline) Library by High-Throughput, Automated Contact-Angle Measurements and Surface-Energy Calculations*. Macromolecular Rapid Communications, 2004. **25**(23): p. 1958-1962.
- [14] Balazs, A.C., T. Emrick, and T.P. Russell, *Nanoparticle polymer composites: where two small worlds meet*. Science, 2006. **314**(5802): p. 1107-1110.
- [15] Collins, K.D., T. Gensch, and F. Glorius, *Contemporary screening approaches to reaction discovery and development*. Nat Chem, 2014. **6**(10): p. 859-871.

- [16] Kantheti, S., R. Narayan, and K.V.S.N. Raju, *The impact of 1,2,3-triazoles in the design of functional coatings*. RSC Adv., 2015. **5**(5): p. 3687-3708.
- [17] Kolb, H.C., M. Finn, and K.B. Sharpless, *Click chemistry: diverse chemical function from a few good reactions*. Angewandte Chemie International Edition, 2001. **40**(11): p. 2004-2021.
- [18] Lutz, J.F. and G. Nanotechnology for Life Science Research, *1,3-dipolar cycloadditions of azides and alkynes: a universal ligation tool in polymer and materials science*. Angew Chem Int Ed Engl, 2007. **46**(7): p. 1018-25.
- [19] Ackerman, P., G. Harris, R. Klimpel, and F. Aplan, *Use of chelating agents as collectors in the flotation of copper sulfides and pyrite*. Minerals & metallurgical processing, 1999. **16**(1): p. 27-35.
- [20] ASTM, *D1193 - 06 Standard Specification for Reagent Water*. ASTM Standard Manual. 2006 (2011), West Conshohocken: ASTM International. 6.
- [21] Ouadahi, K., E. Allard, B. Oberleitner, and C. Larpent, *Synthesis of azide-functionalized nanoparticles by microemulsion polymerization and surface modification by click chemistry in aqueous medium*. Journal of Polymer Science Part A: Polymer Chemistry, 2012. **50**(2): p. 314-328.
- [22] Staff, R.H., J. Willersinn, A. Musyanovych, K. Landfester, and D. Crespy, *Janus nanoparticles with both faces selectively functionalized for click chemistry*. Polymer Chemistry, 2014. **5**(13): p. 4097.
- [23] Abarca, C., M.M. Ali, D. Bowie, and R.H. Pelton, *A simple assay for azide surface groups on clickable polymeric nanoparticles*. Colloids and Surfaces A: Physicochemical and Engineering Aspects, 2016. **508**: p. 192-196.
- [24] Bräse, S., C. Gil, K. Knepper, and V. Zimmermann, *Organic azides: an exploding diversity of a unique class of compounds*. Angewandte Chemie International Edition, 2005. **44**(33): p. 5188-5240.
- [25] Worrell, B., J. Malik, and V. Fokin, *Direct evidence of a dinuclear copper intermediate in Cu (I)-catalyzed azide-alkyne cycloadditions*. Science, 2013. **340**(6131): p. 457-460.
- [26] Smith, P.A.S., *Open-Chain Nitrogen Compounds*. Vol. 2. 1966, New York: Benjamin.
- [27] Meldal, M. and C.W. Tornøe, *Cu-Catalyzed Azide–Alkyne Cycloaddition*. Chemical Reviews, 2008. **108**(8): p. 2952-3015.
- [28] Pearse, M.J., *An overview of the use of chemical reagents in mineral processing*. Minerals Engineering, 2005. **18**(2): p. 139-149.
- [29] Fischer, B.J., *Particle Convection in an Evaporating Colloidal Droplet*. Langmuir, 2002. **18**(1): p. 60-67.
- [30] Weon, B.M. and J.H. Je, *Self-pinning by colloids confined at a contact line*. Phys Rev Lett, 2013. **110**(2): p. 028303.
- [31] Fritz, G., V. Schädler, N. Willenbacher, and N.J. Wagner, *Electrosteric stabilization of colloidal dispersions*. Langmuir, 2002. **18**(16): p. 6381-6390.
- [32] Ralston, J., S. Dukhin, and N. Mishchuk, *Wetting film stability and flotation kinetics*. Advances in colloid and interface science, 2002. **95**(2): p. 145-236.

- [33] Sinz, A., *Chemical cross-linking and mass spectrometry for mapping three-dimensional structures of proteins and protein complexes*. *Journal of Mass Spectrometry*, 2003. **38**(12): p. 1225-1237.
- [34] Green, T.W. and P. Wuts, *Protective Groups in Organic Synthesis*. 1999, New York: Wiley-Interscience.

**Appendix: Supporting Information for Chapter 5****Throughput Screening of Click Nanoparticle Collectors: A Platform for Modular Functionalization**

Carla Abarca, M. Monsur Ali, and Robert H. Pelton\*

Appendix: Supporting Information for Chapter 5.....	117
Fabrication of triazole nanoparticles: Supporting information.....	118
Experimental .....	118
Materials. ....	118
Synthesis of monomer 4-vinylbenzylazide (VBAz) .....	118
Synthesis of Rhodamine Alkyne (Rho-Alk) .....	119
Attenuated Total Reflection Fourier-Transform Infrared Spectroscopy (atr FT-IR) .....	121
Nuclear Magnetic Resonance (NMR).....	121
Azide nanoparticles recipes, properties and characterization .....	124
Experimental design of miniblock reactions.....	125
Triazole nanoparticles recipes and properties.....	126
Triazole nanoparticle candidates properties plots.....	129
Best triazole nanoparticle candidates properties plots.....	130
Miscellaneous Calculations of Azide Surface Density.....	131
Automated hydrophobicity assay: supporting information .....	132
References Appendix Chapter 5 .....	134

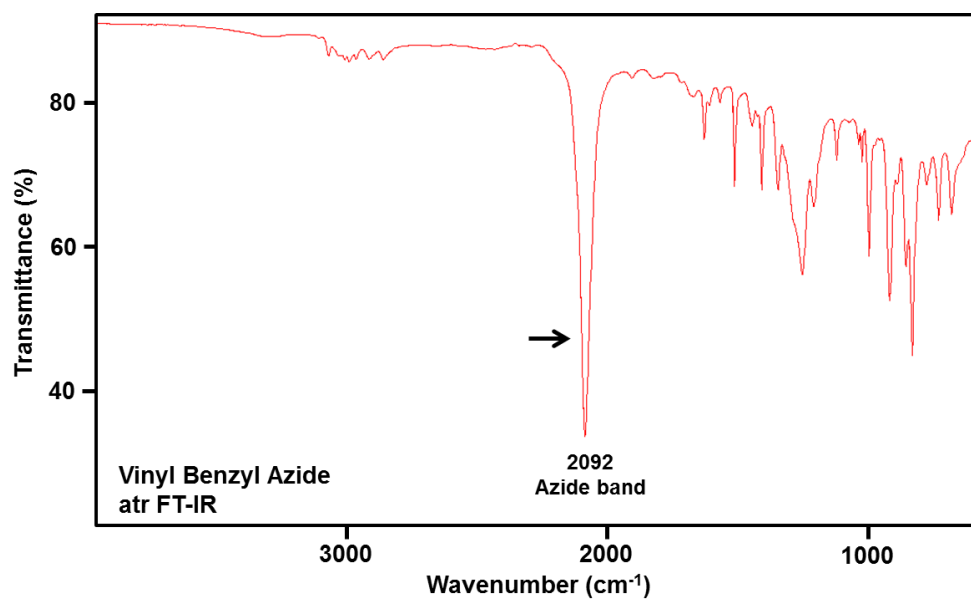
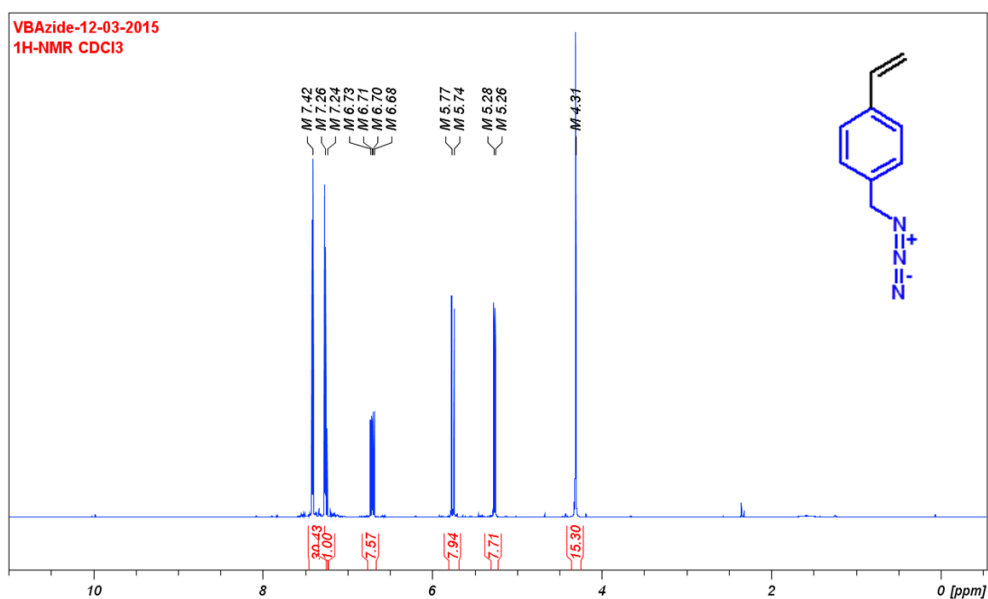
## Fabrication of triazole nanoparticles: Supporting information

### *Experimental*

**Materials.** All the reagents were purchase in Sigma Aldrich unless otherwise noted. In the fabrication of parent azide nanoparticles and synthesis of monomers, Styrene (99%) and 4-vinylbenzylchloride (90%) were purified using distillation. Sodium azide (99%) and sodium iodide (99%) were used without previous purification. Other reagents were Rhodamine B (95%), 4-dimethylaminopyridine (DMAP) (99%), propargyl alcohol (99%), N,N'-Dicyclohexylcarbodiimide (DCC) (99%), sodium bicarbonate (99.5%), anhydrous magnesium sulfate (97%) were used without previous purification. The solvents dimethyl sulfoxide (DMSO) (Caledon, 99,9%), acetonitrile (Caledon, 99%), anhydrous diethyl ether (Caledon, 99%), dichloromethane (Caledon, 99.5%) and water type 1 (as per ASTM D1193-6<sup>[1]</sup>, resistivity 18 M $\Omega$ -cm) were used in experiments accordingly.

### *Synthesis of monomer 4-vinylbenzylazide (VBAz)*

The monomer was prepared by following Ouadahi et al<sup>[2]</sup> procedure with modifications. In a 50 mL 1-neck round bottom flask 10.2 g of sodium azide and 0.58 g of sodium iodide were slowly added to mixture of 5.95 g of 4-vinylbenzylchloride and 25 mL of DMSO. The reaction was stirred at room temperature for 24 hours. The reactions products were extracted in a separatory funnel with 100 mL of water and 100 mL of ether. The organic phase was washed two more times with 100 mL of water. The organic phase was dried with anhydrous magnesium sulfate and filtered by vacuum filtration. Organic solvents were evaporated under vacuum in a rotavapor at room temperature resulting in yellow oil (5.64 g, 94%). This product was analyzed by FT-IR and proton NMR. Relevant signals: FT-IR (ATR diamond crystal): 2092 (azide band), 1288, 1250, 822 cm<sup>-1</sup>. <sup>1</sup>H-NMR (600 MHz, CDCl<sub>3</sub>):  $\delta$  7.42 (d, 2H, Ar-H),  $\delta$  7.26 (d, 2H, Ar-H),  $\delta$  6.73 (dd, 1H, CH=C),  $\delta$  5.77 (dd, 1H, C=CH<sub>2</sub>),  $\delta$  5.28 (dd, 1H, C=CH<sub>2</sub>),  $\delta$  4.31 (s, 2H, CH<sub>2</sub>N<sub>3</sub>, azide peak).

**Figure A 5-1:** atr FT-IR spectrum of monomer vinyl benzyl azide**Figure A 5-2:** <sup>1</sup>H-NMR spectrum of vinyl benzyl azide

### *Synthesis of Rhodamine Alkyne (Rho-Alk)*

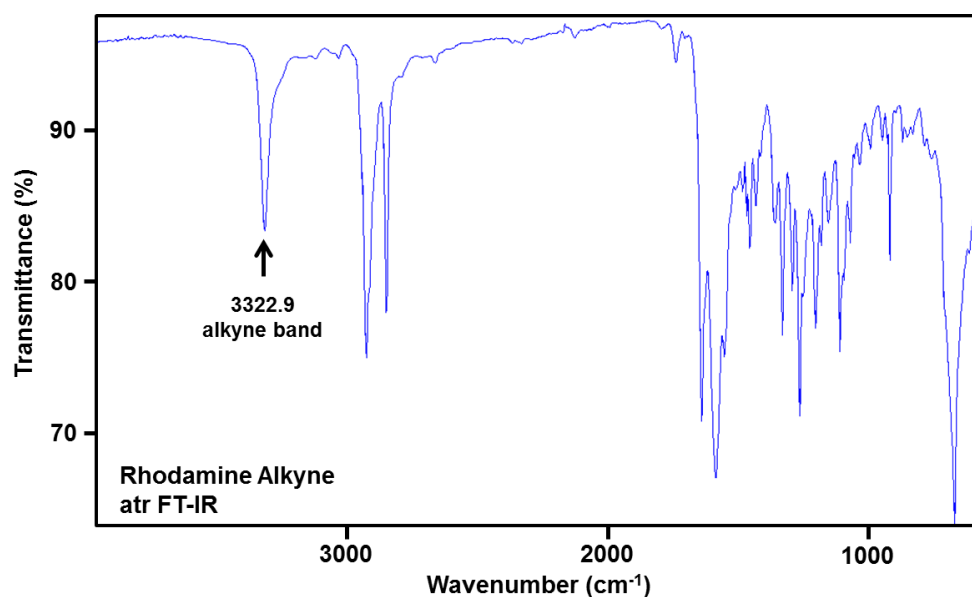
Alkyne functional groups were introduced into Rhodamine B following a reported protocol by Staff and colleagues<sup>[3]</sup> with some modifications. 9.5 g of Rhodamine B,

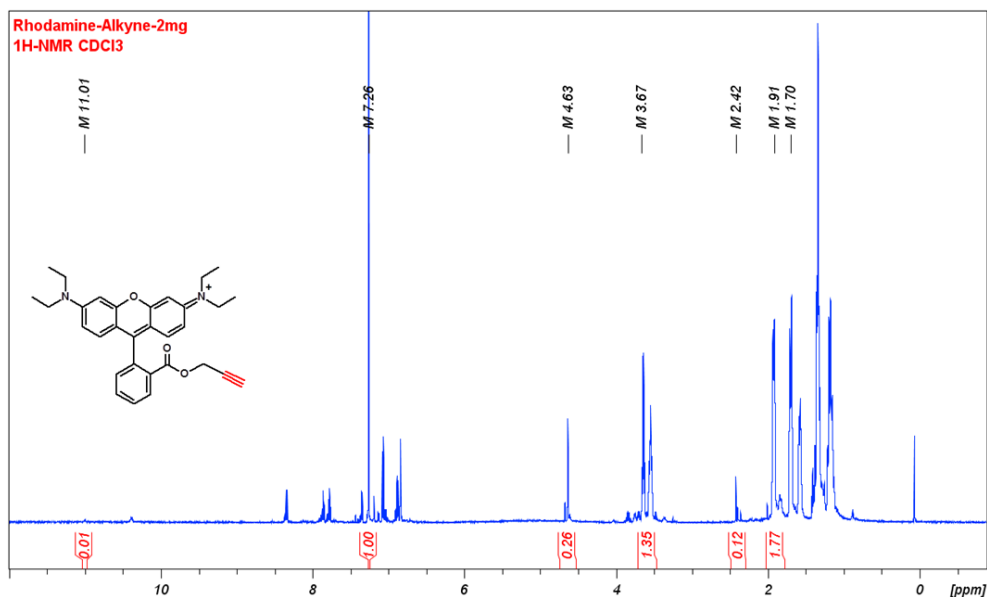
0.024 g of DMAP were added to a dried 3-neck round bottom flask with a stir bar. The mixture was purged in nitrogen for 30 minutes, and 1.27 mL of propargyl alcohol and 90 mL of dichloromethane were added. The flask was cooled to 0° C with an ice bath before adding 8.3 g of DCC dissolved in 10 mL of dichloromethane. The mixture was stirred at 300 RPM for 30 minutes and then allowed to stir for 24 h at room temperature.

The resulting mixture was filtered through a gravity funnel and washed in dichloromethane until approximately 200 mL of solution was obtained. The solution was added to a 500 mL separatory funnel and washed 2 more times with 200 mL of saturated sodium bicarbonate. A final wash step was conducted with water. The organic phase was collected and was dried overnight with magnesium sulfate. Vacuum filtration with a fritted glass funnel was used to remove the magnesium sulfate. The remaining dichloromethane was evaporated in a vacuum rotavap.

The residue was re-dissolved in acetonitrile and re-precipitated in diethyl ether 3 times and filtrated by vacuum filtration in a ceramic funnel provided with a Whatman #1 filter paper. The residue was washed 3 times in diethyl ether and dried in a vacuum oven overnight. 5.1 g of a golden powder were produced (45%, relevant bands: atr FT-IR: 3322.9 cm<sup>-1</sup> alkyne band. <sup>1</sup>H-NMR (600 MHz, CDCl<sub>3</sub>): δ 2.42, δ 1.91 (alkyne bands), carboxylic acid band at ~ δ 11 disappeared.

**Figure A 5-3:** atr FT-IR spectrum of Rhodamine Alkyne



**Figure A 5-4:**  $^1\text{H-NMR}$  spectrum of Rhodamine Alkyne

### ***Attenuated Total Reflection Fourier-Transform Infrared Spectroscopy (atr FT-IR)***

atr FT-IR spectra were acquired for the monomers and nanoparticle samples in order to confirm the reactions were successful. In the experiment, around 5 mg were placed onto the diamond crystal at the atr accessory and it was pressed against the swivel pressure tower of a TENSOR II FT-IR Spectrometer (Bruker Corp. ). The spectra were obtained with the OPUS Spectroscopy Software (Bruker) and analyzed by Thermo Scientific™ OMNIC™ Software. Spectra of monomers and nanoparticles prepared are shown in Figure A 5-1, Figure A 5-3, Figure A 5-5 and Figure A 5-6.

### ***Nuclear Magnetic Resonance (NMR)***

$^1\text{H-NMR}$  spectra were obtained in monomers for characterization and in all the nanoparticle samples to calculate the total azide content on each nanoparticle.  $^{13}\text{C-NMR}$ , 2D-HSQC and 2D-HMBC were acquired in selected nanoparticles to confirm reaction completion. In a typical experiment, a measured amount between 10-15 mg of dry sample was dissolved in 1 mL of deuterated chloroform,  $\text{CDCl}_3$ , and measured in a 600 MHz NMR spectrophotometer at 25 °C. The nanoparticles with a high concentration of azide needed longer time to dissolve in chloroform and in some cases mild sonication was required.



Spectra are shown in Figure A 5-2, Figure A 5-4, Figure A 5-7, Figure A 5-8 and Figure A 5-9

Figure A 5-5: FT-IR spectra for azide nanoparticles, series SA-400. A) Full spectra; B) Zoom-in at 2300 - 1900  $\text{cm}^{-1}$ .

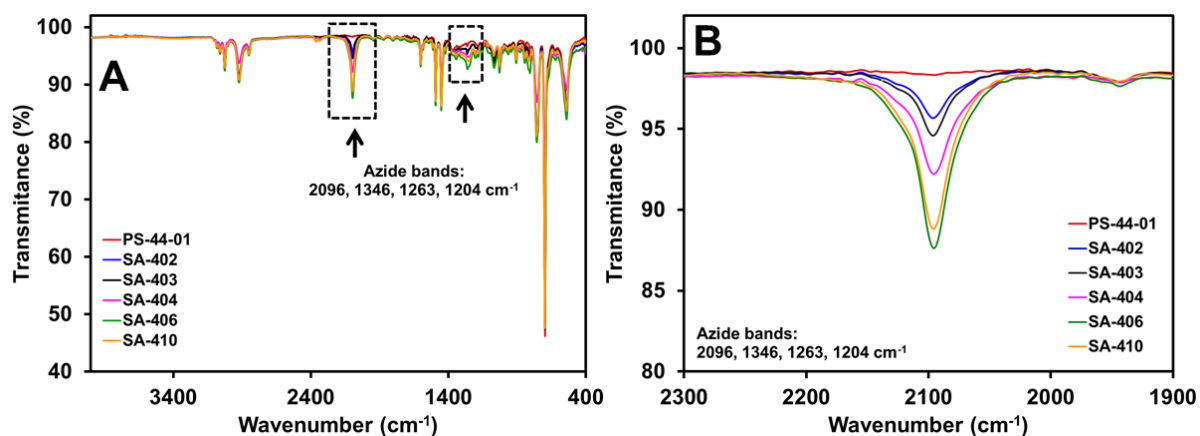
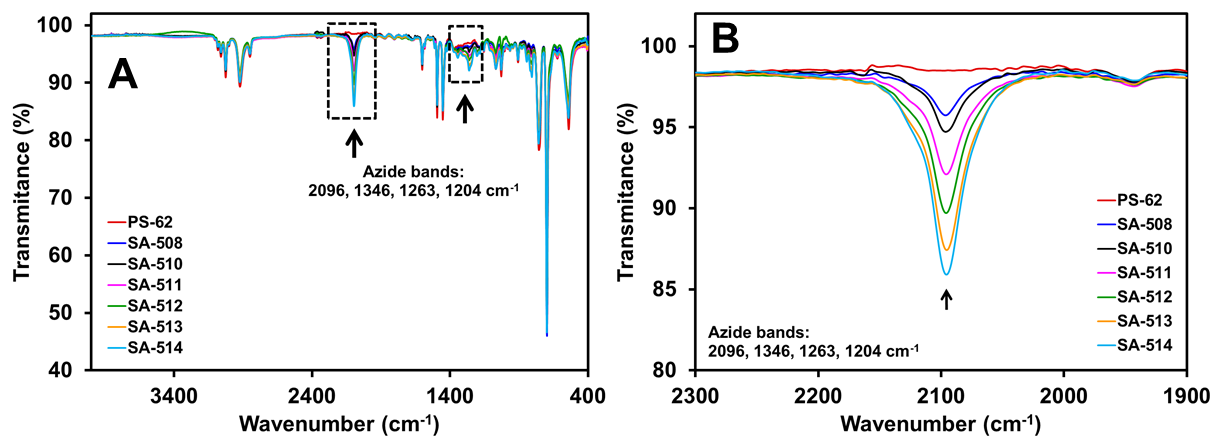
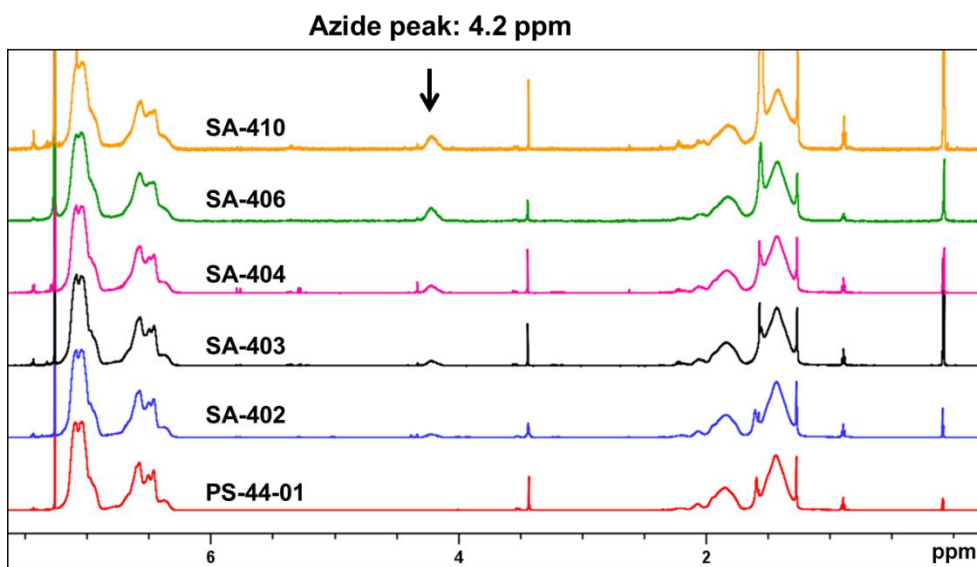
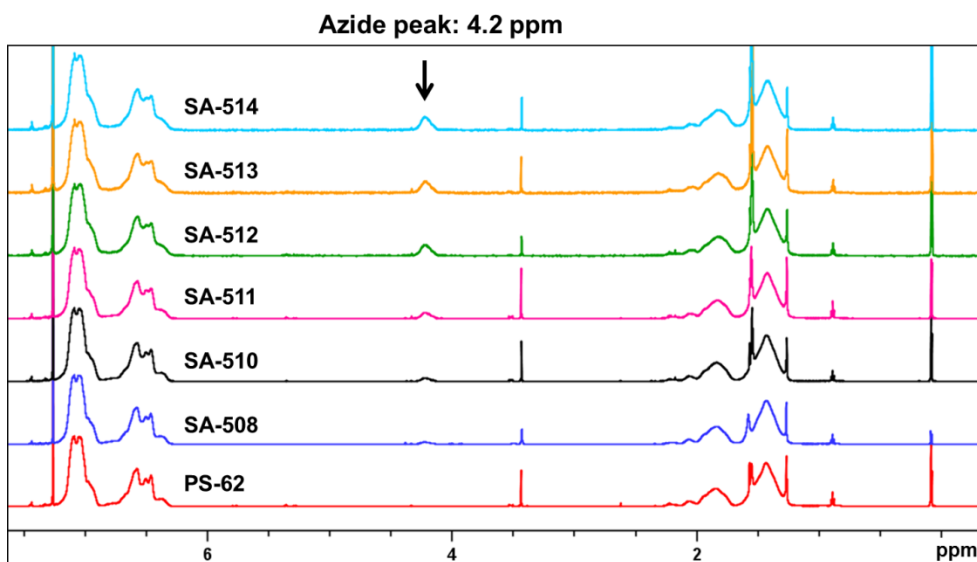
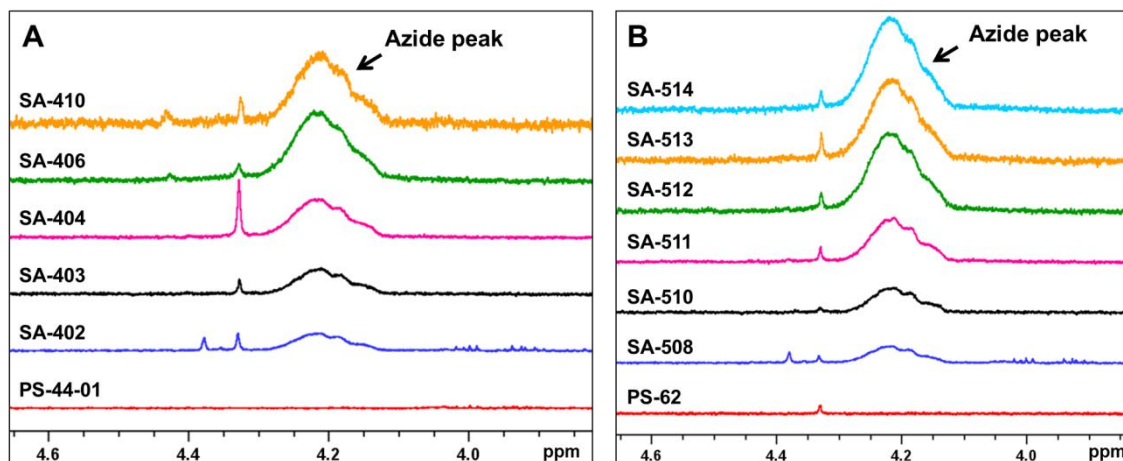


Figure A 5-6: FT-IR spectra for azide nanoparticles, series SA-500. A) Full spectra; B) Zoom-in at 2300 - 1900  $\text{cm}^{-1}$ .



**Figure A 5-7:**  $^1\text{H}$ -NMR spectra for azide nanoparticles, series SA-400.**Figure A 5-8:**  $^1\text{H}$ -NMR spectra for azide nanoparticles, series SA-500.

**Figure A 5-9:** Zoom-in of  $^1\text{H-NMR}$  spectra for azide nanoparticles. A) series SA-500; B) series SA-400.



### *Azide nanoparticles recipes, properties and characterization*

**Table A 5-1:** Properties of parent azide latexes. Polymerizations were conducted in 0.1 g CTAB as surfactant for 48 hrs. The 500 series was initiated with V50 whereas the 400 series was made with V44.

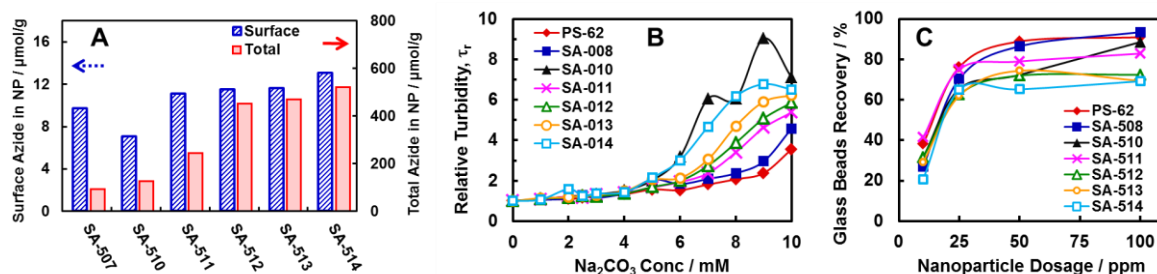
Sample Designation	Azide Monomer added, mg	Azide/Styrene Mole <sup>b</sup> , %	Solids Content, g/L	Diameter <sup>a</sup> , nm (PDI)	EM <sup>a</sup> , $\times 10^{-8} \text{m}^2 \text{s}^{-1} \text{V}^{-1}$	Total Azide <sup>b</sup> , $\lambda_{\text{Taz}}$ ( $\mu\text{mol/g}$ )	Surface Azide <sup>c</sup> , $\lambda_{\text{SAz}}$ ( $\mu\text{mol/g}$ )
PS-62	/	/	43	62 (0.01)	3.3	/	/
SA-507	125	59.8	39	55 (0.05)	3.2	94.2	11.3
SA-508	125	60.4	40	62 (0.06)	2.6	94.2	10.8
SA-510	250	40.1	40	53 (0.06)	2.7	125.6	8.6
SA-511	375	50.2	38	53 (0.05)	2.4	245.0	12.6
SA-512	500	67.3	39	59 (0.07)	2.3	452.3	13.1
SA-513	750	46.8	48	59 (0.05)	3.2	471.1	13.2
SA-514	1000	37.8	49	57 (0.07)	2.7	521.4	14.6
PS-62-4	/	/	45	62 (0.04)	3.0	/	/
SA-402	125	62.5	46	53 (0.06)	2.1	100.5	12.2
SA-403	250	44.4	43	61 (0.03)	2.5	144.5	10.8
SA-404	375	49.0	44	54 (0.09)	2.4	238.7	15.4
SA-406	750	42.0	46	58 (0.02)	3.2	427.2	15.5
SA-410	1000	31.3	49	64 (0.03)	3.4	414.6	13.6

a Particle diameters and electrophoretic mobilities (EM) were measured in 5 mM NaCl.

b The total azide compositions were measured by  $^1\text{H-NMR}$ .

c Surface azide content was obtained from a paper chromatography assay previously published [4].

**Figure A 5-10:** Azide nanoparticle analysis for series SA-500: A) Surface azide ( $\lambda_{SAZ}$ ), versus total azide ( $\lambda_{TAZ}$ ); B) Relative turbidity plots; and C) Glass beads flotation in 5 mM sodium carbonate at different nanoparticle dosage.



### Experimental design of miniblock reactions

**Table A 5-2:** Example of a miniblock experimental design. Reagents concentrations on each vessel are detailed in  $\mu\text{L}$ . The total volume of reaction was 10 mL. A to D: rows in the miniblock; 1 to 6: columns.

<b>Factor</b>		<b>PS-44-01</b>	<b>SA-402</b>	<b>water</b>	<b>PS44-01</b>	<b>SA-402</b>	<b>water</b>
Controls	10 g/L	0.5 mM	1 mM	1 mM	1 mM	1 mM	1 mM
[uL]	Reagents	<b>1</b>	<b>2</b>	<b>3</b>	<b>4</b>	<b>5</b>	<b>6</b>
<b>A</b>	Water	7400	7400	7400	8000	8000	8000
	Cu	200	200	200	0	0	0
	NaAsc	200	200	200	0	0	0
	PMDETA	200	200	200	0	0	0
	Alkyne	0	0	0	0	0	0
	NP	2000	2000	2000	2000	2000	2000
<b>Factor</b>	<b>SA-402</b>	<b>Rho-Alk</b>	<b>Am-PEG4</b>	<b>Hexyne</b>	<b>Pentyne</b>	<b>PrAm</b>	<b>PrOH</b>
1:1	10 g/L	0.5 mM	1 mM	1 mM	1 mM	1 mM	1 mM
[uL]	Reagents	<b>1</b>	<b>2</b>	<b>3</b>	<b>4</b>	<b>5</b>	<b>6</b>
<b>B</b>	Water	6760	7080	7080	7080	7080	7080
	Cu	200	200	200	200	200	200
	NaAsc	200	200	200	200	200	200
	PMDETA	200	200	200	200	200	200
	Alkyne	640	320	320	320	320	320
	NP	2000	2000	2000	2000	2000	2000
<b>Factor</b>	<b>SA-402</b>	<b>Rho-Alk</b>	<b>Am-PEG4</b>	<b>Hexyne</b>	<b>Pentyne</b>	<b>PrAm</b>	<b>PrOH</b>
1:0.5	10 g/L	0.5 mM	1 mM	1 mM	1 mM	1 mM	1 mM
[uL]	Reagents	<b>1</b>	<b>2</b>	<b>3</b>	<b>4</b>	<b>5</b>	<b>6</b>
<b>C</b>	Water	7080	7240	7240	7240	7240	7240
	Cu	200	200	200	200	200	200
	NaAsc	200	200	200	200	200	200
	PMDETA	200	200	200	200	200	200
	Alkyne	320	160	160	160	160	160
	NP	2000	2000	2000	2000	2000	2000
<b>Factor</b>	<b>SA-402</b>	<b>Rho-Alk</b>	<b>Am-PEG4</b>	<b>Hexyne</b>	<b>Pentyne</b>	<b>PrAm</b>	<b>PrOH</b>
1:0.25	10 g/L	0.5 mM	1 mM	1 mM	1 mM	1 mM	1 mM
[uL]	Reagents	<b>1</b>	<b>2</b>	<b>3</b>	<b>4</b>	<b>5</b>	<b>6</b>
<b>D</b>	Water	7240	7320	7320	7320	7320	7320
	Cu	200	200	200	200	200	200
	NaAsc	200	200	200	200	200	200
	PMDETA	200	200	200	200	200	200
	Alkyne	160	80	80	80	80	80
	NP	2000	2000	2000	2000	2000	2000



*Triazole nanoparticles recipes and properties*

**Table A 5-3:** Recipes and properties of triazole nanoparticles made from SA-402 as parent azide. Other reagents were 2 mL of SA-402 10 g/L; 200  $\mu$ L of 1 mM copper sulfate; 200  $\mu$ L of 1 mM PMDETA and 200  $\mu$ L of 10 mM sodium ascorbate, and water to complete a volume of 10 mL on each vessel. Note: results are grouped by alkyne type.

Sample Name	Alkyne sol. $C_f$ ( $\mu$ mol/L)	Alkyne surf. density, $\lambda_{SAIk}$ (molecules / $nm^2$ )	Alkyne / surf. azide ratio	Alkyne stock sol. $C_i$ (mM)	Alkyne vol. , $V$ ( $\mu$ L)	CCC in $Na_2CO_3$ (mM)	Water contact angle, $\theta$ ( $^\circ$ )	Contact angle std. error	Glass bead flotation recovery (%)
PS-44-01	0	0	0.00	0	0	6.5	85.1	1.1	69.2
SA-402	0	0	0.00	0	0	6.5	92.1	2.0	73.1
SA-406	0	0	0.00	0	0	5.0	91.6	2.4	69.2
T-PrAm-8	8	0.022	0.25	1	80	7.5	87.2	0.2	76.6
T-PrAm-16	16	0.045	0.50	1	160	5.5	78.8	1.4	65.5
T-PrAm-32	32	0.089	1.00	1	320	7.5	69.0	0.4	87.4
T-NdMPrAm-8	8	0.022	0.25	1	80	6.5	80.3	0.9	68.0
T-NdMPrAm-16	16	0.045	0.50	1	160	6.5	73.2	1.6	70.6
T-NdMPrAm-32	32	0.089	1.00	1	320	7.5	66.1	0.6	85.0
T-BocPrAm-8	8	0.022	0.25	1	80	8.0	76.7	0.9	65.0
T-BocPrAm-16	16	0.045	0.50	1	160	7.0	74.7	1.8	67.2
T-BocPrAm-32	32	0.089	1.00	1	320	8.0	67.0	1.9	66.7
T-Parg-8	8	0.022	0.25	1	80	6.0	90.2	1.3	ND
T-Parg-16	16	0.045	0.50	1	160	5.5	92.1	1.7	ND
T-Parg-32	32	0.089	1.00	1	320	5.5	95.5	1.0	ND
T-RhoAlk-8	8	0.022	0.25	0.5	160	5.0	74.3	0.2	63.0
T-RhoAlk-16	16	0.045	0.50	0.5	320	5.0	71.7	0.9	65.6
T-RhoAlk-32	32	0.089	1.00	0.5	640	8.0	67.1	0.5	92.9
T-AmPEG4-8	8	0.022	0.25	1	80	7.0	75.8	1.0	65.0
T-AmPEG4-16	16	0.045	0.50	1	160	8.0	72.1	1.5	69.3
T-AmPEG4-32	32	0.089	1.00	1	320	9.5	68.5	0.8	90.4
T-PEG4MI-8	8	0.022	0.25	1	80	4.0	79.6	1.2	ND
T-PEG4MI-16	16	0.045	0.50	1	160	3.0	75.2	1.7	ND
T-PEG4MI-32	32	0.089	1.00	1	320	2.5	62.2	1.7	ND
T-Pen-8	8	0.022	0.25	1	80	5.0	101.4	1.1	ND
T-Pen-16	16	0.045	0.50	1	160	5.0	99.0	0.7	ND
T-Pen-32	32	0.089	1.00	1	320	5.0	98.1	0.4	ND
T-Hex-8	8	0.022	0.25	1	80	5.0	94.4	0.2	ND
T-Hex-16	16	0.045	0.50	1	160	5.0	94.3	0.3	ND
T-Hex-32	32	0.089	1.00	1	320	5.0	90.7	0.4	ND
T-PrBr-8	8	0.022	0.25	1	80	5.0	91.6	0.8	ND
T-PrBr-16	16	0.045	0.50	1	160	6.5	78.8	1.8	ND

T-PrBr-32	32	0.089	1.00	1	320	6.5	69.1	0.5	ND
T-BrBu-8	8	0.022	0.25	1	80	6.5	95.3	0.6	ND
T-BrBu-16	16	0.045	0.50	1	160	5.5	93.2	1.6	ND
T-BrBu-32	32	0.089	1.00	1	320	6.0	89.2	2.0	ND
T-PrOH-8	8	0.022	0.25	1	80	5.5	85.6	0.5	ND
T-PrOH-16	16	0.045	0.50	1	160	5.5	73.3	2.3	ND
T-PrOH-32	32	0.089	1.00	1	320	5.5	61.5	1.6	ND
T-BuTos-8	8	0.022	0.25	1	80	8.5	84.9	0.5	81.1
T-BuTos-16	16	0.045	0.50	1	160	8.0	79.8	1.2	71.7
T-BuTos-32	32	0.089	1.00	1	320	9.0	82.5	0.2	84.0

**Table A 5-4:** Recipes and properties of triazole nanoparticles made from SA-508 as parent azide. Other reagents were 2 mL of SA-508 10 g/L; 200  $\mu$ L of 1 mM copper sulfate; 200  $\mu$ L of 1 mM PMDETA and 200  $\mu$ L of 10 mM sodium ascorbate, and water to complete a volume of 10 mL on each vessel. Note: results are grouped by alkyne type.

Sample Name	Alkyne sol. $C_f$ ( $\mu$ mol/L)	Alkyne surf. density, $\lambda_{SAIk}$ (molecules/ $\text{nm}^2$ )	Alkyne to surface azide ratio	Alkyne stock sol. $C_i$ (mM)	Alkyne vol. , V ( $\mu$ L)	CCC in $\text{Na}_2\text{CO}_3$ (mM)	Water contact angle, $\theta$ ( $^\circ$ )	Contact angle std. error
PS-62	0	0	0.00	0	0	7.0	83.0	0.8
SA-508	0	0	0.00	0	0	6.0	89.0	1.3
SA-513	0	0	0.00	0	0	5.0	85.0	0.8
T8-PrAm-8	8	0.022	0.25	1	80	7.0	80.7	0.9
T8-PrAm-16	16	0.045	0.50	1	160	5.5	76.0	0.4
T8-PrAm-32	32	0.089	1.00	1	320	5.0	63.4	0.4
T8-NdMPrAm-8	8	0.022	0.25	1	80	7.0	77.4	0.2
T8-NdMPrAm-16	16	0.045	0.50	1	160	6.0	68.9	0.8
T8-NdMPrAm-32	32	0.089	1.00	1	320	5.5	60.6	0.9
T8-BocPrAm-8	8	0.022	0.25	1	80	7.5	73.4	0.7
T8-BocPrAm-16	16	0.045	0.50	1	160	7.0	67.7	0.2
T8-BocPrAm-32	32	0.089	1.00	1	320	7.0	60.2	0.5
T8-Parg-8	8	0.022	0.25	1	80	5.5	91.1	0.6
T8-Parg-16	16	0.045	0.50	1	160	5.0	93.9	0.3
T8-Parg-32	32	0.089	1.00	1	320	5.0	95.1	0.5
T8-RhoAlk-8	8	0.022	0.25	0.5	160	5.0	72.2	0.5
T8-RhoAlk-16	16	0.045	0.50	0.5	320	6.0	65.9	0.4
T8-RhoAlk-32	32	0.089	1.00	0.5	640	7.5	61.7	1.1
T8-AmPEG4-8	8	0.022	0.25	1	80	7.5	68.5	0.3
T8-AmPEG4-16	16	0.045	0.50	1	160	7.0	67.2	0.6
T8-AmPEG4-32	32	0.089	1.00	1	320	8.0	62.7	0.7
T8-PEG4MI-8	8	0.022	0.25	1	80	3.0	76.1	0.6
T8-PEG4MI-16	16	0.045	0.50	1	160	3.0	68.6	1.1
T8-PEG4MI-32	32	0.089	1.00	1	320	2.5	58.9	0.8

T8-Pen-8	8	0.022	0.25	1	80	4.5	95.1	0.2
T8-Pen-16	16	0.045	0.50	1	160	5.0	95.8	0.3
T8-Pen-32	32	0.089	1.00	1	320	4.5	96.7	0.9
T8-Hex-8	8	0.022	0.25	1	80	5.0	93.9	0.4
T8-Hex-16	16	0.045	0.50	1	160	5.0	99.7	1.7
T8-Hex-32	32	0.089	1.00	1	320	4.0	95.4	0.6
T8-PrBr-8	8	0.022	0.25	1	80	5.0	91.6	0.2
T8-PrBr-16	16	0.045	0.50	1	160	5.5	75.0	0.6
T8-PrBr-32	32	0.089	1.00	1	320	5.5	61.4	0.5
T8-BrBu-8	8	0.022	0.25	1	80	6.5	91.6	0.6
T8-BrBu-16	16	0.045	0.50	1	160	6.0	83.7	0.7
T8-BrBu-32	32	0.089	1.00	1	320	6.0	82.6	0.3
T8-PrOH-8	8	0.022	0.25	1	80	5.5	80.0	0.3
T8-PrOH-16	16	0.045	0.50	1	160	5.5	62.6	0.8
T8-PrOH-32	32	0.089	1.00	1	320	6.0	59.3	1.3
T8-BuTos-8	8	0.022	0.25	1	80	8.0	79.8	0.3
T8-BuTos-16	16	0.045	0.50	1	160	8.0	80.5	0.6
T8-BuTos-32	32	0.089	1.00	1	320	7.0	78.0	1.4

**Table A 5-5:** Nanoparticle candidates results for SA-402 as parent azide: High throughput critical coagulation concentrations, automated water contact angle and glass beads recovery. Note: results are grouped by alkyne concentration in nanoparticle ( $\mu\text{M}$ ).

Alkyne	CCC in Sodium Carbonate, mM			Water Contact Angle, $\theta$			Glass Beads Flotation Recovery, %		
	8 $\mu\text{M}$	16 $\mu\text{M}$	32 $\mu\text{M}$	8 $\mu\text{M}$	16 $\mu\text{M}$	32 $\mu\text{M}$	8 $\mu\text{M}$	16 $\mu\text{M}$	32 $\mu\text{M}$
T-RhoAlk	5.0	5.0	8.0	74.3	71.7	67.1	63.0	65.6	92.9
T-AmPEG4	7.0	8.0	9.5	75.8	72.1	68.5	65.0	69.3	90.4
T-PrAm	7.5	5.5	7.5	87.2	78.8	69.0	76.6	65.5	87.4
T-N-dMPrAm	6.5	6.5	7.5	80.3	73.2	66.1	68.0	70.6	85.0
T-BuTos	8.5	8.0	9.0	84.9	79.8	82.5	81.1	71.7	84.0
T-BocPrAm	8.0	7.0	8.0	76.7	74.7	67.0	65.0	67.2	66.7
T-PrBr	5.0	6.5	6.5	91.6	78.8	69.1	ND	ND	ND
T-BrBu	6.5	5.5	6.0	95.3	93.2	89.2	ND	ND	ND
T-Parg	6.0	5.5	5.5	90.2	92.1	95.5	ND	ND	ND
T-PrOH	5.5	5.5	5.5	85.6	73.3	61.5	ND	ND	ND
T-Pentyne	5.0	5.0	5.0	101.4	99.0	98.1	ND	ND	ND
T-Hexyne	5.0	5.0	5.0	94.4	94.3	90.7	ND	ND	ND
T-PEG4MI	4.0	3.0	2.5	79.6	75.2	62.2	ND	ND	ND

\*\* ND: Not determined because nanoparticle candidates did not fall on the green flotation domain.

*Triazole nanoparticle candidates properties plots*

**Figure A 5-11:** Advancing water contact angles: A) amine-based triazole nanoparticles; B) miscellaneous triazole nanoparticles. Note: results are grouped by alkyne type and by alkyne concentration in nanoparticle ( $\mu\text{M}$ ).

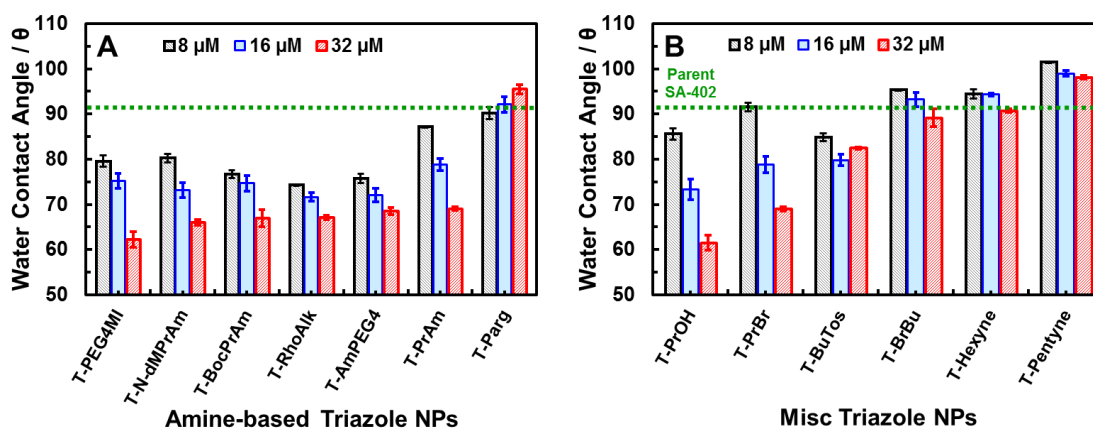
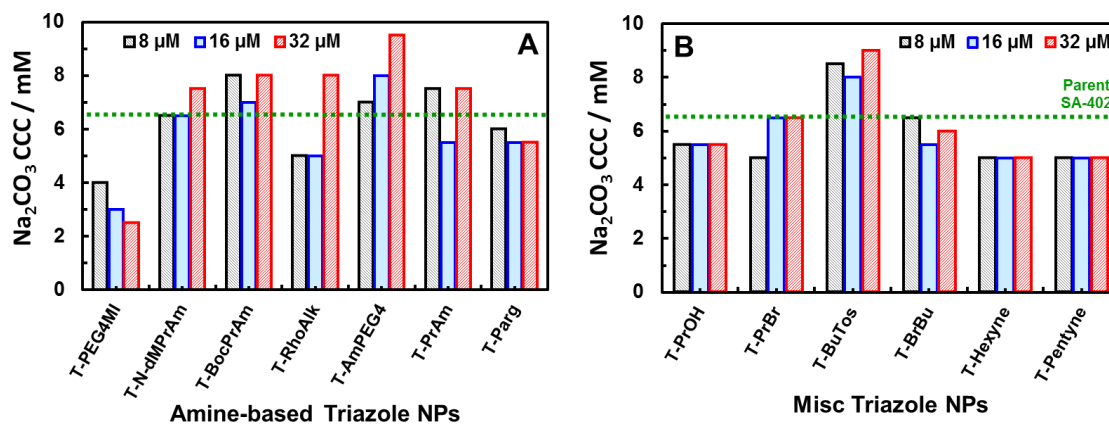


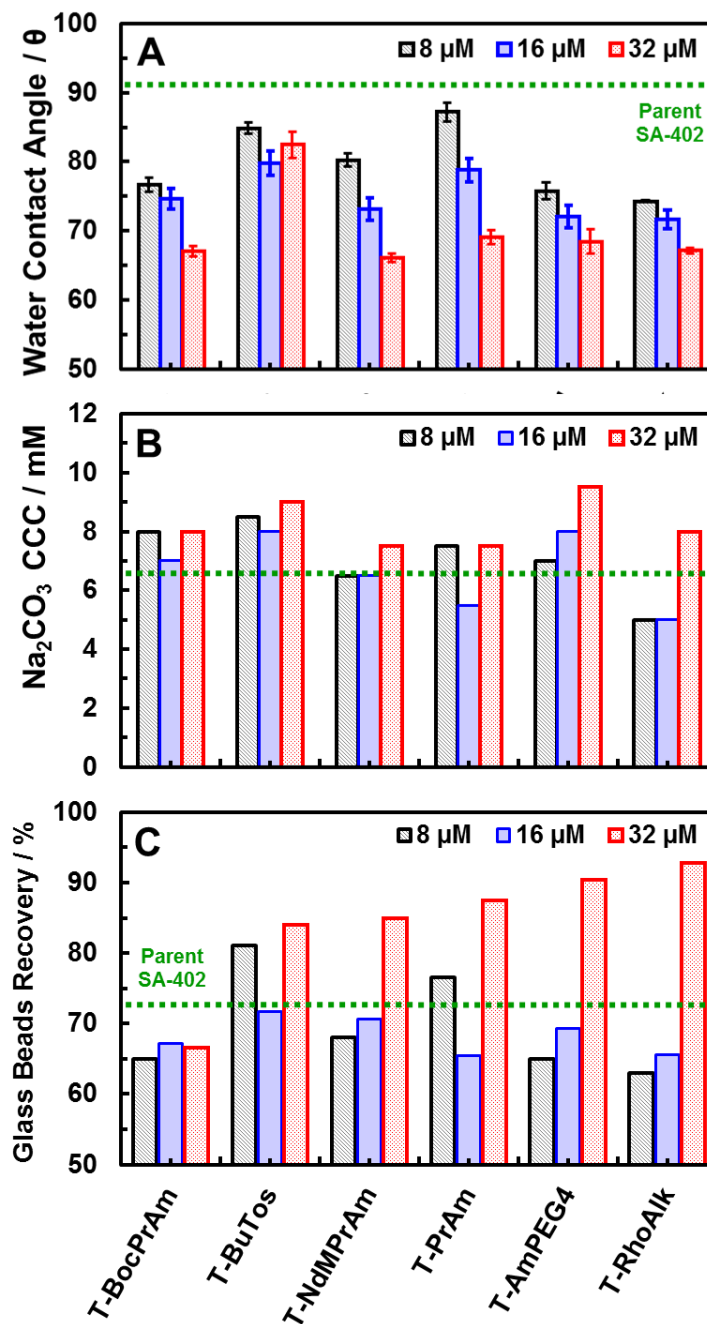
**Figure A 5-12:** Critical coagulation concentrations in sodium carbonate: A) amine-based triazole nanoparticles; B) miscellaneous triazole nanoparticles. Note: results are grouped by alkyne type and by alkyne concentration in nanoparticle ( $\mu\text{M}$ ).





### Best triazole nanoparticle candidates properties plots

**Figure A 5-13:** Best candidates results of: A) water contact angle; B) critical coagulation concentrations and; C) glass beads flotation in 5 mM of sodium carbonate. Green dashed line indicates parent nanoparticle, SA-402, value. Note: results are grouped by alkyne type and by alkyne concentration in nanoparticle ( $\mu\text{M}$ ).



### Miscellaneous Calculations of Azide Surface Density

As example, PTC Mathcad calculations for surface density of SA-402, parent nanoparticle, calculated from the azide concentration in the click reaction (32  $\mu\text{mol/L}$ ), is shown below:

$$\begin{aligned}
 d_{NP} &:= 53 \text{ nm} && \text{diameter of nanoparticle} && \rho_{NP} &:= 1.05 \frac{\text{gm}}{\text{mL}} && \text{density of nanoparticle} \\
 m_{iNP} &:= 10 \frac{\text{mg}}{\text{mL}} && \text{Initial Mass concentration of NP} && m_{fNP} &:= 2 \frac{\text{mg}}{\text{mL}} && \text{Mass concentration of NP in reaction} \\
 V_{NP} &:= 2000 \mu\text{L} && V_T &:= 10000 \mu\text{L} \\
 M_{SAz} &:= 32 \frac{\mu\text{mol}}{\text{L}} && \text{Concentration of Alkyne in reaction} \\
 \lambda_{SAz} &:= \frac{M_{SAz}}{m_{fNP}} = 16 \frac{\mu\text{mol}}{\text{gm}} && \text{Surface azide per NP mass in reaction (umol/gm)} \\
 \end{aligned}$$

Specific surface area of nanoparticle (m<sup>2</sup>/gm):

$$\sigma_{NP} := \frac{4 \pi \cdot \left(\frac{d_{NP}}{2}\right)^2}{\frac{4}{3} \pi \cdot \left(\frac{d_{NP}}{2}\right)^3 \cdot \rho_{NP}} = 107.817 \frac{\text{m}^2}{\text{gm}}$$

Surface Area of 1 nanoparticle:

$$A_{NP} := 4 \pi \cdot \left(\frac{d_{NP}}{2}\right)^2 = (8.825 \cdot 10^3) \text{ nm}^2$$

Surface Azide density per area of NP (nmol/m<sup>2</sup>):

$$\sigma_{SAz} := \lambda_{SAz} \cdot \frac{1}{\sigma_{NP}} = 0.148 \frac{\mu\text{mol}}{\text{m}^2}$$

Azide Molecules per nm<sup>2</sup>:

$$\sigma_{SAz} := \frac{\lambda_{SAz}}{\sigma_{NP}} \cdot N_A = 0.089 \frac{1}{\text{nm}^2}$$

Azide molecules in 1 single nanoparticle:

$$n_{SAz} := \frac{\lambda_{SAz}}{\sigma_{NP}} \cdot N_A \cdot A_{NP} = 788.654$$

## Automated hydrophobicity assay: supporting information

**Figure A 5-14:** Parallel and automated spin coating and dip coating procedures.

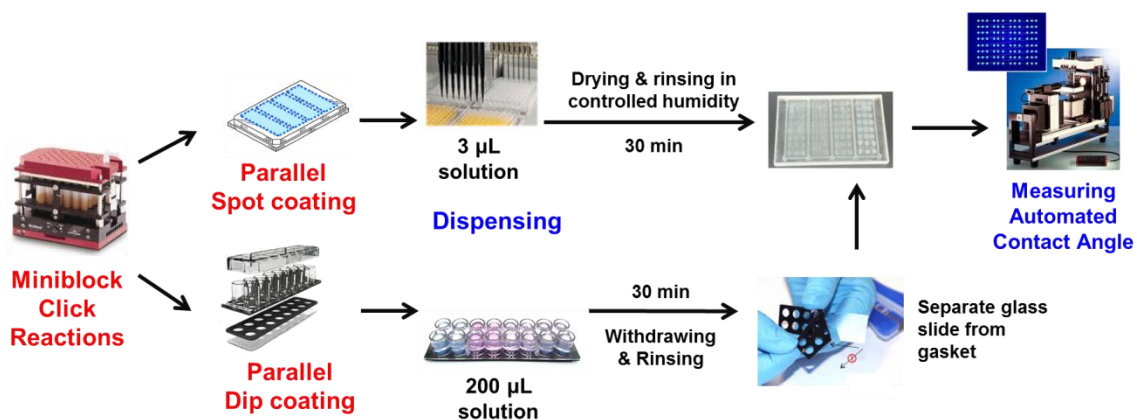


**Figure A 5-15:** Additional SEM micrographs for: A, B) spot coating of triazole Rho-Alk nanoparticles; C, D) automated dip coating of triazole Rho-Alk nanoparticles.

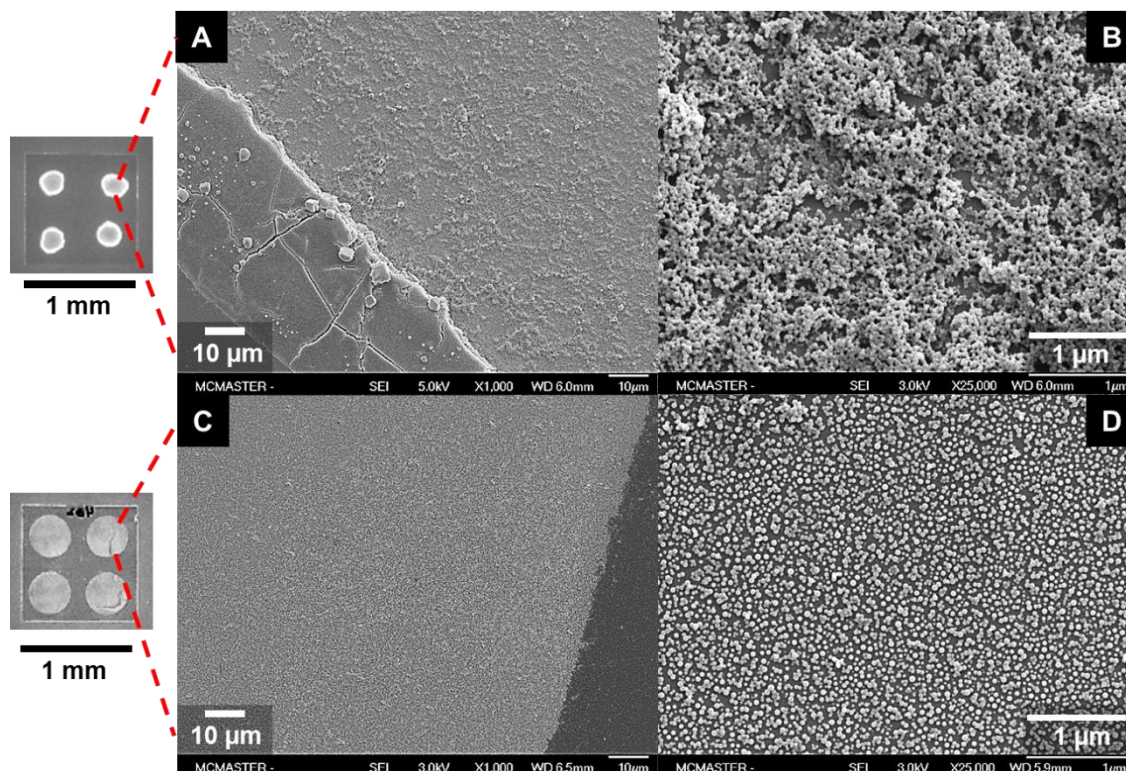
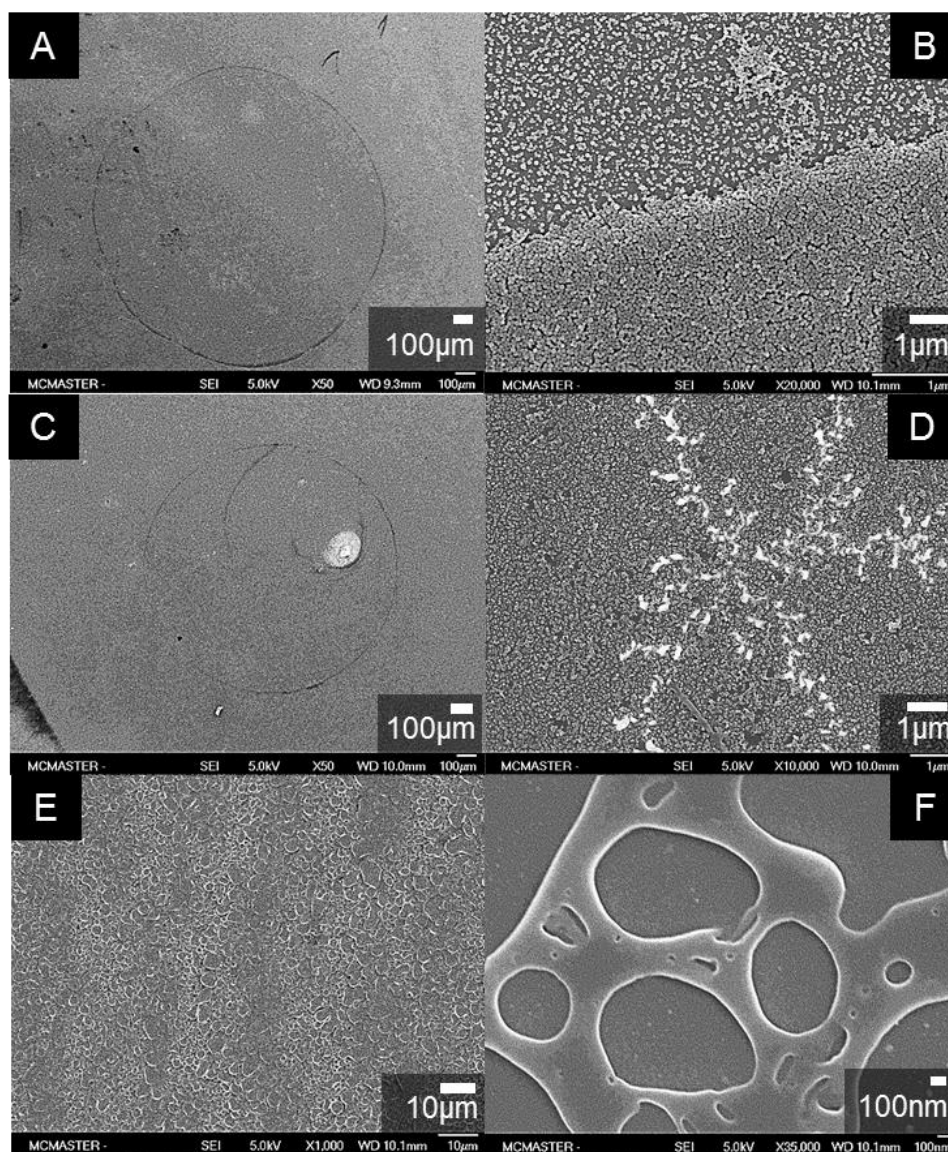


**Figure A 5-16:** SEM micrographs of glass slides surface after advancing water contact angle measurements. A, B) Automated spot coating method with previous rinsing on water; C, D) Automated spot coating method without previous rinsing on water; E, F) Automated spot coating, and further chloroform coating on the slide to dissolve the nanoparticles on the surface of the glass slides.



**References Appendix Chapter 5**

- [1] ASTM, *D1193 - 06 Standard Specification for Reagent Water*. ASTM Standard Manual. 2006 (2011), West Conshohocken: ASTM International. 6.
- [2] Ouadahi, K., E. Allard, B. Oberleitner, and C. Larpent, *Synthesis of azide-functionalized nanoparticles by microemulsion polymerization and surface modification by click chemistry in aqueous medium*. Journal of Polymer Science Part A: Polymer Chemistry, 2012. **50**(2): p. 314-328.
- [3] Staff, R.H., J. Willersinn, A. Musyanovych, K. Landfester, and D. Crespy, *Janus nanoparticles with both faces selectively functionalized for click chemistry*. Polymer Chemistry, 2014. **5**(13): p. 4097.
- [4] Abarca, C., M.M. Ali, D. Bowie, and R.H. Pelton, *A simple assay for azide surface groups on clickable polymeric nanoparticles*. Colloids and Surfaces A: Physicochemical and Engineering Aspects, 2016. **508**: p. 192-196.

## Chapter 6: Concluding Remarks

This thesis has focused in developing a platform for rapid fabrication and screening of nanoparticle libraries, specifically polystyrene modified with hydrophilic and hydrophobic chemicals, that function as collectors in froth flotation of minerals. By following a high throughput screening perspective, this work has investigated and implemented parallel and automated techniques for screening materials. In this work, we have presented the first uses of high throughput technologies applied to the development of mineral flotation collectors, in order to accelerate the discovery of nanoparticle collectors.

### 6.1. Key Findings and Contributions

The research objectives presented in chapter 1 have been achieved, and the key findings of this work include:

- 6.1.1. Our overall objective, an accelerated process to develop polystyrene nanoparticles that can function as collectors, has been proposed and implemented. Although, previous approaches to produce nanoparticle collectors, involving individual synthesis and characterization, were very useful to understand the mechanisms of this technology, they were too inefficient to find new surface chemistries that could improve the flotation performance of nanoparticle collectors. With the establishment of a faster process for discovery and development of nanoparticle collectors, researchers can now screen numerous types of nanoparticles for this application, as shown in chapter 2 and chapter 5 of this work.
- 6.1.2. Investigations on colloidal stability and hydrophobicity of nanoparticles allowed us to screen nanoparticles libraries to find the most suitable candidates for froth flotation. Our analysis included the novel mapping of nanoparticle properties on the CCC/contact angle domain - we call “stability maps”. One of the main challenges in nanoparticle collector technology is to control the delicate balance between colloidal stability and hydrophobicity. We found that this balance was better controlled by using post-modification of nanoparticles than fabricating each of them by polymerization. Chapter 2 presented the stability map approach, while chapter 5 expanded this approach to analyzing a triazole nanoparticles library with the same principle.
- 6.1.3. A PEG-methacrylate nanoparticles library was investigated in chapter 2 to screen sterically stabilized candidates. It was found that emulsion polymerization with PEG macromonomers led to extremely stable but too hydrophilic polystyrene

nanoparticles, thus their flotation performance was poor, less than 36% of glass beads recovery. Only nanoparticles with a dense PEG surface layer gave recoveries higher than 50% due to enhanced entrainment, since hydrophilic moieties stabilized the bubbles and decreased their size.

- 6.1.4. In chapter 3, the design and implementation of a high throughput colloidal stability assay was accomplished. The most robust assay comprised four steps: (1) addition of the coagulant agent by robots; (2) addition of nanoparticle dispersions, stirring, turbidity measurement and imaging; (3) centrifugation of multiwell plates; and (4) supernatant extraction and turbidity measurements. This method resulted suitable for nanoparticles with diameters higher than 50 nm; even though when working with nanoparticles with diameters lower than 150 nm the 3<sup>rd</sup> and 4<sup>th</sup> steps in the procedure can be dismissed, since good results are obtained in the first measurements. To analyze nanoparticles with diameters higher than 150 nm, we recommend to follow the full procedure as the plate readers measured absorbance vertically through the bottom of the wells, hence floc sediments interfered with the readings if large aggregates or concentrated dispersions are not isolated.
- 6.1.5. An automated hydrophobicity assay, based on measuring water contact angles on homogeneous coatings of nanoparticle dispersions, was also developed and optimized in chapter 5. We have found that the most effective method for sample preparation was an automated dip coating procedure, in which a monolayer of nanoparticles was deposited at the surface of glass squares. The method allowed obtaining reproducible water contact angles when dispensing 1- $\mu$ L water drop on the surface of the coated glass slide, with a maximum standard deviation of  $\pm 2.0$  degrees, in three repeats per each slide and experiment triplicates for each sample.
- 6.1.6. In chapter 5 the parallel fabrication via post modification of triazole nanoparticles for a single parent azide nanoparticle was described. We produced and screened over 40 nanoparticles samples, determining the most promising nanoparticle candidates to work as collectors. This library presented a wide range of critical coagulation concentrations and contact angles. For example, SA-402 parent nanoparticle, produced derivatives triazole nanoparticles with contact angles ranged from 62 to 101 degrees, depending upon the type of click reagent and its density. Likewise, critical coagulations concentrations ranged between 2.5 mM to 9.5 mM of sodium carbonate.
- 6.1.7. Since an accurate determination of the surface density of functional groups is critical for optimizing click reactions, a paper chromatographic assay was



developed and discussed in chapter 4. This method allowed us to calculate the surface azide available to react with alkynes in post modification reactions. The assay also provided a key advantage; it could be applied to any click alkyne reagents without modifying the assay for each new alkyne to test, making this experiment specifically attractive when working with libraries and high throughput screening.

- 6.1.8. From all the triazole nanoparticles combinations screened in chapter 5, the derivatives containing amino PEG4, butynyl tosylate, rhodamine, propargyl amine and dimethyl propargylamine, with a surface density of  $0.09 \text{ molecules/nm}^2$ , improved the glass beads recovery in sodium carbonate respect to their parent nanoparticle, SA-402. Although in previous studies we defined that suitable nanoparticle candidates had contact angles higher than 50 degrees, the triazole nanoparticles screening allowed us to establish a narrower criterion for the click library, since the most of the best triazole nanoparticles candidates had contact angles between 65 and 75 degrees. The colloidal stability revealed to be a more precise predictor of glass beads recovery than the water contact angle, when the nanoparticles are past the threshold of 50 degrees, as a higher critical coagulation concentration value led to higher glass beads recovery in most of the nanoparticle samples, selected via stability mapping.
- 6.1.9. The advantage of stability map analysis is that compared to pass/fail assays typically used in high throughput screening, the maps reveal how far specific nanoparticles are from target properties. Consequently, the design of new nanoparticle candidates via high throughput screening can consider models of target properties in narrower thresholds of colloidal stability and hydrophobicity.

## 6.2. Future Work Outlook

Studies of flotation of real ores by using the best nanoparticle candidates along with scaled-up fabrication of these materials would be the next steps in this project. Furthermore, modeling of stability maps and more detailed physicochemical investigations conducted with the most promising candidates would aid to understand how slight variations on the surface chemistry of nanoparticles can produce dramatic effects on their flotation performance. Also, the development of a high throughput assay for selectivity to different minerals would help to narrow even more the spectrum of nanoparticles that can be suitable as collectors.



The high throughput philosophy relays on the fact that countless nanoparticles surfaces could be analyzed. However, the bottleneck for our platform is the fabrication step. The presented thesis explored a parallel fabrication of nanoparticles to accelerate this process. The production implemented can be used for post-modification of nanoparticles by using other click reactions, such as thiol-ene reactions and epoxy nucleophilic substitutions, in order to produce other surfaces that could be interesting to explore as nanoparticles candidates.

Increasing the library database of nanoparticle collectors would be a feasible possibility as long as implementations of data management and statistical multivariate analysis are conducted for this project. Also, chemical structure-property modeling would be another promising approach to theoretically predict good candidates for flotation. These tools would be very useful to expand the knowledge of nanoparticle collectors and their application in froth flotation.

Finally, this work has demonstrated approaches to large library preparation of polystyrene-modified nanoparticle collectors, and high throughput screening for mineral processing. This methodology could be applied to other applications and should not be limited to froth flotation of minerals only. Other applications for this technology might include: their use as additives in flotation of plastics, water treatment flocculants, drug delivery carriers, functional coatings for antifouling, functional surfactants, among others.